Wydział Biologii
Uniwersytetu Gdańskiego

mgr Joanna Morcinek-Orłowska

Powiązania między replikacją DNA a innymi procesami komórkowymi *Escherichia coli* oraz ich rola w koordynacji bakteryjnego cyklu komórkowego

Links between DNA replication and other cellular processes in *Escherichia coli* and their role in bacterial cell cycle coordination

Praca przedstawiona
Radzie Dyscypliny Nauki biologiczne Uniwersytetu Gdańskiego
celem uzyskania stopnia doktora
w dziedzinie nauk ścisłych i przyrodniczych
w dyscyplinie nauki biologiczne

Promotor: dr hab. Monika Glinkowska, prof. UG
Katedra Genetyki Molekularnej Bakterii,
Wydział Biologii, Uniwersytet Gdański

GDAŃSK 2026

Składam najserdeczniejsze podziękowania mojej Promotor, dr hab. Monice Glinkowskiej, prof. UG za opiekę naukową podczas pracy nad projektem doktorskim i przygotowywania rozprawy. Serdecznie dziękuję za wsparcie, cierpliwość, umożliwienie mi rozwoju naukowego w wielu kierunkach, a także mądre mentorstwo, które dało mi możliwość uczenia się na błędach, ale i sukcesach.

Jestem bardzo wdzięczna Współpracownikom, z którymi miałam przyjemność pracy podczas mojego doktoratu. W szczególności dziękuję dr Aleksandrze Bebel za naukę pracy z białkami, dr Monice Maciąg-Dorszyńskiej za wspólne zdobywanie doświadczenia w cytometrii przepływowej oraz mgr Justynie Galińskiej za niezapomnianą współpracę podczas jej studiów magisterskich. Dziękuję również wszystkim Pracownikom i Doktorantom Katedry Genetyki Molekularnej Bakterii, Katedry Biologii Molekularnej oraz Katedry Biologii i Genetyki Medycznej za miłą, wspierającą atmosferę.

Bardzo dziękuję prof. dr. hab. Grzegorzowi Węgrzynowi za możliwość dokończenia eksperymentów i analiz w ramach mojego doktoratu równolegle z pracą nad nowym projektem w Katedrze Biologii Molekularnej, co pozwoliło mi zakończyć projekt doktorski i opublikować wyniki.

Ogromnie dziękuję dr Lidii Boss i dr Klaudynie Krause za nieocenione wsparcie, motywację i życzliwą pomoc, kiedy tylko tego potrzebowałam. Coś, co zaczęło się jako praca naukowa w tej samej Katedrze się, przerodziło się w wartościowe przyjaźnie na – mam nadzieję – długie lata, za co jestem Wam ogromnie wdzięczna.
I would also like to thank mgr Adela Bledea for her valuable support and help, and for reminding me every day that the best view comes after the hardest climb.

Jestem szczególnie wdzięczna Autorytetom, które spotkałam na swojej naukowej drodze. Dziękuję Promotor mojej pracy magisterskiej, dr hab. Dorocie Dziadkowiec, za uświadomienie mi, jak bardzo chcę być naukowcem, za życzliwe rady, o które mogłam poprosić nawet po zakończeniu studiów. Bardzo dziękuję także mojemu obecnemu Przełożonemu, dr hab. Michałowi Szymańskiemu, prof. UG, za możliwość kontynuowania pracy naukowej, a przede wszystkim za pokazywanie mi, jakim naukowcem chcę się stawać i że warto jest mierzyć wyżej. Dziękuję także za wyrozumiałość podczas pisania rozprawy doktorskiej.

Dziękuję mojej Rodzinie, a w szczególności Babci, która udowadnia, że prawdziwa więź nie zna odległości – ani w kilometrach, ani w pokoleniach. Szczególnie dziękuję mojemu Mężowi za każdy wspólny dzień, za ogrom wsparcia i cierpliwości, a nade wszystko za bezustanną wiarę we mnie – szczególnie wtedy, kiedy ja nie wierzyłam.

Spis treści

Streszczenie

Cykl komórkowy bakterii to uporządkowany ciąg zdarzeń prowadzący do powstania dwóch komórek potomnych. Obejmuje on wzrost, replikację DNA oraz podział komórki. Replikacja DNA ma kluczowe znaczenie w cyklu komórkowym, gdyż zapewnia wierność i integralność materiału genetycznego przekazywanego komórkom potomnym. Proces ten zachodzi dzięki skoordynowanej aktywności wyspecjalizowanej maszynerii białkowej zwanej replisomem.

Podczas inicjacji replikacji białko inicjatorowe DnaA doprowadza do rozplecenia dupleksu DNA w rejonie *oriC*, co umożliwia przyłączenie helikazy, prymazy oraz wielopodjednostkowej polimerazy DNA III. Precyzyjna regulacja aktywności DnaA w cyklu komórkowym zachodzi przy udziale białek regulatorowych – pozytywnego regulatora DiaA promującego inicjację oraz negatywnych białek regulatorowych Hda i SeqA, które zapobiegają przedwczesnej reinicjacji. W etapie elongacji katalityczna podjednostka polimerazy III wydłuża nić DNA w kierunku 5'-3', używając substratów (deoksyrybonukleotydów) dostarczanych przez reduktazę nukleotydów. Procesywność polimerazy zapewnia podjednotska β, tak zwana klamra, przyłączana do DNA dzięki aktywności podjednostek tworzących kompleks ładujący klamrę. Replikacja chromosomu postępuje w obydwu kierunkach aż do osiągnięcia miejsca *ter*, gdzie następuje jej terminacja.

Kluczowe procesy w cyklu komórkowym bakterii – replikacja DNA i podział komórki – muszą być nie tylko ściśle kontrolowane, ale i skoordynowane ze wzrostem, którego tempo w różnorodnym środowisku naturalnym mikroorganizmów może ulegać bardzo szybkim zmianom. Mechanizm tej koordynacji nadal nie jest w pełni poznany. Coraz więcej przesłanek sugeruje jednak, że zależna od wzrostu regulacja replikacji jest sprzęgana z różnorodnymi procesami metabolicznymi.

Celem niniejszej rozprawy doktorskiej jest scharakteryzowanie powiązań pomiędzy replikacją DNA a innymi procesami komórkowymi w modelowej Gram-ujemnej bakterii *Escherichia coli.* Główna postawiona hipoteza badawcza zakłada, że białka zaangażowane w przebieg i regulację replikacji mogą bezpośrednio oddziaływać z białkami metabolicznymi i/lub drobnocząsteczkowymi metabolitami. Te interakcje, występujące w komórce w danym momencie cyklu komórkowego i w określonych warunkach wzrostu, mogą regulować

aktywność białek replikacyjnych i stanowić mechanizm koordynujący replikację DNA ze wzrostem komórki bakteryjnej.

Badania obejmowały osiem kluczowych białek zaangażowanych w przebieg oraz regulację replikacji DNA *E. coli* – DnaA (białko inicjatorowe), DiaA, Hda, SeqA (białka regulatorowe inicjacji), DnaB (helikazę), DnaG (prymazę), HolD (podjednostkę ψ polimerazy DNA III, część kompleksu ładującego klamrę) oraz NrdB (podjednostkę β reduktazy nukleotydów). Przeprowadziłam analizę sieci interakcji, które tworzą wspomniane białka w warunkach szybkiego oraz wolnego wzrostu komórek. Izolacja kompleksów białkowych powstających bezpośrednio w komórce bakteryjnej jest możliwa dzięki dołączeniu do sekwencji kodującej sekwencji znacznika SPA. Umożliwia on oczyszczanie białka oraz oddziałujących z nim molekuł z wykorzystaniem chromatografii powinowactwa, a następnie identyfikację składu kompleksów metodą spektrometrii mas poprzedzonej chromatografią cieczową. W eksperymencie uwzględniłam próby kontrolne oraz zaproponowałam dwie strategie analizy specyficzności uzyskanych interakcji – jakościową i ilościową.

Profile interakcji białek replikacyjnych wykazują dużą zależność wobec warunków wzrostu komórek. Ponadto każde z nich tworzy odrębne sieci interakcji, a pula białek oddziałujących z więcej niż jednym białkiem-przynętą jest stosunkowo niewielka. Białka oddziałujące z aparatem replikacyjnym reprezentują różne procesy funkcjonalne, spośród których można wyróżnić biogenezę rybosomu, obróbkę i degradację RNA oraz metabolizm nukleotydów. Szczególnie istotna jest identyfikacja białek zaangażowanych w syntezę powłok komórkowych – fosfolipidów błonowych, peptydoglikanu oraz lipopolisacharydu (LPS). Różni przedstawiciele tej grupy funkcjonalnej pojawiają się konsekwentnie w interaktomach prawie wszystkich analizowanych białek.

Spośród zidentyfikowanych partnerów interakcyjnych wybrałam kilka białek do dalszych analiz, po czym określiłam wpływ delecji ich genów na zawartość DNA w komórkach metodą cytometrii przepływowej po zatrzymaniu replikacji. Wykazałam, że pozbawienie komórki białka RfaD, zaangażowanego w jeden z etapów syntezy rdzenia LPS, przyczynia się do asynchronicznej inicjacji replikacji w komórce oraz zaburzeń czasu inicjacji replikacji w cyklu komórkowym, widocznych zwłaszcza w warunkach wolnego wzrostu komórek. Delecja genu *rlmE*, kodującego metylotransferazę rRNA, opóźnia inicjację replikacji w cyklu komórkowym i zaburza jej synchroniczność, jednak efekt ten manifestuje się

w warunkach szybkiego wzrostu komórek. Uzyskane przeze mnie wyniki wskazują, że mechanizmy kontroli replikacji, w które zaangażowane są białka oddziałujące z aparatem replikacyjnym, są istotnie zależne od warunków wzrostu.

W ramach współpracy naukowej uczestniczyłam również w badaniach nad funkcją lipoprotein wspomagających kompleksu Bam, odpowiedzialnego za fałdowanie białek zewnętrznej błony komórkowej. Ze względu na obserwowane interakcje genetyczne genu *bamB* z podjednostkami polimerazy DNA III oraz regulatorami replikacji, określiłam wpływ jego delecji na regulację replikacji w cyklu komórkowym metodą cytometrii przepływowej po zatrzymaniu replikacji. Wykazałam, że delecja genu *bamB* w komórce może prowadzić do wcześniejszej i częściowo asynchronicznej replikacji w cyklu komórkowym. Wyniki te stanowią dodatkowe potwierdzenie funkcjonalnych zależności między homeostazą powłok komórkowych a regulacją replikacji u *E. coli.*

W strukturze białka DiaA – pozytywnego regulatora inicjacji replikacji – wyróżnić można domenę wiążącą fosfocukry, typową dla izomeraz cukrowych, co skłoniło nas do zadania pytania nie tylko o jej możliwą rolę, ale też o potencjalne interakcje białek replikacyjnych z metabolitami. Pokazaliśmy, że DiaA może oddziaływać z sedoheptulozo-7-fosforanem (S7P) *in vitro*, a interakcja ta hamuje pozytywny efekt DiaA na wiązanie białka inicjatorowego w rejonie *oriC*. Ponadto zaobserwowałam, że obniżenie poziomu S7P *in vivo* powoduje deregulację czasu inicjacji replikacji w cyklu komórkowym. S7P jest zaangażowany w syntezę bakteryjnego LPS, jak również w cykl pentozofosforanowy uczestniczący w produkcji nukleotydów. Odkryte powiązania wskazują na istnienie zależności między syntezą zewnętrznych powłok komórki, syntezą nukleotydów i inicjacją replikacji, które mogłyby odpowiadać za koordynację cyklu komórkowego w sposób zależny od stężenia metabolitów i aktywności enzymów metabolicznych.

Wyniki uzyskane w ramach rozprawy są punktem wyjścia do dalszych badań prowadzących do ustalenia funkcjonalnego znaczenia odkrytych oddziaływań, a w konsekwencji do lepszego zrozumienia mechanizmów sprzęgających replikację i inne procesy w komórce. Koordynacja cyklu komórkowego bakterii ma kluczowe znaczenie dla przeżycia mikroorganizmów w zmiennym środowisku, a także dla wirulencji bakterii patogennych. Co za tym idzie, odkryte mechanizmy mogą stanowić cele molekularne dla nowych leków przeciwbakteryjnych, a z drugiej strony pozwolą na wspieranie wzrostu bakterii tam, gdzie jest to pożądane, na przykład w bioreaktorach.

Abstract

The bacterial cell cycle is a set of consecutive events that leads to the formation of two daughter cells. It comprises cell growth, DNA replication, and cell division. DNA replication is central to the cell cycle, as it ensures the fidelity and integrity of the genetic material passed to progeny cells. This process relies on the coordinated activity of highly specialized protein machinery known as the replisome.

During replication initiation, the initiator protein DnaA unwinds the DNA duplex within the *oriC* region, allowing the helicase, primase, and the multisubunit DNA polymerase III to assemble. The activity of DnaA is tightly regulated throughout the cell cycle by regulatory proteins – a positive regulator, DiaA, which promotes initiation, and negative regulators, Hda and SeqA, which prevent premature reinitiation. During elongation, the catalytic subunit of DNA polymerase III extends the DNA strand in the 5'-3' direction, using deoxyribonucleotides supplied by ribonucleotide reductase. Polymerase processivity is ensured by the sliding clamp (β subunit), which is loaded onto DNA by the clamp-loader complex. Replication proceeds bidirectionally on the chromosome until it reaches the *ter* region, where the process is completed.

Key events in the bacterial cell cycle – DNA replication and cell division – need to be not only strictly controlled but also tightly coordinated with cell growth, whose rate can change rapidly under the diverse environmental conditions in microorganisms' habitats. The mechanisms underlying this coordination still remain not fully understood. Increasing evidence, however, suggests that growth-dependent regulation of replication is coupled to various metabolic processes.

The goal of my doctoral thesis is to characterize the links between DNA replication and other cellular processes in the model Gram-negative bacterium *Escherichia coli*. The central research hypothesis posits that replication proteins can directly interact with metabolic proteins and/or small-molecule metabolites. These interactions – occurring in the cell at specific stages of the cell cycle and under defined growth conditions – may modulate the activity of replication proteins and constitute a mechanism coordinating DNA replication with bacterial cell growth.

The study focused on eight key *E. coli* proteins involved in the progression and regulation of DNA replication: DnaA (the initiator protein), DiaA, Hda, SeqA (regulatory proteins), DnaB (helicase), DnaG (primase), HolD (the ψ subunit of DNA polymerase III, part of the clamp-loader complex), and NrdB (the β subunit of ribonucleotide reductase). I mapped the interaction networks formed by these proteins under conditions supporting fast and slow bacterial growth. Isolation of protein complexes formed directly in the bacterial cell was enabled by chromosomal fusion of the respective coding sequences with SPA-tag sequence. This tag allows affinity purification of the bait protein together with its interacting partners, followed by liquid chromatography-tandem mass spectrometry to identify complex components. The experimental design included appropriate control samples, based on which we developed tailored qualitative and quantitative data processing strategies to filter out non-specific interactions.

Interaction profiles formed by replication proteins exhibit strong dependence on bacterial growth conditions used. Moreover, each bait protein forms a distinct interaction network, and the set of proteins interacting with more than one bait is relatively small. Proteins associating with the replication machinery represent several functional categories, including ribosome biogenesis, RNA processing and degradation, and nucleotide metabolism. Particularly notable is the identification of proteins involved in the synthesis of cell envelope components – membrane phospholipids, peptidoglycan, and lipopolysaccharide (LPS). Different representatives of this functional group appear consistently across nearly all analyzed interactomes.

From among the identified interaction partners, I selected a few proteins representing distinct functional classes for further analysis. I determined the effect of their gene deletion on DNA content in fast- and slow-growing cells using flow cytometry after replication run-out. I showed that depletion of RfaD, an enzyme involved in one of the steps of LPS core biosynthesis, leads to asynchronous replication initiation and disturbances in replication-timing control within the cell cycle, particularly evident under slow-growth conditions. Deletion of *rlmE*, encoding an rRNA methyltransferase delays replication initiation and disrupts its synchrony, but this effect manifests under conditions of rapid cell growth. My results indicate that the potential coordination mechanisms involving proteins interacting with the replication machinery are strongly dependent on growth conditions.

As part of a scientific collaboration, I also participated in studies aimed at elucidating the function of accessory lipoproteins of the Bam complex, which is responsible for the folding of outer membrane proteins. Given the observed genetic interactions of the *bamB* gene with subunits of DNA polymerase III and replication regulatory proteins, I investigated the effect of its deletion on the regulation of DNA replication during the cell cycle using flow cytometry after replication run-out. I demonstrated that the *bamB* gene deletion can lead to earlier and partially asynchronous replication in the cell cycle. These results further support the functional interplay between cell envelope homeostasis and replication regulation in *E. coli*.

The structure of DiaA, a positive regulator of replication initiation, contains phosphosugar-binding domain, characteristic of sugar isomerases, which prompted us to ask not only about its role, but also about possible interactions between replication proteins and metabolites. We showed that DiaA binds sedoheptulose-7-phosphate (S7P) *in vitro*, and that this interaction impedes the stimulatory effect of DiaA on DnaA oligomerization at *oriC*. I also demonstrated that lowering intracellular S7P levels deregulates replication initiation timing in the cell cycle, resulting in earlier initiation. S7P is an intermediate of the pentose phosphate pathway, and a key metabolite for the bacterial lipopolysaccharide biosynthesis. The identified interaction points to interconnection between nucleotide biosynthesis, cell envelope biogenesis and replication regulation, which may coordinate the bacterial cell cycle in response to metabolite concentration and metabolic enzyme activities.

The results of this dissertation provide a foundation for future studies aimed at determining the functional significance of the identified interactions. It would ultimately contribute to a deeper understanding of the mechanisms coupling DNA replication with other cellular processes. Coordination of the bacterial cell cycle is crucial not only for microbial survival in dynamically changing environments, but also for the virulence of pathogenic bacteria. Consequently, discovered mechanisms may constitute novel molecular targets for antimicrobial therapies and, conversely, may support bacterial growth where desirable, such as in bioreactors.

Lista prac wchodzących w skład rozprawy doktorskiej

1. Artykuł przeglądowy:

   Morcinek-Orłowska J., Galińska J., Glinkowska M.K. When size matters - coordination of growth and cell cycle in bacteria. Acta Biochim Pol. 2019 Apr 10;66(2):139-146.

   DOI: https://doi.org/10.18388/abp.2018_2798.

   PMID: 30970043.

2. Artykuł oryginalny (badawczy):

   Morcinek-Orłowska J., Walter B., Forquet R., Cysewski D., Carlier M., Mozolewski M., Meyer S., Glinkowska M. Interaction networks of *Escherichia coli* replication proteins under different bacterial growth conditions. Sci Data. 2023 Nov 10;10(1):788.

   DOI: https://doi.org/10.1038/s41597-023-02710-1.

   PMID: 37949936; PMCID: PMC10638427.

3. Preprint artykułu oryginalnego (badawczego):

   Morcinek-Orłowska J., Walter B., Forquet R., Cysewski D., Carlier M., Meyer S., Glinkowska M. Protein interaction network analysis reveals growth conditions-specific crosstalk between chromosomal DNA replication and other cellular processes in *E. coli*. bioRxiv 2021.12.08.471875.

   DOI: https://doi.org/10.1101/2021.12.08.471875.

4. Preprint (recenzowany) artykułu oryginalnego (badawczego):

   Bryant J.A., Staunton K.A., Doherty H.M., Alao M.B., Ma X., **Morcinek-Orłowska J.**, Goodall E.C.A., Gray J., Milner M., Cole J.A., de Cogan F., Knowles T.J., Glinkowska M., Moradigaravand D., Henderson I.R., Banzhaf M. (2024) Bam complex associated proteins in *Escherichia coli* are functionally linked to peptidoglycan biosynthesis, membrane fluidity and DNA replication. eLife 13:RP99955.

   DOI: https://doi.org/10.7554/eLife.99955.1.

5. Manuskrypt artykułu oryginalnego (badawczego) przygotowany do publikacji:

   Bebel A.*, **Morcinek-Orłowska J.***, Banzhaf M., Galińska J., Waldminghaus T., Zawilak-Pawlik A., Glinkowska M., Interaction of the replication factor DiaA and primary metabolite sedoheptulose 7-phosphate regulates DNA replication in *Escherichia coli*.

   * wkład równorzędny.

Komentarz do rozprawy doktorskiej

Wprowadzenie

Cykl komórkowy bakterii to sekwencja zdarzeń obejmujących wzrost, replikację chromosomu oraz podział komórki, prowadząca do powstania dwóch komórek potomnych. Tradycyjnie dzieli się go na określone etapy: fazę B (ang. *birth*, okres od narodzin komórki do inicjacji replikacji), fazę C (duplikacja chromosomu) oraz fazę D (czas od ukończenia replikacji do cytokinezy) [1]. W komórkach eukariotycznych poszczególne procesy cyklu komórkowego zachodzą w wyspecjalizowanych organellach, a przejścia między fazami są ściśle kontrolowane przez zestaw białek tzw. punktów kontrolnych (ang. *cell cycle checkpoints*). U bakterii analogiczne systemy nie zostały zidentyfikowane, a wszystkie etapy cyklu zachodzą równolegle w cytoplazmie [2]. Taka współbieżność wymaga precyzyjnej koordynacji, zwłaszcza w warunkach zmiennej dostępności składników odżywczych. W tym kontekście replikacja jest uważana za centralny etap cyklu komórkowego – decyzja o jej rozpoczęciu musi być dostosowana do stanu fizjologicznego komórki oraz jej tempa wzrostu, tak, aby każda komórka potomna otrzymała kompletną kopię genomu.

Replikacja DNA obejmuje trzy główne fazy – inicjację, elongację oraz terminację – a ich niezakłócony przebieg zależy od skoordynowanej aktywności wielu białek [3]. W modelowej Gram-ujemnej bakterii *Escherichia coli* replikacja rozpoczyna się w pojedynczym, ściśle określonym miejscu zwanym *origin* (*oriC*). Zawiera ono region o powinowactwie do białka inicjatorowego DnaA (ang. *DnaA-oligomerization region*, DOR) oraz region bogaty w pary AT podlegający rozpleceniu (ang. *duplex unwinding element*, DUE). DnaA związane z ATP oligomeryzuje na DOR, a po osiągnięciu krytycznego poziomu doprowadza do rozplecenia DNA w miejscu DUE [4]. Proces ten wspierają białka DiaA i IHF, które wraz z DnaA tworzą kompleks inicjacyjny. DiaA promuje oligomeryzację DnaA i wiązanie do rejonów *oriC* o słabszym powinowactwie, a IHF silnie zagina helisę, umożliwiając tworzenie przestrzennej struktury ułatwiającej rozplecenie DNA [5].

Powstała w wyniku rozplecenia „bańka replikacyjna” stanowi platformę do stopniowego przyłączania wysoce zorganizowanego białkowego kompleksu – replisomu

[3]. W pierwszym etapie do DNA rekrutowana jest heksameryczna helikaza DnaB, której załadowanie zachodzi przy udziale pomocniczego białka DnaC, w sposób zależny od ATP i interakcji z DnaA [6]. Dysocjacja DnaC umożliwia następnie przyłączenie prymazy DnaG, odpowiedzialnej za syntezę starterów – krótkich odcinków RNA stanowiących punkt wyjścia do syntezy nowych nici DNA [7]. Obecność starterów na jednoniciowym DNA stanowi sygnał do rekrutacji polimerazy DNA III. Składa się ona z 10 podjednostek zorganizowanych w trzy moduły funkcjonalne: rdzeń katalityczny (podjednostki DnaE, DnaQ i HolE), dimeryczną β-klamrę $(DnaN)_2$ oraz kompleks ładujący klamrę (ang. *clamp-loader complex*, CLC), tworzony przez podjednostki $(DnaX)_3$, HolB, HolA, HolC i HolD [8].

Włączenie polimerazy do replisomu ma charakter sekwencyjny. Związane z matrycą startery są najpierw rozpoznawane przez CLC, który, wykorzystując energię z hydrolizy ATP, montuje β-klamrę na DNA. Umożliwia ona polimerazie sprawne poruszanie się po nici DNA i zapewnia jej procesywność [3, 8]. Do klamry przyłącza się następnie rdzeń polimerazy. Podjednostka DnaE katalizuje przyłączanie nukleotydów do wolnej grupy hydroksylowej końca 3', wydłużając nić w kierunku 5'-3'. Tym samym nić wiodąca syntezowana jest w sposób ciągły, natomiast nić opóźniona powstaje w formie krótkich odcinków DNA zwanych fragmentami Okazaki, z których każdy wymaga syntezy nowego startera [7, 8].

W wyniku pojedynczej inicjacji replikacji na przeciwległych końcach bańki replikacyjnej formują się dwa siostrzane replisomy, prowadzące syntezę DNA w przeciwnych kierunkach [8]. Najnowsze badania wskazują, że nie poruszają się one po chromosomie jako niezależne jednostki, lecz mogą pozostawać ze sobą sprzężone, tworząc tak zwaną „fabrykę replikacyjną", w której chromosom jest dynamicznie przemieszczany przez względnie nieruchomą maszynerię białkową [9, 10]. Efektywna elongacja wymaga stałej dostępności substratów do syntezy DNA – deoksyrybonukleotydów. Są one produkowane przez reduktazę rybonukleotydową NrdAB, której poziom w komórkach jest ściśle zależny od postępu cyklu komórkowego i liczby aktywnych replisomów [11]. Coraz więcej przesłanek sugeruje, że NrdAB może kolokalizować z replisomem [12], a nawet fizycznie z nim oddziaływać, zapewniając precyzyjne dostarczanie dNTP do centrum aktywnego polimerazy DNA III. Synteza nowych nici DNA postępuje aż do osiągnięcia na chromosomie regionu *terminus*, gdzie progresja widełek replikacyjnych zostaje zatrzymana i proces ulega zakończeniu [8].

Mechanizmy regulacji replikacji DNA w komórkach *Escherichia coli* koncentrują się przede wszystkim na etapie inicjacji. Zapewniają one precyzyjne zsynchronizowanie rozpoczęcia replikacji z przebiegiem cyklu komórkowego oraz gwarantują, że inicjacja zachodzi dokładnie raz na cykl, zapobiegając zbyt szybkiej reinicjacji po jej zajściu. Na poziomie molekularnym kontrola ta opiera się przede wszystkim na regulacji aktywności białka inicjatorowego DnaA oraz dostępności regionu *oriC* [13]. DnaA występuje w komórce w dwóch funkcjonalnie odmiennych formach – związanej z ATP, aktywnej inicjacyjnie, oraz związanej z ADP, niezdolnej do inicjacji – a ich stosunek ulega dynamicznym zmianom w trakcie cyklu komórkowego i jest ściśle regulowany [14]. Po zainicjowaniu replikacji pula DnaA-ATP jest szybko obniżana. Odpowiada za to przede wszystkim system RIDA (ang. *Regulatory Inactivation of DnaA*). Opiera się on na aktywności białka Hda, które oddziałuje z załadowaną na DNA β-klamrą i w tej formie stymuluje hydrolizę DnaA-ATP w sposób sprzężony z elongacją replikacji [4, 13]. Obniżenie poziomu DnaA-ATP jest dodatkowo stymulowane poprzez jego asocjację z chromosomalnym locus *datA*, które promuje hydrolizę (ang. *datA-dependent DnaA-ATP hydrolysis*, DDAH) [14]. Z kolei wiązanie nieaktywnego inicjacyjnie DnaA do sekwencji DARS (ang. *DnaA reactivating sequences*) pozwala na wymianę ADP na ATP i reaktywację DnaA [14]. Podobny proces wspierany jest przez kwaśne fosfolipidy i wymaga asocjacji DnaA do wewnętrznej błony komórkowej [15], co prowadzi do stopniowego odbudowania puli aktywnego inicjatora przed kolejną rundą inicjacji.

Równolegle do mechanizmów regulujących aktywność DnaA funkcjonuje system, którego bezpośrednim celem molekularnym jest *origin* replikacji. W komórkach bakteryjnych DNA podlega metylacji za pośrednictwem metylazy Dam, jednak we wczesnej fazie elongacji replikacji nowo zsyntetyzowana nić pozostaje przejściowo niezmetylowana. Powstałe w ten sposób hemimetylowane *oriC* jest wiązane przez białko SeqA, co uniemożliwia przyłączenie DnaA-ATP i zapobiega przedwczesnej reinicjacji replikacji [16]. Efekt ten, określany jako sekwestracja *origin*, utrzymuje się do momentu metylacji nowej nici przez metylazę Dam, której aktywność również wykazuje zależność od cyklu komórkowego [17]. Oprócz *oriC* SeqA wiąże się też z innymi miejscami rozmieszczonymi w obrębie całego chromosomu i może oddziaływać z topoizomerazami – enzymami regulującymi stopień i kierunek superskręcenia helisy DNA [18]. Wskazuje to na jego dodatkową, bardziej globalną rolę w utrzymaniu właściwej architektury chromosomu podczas cyklu komórkowego [19].

Pomimo szczegółowego poznania mechanizmów regulacji replikacji w komórkach *Escherichia coli*, ich koordynacja oraz integracja z tempem wzrostu i stanem fizjologicznym komórki, które determinują czas inicjacji replikacji w cyklu komórkowym, nadal nie są w pełni wyjaśnione. Podstawy współczesnego rozumienia kontroli cyklu komórkowego bakterii wywodzą się z badań populacyjnych prowadzonych na *Salmonella* spp. niemal siedem dekad temu. Wykazały one liniową zależność między tempem wzrostu a rozmiarem komórki i jej makromolekularną kompozycją, znaną jako „prawo wzrostu" (ang. *growth law*) [20]. Spójny z tymi obserwacjami sposób organizacji replikacji DNA w warunkach szybkiego wzrostu został zaproponowany przez Coopera i Helmstettera w modelu wielowidełkowej replikacji (ang. *multifork replication*), zgodnie z którym kolejne rundy replikacji są inicjowane przed zakończeniem poprzednich, co umożliwia podziały w czasie krótszym niż minimalny czas wymagany do pełnej replikacji chromosomu [21]. Integracja powyższych założeń doprowadziła do sformułowania koncepcji masy inicjacyjnej (ang. *initiation mass*), zakładającej, że rozmiar komórki w momencie inicjacji replikacji stanowi wielokrotność krytycznej masy przypadającej na pojedyncze *origin* replikacji. Według jej autora, Williama Donachiego, osiągnięcie tej krytycznej masy jest skorelowane z zależną od wzrostu akumulacją molekularnego czynnika wyzwalającego inicjację replikacji [22, 23]. Paradygmat ten po raz pierwszy bezpośrednio powiązał kontrolę rozmiaru komórki z progresją cyklu komórkowego. Za postulowany czynnik wyzwalający przez długi czas uznawano białko inicjatorowe DnaA. Późniejsze badania wykazały jednak, że manipulacje poziomem DnaA w komórce nie przekładają się jednoznacznie na proporcjonalne zmiany w masie inicjacyjnej ani czasie inicjacji w cyklu komórkowym [24, 25]. Tym samym mechanizmy koordynacji cyklu komórkowego ze wzrostem wydają się bardziej złożone, niż wynikałoby to z prostego modelu jednoczynnikowego.

Dane populacyjne, na których opierają się klasyczne modele bakteryjnego cyklu komórkowego, opisują zachowanie wyidealizowanej "komórki średniej", podczas gdy rzeczywiste komórki wykazują stochastyczną zmienność rozmiaru, tempa wzrostu oraz czasu kluczowych zdarzeń cyklu [2]. Uśrednianie procesów o takim charakterze może prowadzić do pozornie deterministycznych zależności, które niekoniecznie odzwierciedlają mechanizmy zachodzące na poziomie pojedynczej komórki. Rozwój wysokoprzepustowych technik mikroprzepływowych i mikroskopowych umożliwił bezpośrednie śledzenie parametrów cyklu komórkowego w dużej liczbie pojedynczych komórek, co – w połączeniu z zaawansowanym

modelowaniem matematycznym – doprowadziło do rewizji dotychczasowych modeli i ram pojęciowych opisujących kontrolę rozmiaru komórki w cyklu komórkowym. Praca przeglądowa *When size matters – coordination of growth and cell cycle in bacteria*, stanowiąca część niniejszej rozprawy doktorskiej (**Artykuł nr 1**), podsumowuje te osiągnięcia oraz wynikającą z nich zmianę w postrzeganiu koordynacji cyklu komórkowego bakterii. Wysokoprzepustowe dane z pojedynczych komórek wykazały bowiem, że kontrola rozmiaru w progresji cyklu komórkowego nie opiera się na osiąganiu całkowitego rozmiaru krytycznego (‘*sizer*’), lecz na dodawaniu stałej objętości, niezależnie od początkowego rozmiaru komórki (‘*adder*’) [26]. Model ten potwierdzono w wielu gatunkach bakterii, co wskazuje na jego uniwersalny charakter [2, 27]. Niemniej, etap cyklu komórkowego, na którym nakładana jest kontrola dodawanego rozmiaru, jak również molekularny mechanizm tej kontroli, pozostają przedmiotem dyskusji. Aktualne modele sugerują, że może być ona realizowana zarówno na etapie inicjacji replikacji, jak i podziału komórki. W takim ujęciu podwójny ‘*adder*’ może wynikać z współbieżnego działania dwóch procesów, gdzie przejście między cyklami jest determinowane przez wolniejszy z nich [28] lub – jak wskazują nowsze analizy rewidujące wcześniejsze modele – z całkowicie niezależnej kontroli tych zdarzeń [29, 30].

Modele cyklu komórkowego, chociaż pozwalają na określenie zależności między wzrostem, replikacją i podziałem komórki, nie definiują natury sygnału przekazującego informację o tempie wzrostu bezpośrednio do aparatu replikacyjnego. Metabolizm, jako pierwszy proces odpowiadający na zmiany dostępności składników odżywczych i warunków środowiska, jest naturalnym kandydatem na pośrednika w tej replikacji, co pozwala założyć, że replikacja DNA i metabolizm komórki są ze sobą sprzężone [31]. Analizy genetyczne prowadzone dla *Bacillus subtilis* i *Escherichia coli* wykazały, że delecje genów kodujących enzymy centralnego metabolizmu węgla specyficznie redukują negatywny efekt punktowych mutacji w białku DnaA i komponentach replisomu, co wskazuje na korelację pomiędzy stanem metabolicznym komórki a etapami inicjacji oraz elongacji replikacji [32, 33]. Ponadto wykazano, że suplementacja niektórych metabolitów centralnego metabolizmu węgla również moduluje fenotypy punktowych mutantów białek replikacyjnych, co sugeruje, że komunikacja między replikacją a metabolizmem może zachodzić zarówno na poziomie proteomicznym, jak i metabolomicznym [34, 35]. Zgodnie z aktualną perspektywą, metaboliczna kontrola replikacji działa jako zestaw równolegle dostępnych elementów regulacyjnych, z których

komórka może korzystać w sposób zależny od warunków wzrostu, aktualnego stanu metabolicznego i dostępnych zasobów molekularnych, prowadząc do dostowania inicjacji i przebiegu replikacji DNA do stanu fizjologcznego komórki [31, 36]. Niemniej, dokładne mechanizmy molekularne leżące u podstaw tego sprzężenia pozostają w dużej mierze niepoznane.

Oprócz omówionego powyżej artykułu przeglądowego, niniejsza rozprawa obejmuje cztery prace eksperymentalne, w których analizowane są powiązania między replikacją DNA a innymi procesami zachodzącymi w komórce *Escherichia coli*, w funkcjonalnym kontekście koordynacji bakteryjnego cyklu komórkowego.

Cel pracy

Celem badań prowadzonych w ramach niniejszej rozprawy doktorskiej było określenie powiązań pomiędzy replikacją DNA a innymi procesami komórkowymi (ze szczególnym uwzględnieniem metabolizmu) w modelowej Gram-ujemnej bakterii *Escherichia coli.* Główna postawiona hipoteza badawcza zakłada, że białka zaangażowane w przebieg i regulację replikacji mogą bezpośrednio oddziaływać z czynnikami funkcjonalnie odrębnych procesów komórkowych – głównie z białkami metabolicznymi i/lub drobnocząsteczkowymi metabolitami. Te interakcje, występujące w komórce w danym momencie cyklu komórkowego i w określonych warunkach wzrostu, mogą regulować aktywność białek replikacyjnych i stanowić mechanizm koordynujący replikację DNA ze wzrostem komórki bakteryjnej.

Cel zrealizowałam poprzez:

- zidentyfikowanie sieci interakcji białko-białko dla 8 białek (DnaA, DiaA, Hda, SeqA, DnaB, DnaG, HolD, NrdB) związanych z replikacją DNA, w warunkach szybkiego oraz wolnego wzrostu komórek, a także po przejściu hodowli w fazę stacjonarną,
- ocenę wpływu delecji 2 genów (*rfaD*, *rlmE*) kodujących białka potencjalnie oddziałujące z białkami replikacyjnymi oraz genu zaangażowanego w interakcje genetyczne z genami podjednostek polimerazy DNA i regulatorów replikacji (*bamB*) na czas inicjacji replikacji w bakteryjnym cyklu komórkowym,

- charakteryzację oddziaływania białka regulatorowego DiaA z sedoheptulozo-7-fosforanem (S7P) oraz określenie możliwego wpływu tej interakcji oraz wewnątrzkomórkowego poziomu S7P na regulację inicjacji replikacji w bakteryjnym cyklu komórkowym.

Omówienie prac eksperymentalnych

Artykuł nr 2 – *Interaction networks of Escherichia coli replication proteins under different bacterial growth conditions*

Sprawne funkcjonowanie komórki na poziomie molekularnym zachodzi dzięki skomplikowanym sieciom interakcji białkowych. Odpowiadają one za organizację procesów biologicznych w przestrzeni i czasie, koordynację poszczególnych funkcji komórkowych oraz reakcję na bodźce zewnętrzne. Kompleksy białkowe często zyskują właściwości, których nie mają ich pojedyncze składniki. Tworzone w ten sposób zintegrowane moduły funkcjonalne charakteryzują się dużą dynamiką i zdolnością do reorganizacji w odpowiedzi na zmieniające się warunki środowiska [37-39]. Identyfikacja zmian w sieciach interakcji konkretnych białek w zależności od tempa wzrostu komórek może zatem sprzyjać odkryciu mechanizmów wykorzystywanych przez bakterie do dostosowywania fizjologii komórki do dostępności składników odżywczych.

Jedną ze strategii stosowanych w badaniach proteomicznych do identyfikacji interakcji białkowych jest chromatografia powinowactwa sprzężona ze spektrometrią mas (ang. *affinity purification coupled with mass spectrometry*, AP-MS). Metoda ta polega na izolacji kompleksów białkowych tworzonych przez wybrane białko-przynętę, wyposażone w sekwencję znacznika umożliwiającego jego selektywne oczyszczenie bezpośrednio z lizatu komórkowego wraz ze związanymi z nim partnerami. Skład wyizolowanych kompleksów identyfikuje się następnie za pomocą spektrometrii mas, co umożliwia mapowanie fizjologicznych oddziaływań białkowych na dużą skalę [40]. Dotychczas opublikowane wysokoprzepustowe analizy sieci interakcji w komórkach *Escherichia coli* obejmowały szeroki zakres białek-przynęt, jednak ograniczały się do standardowych warunków hodowli laboratoryjnej z użyciem bogatej, niezdefiniowanej pożywki [41-43]. Ponadto większość tych

eksperymentów prowadzono w tle genetycznym szczepu *Escherichia coli* DY330 (wyposażonego w chromosomalnie zintegrowany system rekombinacji λ-red [44]), którego proteom może odbiegać od proteomu szczepu typu dzikiego. **Dlatego też naszym celem było określenie zależnego od warunków wzrostu profilu interakcji białek replikacyjnych w laboratoryjnym szczepie typu dzikiego *Escherichia coli* MG1655. Ponadto, istotnym zadaniem tej pracy było również zaproponowanie systemu kontroli negatywnych oraz strategii analizy danych, które mogą zostać wykorzystane w przyszłych badaniach tego typu.**

Zastosowana koncepcja eksperymentalna obejmowała kilka etapów (graficzna reprezentacja: **Artykuł nr 2, Fig. 1**). Wybraliśmy 8 białek-przynęt, obejmujących białko inicjatorowe DnaA, białka regulatorowe replikacji DiaA, Hda i SeqA, komponenty replisomu – helikazę DnaB, prymazę DnaG oraz podjednostkę ψ polimerazy DNA III HolD, a także podjednostkę β reduktazy rybonukleotydowej – NrdB. Do chromosomalnych sekwencji kodujących te białka dołączyłam sekwencję tandemowego znacznika SPA (ang. *sequential purification affinity tag*) za pomocą rekombinacji zależnej od systemu λ-red [45] (**Artykuł nr 2, Fig. 2**). Skonstruowane w ten sposób fuzje genowe zachowują poziom ekspresji zbliżony do natywnego, co pozwala na uchwycenie fizjologicznych interakcji białkowych w komórce. Fuzyjne szczepy *Escherichia coli* hodowałam w trzech niezależnych powtórzeniach biologicznych w warunkach szybkiego oraz wolnego wzrostu komórek (definiowanego przez różne źródła węgla w pożywce) do późnej fazy logarytmicznej, a także – w warunkach szybkiego wzrostu – do fazy stacjonarnej. Z uzyskanych w ten sposób komórek izolowałam kompleksy białkowe metodą tandemowej chromatografii powinowactwa. Zastosowany znacznik SPA składa się z trzykrotnie powtórzonego peptydu FLAG oraz białka wiążącego kalmodulinę CBP (ang. *calmodulin binding protein*) oddzielonych miejscem cięcia dla proteazy TEV (ang. *tobacco etch virus protease*). Taki układ umożliwia sekwencyjne oczyszczanie białka-przynęty wraz z oddziałującymi partnerami na dwóch złożach chromatograficznych, a trawienie TEV bezpośrednio na złożu wiążącym FLAG pozwala na elucję specyficznie związanych do przynęty białek [46] (**Artykuł nr 2, Fig. 3**). Oczyszczone kompleksy białkowe poddano tandemowej spektrometrii mas poprzedzonej chromatografią cieczową (ang. *liquid chromatography-tandem mass spectrometry*, LC-MS/MS). Identyfikację białek na podstawie

widm MS przeprowadzono za pomocą oprogramowania MaxQuant, wykorzystując referencyjny proteom *Escherichia coli* K-12 zdeponowany w bazie UniProt.

Badania AP-MS cechują się zwykle dość dużym poziomem fałszywie pozytywnych interakcji wynikających z niespecyficznego oddziaływania białek ze złożami chromatograficznymi oraz znacznikami molekularnymi. Zastosowanie tandemowego oczyszczania kompleksów na różnych złożach pozwala ograniczyć poziom takich kontaminacji, jednak nie eliminuje ich całkowicie. W związku z tym niezbędne jest zastosowanie odpowiednio dobranych kontroli negatywnych, umożliwiających rozróżnienie rzeczywistych interakcji od tła eksperymentu [47].

W niniejszej pracy zastosowaliśmy dwa rodzaje prób kontrolnych. Pierwsza obejmowała szczep MG1655 (tło genetyczne eksperymentu) pozbawiony jakiegokolwiek znacznika, co pozwalało na ocenę poziomu niespecyficznych interakcji białek ze złożami chromatograficznymi. Druga kontrola odzwierciedlała sytuację, gdy przynętą jest losowe białko z C-terminalnym znacznikiem SPA – w tym przypadku białko mVenus – służące do oszacowania niespecyficznego wiązania białek do znacznika. Próby kontrolne przygotowałam dla wszystkich warunków wzrostu i traktowałam identycznie jak próby eksperymentalne, a zidentyfikowane w nich białka posłużyły do oceny specyficzności interakcji w próbach eksperymentalnych na podstawie dwóch opracowanych strategii. W podejściu jakościowym pula białek wspólna dla trzech powtórzeń prób eksperymentalnych była porównana z analogicznymi zestawami dla obu kontroli. Każde białko wykryte w którejkolwiek próbie kontrolnej klasyfikowaliśmy jako wynik fałszywie pozytywny. Podstawą ilościowej strategii analizy danych było podejście bez zastosowania znakowania, tzw. *label-free*, w którym oceniane były wartości intensywności jonów prekursorowych obliczane w programie MaxQuant jako pole powierzchni pików chromatograficznych dla poszczególnych peptydów [48, 49]. Jeśli dane białko zostało wykryte przynajmniej w jednym powtórzeniu którejś z prób kontrolnych, wykonaliśmy testy statystyczne, za swoiste uznając jedynie interaktanty spełniające ustalone kryteria istotności względem obu kontroli. Tym samym w podejściu ilościowym klasyfikowaliśmy interaktant jako specyficzny, o ile nie pojawiał się w żadnej z prób kontrolnych lub o ile przekształcony logarytmicznie stosunek intensywności jego sygnału w próbach eksperymentalnych względem prób kontrolnych przekraczał ustalony próg

krytyczny (*log2 intensity magnitude ratio* $\geq$ 1,5) oraz spełniał kryterium istotności statystycznej (*p-value* $\leq$ 0,01) (**Fig. 4, Artykuł nr 2**).

Przygotowany w ramach niniejszej pracy zestaw danych AP-MS pozwolił na łączną identyfikację 1596 różnych białek spośród 4391 białek proteomu referencyjnego. W pojedynczej próbie liczba identyfikacji mieściła się zwykle w zakresie 210-250, zależnie od zastosowanych warunków wzrostu hodowli bakteryjnej. W przypadku prób eksperymentalnych białko-przynęta było zawsze najobficiej reprezentowanym składnikiem, co potwierdza skuteczność zastosowanej procedury AP-MS. Pomimo różnic w natywnych poziomach ekspresji genów kodujących poszczególne białka-przynęty, ich intensywność w próbach eksperymentalnych była zbliżona (**Fig. S4, Artykuł nr 2)**. Może to wskazywać na wysycenie złóż chromatograficznych, wskutek którego część puli przynęt o wyższym natywnym poziomie w komórce pozostawała niezwiązana. Do dalszej analizy specyficzności danych metodą jakościową i ilościową włączyliśmy wyłącznie interaktanty pojawiające się w trzech powtórzeniach danej próby. Stanowiły one, w zależności od przynęty i warunków wzrostu, 10.8-42.7% wszystkich zidentyfikowanych białek (**Fig. 9, Artykuł nr 2)**.

Zestaw danych uzyskany w niniejszym eksperymencie AP-MS został udostępniony jako surowe widma MS, wyniki przeszukiwania i identyfikacji w programie MaxQuant oraz listy białek przeanalizowane pod kątem specyficzności interakcji dwoma opisanymi wyżej metodami. Aby ułatwić przegląd i wizualizację danych, przygotowałam sieci interakcji udostępnione w formie interaktywnej w repozytorium NDEX, przypisując interaktanty do 10 utworzonych przeze mnie kategorii funkcjonalnych (**Tab. 5 i Fig. 6, Artykuł nr 2**). Mimo iż podział ten jest w wielu przypadkach arbitralny (zwłaszcza w przypadku białek wielofunkcyjnych), pozwala szybko zauważyć możliwe powiązania między replikacją a innymi procesami, co tworzy punkt wyjścia do szerszych badań funkcjonalnych.

Liczba istotnie zidentyfikowanych białek w zależności od warunków wzrostu wskazuje, że najbardziej rozbudowane sieci interakcji tworzą się podczas szybkiego wzrostu bakterii. Profile ilościowe obejmują nieco węższy zestaw interakcji niż te uzyskane za pomocą analizy jakościowej, prawdopodobnie ze względu na bardziej rygorystyczne kryteria oceny istotności wyników. Co istotne, zidentyfikowane sieci interakcji są silnie zależne od warunków wzrostu. Stopień nakładania się wyników zarówno między warunkami wzrostu dla jednej przynęty (**Fig.**

10, Artykuł nr 2), jak i między poszczególnymi przynętami jest niewielki (**Fig. 11, Artykuł nr 2**). Jednocześnie powtarzalna identyfikacja stabilnych, dobrze scharakteryzowanych kompleksów we wszystkich warunkach wzrostu potwierdza wiarygodność uzyskanych wyników. Sugeruje to zatem, że białka replikacyjne *Escherichia coli* tworzą unikalne konstelacje oddziaływań, cechujące się dużą dynamiką w odpowiedzi na zmieniające się warunki środowiska.

Artykuł nr 2 stanowi przede wszystkim opis, walidację i ocenę jakości uzyskanego zestawu danych AP-MS, bez szczegółowej analizy znaczenia biologicznego uzyskanych interakcji. Niemniej jednak zdeponowane dane dotyczące zależnych od warunków wzrostu sieci interakcji białek replikacyjnych *Escherichia coli* dostarczają podstaw do dalszych badań nad ich znaczeniem. Interpretcja funkcjonalna oraz potencjalne dalsze kierunki badań zostały szerzej opisane w Artykule nr 3.

Artykuł nr 3 – *Protein interaction network analysis reveals growth conditions-specific crosstalk between chromosomal DNA replication and other cellular processes in E. coli.*

Podczas gdy Artykuł nr 2 koncentrował się na charakterystyce zestawu danych AP-MS ze szczególnym uwzględnieniem walidacji modelu eksperymentalnego i jakości uzyskanych danych, niniejsza praca rozszerza tę perspektywę, przechodząc od opisu interaktomów, przez analizę funkcjonalną, do określenia biologicznego znaczenia wybranych powiązań. Wszystkie przedstawione w niniejszej pracy analizy wyników i eksperymenty uzupełniające oparliśmy na opisanym powyżej zestawie danych opracowanych metodą ilościową.

Należy podkreślić, że wyniki uzyskane metodą AP-MS rozpatrywane są jako wskazania potencjalnych oddziaływań białkowych. Obejmują one zarówno bezpośrednie interakcje białka-przynęty, jak i powiązania pośrednie, mediowane przez inne składniki kompleksów białkowych, a także – mimo zastosowania restrykcyjnych kryteriów obróbki surowych danych – możliwe wyniki fałszywie pozytywne. Z tego względu każda zidentyfikowana w ten sposób interakcja wymaga dalszego potwierdzenia z wykorzystaniem niezależnych metod eksperymentalnych, takich jak analizy in vitro typu *pull-down* czy metody znakowania proksymalnego [50]. Dla uproszczenia narracji, w dalszej części opisu będę jednak posługiwać się terminami “oddziaływania” oraz “interakcje”.

W naszym zestawie danych potwierdziliśmy część interakcji ujętych w bazie sieci funkcjonalnych STRING (**Fig. 2, Plik S3, Artykuł nr 3**). Oprócz interakcji o wysokim powinowactwie, tworzących stabilne kompleksy w komórce (takich jak podjednostki Polimerazy III DNA, Hda-DnaN, NrdB-NrdA), zidentyfikowaliśmy także oddziaływania opisane wcześniej jako podlegające regulacji czasowo-przestrzennej w cyklu komórkowym (DnaA-DiaA, DnaB-DnaC, DnaB-DnaG, HolD-SSB, DnaB-Rep) (**Fig. 1C, Plik S3, Artykuł nr 3**) [51, 52]. Ponadto część interakcji wykrytych wcześniej w ramach analiz genetycznych znajduje potwierdzenie w naszym zestawie danych AP-MS, co dodatkowo wskazuje na potencjalne znaczenie biologiczne uzyskanego interaktomu [53, 54]. Są to między innymi pary HolD-SspA (czynnik transkrypcyjny związany z odpowiedzią ścisłą) czy NrdB-RlmE (metylotransferaza rRNA). Zdecydowana większość zidentyfikowanych w niniejszej pracy oddziaływań stanowi natomiast nowe, nieopisane dotąd powiązania z maszynerią replikacyjną, co otwiera szerokie możliwości dalszych badań nad ich znaczeniem. W kolejnej części podsumowania proponuję funkcjonalną interpretację zidentyfikowanych interakcji w świetle aktualnego stanu wiedzy oraz omawiam możliwe kierunki dalszych badań.

Stosunkowo duża część interaktomu analizowanych białek replikacyjnych to białka rybosomalne (podjednostki rybosomu oraz białka związane z translacją), jednak ich procentowy udział pomiędzy poszczególnymi przynętami jest wyraźnie zróżnicowany, a część z nich wykazuje specyficzność tylko względem określonej grupy przynęt. Największe wzbogacenie funkcjonalne tej grupy białek zaobserwowaliśmy dla SeqA oraz DnaA (**Fig. 3, Fig. 6, Artykuł nr 3**), stanowiły one odpowiednio 69 i 49% wszystkich interaktantów. Podjednostki rybosomu L16 (RplP) i L23 (RplW) są specyficzne wobec SeqA, a także helikazy i prymazy, ale nie DnaA (**Plik S4, Artykuł nr 3**). Selektywność wymienionych oddziaływań sugeruje możliwe zaangażowanie tych białek w tworzenie odrębnych kompleksów. Oprócz elementów strukturalnych rybosomu, wykryliśmy również szereg interakcji z metylotransferazami rRNA, zaangażowanymi w biogenezę podjednostki 50S [55]. Co interesujące, wspomniana wcześniej metylotransferaza RlmE została zidentyfikowana jako istotne oddziaływanie tylko w przypadku NrdB, podczas gdy interakcje z pozostałymi wykrytymi metylotransferazami (RluB, RluC, RlmN, RlmL) obserwowaliśmy powtarzalnie dla kilku przynęt (**Fig. 3, Plik S4, Artykuł nr 3**).

DnaA tworzy z kolei interakcje z syntetazami aminoacylo-tRNA (aaRS) (**Fig. 3, Fig. 6, Artykuł nr 3**), katalizującymi ATP-zależne przyłączenie aminokwasu do właściwego tRNA [56].

Na uwagę zasługuje syntetaza izoleucylo-tRNA (IleS), zidentyfikowana jedynie jako interaktant DnaA (**Plik S4, Artykuł nr 3**). Interakcja ta mogłaby umożliwiać lokalne wykorzystanie przez aaRS ATP związanego z DnaA, potencjalnie obniżając pulę DnaA-ATP w komórce. Oprócz translacji, aminoacylo-tRNA wykorzystywane są jako substraty w aminoacylacji lipidów, która modyfikuje ich sumaryczny ładunek [57]. W tym kontekście oddziaływanie aaRS z zakotwiczonym w błonie DnaA mogłoby prowadzić do neutralizacji kwaśnych fosfolipidów błonowych (m.in. fosfatydyloglicerolu), a w konsekwencji do obniżenia wydajności procesu reaktywacji DnaA [58].

W przypadku sieci interakcji dla czterech analizowanych przynęt (DnaA, DnaB, DnaG, SeqA) zaobserwowaliśmy wzbogacenie funkcjonalne w białka zaangażowane w wiązanie i procesowanie RNA (Fig. 3, Fig. 6, Artykuł nr 3). Są to m.in. komponenty degradosomu – multibiałkowego kompleksu degradującego mRNA [59]. Specyficzne oddziaływania związane z degradosomem tworzone są przez DnaB w warunkach szybkiego wzrostu (RNAzy Rne, Rnr, helikaza RhlB) oraz przez SeqA i DnaG w fazie stacjonarnej (SrmB), w której SeqA wchodzi również w interakcję z DnaG. Udowodniono, że mitochondrialny degradosom zapobiega akumulacji hybryd RNA-DNA (w tym pętli R) w genomie, a tym samym umożliwia procesywność replisomu i stabilność mitochondrialnego DNA [60]. Dzięki interakcji z helikazą degradosom *Escherichia coli* mógłby być kierowany bezpośrednio w rejon poruszających się widełek replikacyjnych, gdzie pełniłby analogiczną funkcję.

Największy udział białek zaangażowanych w procesy metaboliczne zaobserwowaliśmy w sieciach interakcji HolD – podjednostki ψ polimerazy III. Szczególnie wyróżnia się oddziaływanie z ligazą γ-glutamylocysteiny (GshA), katalizującą pierwszy etap syntezy glutationu – tripeptydu, którego główną funkcją jest utrzymanie właściwego potencjału oksydacyjno-redukcyjnego komórki [61]. Interakcję tę wykryliśmy jedynie dla HolD, wyłącznie w warunkach szybkiego wzrostu, co sugeruje jej zależność od fizjologicznego stanu komórki (**Plik S4, Fig. 3, Artykuł nr 3**). Niedawne badania metabolomiczne wskazują na rolę glutationu w kontroli rozmiaru komórki i progresji cyklu komórkowego u *Caulobacter crescentus* – poziom tego metabolitu zmienia się w czasie cyklu komórkowego, osiągając maksimum w fazie S (etap replikacji DNA), a jego niedobór prowadzi do zaburzonej dystrybucji długości komórek [62]. Oddziaływanie HolD-GshA może wskazywać zatem na bezpośrednie zaangażowanie białek replisomu w zależną od wzrostu regulację syntezy glutationu. Zgodnie z naszymi danymi HolD

tworzy także kompleks z syntetazą glutamylo-tRNA (GltX), co dodatkowo wzmacnia tę interpretację.

W uzyskanym przez nas interaktomie białek replikacyjnych obecne są także białka błonowe (głównie poryny, stanowiące istotną część sieci interakcji DnaB) oraz enzymy zaangażowane w biogenezę powłok komórkowych bakterii, obejmujących szlaki syntezy fosfolipidów błonowych, peptydoglikanu i lipopolisacharydu (LPS) w przypadku bakterii Gram-ujemnych [63]. DnaA wyizolowaliśmy z szybko rosnących komórek razem z enzymami szlaku syntezy peptydoglikanu (MurG i MrcB). W obrębie wszystkich przynęt, z wyjątkiem DnaG zaobserwowaliśmy również interakcje z białkami uczestniczącymi w syntezie lipopolisacharydu (LPS) – głównie RfaF, ale także HldE, LpxD i WecF (**Fig. 3, Fig. 9B, Artykuł nr 3**). Powiązania między regulacją replikacji DNA a metabolizmem powłok komórkowych są dobrze udokumentowane. Wykazano m.in., że białko SeqA, podobnie jak DnaA, może być wiązane przez wewnętrzną błonę komórkową [64]. Komórki *Escherichia coli* pozbawione SeqA wykazują zwiększoną fosforylację LPS, co koreluje ze zwiększoną częstością inicjacji replikacji [65]. Ponadto, mechanizmy syntezy powłok komórkowych mogą również uczestniczyć w kontroli rozmiaru komórki i związaną z tym koordynacją cyklu komórkowego [66, 67]. Oddziaływania zidentyfikowane w naszym zestawie danych mogą stanowić dodatkowe czynniki w już opisanych mechanizmach regulacyjnych lub wskazywać na nieopisane dotąd połączenia.

Aby ocenić, czy zidentyfikowane interaktanty białek replikacyjnych są funkcjonalnie zaangażowane w regulację cyklu komórkowego, zbadałam wpływ delecji wybranych genów kodujących te białka na czas inicjacji replikacji w cyklu komórkowym. Do delecji wybraliśmy geny z dwóch grup funkcjonalnych – *rlmE*, kodujący wcześniej wspomnianą metylotransferazę 23S rRNA, oddziałującą z NrdB, oraz *rfaD*, kodujący 6-epimerazę ADP-L-glicero-D-mannoheptozy, enzym zaangażowany w ostatni etap syntezy prekursora rdzenia LPS, występujący w sieciach interakcji SeqA. Produkt reakcji RfaD jest bezpośrednio wykorzystywany przez RfaF – enzym licznie występujący w interaktomie białek replikacyjnych – a ekspresja obu genów jest współregulowana, stąd przypuszczenie, że mogą one pełnić zależną od siebie funkcję w koordynacji replikacji i wzrostu komórki. Szczepy delecyjne poddałam analizie zawartości DNA w komórkach, metodą cytometrii przepływowej po zatrzymaniu replikacji (ang. *replication run-out assay*). Traktowanie aktywnie dzielących się

komórek rifampicyną i cefaleksyną blokuje odpowiednio kolejne rundy inicjacji replikacji oraz podziały komórki, umożliwiając dokończenie trwających rund replikacji. Uzyskana liczba chromosomów w komórce odzwierciedla liczbę aktywnych *origin* w momencie dodania antybiotyków. W prawidłowym przebiegu replikacji obserwuje się dwie populacje komórek (przed i po inicjacji), a liczba chromosomów w zależności od tempa wzrostu powinna wynosić 2^n [68]. Odchylenia od tej wartości (np. nieparzysta liczba chromosomów w komórce) świadczą o asynchronicznej inicjacji replikacji. Zmiany udziału populacji komórek względem szczepu referencyjnego, analizowane w funkcji rozmiaru komórki i tempa wzrostu, pozwalają z kolei określić czas inicjacji w cyklu komórkowym (ang. *initiation timing*).

Uzyskane przeze mnie wyniki wskazują, że delecje obu analizowanych genów zaburzają regulację replikacji w cyklu komórkowym. W komórkach szczepów Δ*rlmE* i Δ*rfaD* hodowanych w bogatej pożywce (szybki wzrost) zaobserwowałam populacje komórek z asynchronicznymi inicjacjami replikacji i mniejszą liczbą chromosomów niż w komórkach szczepu dzikiego dla tych samych warunków wzrostu (**Fig. 7-8, Fig. S2, Artykuł nr 3**). Podczas gdy w szczepie Δ*rfaD* wiązała się ona z nieznacznie mniejszym rozmiarem komórek i wolniejszym wzrostem, w przypadku Δ*rlmE* zależności między zawartością DNA, objętością komórek i czasem generacji były wyraźnie zaburzone **(Fig. 7, Tabela S5, Artykuł nr 3)**. W warunkach wolnego wzrostu komórek obserwowany efekt był odwrotny, – szczep pozbawionym RfaD charakteryzował się obecnością frakcji komórek z podwyższoną zawartością DNA przy dużo mniejszym rozmiarze i wolniejszym wzroście **(Fig. 8, Tabela S5, Artykuł nr 3)**, podczas gdy dla Δ*rlmE* nie stwierdziłam różnic względem szczepu typu dzikiego. Oba białka mogą zatem uczestniczyć w mechanizmach kontroli czasu replikacji w cyklu komórkowym, jednak ich udział jest zależny od warunków wzrostu, a co za tym idzie, stanu metabolicznego komórki.

Uzyskane dane AP-MS dostarczają nowych informacji o dynamice sieci interakcji białek replikacyjnych w różnych warunkach wzrostu komórek oraz o powiązaniach replikacji DNA z procesami funkcjonalnie odległymi, takimi jak biogeneza rybosomów, procesowanie RNA, czy synteza składników powłok komórkowych. Aby potwierdzić bezpośredni, fizyczny charakter zidentyfikowanych oddziaływań i dokładnie określić ich fizjologiczne znaczenie, konieczne są jednak dalsze badania, zarówno *in vivo*, jak i *in vitro*.

Artykuł nr 4 – *Bam complex associated proteins in Escherichia coli are functionally linked to peptidoglycan biosynthesis, membrane fluidity and DNA replication*

Opisane w poprzednich artykułach analizy powiązań między replikacją DNA a innymi procesami komórkowymi kierują uwagę na interakcje białek replikacyjnych z czynnikami zaangażowanymi w syntezę i homeostazę powłok komórkowych i ich możliwą rolę w koordynacji bakteryjnego cyklu komórkowego. Do tej samej grupy funkcjonalnej należy kompleks Bam (ang. *β-barrel assembly machine*), wielobiałkowy system odpowiedzialny za właściwe fałdowanie i wbudowywanie białek błonowych (ang. *outer membrane proteins*, OMP) w zewnętrzną błonę *Escherichia coli*. Składa się z transmembranowego białka BamA zlokalizowanego w błonie zewnętrznej oraz czterech lipoprotein (BamB, BamC, BamD i BamE), tworzących pierścień peryplazmatyczny. Podczas gdy BamA i BamD są niezbędne do przeżycia komórki, odgrywając kluczową rolę w fałdowaniu i integracji białek błonowych, pozostałe lipoproteiny pełnią funkcje wspomagające, które nie są do tej pory szczegółowo zbadane [69]. Wyniki dotychczasowych badań wskazują natomiast, że dodatkowe podjednostki mogą być zaangażowane również w inne procesy, potencjalnie przyczyniając się do sprzęgania różnych procesów komórkowych z biogenezą błony zewnętrznej. OMP są syntetyzowane w cytoplazmie i dzięki aktywności maszynerii sekrecyjnej podlegają transportowi do przestrzeni peryplazmatycznej, gdzie przechwytywane są przez pierścień Bam. Dodatkowa aktywność trzech białek opiekuńczych – SurA, Skp i DegP – przeciwdziała agregacji i niewłaściwemu fałdowaniu OMP [70].

W celu określenia dokładnej roli lipoprotein wspomagających, a także wzajemnych zależności między aktywnością kompleksu Bam a homeostazą błony zewnętrznej, przeprowadzono wysokoprzepustowe analizy interakcji genetycznych dla pojedynczych mutantów pozbawionych poszczególnych komponentów kompleksu. Takie podejście umożliwia identyfikację warunkowo niezbędnych genów, których delecja w tle genetycznym analizowanego mutanta daje efekt letalny (lub znaczne pogorszenie wzrostu). Możliwe jest również zbadanie w ten sposób interakcji o odwrotnej zależności, tzn. takich, w których delecja genu skutkuje poprawą przeżywalności mutantów w danych warunkach.

Delecja genu *bamB* pozwoliła na identyfikację warunkowo niezbędnych genów zaangażowanych w replikację DNA. Stwierdzono syntetyczny efekt letalny w połączeniu z

genami negatywnych regulatorów inicjacji replikacji (*hda, seqA*) oraz podjednostek polimerazy DNA III (*holC, holD*). Co istotne, zauważono, że dodatkowa delecja genu *diaA*, kodującego pozytywny regulator inicjacji replikacji, niwelowała defekt wzrostowy szczepu *ΔbamB* (**Fig. 6A-D, Artykuł nr 4**). Na tej podstawie postawiono hipotezę, że BamB może być funkcjonalnie zaangażowane w kontrolę replikacji DNA. **Celem eksperymentów przeprowadzonych przeze mnie w ramach niniejszej pracy było określenie wpływu delecji genów *bam* na regulację replikacji w cyklu komórkowym.**

Wykorzystując doświadczenie zdobyte podczas wcześniejszych badań, przeprowadziłam analizę zawartości DNA w komórkach po zatrzymaniu replikacji, metodą cytometrii przepływowej. Uzyskane przeze mnie wyniki pokazały, że delecja *bamB* istotnie skutkuje wcześniejszą inicjacją replikacji w cyklu komórkowym – zaobserwowałam nieco większą frakcję komórek po inicjacji replikacji w porównaniu do szczepu wyjściowego przy podobnym rozmiarze komórek, jak również występowanie subpopulacji o asynchronicznej inicjacji replikacji (**Fig. 6E, Artykuł nr 4**). W przypadku delecji genów kodujących pozostałe lipoproteiny wspomagające (BamC, BamE) oraz białko opiekuńcze Skp nie zaobserwowałam istotnych różnic (**Fig. S11, Artykuł nr 4**).

Co interesujące, w analizie genetycznych interakcji genów kompleksu *bam* ujawniono również syntetyczny efekt letalny w połączeniu z genami *gmhA*, *gmhB*, *hldE* i *rfaD*, których produkty uczestniczą w syntezie heptozy – prekursora rdzenia LPS (**Fig. 3, Artykuł nr 4**). Nasze badania sieci interakcji białek replikacyjnych wskazują na bezpośrednie oddziaływania tych enzymów z białkami replikacyjnymi. Ponadto delecja genu *rfaD*, podobnie jak *bamB*, zaburzała prawidłową regulację replikacji w cyklu komórkowym. Sugeruje to istnienie funkcjonalnej korelacji pomiędzy kontrolą replikacji DNA a mechanizmami utrzymującymi homeostazę zewnętrznych powłok komórkowych, w których istotnymi czynnikami są zarówno białka biogenezy OMP, jak i enzymy uczestniczące w syntezie LPS.

Artykuł nr 5 ***Interaction of the replication factor DiaA and primary metabolite sedoheptulose 7-phosphate regulates DNA replication in Escherichia coli***

Dotychczas opublikowane dane literaturowe wskazują, że drobnocząsteczkowe metabolity centralnego metabolizmu węgla mogą pośrednio wpływać na funkcjonowanie

białek replikacyjnych, m.in. poprzez znoszenie skutków punktowych mutacji w kodujących je genach, co sugeruje istnienie dodatkowego poziomu sprzężenia między metabolizmem a replikacją DNA [35]. Ponadto wykazano, że zmiany wewnątrzkomórkowego przepływu metabolitów mogą być wykorzytsywane przez komórkę do regulacji jej stanu fizjologicznego [71]. Na tej podstawie postawiliśmy hipotezę, że metabolity mogą również bezpośrednio oddziaływać z białkami replikacyjnymi i modulować ich funkcję w zależności od stanu metabolicznego komórki.

DiaA zostało opisane w literaturze jako białko regulatorowe inicjacji replikacji pełniące podwójną funkcję. Z jednej strony stymuluje ono oligomeryzację DnaA-ATP i jego wiązanie do rejonów *oriC* o słabszym powinowactwie oraz ułatwia rozplatanie dupleksu [72, 73]. Z drugiej – konkuruje z helikazą DnaB o wiązanie do DnaA, co oznacza, że rekrutacja helikazy wymaga uprzedniego odłączenia się DiaA od białka inicjatorowego [74]. Ta negatywna regulacja ładowania helikazy może stanowić mechanizm precyzyjnej kontroli przejścia z etapu formowania kompleksu pre-replikacyjnego do utworzenia replisomu w cyklu komórkowym. Wciąż jednak nie ustalono, w jaki sposób w komórkach *Escherichia coli* dochodzi do wymiany DiaA na DnaB ani czy proces ten wymaga udziału dodatkowego czynnika regulacyjnego.

Struktura krystaliczna DiaA ujawniła obecność konserwowanej domeny izomerazy cukrowej SIS (ang. *sugar isomerase domain*) [73]. Przypomina ona tę samą domenę występującą w GmhA, enzymie zaangażowanym w izomeryzację sedoheptulozo-7-fosforanu (S7P) do D-glycero-D-manno-heptozo-7-fosforanu (M7P) w pierwszy etapie wspomnianego już wcześniej szlaku syntezy heptozy – kluczowego prekursora rdzenia LPS. Analiza dotychczas zdeponowanych struktur wskazuje, że GmhA przyjmuje dwie konformacje, określane jako otwarta i zamknięta. Obserwowana zmienność konformacyjna może odzwierciedlać różnice w stanie wiązania fosfocukru (S7P lub M7P) lub stanowić cechę charakterystyczną GmhA poszczególnych gatunków bakterii [75]. Podobieństwo domeny SIS DiaA do domeny GmhA nasuwa pytanie o jej możliwą rolę w regulacji replikacji DNA i funkcjonalne powiązanie DiaA z metabolizmem fosfocukrów. **Celem niniejszej pracy było ustalenie, czy DiaA może oddziaływać z S7P i czy potencjalna interakcja wpływa na jego aktywność w inicjacji replikacji *Escherichia coli*.** Zastosowaliśmy podejście *in vitro*, analizując wpływ punktowych substytucji w domenie SIS na zdolność DiaA do wiązania S7P, ewentualną aktywność izomerazową, a także oligomeryzację i interakcję z DnaA. Ponadto w badaniach *in vivo*

oceniliśmy, jak mutacje w genie *diaA* oraz obniżenie wewnątrzkomórkowego poziomu S7P w komórce wpływają na parametry inicjacji replikacji w cyklu komórkowym.

Geny *gmhA* i *diaA* zostały sklonowane do wektora ekspresyjnego pET28, umożliwiającego ekspresję N-terminalnych fuzji ze znacznikiem His-SUMO w bakteryjnym systemie T7, a nadprodukcja i izolacja pozwoliła uzyskać preparaty o wysokiej czystości. Następnie oceniliśmy oddziaływanie obu białek ze znakowanym radioaktywnie S7P *in vitro* metodą EMSA (ang. *electrophoretic mobility shift assay*). W obu przypadkach zaobserwowaliśmy sygnał odpowiadający kompleksom białko-S7P (**Fig. 2A, Artykuł nr 5**). Analiza podobieństwa strukturalnego domeny SIS obu białek pozwoliła wybrać reszty aminokwasowe, których zmiana mogłaby upośledzić wiązanie fosfocukru przez DiaA lub przeciwnie – nadać DiaA właściwości izomerazy GmhA (**Fig. 1, Artykuł nr 5**). Jednakże spośród kilkunastu skonstruowanych wariantów DiaA z pojedynczymi lub wielokrotnymi substytucjami w obrębie domeny SIS, tylko jeden (N180E) wykazywał upośledzenie wiązania S7P. Zauważyliśmy ponadto, że część wprowadzonych mutacji (np. N65E) destabilizuje tetramery DiaA, prowadząc do powstania dimerów, które jednak zachowują zdolność wiązania S7P (**Fig. 2B-C, Artykuł nr 5**).

Aby ocenić wpływ wiązania S7P przez DiaA na regulację replikacji w cyklu komórkowym, wprowadziliśmy punktowe mutacje do chromosomalnego locus *diaA* i przeanalizowaliśmy czas inicjacji replikacji w cyklu komórkowym. Zaobserwowałam, że szczepy z punktowymi mutacjami zaburzającymi wiązanie S7P lub tetrameryzację DiaA wykazują fenotyp zbliżony do szczepu Δ*diaA* (**Fig. 3, Artykuł nr 5**). Co istotne, dodatkowa analiza stanu oligomerycznego białek *in vitro* pozwala stwierdzić, że wariant N180E przynajmniej częściowo zachowuje zdolność do tetrameryzacji (**Fig. S1, Artykuł nr 5**) oraz wiązania DnaA (**Fig. 4, Artykuł nr 5**), co pozwala stwierdzić, że obserwowany efekt może być związany z brakiem interakcji DiaA-S7P w komórce.

Uzyskane wyniki pozwalały przypuszczać, że S7P może uczestniczyć w mechanizmie regulowania aktywności DiaA. Dlatego też kolejnym etapem było sprawdzenie, czy zmiana wewnątrzkomórkowego poziomu tego metabolitu w komórce również miałaby wpływ na parametry inicjacji replikacji w cyklu komórkowym. W tym celu zbadałam szczep pozbawiony transketolazy TktA – enzymu produkującego S7P w szlaku pentozofosforanowym

[76]. W warunkach szybkiego wzrostu komórek komórki szczepu Δ*tktA* charakteryzowały się nieznacznie wolniejszym wzrostem i mniejszym rozmiarem komórki. Udział populacji komórek po inicjacji replikacji (o większej zawartości DNA) był jednak podwyższony, co sugeruje, że inicjacja replikacji w cyklu komórkowym zachodzi wcześniej w porównaniu do szczepu typu dzikiego (**Fig. 5, Artykuł nr 5**).

Aby ocenić możliwy wpływ interakcji z S7P na funkcję DiaA w inicjacji replikacji, przeprowadziłam analizę wiązania DnaA do regionu *oriC* metodą EMSA, w obecności DiaA oraz kompleksu DiaA-S7P. Zgodnie z oczekiwaniami, DiaA promowało wiązanie i oligomeryzację DnaA w obrębie sekwencji o niższym powinowactwie, czego przejawem było pojawienie się wolniej migrującego kompleksu o wyższej masie. Preinkubacja DiaA z S7P znosiła ten efekt, co sugeruje, że wiązanie metabolitu osłabia zdolność DiaA do stymulowania oligomeryzacji DnaA na DNA (**Fig. 6, Artykuł nr 5**).

Wyniki uzyskane w niniejszej pracy wskazują, że w kontroli inicjacji replikacji uczestniczą nie tylko białka metaboliczne, ale także drobnocząsteczkowe metabolity. S7P służy prawdopodobnie jako negatywny modulator aktywności białka DiaA. Uprzednio związane z S7P białko traci bowiem zdolność stymulowania oligomeryzacji DnaA-ATP w rejonie *oriC*. Konsekwentnie, szczep pozbawiony enzymu dostarczającego S7P cechuje się wcześniejszą inicjacją replikacji w cyklu komórkowym, która może wynikać z niższej podaży metabolitu i braku hamującego efektu na aktywność DiaA. Co istotne, wyniki te stanowią kolejny dowód na możliwe zaangażowanie szlaków syntezy powłok komórkowych w mechanizmy koordynacji replikacji. S7P mogłoby pełnić rolę sygnałową, przekazującą informacje o przyroście rozmiaru komórki i tempie syntezy nukleotydów bezpośrednio do aparatu replikacyjnego. DiaA i GmhA wydają się pochodzić od tego samego białkowego przodka, z którego wyewoluowały dwa białka o odrębnych funkcjach, jednak z zachowaną zdolnością wiązania fosfocukrów. W niektórych gatunkach bakterii, np. *Pseudomonas aeruginosa*, nie zidentyfikowano białka regulatorowego o analogicznej do DiaA funkcji. Białko GmhA tej bakterii zawiera jednak aminokwasy odpowiadające kluczowym resztom dla formowania kompleksu DiaA-DnaA w *Escherichia coli*, co sugeruje, że izomeraza S7P może częściowo pełnić funkcje regulacyjne w inicjacji replikacji [73, 75]. Stanowi to niezwykle interesujący kierunek dalszych badań, tym bardziej, że dokładny mechanizm molekularny stojący za oddziaływaniem DiaA-S7P i jego biologicznym znaczeniem pozostaje nie w pełni wyjaśniony.

Wnioski i dyskusja

W ramach niniejszej rozprawy doktorskiej prowadziłam badania nad powiązaniami replikacji *Escherichia coli* i innych procesów zachodzących w komórce bakteryjnej ze szczególnym naciskiem na szeroko pojęty metabolizm komórki. Realizując cel pracy, skupiłam się przede wszystkim na podejściu proteomicznym, badając dynamikę interakcji białko-białko głównych białek replikacyjnych w zależności od warunków wzrostu komórek (**Artykuł nr 2, Artykuł nr 3**) W ramach potwierdzenia biologicznego znaczenia interakcji zidentyfikowanych w moich badaniach, a także w badaniach interakcji genetycznych wykonanych we współpracy, oceniłam efekt delecji genów kodujących potencjalne interaktanty na regulację replikacji DNA w cyklu komórkowym. (**Artykuł nr 3, Artykuł nr 4**). Dodatkowo w pracy opisałam interakcję białka DiaA z drobnocząsteczkowym metabolitem S7P i za pomocą analiz biochemicznych oraz eksperymentów *in vivo* scharakteryzowałam możliwą rolę tej interakcji w regulacji replikacji *Escherichia coli* (**Artykuł nr 5**). Poniżej skrótowo przedstawiam najważniejsze tezy i wnioski mojej rozprawy doktorskiej:

1. **Profile interakcji białek replikacyjnych *Escherichia coli* różnią się znacząco w zależności od warunków wzrostu komórek i użytego białka-przynęty.**

   Głównym rezultatem niniejszej pracy są dane proteomiczne uzyskane za pomocą AP-MS. Złożona walidacja techniczna potwierdza ich jakość i wiarygodność. Zdeponowany zestaw danych może stanowić podstawę do dalszej interpretacji funkcjonalnej lub ponownej analizy z użyciem alternatywnych strategii. Dobór odpowiednich prób kontrolnych oraz kryteriów analizy jest kluczowy dla ostatecznych wyników, co potwierdza różna ilość specyficznych interaktantów uzyskana w ramach podejścia jakościowego lub ilościowego. Większa restrykcyjność zwiększa specyficzność, ale też ryzyko pominięcia istotnych biologicznie interakcji.

2. **W interaktomie białek replikacyjnych widoczne jest wzbogacenie w białka reprezentujące różne procesy komórkowe.**

Zidentyfikowane interaktanty obejmują białka zaangażowane m.in. w biogenezę rybosomów, obróbkę RNA oraz metabolizm, ze szczególnym uwzględnieniem szlaków syntezy nukleotydów oraz powłok komórkowych, zwłaszcza komponentów LPS. Powiązania białek replikacyjnych z tymi procesami przyjmują różne formy – od pojedynczych, izolowanych interakcji (np. DnaA-IleS, HolD-GshA, NrdB-RlmE), przez zespoły białek oddziałujących z jedną przynętą lub grupą przynęt (np. DnaB-składniki degradosomu, SeqA-białka podjednostek rybosomu), aż po interaktanty tej samej grupy funkcjonalnej rozproszone w całym interaktomie (interakcje białek replikacyjnych z RfaF i innymi enzymami syntezy LPS). Zróżnicowanie wzorców oddziaływań sugeruje wielopoziomową molekularną komunikację replikacji z innymi aspektami fizjologii komórki.

3. **Delecja genów potencjalnie zaangażowanych w interakcje z maszynerią replikacyjną wpływa na regulację replikacji w cyklu komórkowym.**

Analiza zawartości chromosomów po zatrzymaniu replikacji wykazała, że pozbawienie komórki wybranych białek potencjalnie oddziałujących z aparatem replikacyjnym wpływa zarówno na czas inicjacji replikacji w cyklu komórkowym, jak i na jej synchroniczność. Efekt ten w analizowanych przeze mnie przypadkach był zależny od tempa wzrostu komórek – zaburzenia w szczepie Δ*rlmE* obserwowałam jedynie w warunkach szybkiego wzrostu, podczas gdy dla szczepu Δ*rfaD* były one wyraźniejsze w warunkach wolnego wzrostu. Deregulację inicjacji replikacji w szybko dzielących się komórkach wykazałam również w szczepie z delecją genu *bamB*. Obserwowane zmiany w kontroli replikacji DNA w cyklu komórkowym mogą wynikać z bezpośredniej utraty istotnej interakcji, ale nie można też wykluczyć, że odzwierciedlają one również wtórne zmiany w ekspresji wspólnie regulowanych genów lub w funkcjonowaniu białek zależnych od usuniętego czynnika. Dlatego też dla pełnego potwierdzenia wpływu delecji analizowanych genów należałoby wykonać testy komplementacji.

4. **Interakcja z drobnocząsteczkowym metabolitem S7P może modulować aktywność białka DiaA w komórce w sposób zależny od wewnątrzkomórkowego poziomu metabolitu.**

DiaA wiąże S7P *in vitro*, a interakcja ta osłabia jego zdolność do promowania tworzenia kompleksu DnaA-oriC. Zarówno zaburzenie oddziaływania DiaA-S7P, jak i obniżenie poziomu metabolitu w komórce prowadzą do zmian czasu inicjacji replikacji w cyklu komórkowym. Wyniki te wskazują, że drobnocząsteczkowe metabolity mogą bezpośrednio kontaktować się z białkami replikacyjnymi i pełnić funkcje sygnałowe. S7P jest metabolitem pośrednim szlaku pentozofosforanowego, prekursorem syntezy zarówno LPS, jak i nukleotydów, co wskazuje na wzajemne zależności funkcjonalne tych procesów z kontrolą replikacji DNA. Niestety, większość reszt aminokwasowych zaangażowanych w wiązanie S7P przez DiaA wpływa również na właściwą oligomeryzację białka, co utrudnia jednoznaczne rozdzielenie obserwowanych efektów. Wyjaśnienie dokładnego mechanizmu, poprzez który interakcja DiaA z S7P moduluje regulację replikacji, wymaga dalszych badań.

Sieci interakcji białek replikacyjnych *Escherchia coli* są bardzo rozległe – każde z nich tworzy odrębne oddziaływania, podlegające dynamicznym zmianom w zależności od warunków wzrostu komórek. Uzyskane w ramach niniejszej rozprawy doktorskiej wyniki poszerzają znacząco zakres dotychczas opisanych procesów, które mogą brać udział w koordynacji cyklu komórkowego bakterii w odpowiedzi na zróżnicowane warunki środowiska.

Chociaż od opublikowania klasycznego modelu Coopera i Helmstettera minęło niemal 60 lat, problem koordynacji replikacji DNA ze wzrostem komórki bakteryjnej pozostaje nadal przedmiotem aktywnych badań i dyskusji. W ostatnim czasie obserwuje się powrót zainteresowania koncepcją czynnika wyzwalającego inicjację replikacji – opublikowano kilka modeli opartych na wykrywaniu liczby kopii białka inicjatorowego DnaA w warunkach zbalansowanej biosyntezy białek [77, 78, 79]. Nowe podejścia wskazują, że inicjacja replikacji nie jest wyzwalana w sposób zależny od całkowitego poziomu DnaA w komórce, ale od dynamicznej regulacji stosunku aktywnego inicjacyjnie DnaA-ATP do DnaA-ADP. Wyczuwana przez komórkę liczba kopii DnaA-ATP oscyluje w cyklu komórkowym, przy czym może być szybko dostosowana do tempa wzrostu i liczby aktywnych widełek replikacyjnych

dzięki rezerwuarowi DnaA-ADP [77, 80]. Taka forma kontroli replikacji w cyklu komórkowym pozwala również częściowo wyjaśnić, dlaczego sztuczna manipulacja poziomem DnaA w komórce nie koreluje jednoznacznie z czasem inicjacji replikacji w cyklu komórkowym oraz masą inicjacyjną komórki [24, 25].

W powyższym świetle wyniki danych AP-MS uzyskane w niniejszej pracy mogą przyczynić się do zrozumienia, w jaki sposób informacja o warunkach wzrostu komórki jest przekazywana bezpośrednio do aparatu inicjacyjnego. Co istotne, zidentyfikowane dotychczas systemy promujące hydrolizę DnaA-ATP (RIDA, DDAH) oraz konwersję DnaA-ADP do DnaA-ATP (DARS, regeneracja z udziałem fosfolipidów błonowych) nie są niezbędne do przeżycia komórki. Jednoczesne upośledzenie wszystkich tych mechanizmów nie zaburza w znaczący sposób progresji cyklu komórkowego w warunkach wolnego wzrostu, prowadząc do perturbacji dopiero w warunkach nakładających się cykli replikacyjnych [81, 25]. Obserwacje te wskazują, że mechanizmy zapewniające dynamiczną zmianę stosunku DnaA-ATP/DnaA-ADP stanowią ewolucyjne przystosowanie do szybkiego wzrostu. Zarówno w oscylację poziomu dostępnego DnaA-ATP w cyklu komórkowym, jak i wyczuwanie liczby kopii aktywnej formy inicjatora, zaangażowane mogą być alternatywne, komplementarne mechanizmy, a białka zidentyfikowane w sieciach interakcji uzyskanych w niniejszej pracy mogą stanowić ich komponenty.

Istnienie wielu mechanizmów regulacyjnych aktywowanych w danych warunkach wzrostu komórki jest również spójne z koncepcją alokacji proteomu, zgodnie z którą komórki bakteryjne globalnie dostosowują jego skład do tempa wzrostu i dostępności zasobów. Szybki wzrost przesuwa równowagę proteomu w stronę białek rybosomalnych i translacyjnych, natomiast w warunkach wolnego wzrostu zwiększa się udział białek metabolicznych, przy czym zasada ta wydaje się być szeroko konserwowana ewolucyjnie [82, 83]. W tym ujęciu regulacja replikacji może być postrzegana jako element szerszej strategii optymalizacji wykorzystania zasobów komórkowych. Identyfikacja potencjalnych oddziaływań aparatu replikacyjnego z podjednostkami rybosomu oraz aaRS może odzwierciedlać taki zależny od wzrostu tryb regulacji.

Spośród znanych mechanizmów regulujących poziom DnaA-ATP/DnaA-ADP w komórkach Escherichia coli szczególną rolę przypisuje się systemowi RIDA, który – mimo że molekularnie ukierunkowany na negatywną kontrolę inicjacji – jest bezpośrednio zależny

od aktywnych widełek replikacyjnych, a zatem od etapu elongacji [25]. Coraz więcej danych wskazuje, że elongacja replikacji może być celem mechanizmów sprzęgających replikację ze stanem metabolicznym komórki. Wykazano, że tempo progresji widełek replikacyjnych nie jest stałe w trakcie cyklu komórkowego, lecz zależy od liczby aktywnych replisomów oraz dostępności nukleotydów [84]. Manipulacja wewnątrzkomórkowym poziomem dNTP wpływa bezpośrednio na tempo elongacji, co sugeruje rolę aktywności reduktazy rybonukleotydowej w kontroli replikacji DNA [12, 84]. Sporządzone w niniejszej pracy sieci interakcji podjednostki β reduktazy rybonukleotydowej (szczególnie interesująca interakcja NrdB-RlmE) dostarczają nowych przesłanek dotyczących potencjalnych mechanizmów takiej kontroli. Ponadto zidentyfikowane możliwe oddziaływania podjednostki ψ polimerazy DNA III z białkami metabolicznymi, zwłaszcza z enzymami zaangażowanymi w biosyntezę prekursorów nukleotydów, wskazują na liczne punkty styczne pomiędzy elongacją replikacji a metabolizmem nukleotydów. Obserwacje te poszerzają klasyczne, skoncentrowane na inicjacji ujęcie regulacji replikacji, sugerując, że ważnym elementem kontroli cyklu komórkowego jest również modulacja elongacji w odpowiedzi na zmieniający się stan metaboliczny komórki.

Podsumowując, wyniki przedstawione w niniejszej pracy, osadzone w kontekście aktualnych modeli teoretycznych i danych literaturowych, wspierają ujęcie kontroli bakteryjnego cyklu komórkowego jako wielowarstwowego systemu, w którym poszczególne mechanizmy wzajemnie się uzupełniają. Koordynacja replikacji DNA ze wzrostem komórki opiera się na dynamicznej regulacji aktywności białka inicjatorowego, globalnej alokacji zasobów proteomicznych zależnej od tempa wzrostu, kontroli progresji elongacji replikacji oraz sprzężeniu tych procesów z metabolizmem. Tak szeroko zintegrowana architektura regulacyjna stanowi efektywne rozwiązanie ewolucyjne, umożliwiające szybką adaptację do zmiennych warunków środowiska. Wyniki uzyskane w niniejszej rozprawie doktorskiej wskazują na dotychczas nieopisane poziomy tej integracji, otwierając nowe perspektywy badań nad regulacją replikacji DNA u bakterii w kontekście biologii systemowej.

Wykaz skrótów

DOR – *DnaA-oligomerization region*

DUE – *duplex unwinding element*

CLC – *clamp-loader complex*

RIDA – *Regulatory Inactivation of DnaA*

DDAH – *datA-dependent DnaA-ATP hydrolysis*

DARS – *DnaA reactivating sequences*

S7P – sedoheptulozo-7-fosforan

AP-MS – *affinity purification coupled with mass spectrometry*

SPA – *sequential purification affinity tag*

CBP – *calmodulin binding protein*

TEV –*tobacco etch virus protease*

LC-MS/MS – *liquid chromatography-tandem mass spectrometry*

aaRS – *aminoacyl-tRNA synthetase*

LPS – lipopolisacharyd

OMP – *outer membrane proteins*

SIS – *sugar isomerase domain*

M7P – D-glicero-D-manno-heptozo-7-fosforan

EMSA – *electrophoretic mobility shift assay*

Literatura

[1] Dewachter L, Verstraeten N, Fauvart M, Michiels J. An integrative view of cell cycle control in Escherichia coli. FEMS Microbiol Rev. 2018 Mar 1;42(2):116-136. doi: 10.1093/femsre/fuy005. PMID: 29365084.

[2] Meunier A, Govers SK. Cell cycle regulation in Escherichia coli: from governing principles, checkpoints, and control variables to molecular mechanisms. Curr Opin Microbiol. 2025 Aug;86:102616. doi: 10.1016/j.mib.2025.102616. Epub 2025 Jun 7. PMID: 40483873.

[3] Łazowski K, Woodgate R, Fijalkowska IJ. Escherichia coli DNA replication: the old model organism still holds many surprises. FEMS Microbiol Rev. 2024 Jun 20;48(4):fuae018. doi: 10.1093/femsre/fuae018. PMID: 38982189; PMCID: PMC11253446.

[4] Katayama T. Initiation of DNA Replication at the Chromosomal Origin of E. coli, oriC. Adv Exp Med Biol. 2017;1042:79-98. doi: 10.1007/978-981-10-6955-0_4. PMID: 29357054.

[5] Kasho K, Ozaki S, Katayama T. IHF and Fis as *Escherichia coli* Cell Cycle Regulators: Activation of the Replication Origin *oriC* and the Regulatory Cycle of the DnaA Initiator. Int J Mol Sci. 2023 Jul 18;24(14):11572. doi: 10.3390/ijms241411572. PMID: 37511331; PMCID: PMC10380432.

[6] Liu B, Eliason WK, Steitz TA. Structure of a helicase-helicase loader complex reveals insights into the mechanism of bacterial primosome assembly. Nat Commun. 2013;4:2495. doi: 10.1038/ncomms3495. PMID: 24048025; PMCID: PMC3791466.

[7] Oakley AJ. A structural view of bacterial DNA replication. Protein Sci. 2019 Jun;28(6):990-1004. doi: 10.1002/pro.3615. Epub 2019 Apr 17. PMID: 30945375; PMCID: PMC6511741.

[8] Xu ZQ, Dixon NE. Bacterial replisomes. Curr Opin Struct Biol. 2018 Dec;53:159-168. doi: 10.1016/j.sbi.2018.09.006. Epub 2018 Oct 4. PMID: 30292863.

[9] Chen PJ, McMullin AB, Visser BJ, Mei Q, Rosenberg SM, Bates D. Interdependent progression of bidirectional sister replisomes in *E. coli*. Elife. 2023 Jan 9;12:e82241. doi: 10.7554/eLife.82241. PMID: 36621919; PMCID: PMC9859026.

[10] Gras K, Fange D, Elf J. The Escherichia coli chromosome moves to the replisome. Nat Commun. 2024 Jul 17;15(1):6018. doi: 10.1038/s41467-024-50047-z. PMID: 39019870; PMCID: PMC11255300.

[11] Herrick J, Sclavi B. Ribonucleotide reductase and the regulation of DNA replication: an old story and an ancient heritage. Mol Microbiol. 2007 Jan;63(1):22-34. doi: 10.1111/j.1365-2958.2006.05493.x. PMID: 17229208.

[12] Sánchez-Romero MA, Molina F, Jiménez-Sánchez A. Organization of ribonucleoside diphosphate reductase during multifork chromosome replication in Escherichia coli. Microbiology (Reading). 2011 Aug;157(Pt 8):2220-2225. doi: 10.1099/mic.0.049478-0. Epub 2011 Jun 9. PMID: 21659325.

[13] Skarstad K, Katayama T. Regulating DNA replication in bacteria. Cold Spring Harb Perspect Biol. 2013 Apr 1;5(4):a012922. doi: 10.1101/cshperspect.a012922. PMID: 23471435; PMCID: PMC3683904.

[14] Katayama T, Kasho K, Kawakami H. The DnaA Cycle in *Escherichia coli*: Activation, Function and Inactivation of the Initiator Protein. Front Microbiol. 2017 Dec 21;8:2496. doi: 10.3389/fmicb.2017.02496. PMID: 29312202; PMCID: PMC5742627.

[15] Saxena R, Fingland N, Patil D, Sharma AK, Crooke E. Crosstalk between DnaA protein, the initiator of Escherichia coli chromosomal replication, and acidic phospholipids present in bacterial membranes. Int J Mol Sci. 2013 Apr 17;14(4):8517-37. doi: 10.3390/ijms14048517. PMID: 23595001; PMCID: PMC3645759.

[16] Waldminghaus T, Skarstad K. The Escherichia coli SeqA protein. Plasmid. 2009 May;61(3):141-50. doi: 10.1016/j.plasmid.2009.02.004. Epub 2009 Feb 28. PMID: 19254745.

[17] Løbner-Olesen A, Skovgaard O, Marinus MG. Dam methylation: coordinating cellular processes. Curr Opin Microbiol. 2005 Apr;8(2):154-60. doi: 10.1016/j.mib.2005.02.009. PMID: 15802246.

[18] Donczew R, Zakrzewska-Czerwińska J, Zawilak-Pawlik A. Beyond DnaA: the role of DNA topology and DNA methylation in bacterial replication initiation. J Mol Biol. 2014 Jun 12;426(12):2269-82. doi: 10.1016/j.jmb.2014.04.009. Epub 2014 Apr 18. PMID: 24747048.

[19] Dame RT, Kalmykowa OJ, Grainger DC. Chromosomal macrodomains and associated proteins: implications for DNA organization and replication in gram negative bacteria. PLoS Genet. 2011 Jun;7(6):e1002123. doi: 10.1371/journal.pgen.1002123. Epub 2011 Jun 16. PMID: 21698131; PMCID: PMC3116907.

[20] Schaechter M, Maaloe O, Kjeldgaard NO. Dependency on medium and temperature of cell size and chemical composition during balanced grown of Salmonella typhimurium. J Gen Microbiol. 1958 Dec;19(3):592-606. doi: 10.1099/00221287-19-3-592. PMID: 13611202.

[21] Cooper S, Helmstetter CE. Chromosome replication and the division cycle of Escherichia coli B/r. J Mol Biol. 1968 Feb 14;31(3):519-40. doi: 10.1016/0022-2836(68)90425-7. PMID: 4866337.

[22] Donachie WD. Relationship between cell size and time of initiation of DNA replication. Nature. 1968 Sep 7;219(5158):1077-9. doi: 10.1038/2191077a0. PMID: 4876941.

[23] Levin PA, Taheri-Araghi S. One is Nothing without the Other: Theoretical and Empirical Analysis of Cell Growth and Cell Cycle Progression. J Mol Biol. 2019 May 17;431(11):2061-2067. doi: 10.1016/j.jmb.2019.04.004. Epub 2019 Apr 24. PMID: 31026450; PMCID: PMC6800662.

[24] Flåtten I, Fossum-Raunehaug S, Taipale R, Martinsen S, Skarstad K. The DnaA Protein Is Not the Limiting Factor for Initiation of Replication in Escherichia coli. PLoS Genet. 2015 Jun 5;11(6):e1005276. doi: 10.1371/journal.pgen.1005276. PMID: 26047361; PMCID: PMC4457925.

[25] Knöppel A, Broström O, Gras K, Elf J, Fange D. Regulatory elements coordinating initiation of chromosome replication to the *Escherichia coli* cell cycle. Proc Natl Acad Sci U S A. 2023 May 30;120(22):e2213795120. doi: 10.1073/pnas.2213795120. Epub 2023 May 23. PMID: 37220276; PMCID: PMC10235992.

[26] Campos M, Surovtsev IV, Kato S, Paintdakhi A, Beltran B, Ebmeier SE, Jacobs-Wagner C. A constant size extension drives bacterial cell size homeostasis. Cell. 2014 Dec 4;159(6):1433-46. doi: 10.1016/j.cell.2014.11.022. PMID: 25480302; PMCID: PMC4258233.

[27] Taheri-Araghi S, Bradde S, Sauls JT, Hill NS, Levin PA, Paulsson J, Vergassola M, Jun S. Cell-size control and homeostasis in bacteria. Curr Biol. 2015 Feb 2;25(3):385-391. doi:

10.1016/j.cub.2014.12.009. Epub 2014 Dec 24. Erratum in: Curr Biol. 2017 May 8;27(9):1392. doi: 10.1016/j.cub.2017.04.028. PMID: 25544609; PMCID: PMC4323405.

[28] Micali G, Grilli J, Osella M, Cosentino Lagomarsino M. Concurrent processes set *E. coli* cell division. Sci Adv. 2018 Nov 7;4(11):eaau3324. doi: 10.1126/sciadv.aau3324. PMID: 30417095; PMCID: PMC6224021.

[29] Si F, Le Treut G, Sauls JT, Vadia S, Levin PA, Jun S. Mechanistic Origin of Cell-Size Control and Homeostasis in Bacteria. Curr Biol. 2019 Jun 3;29(11):1760-1770.e7. doi: 10.1016/j.cub.2019.04.062. Epub 2019 May 16. PMID: 31104932; PMCID: PMC6548602.

[30] Le Treut G, Si F, Li D, Jun S. Quantitative Examination of Five Stochastic Cell-Cycle and Cell-Size Control Models for *Escherichia coli* and *Bacillus subtilis*. Front Microbiol. 2021 Oct 26;12:721899. doi: 10.3389/fmicb.2021.721899. PMID: 34795646; PMCID: PMC8594374.

[31] Soultanas P, Janniere L. The metabolic control of DNA replication: mechanism and function. Open Biol. 2023 Aug;13(8):230220. doi: 10.1098/rsob.230220. Epub 2023 Aug 16. PMID: 37582405; PMCID: PMC10427196.

[32] Jannière L, Canceill D, Suski C, Kanga S, Dalmais B, Lestini R, Monnier AF, Chapuis J, Bolotin A, Titok M, Le Chatelier E, Ehrlich SD. Genetic evidence for a link between glycolysis and DNA replication. PLoS One. 2007 May 16;2(5):e447. doi: 10.1371/journal.pone.0000447. PMID: 17505547; PMCID: PMC1866360.

[33] Maciąg M, Nowicki D, Janniere L, Szalewska-Pałasz A, Węgrzyn G. Genetic response to metabolic fluctuations: correlation between central carbon metabolism and DNA replication in Escherichia coli. Microb Cell Fact. 2011 Mar 31;10:19. doi: 10.1186/1475-2859-10-19. PMID: 21453533; PMCID: PMC3080795.

[34] Tymecka-Mulik J, Boss L, Maciąg-Dorszyńska M, Matias Rodrigues JF, Gaffke L, Wosinski A, Cech GM, Szalewska-Pałasz A, Węgrzyn G, Glinkowska M. Suppression of the Escherichia coli dnaA46 mutation by changes in the activities of the pyruvate-acetate node links DNA replication regulation to central carbon metabolism. PLoS One. 2017 Apr 27;12(4):e0176050. doi: 10.1371/journal.pone.0176050. PMID: 28448512; PMCID: PMC5407757.

[35] Krause K, Maciąg-Dorszyńska M, Wosinski A, Gaffke L, Morcinek-Orłowska J, Rintz E, Bielańska P, Szalewska-Pałasz A, Muskhelishvili G, Węgrzyn G. The Role of Metabolites in the

Link between DNA Replication and Central Carbon Metabolism in *Escherichia coli*. Genes (Basel). 2020 Apr 19;11(4):447. doi: 10.3390/genes11040447. PMID: 32325866; PMCID: PMC7231150.

[36] Murray H, Koh A. Multiple regulatory systems coordinate DNA replication with cell growth in Bacillus subtilis. PLoS Genet. 2014 Oct 23;10(10):e1004731. doi: 10.1371/journal.pgen.1004731. PMID: 25340815; PMCID: PMC4207641.

[37] Typas A, Sourjik V. Bacterial protein networks: properties and functions. Nat Rev Microbiol. 2015 Sep;13(9):559-72. doi: 10.1038/nrmicro3508. Epub 2015 Aug 10. PMID: 26256789.

[38] Meng, X., Li, W., Peng, X. et al. Protein interaction networks: centrality, modularity, dynamics, and applications. Front. Comput. Sci. 15, 156902 (2021). https://doi.org/10.1007/s11704-020-8179-0

[39] Lin CY, Lee TL, Chiu YY, Lin YW, Lo YS, Lin CT, Yang JM. Module organization and variance in protein-protein interaction networks. Sci Rep. 2015 Mar 23;5:9386. doi: 10.1038/srep09386. PMID: 25797237; PMCID: PMC4369690.

[40] Dunham WH, Mullin M, Gingras AC. Affinity-purification coupled to mass spectrometry: basic principles and strategies. Proteomics. 2012 May;12(10):1576-90. doi: 10.1002/pmic.201100523. PMID: 22611051.

[41] Butland G, Peregrín-Alvarez JM, Li J, Yang W, Yang X, Canadien V, Starostine A, Richards D, Beattie B, Krogan N, Davey M, Parkinson J, Greenblatt J, Emili A. Interaction network containing conserved and essential protein complexes in Escherichia coli. Nature. 2005 Feb 3;433(7025):531-7. doi: 10.1038/nature03239. PMID: 15690043.

[42] Hu P, Janga SC, Babu M, Díaz-Mejía JJ, Butland G, Yang W, Pogoutse O, Guo X, Phanse S, Wong P, Chandran S, Christopoulos C, Nazarians-Armavil A, Nasseri NK, Musso G, Ali M, Nazemof N, Eroukova V, Golshani A, Paccanaro A, Greenblatt JF, Moreno-Hagelsieb G, Emili A. Global functional atlas of Escherichia coli encompassing previously uncharacterized proteins. PLoS Biol. 2009 Apr 28;7(4):e96. doi: 10.1371/journal.pbio.1000096. PMID: 19402753; PMCID: PMC2672614.

[43] Babu M, Díaz-Mejía JJ, Vlasblom J, Gagarinova A, Phanse S, Graham C, Yousif F, Ding H, Xiong X, Nazarians-Armavil A, Alamgir M, Ali M, Pogoutse O, Pe'er A, Arnold R, Michaut M, Parkinson J, Golshani A, Whitfield C, Wodak SJ, Moreno-Hagelsieb G, Greenblatt JF, Emili A. Genetic interaction maps in Escherichia coli reveal functional crosstalk among cell envelope biogenesis pathways. PLoS Genet. 2011 Nov;7(11):e1002377. doi: 10.1371/journal.pgen.1002377. Epub 2011 Nov 17. PMID: 22125496; PMCID: PMC3219608.

[44] Yu D, Ellis HM, Lee EC, Jenkins NA, Copeland NG, Court DL. An efficient recombination system for chromosome engineering in Escherichia coli. Proc Natl Acad Sci U S A. 2000 May 23;97(11):5978-83. doi: 10.1073/pnas.100127597. PMID: 10811905; PMCID: PMC18544.

[45] Datsenko KA, Wanner BL. One-step inactivation of chromosomal genes in Escherichia coli K-12 using PCR products. Proc Natl Acad Sci U S A. 2000 Jun 6;97(12):6640-5. doi: 10.1073/pnas.120163297. PMID: 10829079; PMCID: PMC18686.

[46] Babu M, Butland G, Pogoutse O, Li J, Greenblatt JF, Emili A. Sequential peptide affinity purification system for the systematic isolation and identification of protein complexes from Escherichia coli. Methods Mol Biol. 2009;564:373-400. doi: 10.1007/978-1-60761-157-8_22. PMID: 19544035.

[47] Nesvizhskii AI. Computational and informatics strategies for identification of specific protein interaction partners in affinity purification mass spectrometry experiments. Proteomics. 2012 May;12(10):1639-55. doi: 10.1002/pmic.201100537. PMID: 22611043; PMCID: PMC3744239.

[48] Zhu W, Smith JW, Huang CM. Mass spectrometry-based label-free quantitative proteomics. J Biomed Biotechnol. 2010;2010:840518. doi: 10.1155/2010/840518. Epub 2009 Nov 10. PMID: 19911078; PMCID: PMC2775274.

[49] Cox J, Mann M. MaxQuant enables high peptide identification rates, individualized p.p.b.-range mass accuracies and proteome-wide protein quantification. Nat Biotechnol. 2008 Dec;26(12):1367-72. doi: 10.1038/nbt.1511. Epub 2008 Nov 30. PMID: 19029910.

[50] Akbarzadeh S, Coşkun Ö, Günçer B. Studying protein-protein interactions: Latest and most popular approaches. J Struct Biol. 2024 Dec;216(4):108118. doi: 10.1016/j.jsb.2024.108118. Epub 2024 Aug 28. PMID: 39214321.

[51] Schaeffer PM, Headlam MJ, Dixon NE. Protein--protein interactions in the eubacterial replisome. IUBMB Life. 2005 Jan;57(1):5-12. doi: 10.1080/15216540500058956. PMID: 16036556.

[52] Xu ZQ, Dixon NE. Bacterial replisomes. Curr Opin Struct Biol. 2018 Dec;53:159-168. doi: 10.1016/j.sbi.2018.09.006. Epub 2018 Oct 4. PMID: 30292863.

[53] Michel B, Sinha AK. The inactivation of rfaP, rarA or sspA gene improves the viability of the Escherichia coli DNA polymerase III holD mutant. Mol Microbiol. 2017 Jun;104(6):1008-1026. doi: 10.1111/mmi.13677. Epub 2017 Apr 12. PMID: 28342235.

[54] Nakayashiki T, Mori H. Genome-wide screening with hydroxyurea reveals a link between nonessential ribosomal proteins and reactive oxygen species production. J Bacteriol. 2013 Mar;195(6):1226-35. doi: 10.1128/JB.02145-12. Epub 2013 Jan 4. Erratum in: J Bacteriol. 2013 Aug;195(16):3796. PMID: 23292777; PMCID: PMC3592001.

[55] Ero R, Leppik M, Reier K, Liiv A, Remme J. Ribosomal RNA modification enzymes stimulate large ribosome subunit assembly in E. coli. Nucleic Acids Res. 2024 Jun 24;52(11):6614-6628. doi: 10.1093/nar/gkae222. PMID: 38554109; PMCID: PMC11194073.

[56] Parker DJ, Lalanne JB, Kimura S, Johnson GE, Waldor MK, Li GW. Growth-Optimized Aminoacyl-tRNA Synthetase Levels Prevent Maximal tRNA Charging. Cell Syst. 2020 Aug 26;11(2):121-130.e6. doi: 10.1016/j.cels.2020.07.005. Epub 2020 Jul 28. PMID: 32726597; PMCID: PMC7484455.

[57] Roy H, Ibba M. Broad range amino acid specificity of RNA-dependent lipid remodeling by multiple peptide resistance factors. J Biol Chem. 2009 Oct 23;284(43):29677-83. doi: 10.1074/jbc.M109.046367. Epub 2009 Sep 4. PMID: 19734140; PMCID: PMC2785599.

[58] Ichihashi N, Kurokawa K, Matsuo M, Kaito C, Sekimizu K. Inhibitory effects of basic or neutral phospholipid on acidic phospholipid-mediated dissociation of adenine nucleotide bound to DnaA protein, the initiator of chromosomal DNA replication. J Biol Chem. 2003 Aug 1;278(31):28778-86. doi: 10.1074/jbc.M212202200. Epub 2003 May 26. PMID: 12767975.

[59] Carpousis AJ, Campo N, Hadjeras L, Hamouche L. Compartmentalization of RNA Degradosomes in Bacteria Controls Accessibility to Substrates and Ensures Concerted

Degradation of mRNA to Nucleotides. Annu Rev Microbiol. 2022 Sep 8;76:533-552. doi: 10.1146/annurev-micro-041020-113308. Epub 2022 Jun 7. PMID: 35671533.

[60] Silva S, Camino LP, Aguilera A. Human mitochondrial degradosome prevents harmful mitochondrial R loops and mitochondrial genome instability. Proc Natl Acad Sci U S A. 2018 Oct 23;115(43):11024-11029. doi: 10.1073/pnas.1807258115. Epub 2018 Oct 9. PMID: 30301808; PMCID: PMC6205488.

[61] Masip L, Veeravalli K, Georgiou G. The many faces of glutathione in bacteria. Antioxid Redox Signal. 2006 May-Jun;8(5-6):753-62. doi: 10.1089/ars.2006.8.753. PMID: 16771667.

[62] Hartl J, Kiefer P, Kaczmarczyk A, Mittelviefhaus M, Meyer F, Vonderach T, Hattendorf B, Jenal U, Vorholt JA. Untargeted metabolomics links glutathione to bacterial cell cycle progression. Nat Metab. 2020 Feb;2(2):153-166. doi: 10.1038/s42255-019-0166-0. Epub 2020 Feb 3. PMID: 32090198; PMCID: PMC7035108.

[63] Deghelt M, Pierre Despas ES, Collet JF. The cell envelope of diderm bacteria: a unified scaffold, not a stack of layers. Curr Opin Microbiol. 2025 Nov 7;88:102681. doi: 10.1016/j.mib.2025.102681. Epub ahead of print. PMID: 41205332.

[64] Sueki A, Stein F, Savitski MM, Selkrig J, Typas A. Systematic Localization of Escherichia coli Membrane Proteins. mSystems. 2020 Mar 3;5(2):e00808-19. doi: 10.1128/mSystems.00808-19. PMID: 32127419; PMCID: PMC7055658.

[65] Rotman E, Bratcher P, Kuzminov A. Reduced lipopolysaccharide phosphorylation in Escherichia coli lowers the elevated ori/ter ratio in seqA mutants. Mol Microbiol. 2009 Jun;72(5):1273-92. doi: 10.1111/j.1365-2958.2009.06725.x. Epub 2009 Apr 30. PMID: 19432803; PMCID: PMC2691451.

[66] Harris LK, Theriot JA. Surface Area to Volume Ratio: A Natural Variable for Bacterial Morphogenesis. Trends Microbiol. 2018 Oct;26(10):815-832. doi: 10.1016/j.tim.2018.04.008. Epub 2018 May 26. PMID: 29843923; PMCID: PMC6150810.

[67] Miguel A, Zietek M, Shi H, Sueki A, Corona F, Maier L, Verheul J, den Blaauwen T, Van Valen D, Typas A, Huang KC. Modulation of bacterial cell size and growth rate via activation of a cell envelope stress response. mBio. 2025 Nov 12;16(11):e0228125. doi: 10.1128/mbio.02281-25. Epub 2025 Sep 22. PMID: 40980883; PMCID: PMC12607864.

[68] Hawkins M, Atkinson J, McGlynn P. Escherichia coli Chromosome Copy Number Measurement Using Flow Cytometry Analysis. Methods Mol Biol. 2016;1431:151-9. doi: 10.1007/978-1-4939-3631-1_12. PMID: 27283308.

[69] Wang X, Peterson JH, Bernstein HD. Bacterial Outer Membrane Proteins Are Targeted to the Bam Complex by Two Parallel Mechanisms. mBio. 2021 May 4;12(3):e00597-21. doi: 10.1128/mBio.00597-21. PMID: 33947759; PMCID: PMC8262991.

[70] Sklar JG, Wu T, Kahne D, Silhavy TJ. Defining the roles of the periplasmic chaperones SurA, Skp, and DegP in Escherichia coli. Genes Dev. 2007 Oct 1;21(19):2473-84. doi: 10.1101/gad.1581007. PMID: 17908933; PMCID: PMC1993877.

[71] Morrison JJ, Banas DA, Madden EK, DiBiasio EC, Rowley DC, Cohen PS, Camberg JL. Metabolic flux regulates growth transitions and antibiotic tolerance in uropathogenic *Escherichia coli*. bioRxiv [Preprint]. 2023 May 10:2023.05.09.540013. doi: 10.1101/2023.05.09.540013. Update in: J Bacteriol. 2024 Jun 20;206(6):e0016224. doi: 10.1128/jb.00162-24. PMID: 37215002; PMCID: PMC10197701.

[72] Ishida T, Akimitsu N, Kashioka T, Hatano M, Kubota T, Ogata Y, Sekimizu K, Katayama T. DiaA, a novel DnaA-binding protein, ensures the timely initiation of Escherichia coli chromosome replication. J Biol Chem. 2004 Oct 29;279(44):45546-55. doi: 10.1074/jbc.M402762200. Epub 2004 Aug 23. PMID: 15326179.

[73] Keyamura K, Fujikawa N, Ishida T, Ozaki S, Su'etsugu M, Fujimitsu K, Kagawa W, Yokoyama S, Kurumizaka H, Katayama T. The interaction of DiaA and DnaA regulates the replication cycle in E. coli by directly promoting ATP DnaA-specific initiation complexes. Genes Dev. 2007 Aug 15;21(16):2083-99. doi: 10.1101/gad.1561207. PMID: 17699754; PMCID: PMC1948862.

[74] Keyamura K, Abe Y, Higashi M, Ueda T, Katayama T. DiaA dynamics are coupled with changes in initial origin complexes leading to helicase loading. J Biol Chem. 2009 Sep 11;284(37):25038-50. doi: 10.1074/jbc.M109.002717. Epub 2009 Jul 24. PMID: 19632993; PMCID: PMC2757208.

[75] Taylor PL, Blakely KM, de Leon GP, Walker JR, McArthur F, Evdokimova E, Zhang K, Valvano MA, Wright GD, Junop MS. Structure and function of sedoheptulose-7-phosphate isomerase, a critical enzyme for lipopolysaccharide biosynthesis and a target for antibiotic adjuvants. J

Biol Chem. 2008 Feb 1;283(5):2835-45. doi: 10.1074/jbc.M706163200. Epub 2007 Dec 3. PMID: 18056714.

[76] Sprenger GA. Genetics of pentose-phosphate pathway enzymes of Escherichia coli K-12. Arch Microbiol. 1995 Nov;164(5):324-30. doi: 10.1007/BF02529978. PMID: 8572885.

[77] Fu H, Xiao F, Jun S. Bacterial Replication Initiation as Precision Control by Protein Counting. PRX Life. 2023 Aug-Oct;1(1):013011. doi: 10.1103/prxlife.1.013011. Epub 2023 Aug 28. PMID: 38550259; PMCID: PMC10977104.

[78] Berger M, Wolde PRT. Robust replication initiation from coupled homeostatic mechanisms. Nat Commun. 2022 Nov 7;13(1):6556. doi: 10.1038/s41467-022-33886-6. PMID: 36344507; PMCID: PMC9640692.

[79] Zhang Q, Zhang Z, Shi H. Cell Size Is Coordinated with Cell Cycle by Regulating Initiator Protein DnaA in E. coli. Biophys J. 2020 Dec 15;119(12):2537-2557. doi: 10.1016/j.bpj.2020.10.034. Epub 2020 Nov 13. PMID: 33189684; PMCID: PMC7822741.

[80] Li D, Zheng H, Bai Y, Zhang Z, Cheng H, Huang X, Wei T, Chang M, Zaritsky A, Hwa T, Liu C. Extrusion-modulated DnaA activity oscillations coordinate DNA replication with biomass growth. Elife. 2025 Nov 18;14:RP107214. doi: 10.7554/eLife.107214. PMID: 41251668; PMCID: PMC12626423.

[81] Boesen TO, Charbon G, Fu H, Jensen C, Sandler M, Jun S, Løbner-Olesen A. Dispensability of extrinsic DnaA regulators in *Escherichia coli* cell-cycle control. Proc Natl Acad Sci U S A. 2024 Aug 13;121(33):e2322772121. doi: 10.1073/pnas.2322772121. Epub 2024 Aug 6. PMID: 40014855; PMCID: PMC11331064.

[82] Wu C, Mori M, Abele M, Banaei-Esfahani A, Zhang Z, Okano H, Aebersold R, Ludwig C, Hwa T. Enzyme expression kinetics by Escherichia coli during transition from rich to minimal media depends on proteome reserves. Nat Microbiol. 2023 Feb;8(2):347-359. doi: 10.1038/s41564-022-01310-w. Epub 2023 Feb 3. PMID: 36737588; PMCID: PMC9994330.

[83] Zhu M, Mori M, Hwa T, Dai X. Distantly related bacteria share a rigid proteome allocation strategy with flexible enzyme kinetics. Proc Natl Acad Sci U S A. 2025 May 6;122(18):e2427091122. doi: 10.1073/pnas.2427091122. Epub 2025 Apr 29. PMID: 40299698; PMCID: PMC12067254.

[84] Skovgaard O. An additional replication origin causes cell cycle specific DNA replication fork speed. Front Microbiol. 2025 Apr 30;16:1584664. doi: 10.3389/fmicb.2025.1584664. PMID: 40371120; PMCID: PMC12075136.

Prace wchodzące w skład rozprawy doktorskiej

Artykuł nr 1 (praca przeglądowa)

Morcinek-Orłowska J., Galińska J., Glinkowska M.K.

When size matters – coordination of growth and cell cycle in bacteria.

(2019) Acta Biochimica Polonica. Vol. 66 No. 2:139-146.

IF (2019) = 1,42

Punktacja MNiSW (2019) = 40

ACTA ABP BIOCHIMICA POLONICA

Vol. 66, No 2/2019
139–146
https://doi.org/10.18388/abp.2018_2798

Review

When size matters – coordination of growth and cell cycle in bacteria

Joanna Morcinek-Orłowska, Justyna Galińska and Monika Glinkowska✉

Department of Bacterial Molecular Genetics, University of Gdansk, Gdańsk, Poland

Bacterial cells often inhabit environments where conditions can change rapidly. Therefore, a lot of bacterial species developed control strategies allowing them to grow and divide very fast during feast and slow down both parameters during famine. Under rich nutritional conditions, fast-growing bacteria can divide with time interval equal to half of the period required to synthesize their chromosomes. This is possible due to multifork replication which allows ancestor cells to start copying genetic material for their descendants. This reproduction scheme was most likely selected for, since it enables maximization of growth rate and hence – effective competition for resources, while ensuring that DNA replication will not become limiting for cell division. Even with this complexity of cell cycle, isogenic bacterial cells grown under defined conditions display remarkably narrow distribution of sizes. This may suggest that mechanisms exists to control cell size at division step. Alternative view, with great support in experimental data is that the only step coordinated with cell growth is the initiation of DNA replication. Despite decades of research we are still not sure what the driving forces in bacterial cell cycle are. In this work we review recent advances in understanding coordination of growth with DNA replication coming from single cell studies and systems biology approaches.

Key words: bacterial cell cycle, DNA replication, cell division, cell size control

Received: 30 March, 2019; revised: 07 April, 2019; accepted: 07 April, 2019; available on-line: 10 April, 2019

✉e-mail: monika.glinkowska@biol.ug.edu.pl
Acknowledgements of Financial Support: This work was supported by the National Science Center (Poland) No. UMO-2016/23/N/NZ2/02378 to J.M.O.

Abbreviations: SMK, Schaechter, Maaloe and Kjeldgaard; DAR, DnaA assembly region; DUE, DNA unwinding element; RIDA, regulatory inactivation of DnaA; DDAH, datA-dependent DnaA-ATP hydrolysis; DARS, DnaA reactivating sequences; NAPs, nucleoid associated proteins; SMC, structural maintenance of chromosome; SA, surface; V, volume; PG, peptidoglycan; PCC, progression control complex; SIS, sugar isomerase; S7P, sedoheptulose-7-phophasphate; M7P, D-glycero-D-manno-heptose-7-phosphate

EARLY MODELS OF CELL CYCLE COORDINATION IN BACTERIA – A BIT OF HISTORY

Bacterial cell cycle is defined as a set of consecutive events leading to production of two daughter cells. It is traditionally divided into three stages: a phase between cell birth and initiation of DNA replication (B period), genome duplication step (C period) and a phase between completion of replication and cell division (D period) (Skarstad *et al.*, 1983; Michelsen *et al.*, 2003). The two main processes of the cell cycle – DNA replication and cell division – have to be coordinated with cellular growth, so that reproduction is accompanied by the maintenance of characteristic cell size and shape. Such coordination is particularly important for microorganisms whose environment of can change very quickly and thus – rapid adaptation of bacterial cell cycle parameters to variable growth conditions is crucial for survival.

Over 60 years ago Schaechter, Maaloe and Kjeldgaard (SMK) formulated the principles of bacterial growth, also known as the growth law (Schechter *et al.*, 1958). They cultivated *Salmonella enterica* in different media and observed that cells grown under conditions supporting faster growth rate exhibit larger size and higher DNA, RNA and protein content per cell, irrespective of particular media composition. In other words, they proposed that the macromolecular composition of cells and their size is a function of growth rate, regardless of the specific nutrients present in the medium (Schaechter *et al.*, 1958). In their results, cell size scaled linearly with growth rate and was inversely correlated with doubling time. These observations linked also cell growth to cell cycle.

The C and D period in Schaechter's experiments were approximately constant and last for 40 and 20 minutes, respectively, whereas doubling time of fast growing bacteria is about 20 minutes. This paradox of bacterial cell cycle was solved in 1968 by Copper and Helmstetter's model, assuming that under fast growth conditions bacteria initiate the subsequent round of chromosome replication before the previous one is finished. Thus, the cell contains several replicating chromosomes, but replication is still initiated only once during the cell cycle (Cooper & Helmstetter, 1968). Cooper-Helmstetter's model of multifork replication together with the growth law led to the hypothesis that in the cell cycle replication is triggered by the achievement of a critical cell size (mass) per origin, which is constant regardless of growth conditions (Donachie, 1968). It was therefore assumed that there is a factor conveying the information about cell size growth directly to the replication machinery, however a perfect candidate for such a mechanism is still missing (for reasons why, see (Flåtten *et al.*, 2015; Barber *et al.*, 2017; Willis & Huang, 2017)).

Recently, development of single-cell techniques which enables testing the rules governing the cell cycle with respect to individual cells, renewed the interest in its principles. In this review we summarize the current knowledge about cell cycle coordination in bacteria, starting from brief description of the molecular mechanisms and regulation of main cell cycle stages followed by the newest insight into the role of cell size in proper cell cycle progression.

TOP-DOWN AND BACK AGAIN – MOLECULAR MECHANISMS UNDERLYING CONTROL OF THE KEY CELL CYCLE PROCESSES

Unless stated otherwise, mechanisms and protein terminology described below refer to the model Gram-negative bacterium *Escherichia coli*.

DNA replication

DNA replication has to be tightly controlled to ensure that bacterial chromosome is duplicated faithfully and only once during the cell cycle. This provides the stability and integrity of the next generations' genome.

The main regulatory mechanisms known so far, focus on the initiation of replication. The central player of that stage and the subject of control mechanisms is a highly conserved initiator protein DnaA, found in almost all eubacteria. DnaA binds to *oriC* and leads to the initial unwinding of the double DNA helix, permitting further formation of the replisome (reviewed in: Leonard & Grimwade, 2015; Jameson & Wilkinson, 2017; Katayama, 2017)

High degree of structural conservation pertains particularly to one of the four domains of DnaA, namely to domain III, responsible for ADP and ATP binding and hydrolysis of the latter (Erzberger *et al*., 2002; Nishida *et al*., 2002; Kawakamii *et al*., 2005). Decades of studies brought detailed understanding of the mechanism of DnaA action and its regulation. It was shown that DnaA binds to several types of sequences within the *oriC* ((Leonard & Grimwade, 2015) and references therein). *OriC* has a modular structure and consists of the DnaA Assembly Region (DAR), where DnaA binds initially, and DNA Unwinding Element (DUE) where DNA strands become separated during the initiation step. Three high affinity DnaA binding sites (R1, R2, R4) present in the *oriC* sequence are occupied throughout most of the cell cycle, and both DnaA- ADP and DnaA-ATP can interact with them. However, only DnaA-ATP can bind several low-affinity sites, forming two oppositely arrays between R1-R2 and R2-R4 DnaA-boxes (Hansen & Atlung, 2018).

Accumulation of a critical amount of DnaA-ATP bound to the oriC eventually results in the unwinding of the AT-rich DUE region (Kurokawa *et al*., 1999; Ozaki & Katayama, 2012; Sakiyama *et al*., 2017). Then further replication proteins are recruited to the so-called „open complex", namely DnaB helicase is loaded with the aid of DnaC, followed by DnaG primase and multi-subunit DNA polymerase III (Katayama, 2017).

DnaA concentration is stable during the cell cycle, but the ratio of the form associated with ATP to that bound to ADP changes – the level of DnaA-ATP peaks at the time of initiation, reaching 80% of the total cell pool of DnaA and shortly after initiation it falls up to around 20% (Kurokawa *et al*., 1999). There are several mechanisms responsible for the fluctuations of the levels of DnaA-ATP and DnaA-ADP and for the access of DnaA to oriC, which allow for precise control of the initiation timing and prevent premature reinitiation.

DnaA-ATP is converted to DnaA-ADP upon initiation via two independent mechanisms – RIDA (regulatory inactivation of DnaA) and DDAH (*datA*-dependent DnaA-ATP hydrolysis). In the first case, Hda protein, a homologue of DnaA, interacting with the β clamp of DNA polymerase III stimulates ATPase activity of DnaA during DNA synthesis (Kato & Katayama, 2001). In the second, chromosomal *datA* region with unusually high DnaA-binding capacity, stimulates ATP hydrolysis by DnaA in a manner dependent on IHF, one of the nucleoid associated, DNA-bending proteins (Kasho & Katayama, 2013; Kasho *et al*., 2017). DnaA-ADP can be also reactivated to DnaA-ATP by acidic phospholipids of the cell membrane (Saxena *et al*., 2013) and two chromosomal regions, called DARS (DnaA Reactivating Sequences) (Fujimitsu *et al*., 2009; Kasho *et al*., 2014) suggesting that cellular membrane synthesis and replication initiation may be related to each other. Moreover, DnaA autoregulates its cognate gene expression in an ATP-dependent manner (Speck *et al*., 1999; Grant *et al*., 2011). After the initiation, when Dna-ATP level is still high, unscheduled re-initiation is prevented by the SeqA protein, which sequesters both *oriC* region and the *dnaA* promoter for about one-third of the cell cycle (von Freiesleben *et al*., 2000; Hiraga *et al*., 2004; Guarné *et al*., 2005; Waldminghaus & Skarstad, 2009).

Another important regulatory protein that positively affects the initiator activity of DnaA is the DiaA (DnaA initiator-associating factor) protein. It directly interacts with DnaA, supporting its assembly to weak DnaA-affinity sites in the *oriC* (Ishida *et al*., 2004). Although DiaA is not an essential protein, its activity significantly promotes the initiation of replication and ensures that every origin in a cell is fired simultaneously (Ishida *et al*., 2004; Keyamura *et al*., 2007). Interestingly, DiaA also has a negative effect on the initiation of replication at its later stage. The protein binds to DnaA at the same site as DnaB helicase. Thus, as long as DiaA is bound to DnaA, it is impossible to recruit DnaB to the replisome and proceed with the initiation stage (Keyamura *et al*., 2009). Mild overexpression of DiaA does not affect the timing of replication in the cell cycle (Flåtten *et al*., 2015), so it is suggested that the inhibitory effect of DiaA on helicase loading does not result simply from binding competition, but a specific molecular mechanism allowing to release DiaA from the DnaA-DiaA complex. However, what cellular factor promotes replacement of DiaA with DnaB, is still unknown.

Chromosome segregation and cell division

Proper segregation of the replicated bacterial chromosome is essential for each of the daughter cells to inherit a full copy of the genome. However, this is the least understood process in bacteria, especially in *Escherichia coli* which lacks specific partition system. In contrast to eukaryotic organisms, chromosome segregation in bacteria occurs concomitantly with DNA replication, so the origin-close region is segregated first, followed by the rest of the chromosome with a certain delay (reviewed in (Badrinarayanan *et al*., 2015)).

It is assumed that the chromosome segregation occurs spontaneously and is driven by physical forces derived from the nucleoid topology, rather than by a biological mechanism (Jun & Wright, 2010; Le Chat & Espéli, 2012). Thus, proteins involved in the proper organization, compaction and maintenance of chromosome may also be involved in segregation process. These are nucleoid-associated proteins (NAPs) – key factors of proper chromosome organization – such as IHF, Fis, HU and H-NS, that are able to wrap, bend or bridge the DNA (Wang *et al*., 2013), as well as global chromosome organization factor – structural maintenance of chromosome (SMC) complex, in *E. coli* consisting of MukBEF proteins (Rybenkov *et al*., 2014).

It is also worth noting that during the replication, the emerging sister chromosomes are topologically in-

terwound – in order to be effectively segregated, they should be separated. Here, topoisomerase IV, which is essential in the segregation process, is involved in sister chromosomes decatenation (Zechiedrich *et al.*, 1997; Sand *et al.*, 2003; Joshi *et al.*, 2011; Zawadzki *et al.*, 2015).

Contrary to *E. coli*, up to 65% of bacterial species possess parABS partitioning system for the origin segregation (for more information see (Funnell, 2016)). It consists of parS sequences located near oriC and two protein components, ParA and ParB. ParB recognizes and binds to parS sequences, to which ParA protein is substequently recruited. The whole nucleoprotein complex is then pulled to the opposite poles of the cell in an ATP-dependent mechanism whose details have not been fully explained yet.

After completion of chromosomal DNA synthesis and segregation, the cell divides into two progeny cells of approximately equal size. This process is controlled by a protein complex called divisosome. Assembly of the division machinery is orchestrated by a tubulin homologue protein – FtsZ, which polymerizes in a GTP-dependent manner into a so-called Z-ring in the future septation region (Erickson *et al.*, 2010; Szwedziak *et al.*, 2014). In *E. coli*, *B. subtilis* and several other bacteria, the divisome structure has been proposed to assemble in two temporally distinct phases. During the first, the Z ring is formed and membrane-associated proteins (ZipA and FtsA in *E. coli*) tether it to the cell envelope, forming a complex called proto-ring. In the second stage, proto-ring recruits late divisome proteins responsible for peptidoglycan synthesis at the septum (FtsI in *E. coli*) and several proteins whose role relies most likely on coordinating the crosstalk between the proto ring and peptidoglycan synthetases (*E. coli* – FtsN, FtsLBQ) (for more detailed information see: (Rowlett & Margolin, 2015; Haeusser & Margolin, 2016). Constriction of the cytoplasmic membrane, cell wall synthesis at the septum and outer membrane invagination by the divisome finish the fission process.

Molecular regulation of cell division in bacteria concentrates basically on proper Z-ring positioning, coordinated in *E. coli* by at least two systems. The first, Min complex, ensures that FtsZ polymerization occurs exactly at midcell. Two components of this system, MinC and MinD oscillate between cell poles thanks to the help of a third protein, MinE. Min complex inhibits FtsZ polymerization, so the Z-ring cannot form at the poles, occupied with MinCD proteins (Rowlett & Margolin, 2013; Shih & Zheng, 2013). Second mechanism, named nucleoid occlusion, consists of SlmA – the protein that binds to the chromosome and represses Z ring formation over the nucleoid (for a recent review and references see: (Ortiz *et al.*, 2016)). The SlmA-specific sequences are dispersed throughout the genome with the exception of the replication terminus site. Thus, SlmA, directly interacting with FtsZ, restrains septum formation until the segregation process is almost completed. FtsZ is additionally linked to the ter region by such proteins as ZapA, ZapB and MatP, which contribute to the coupling between chromosome segregation and cell division (Espeli *et al.*, 2012). DNA translocase FtsK, which is an essential protein for *E. coli*, orchestrates chromosome segregation and cell division by interacting with chromosomal DNA, the divisome and topoisomerase IV (Crozat *et al.*, 2014).

Growth

Rapid growth is a guarantee of outgrowing competitors and producing progeny cells, so a maximization of growth rate and quick adaptation to changes in environmental conditions are the universal evolutionary strategy of most bacteria. However, bacterial growth rate depends directly on environmental conditions, i. e. on the availability of nutrients. Growth rate changes correspond to alterations in the scale of protein production, metabolism and synthesis of external cell layers – cell membranes and peptidoglycan.

The growth rate of bacterial cells is limited by the efficiency of cellular translation machinery, i.e. the amount and activity of rybosomes. Indeed, it has been confirmed that the fraction of ribosomal proteins increases linearly with growth rate (Dennis *et al.*, 2004; Jin *et al.*, 2012). However, apart from proper amount of ribosomes, growth is guaranteed also by a proper supply of aminoacids and tRNA and growth rate maximization is obtained when all rybosomes are saturated with their substrate. The translation rate is therefore regulated by both the amount of ribosomes and the diffusion of the complexes transporting aminoacyl-tRNA in the cytoplasm (Klumpp & Hwa, 2014; Scott *et al.*, 2014).

Systems biology research aiming to discover the complex interaction network within the cell has revealed that the cellular protein pool is partitioned into three fractions: a growth rate-independent fraction, ribosomal protein fraction and metabolic fraction including catabolic and anabolic enzymes (Scott & Hwa, 2011; Scott *et al.*, 2014). Two latter fractions always add up to a constant value as the total cellular protein concentration is fixed. However, the ratio between them changes depending on growth conditions. Namely, in the nutrient-rich environment the supply of nutrients such as amino acids is high and they do not need to be synthesized, so the metabolic fraction of proteins is reduced. As a result, production of ribosomal proteins increases, allowing for the cell to maximize the global translation rate (Scott *et al.*, 2014). Therefore, allocation of proteins between ribosomal and metabolic fraction is correlated with growth rate and – consequently - growth rate-dependent control of gene expression reflects that protein economy (Scott *et al.*, 2010, 2014; Scott & Hwa, 2011).

The genes encoding translational machinery are highly expressed and therefore, they need to be precisely regulated, because any deviation from the optimal level has a large impact on the proteome. Production of tRNA-affiliated and ribosomal proteins is co-regulated (Klumpp & Hwa, 2014). Ribosomes consist of rRNA and r-proteins and it is the rRNA component which is mainly subjected to precise, growth-rate dependent regulation ((Jin *et al.*, 2012) and references therein). rRNA genes are regulated by the alarmone of stringent response – ppGpp ((Potrykus & Cashel, 2008; Hauryliuk *et al.*, 2015) and references therein), and thus ppGpp is considered as a main source of growth rate control (Murphy *et al.*, 2010). In *E. coli* cells, ppGpp is produced by two proteins RelA and SpoT, the former is responsible for ppGpp synthesis during amino acid starvation. Appearance of an uncharged tRNA at the ribosomal A site activates RelA and induces ppGpp production. ppGpp in turn, inhibits rRNA promoters activity at the transcription initiation stage (Gralla, 2005; Brown *et al.*, 2016). As a result, a downshift in amino acids concentration will reduce tRNA charging and hence – increase ppGpp level, resulting in rRNA promoters inhibition. Consequently, a drop of ppGpp level upon an upshift of amino acids supply will have a contrary effect. Taken together, ppGpp-dependent regulation of rRNA synthesis contributes to the balance between amino acid supply and protein synthesis (Scott *et al.*, 2014) and supports the maintenance of

ribosomes saturated with their substrate under different growth conditions (Bosdriesz *et al.*, 2015).

Corse-grained model of growth-dependent protein allocation has also implications for the cell cycle control. Namely, it has been shown that *E. coli* cells during balanced growth under perturbations in various cellular processes, change their sizes and/or growth rate but maintain a remarkably stable initiation mass (mass per origin at the moment of initiation or a unit cell) (Si *et al.*, 2017). The authors proposed that this invariance of the unit cell under perturbations targeting transcription, translation, fatty acids or cell wall synthesis etc. can be explained assuming that cell size is the sum of all unit cells under any steady-state growth conditions. Furthermore, taking into account that cells attain a critical size prior to initiation and that the initiator concentration is constant under different steady-state growth conditions (as was shown for DnaA), the model of protein allocation predicts the existence of a specific protein sector that is constant despite changes of the ribosomal fraction of the proteome under different perturbations. Affiliation of replication initiators with that sector ensures invariance of initiation mass during balanced growth (Si *et al.*, 2017).

BACTERIAL CELL CYCLE COORDINATION – NEW INSIGHTS FROM SINGLE CELL STUDIES AND MATHEMATICAL MODELING

The moments of replication initiation and division in the cell cycle need to be optimally chosen to meet certain criteria. Each initiation of DNA replication needs to be followed by division to maintain one genome duplication per cell cycle. Moreover, it has to be assured that each daughter cell receives a full copy of genetic material and maintains characteristic size after division. Despite availability of often detailed molecular description of mechanism underlying cell cycle progression, the big picture how key events are coordinated is still missing. In eukaryotic organisms it is achieved by a complex system of cell cycle checkpoints, however in bacteria no such cell cycle engine has been identified (Harashima *et al.*, 2013). A recent insight from single cell studies on cell size control and the chromosome cycle brings new scenarios and integrates previously described models, providing hints where to look for molecular control mechanisms. In this chapter, we review the conclusions of those studies and propose the role of metabolic cues in the integration of cell cycle events.

Cells of a defined type, under the same conditions display a narrow distribution of cell sizes (Amir, 2014). Early on, this fact resulted in the search of cell size control mechanisms and two models how such control can be achieved have been proposed. According to the first, cells divide upon reaching a certain size ('sizer') (Fig 1a). In the second, spending a certain amount of time in the cell cycle is the signal to trigger cell division ('timer') (Fig. 1b). The advent of single cell techniques enabled to revise these model by studying rules followed by individual cells. 'Sizer' or 'timer' models can be verified in such studies by analyzing the correlation of cells birth size and the amount of growth within the doubling time interval. Cells behaving like a perfect 'timer' would show no such correlation, whereas in the case of perfect 'sizer', the need to attain a defined size by cells in order to divide, would lead to the negative correlation between the birth size and the amount of growth prior to division (Willis & Huang, 2017).

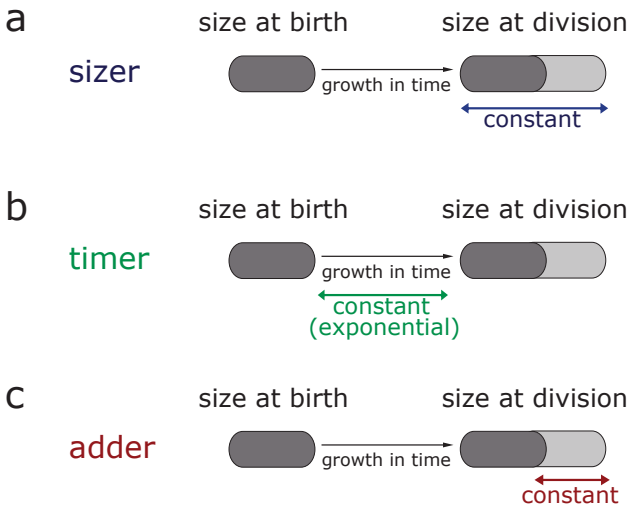

Figure 1. Alternative models of cell size control.
(**a**) "sizer" – bacteria cells divide after reaching defined size; (**b**) "timer" – cells divide after a certain period of time since birth; (**c**) "adder" – cells add a constant amount of volume between subsequent divisions. Adapted from (Willis & Huang, 2017).

Recently, high-throughput microfluidic techniques allowed to monitor the size and cell cycle of many individual bacterial cells simultaneously (reviewed in (Taheri-Araghi *et al.*, 2015a)). High amount of data collected from thousands of cells combined with mathematical modelling brought a third paradigm, dubbed 'adder' (Fig. 1c), stating that cells add a nearly constant volume between subsequent initiations or divisions irrespective of their birth size. 'Adder' principle turned out to be consistent with a large amount of data from evolutionarily distant bacterial species such as *Caulobacter crescentus*, *E. coli*, *Bacillus subtilis* and *Pseudomonas aeruginosa* (Deforet *et al.*, Osella *et al.*, 2014; Taheri-Araghi *et al.*, 2015b; Jun *et al.*, 2017). However, this coarse-grained model does not identify the mechanism by which the cells measure the added size or the point of the cell cycle where such regulation takes place. We also note here, that slow growing *E. coli* cells do not seem to follow "adder" growth mode, which will be described in more detail below.

The 'adder' model seems to finally disprove "sizer" based on feedback size-driven mechanisms. However, the question still remains what are the mechanisms underlying this constant size extension during the cell cycle. Later works based on single-cell data propose different schemes explaining which cell cycle stage is subjected to size-dependent control.

The prevalent view places cell size control at the initiation of DNA replication. The classical model of bacterial cell cycle control derived by Donachie from Cooper and Helmstetter and SMK data claimed that replication is initiated after reaching a critical size per origin at the moment of initiation regardless of growth conditions (Donachie, 1968; Donachie & Blakely, 2003). Cell division occurs after a fixed amount of time needed for completion of DNA replication and chromosome segregation (C+D period of cell cycle). A recent study by Wallden and coworkers (2016) based on monitoring of individual cell behavior supported this view and stated that initiation of DNA replication is set by a constant volume per origin ratio ("sizer" between initiations) and the respective division occurs C+D time after. The duration of C+D period is dependent on growth rate. In fast growing cells with overlapping replication rounds,

the initiation of DNA replication started in previous generations and the respective cell division will occur C+D time after, which is nearly constant under those conditions. Therefore the added size prior to division is uncorrelated to birth size, but depends on the individual cell's growth rate. In addition, Wallden and coworkers (2016) observed that *E. coli* cells grown under slow growth conditions do not follow "adder" behavior and instead behave like "sizers". The authors proposed that the observed negative correlation between birth size and the added volume in slow growing *E. coli* stems from size-dependent control of the initiation of DNA replication. Under conditions supporting only single replication round, cells small at birth add a greater volume before they can start DNA replication – and this results in a greater added volume, and hence – greater size prior to division.

Other works claimed that a threshold of size at any cell cycle stage, assuming nearly constant growth rate, would result in the loss of correlation between the birth volume and the division volume, in contrast to the situation seen in the data underlying "adder" principle. The authors proposed that cells add a constant volume per origin subsequent initiation rounds (behave like "adder" between initiations). This scenario preserves the "memory" of the previous cell cycle and predicts a strict relationship between cell size and the number of origin per cell (Haschemi *et al.*, 2012; Ho & Amir, 2015).

In other words, in those chromosome-centric views – DNA replication and segregation are rate limiting steps for cell division. On the other hand, there are several opposite models, stating that the cell division, not initiation of replication is the rate-limiting process for the cell cycle progression. Along with the parallel discoveries of 'adder' phenomenon by several research group, some of them place control of the a constant volume preferentially at division step (Campos *et al.*, 2014; Osella *et al.*, 2014) or at a sub-period between initiation of replication and cell division (Adiciptaningrum *et al*). According to them, implementing cell size increment at division step ensures the compensation of the stochastic differences of cells' birth size and consequently, maintains cell size homeostasis (Campos *et al.*, 2014).

Recently, another model standing in opposition to the chromosome-centric view has appeared. Namely, Harris and Theriot proposed that cells add a certain surface area between subsequent divisions (Harris & Theriot, 2016). They observed that although single cells may differ in individual sizes and shapes, they maintain surface (SA) to volume (V) ratio characteristic for given conditions (Harris & Theriot, 2016). They proposed that SA/V is the parameter controlled by cells and determined by the ratio of surface growth to volume growth. They based on the assumption that synthesis of cell surface precursors in the cytoplasm sets the rate of surface growth and leads to its scaling with volume. Harris and Theriot noted that as individual cell grows during the cell cycle SA/V drops due to larger proportion of low SA/V cylindrical body to high SA/V end-cap and the synthesis of the new cell polls restores characteristic SA/V, which implies that the rates of volume or surface growth must also display variation over the cell cycle. Indeed, the authors observed that cell volume growth rate is stable over the cell cycle, whereas SA growth speeds up at the end of the cycle which coincides with septation. They proposed that as the cell grows, cell surface material accumulates in the cell and is subsequently used up during the new cell pole synthesis. As artificial reduction of peptidoglycan (PG) synthesis leads to delay of cell division, Harris and Theriot concluded that accumulation of PG precursors may serve as a signal for cell division machinery to end septation process. This strategy ensures that cells accumulated enough material to finish this precursor-demanding step. The model based on accumulation of a threshold amount of cell wall building blocks reproduced the constant amount of volume added from birth to division, postulated by "adder" growth mode (Harris & Theriot, 2016, 2018).

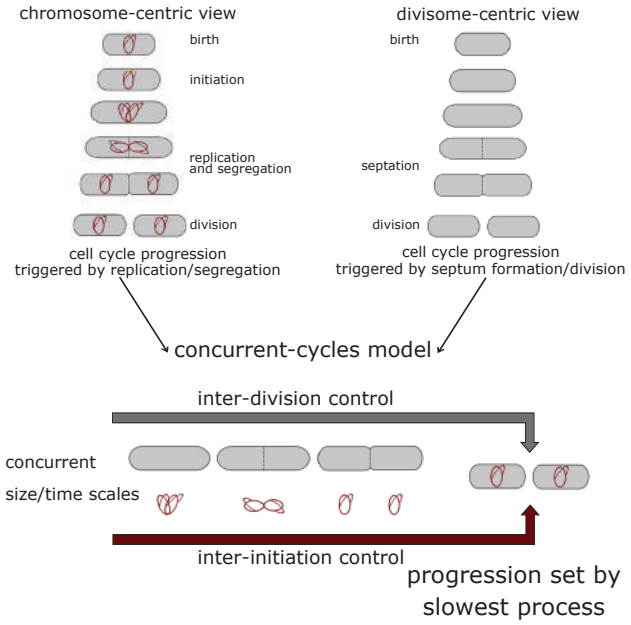

Figure 2. Competing models explaining timing of cell division during the cell cycle.
In the first scheme, DNA replication is always limiting for the cell cycle progression as proposed by Wallden and coworkers (Wallden *et al.*, 2016) and Amir (Amir, 2014). In the second, chromosome replication is never limiting, i.e. division is set by accumulation of a certain amount of cell wall precursors, as proposed by Harris & Theriot (Harris & Theriot, 2016). Recently, Micali and coworkers (Micali *et al.*, 2018a) have shown that neither of the two models recapitulates experimental data and proposed that both conditions have to be fulfilled – chromosome duplication and segregation has to be completed and divisome ready to finish off septation process. Division timing is set by the slowest of the two processes. Adapted from (Micali *et al.*, 2018a).

Cell size control models, centralized either on either replication initiation or cell division seem to be incompatible and contrast one another. On the other hand, it has been shown recently that these models separately do not fit with all experimental observations from single-cell analysis. Namely, Micali et al. (Micali *et al.*, 2018a, 2018b) reexamined previous single-cell data and concluded that neither the model, assuming DNA replication as the sole rate-liming process for cell division, nor models based on chromosome-independent interdivision cycles recapitulate the growth patterns observed in those studies. Instead the authors proposed that both mechanisms are at play and division is set by the slowest process, i.e. when chromosome replication and segregation is completed and when septum-synthesizing machinery is equipped with enough building-blocks (Fig. 2). This concurrent cycles view assumes that both chromosome replication-segregation and cell division are subjected to size-dependent control and these two size scales work in parallel. It results in a model where between subsequent initiations cells behave like 'adders' or 'sizers', depending on growth conditions, whereas interdivision process is

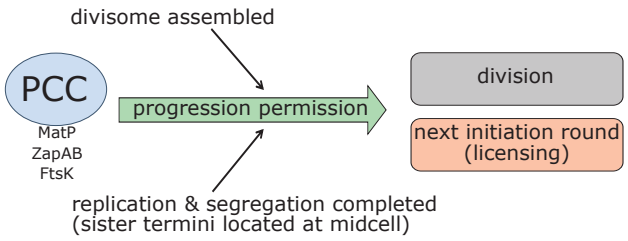

Figure 3. A model explaining cell cycle control by formation of Progression Control Complex (PCC).
Progression Control Complex is formed by physical interaction of the chromosome terminus with cell membrane in the forming septum after replicated sister chromosomes have moved to daughter cell compartments with termini situated on both sides of the septum. When other growth conditions are met and divisome maturates, progression permission is granted, allowing for subsequent cell division and initiation of DNA replication. Thus, progression permission is a licensing decision and it does not decide about timing of the downstream cell cycle events. Adapted from (Stouf *et al.*, 2018).

always an 'adder' (Micali *et al.*, 2018a). Thus, the integration of two processes sets the final decision about cell cycle progression.

The concept of integration of concurrent processes – DNA replication and cell division in setting the division time can be extended with a proposal of molecular progression control complex (PCC) (Stouf *et al.*, 2018). This system would constrain the onset of cell division as well as subsequent initiation of DNA replication until chromosome duplication and segregation is completed AND cells finished divisome maturation (Fig. 3). After both conditions are fulfilled progression permission is granted and cells complete division. At molecular level, this system is suggested to act as a link between chromosome segregation and division by direct physical interaction of the sister chromosomes terminus region with nascent septum, dependent on MatP, ZapAB and FtsK proteins. In support of this proposal, the authors observed that tethering of chromosomal DNA to cell membrane leads to inhibition of next replication rounds most likely due to loss of the negative supercoiling (Magnan & Bates, 2015; Magnan *et al.*, 2015). In addition, the authors argue that in conditional *ftsZ* and *ftsK* mutants chromosomal cell cycle progresses despite the lack of cell division and explain it by the absence of progression control complex in such cells. It is worth emphasizing that progression permission works as a licensing factor, not the mechanism controlling timing of replication initiation or cell division. Assumption that both replication and interdivision processes set division timing allows for existence of processes controlling both replication initiation and cell division. Such models account for the role of numerous proteins found in distinct bacterial species that regulate FtsZ assembly in response to the level of certain metabolites. For instance, moonlighting glucosyltransferases OpgH and UgtP link the UDP-glucose level to cell division in *E. coli* and *B. subtilis*, respectively (Weart *et al.*, 2007; Hill *et al.*, 2012; Westfall & Levin, 2017). For detailed molecular mechanisms and further examples of such proteins we refer the reader to recent excellent reviews on that subject (Chien *et al.*, 2012; Vadia & Levin, 2015; Jun *et al.*, 2017; Sperber & Herman, 2017; Westfall & Levin, 2017).

It is worth noting that eukaryotic cells also follow "adder" behavior leading to cell size homeostasis. To achieve this, they modulate both growth rate and cell cycle duration (Srivastava *et al.*, 2018). Therefore, one could say that genetically distinct organisms use different molecular strategies to achieve the same size control principle. This supports the view that cell size control is a result of coordination of many cellular functions like cell cycle, metabolism, protein synthesis, synthesis of the cell envelope. Indeed, mutation of many genes involved in very different cellular processes lead to changes in cell size (Cornet *et al.*, 2018). At molecular level, this coordination between cellular functions requires flow of information between the processes. Metabolic proteins engaged in the regulation of cell division, mentioned above, are an excellent example of such communication. In this light, it is also interesting that nucleotide sugars, used for cell envelope synthesis provide a link between replication precursors and cell surface expansion. Interestingly, also the level of S7P, a precursor of both nucleotides and outer cell membrane components seems to have a profound effect on the cell size, as shown by opposing effects of deletion of genes encoding enzymes that produce and consume it in the pentose-phosphate pathway (*tktA* and *talB*, respectively) (Westfall & Levin, 2018). Evidence has also accumulated suggesting a direct crosstalk between metabolism and regulation of DNA replication in *E. coli* and *B. subtilis* (Dalmais *et al.*, 2007; Węgrzyn *et al.*, 2011; Barańska *et al.*, 2013). In this light we also propose that DiaA protein could integrate the information on cell surface expansion and/or nucleotide synthesis capacity. DiaA contains a well conserved sugar isomerase domain (SIS) (Keyamura *et al.*, 2007). The role of the SIS domain in DiaA function is unknown. Notably, the SIS domain closely resembles that of another *E. coli* protein, sedoheptulose 7-phosphate isomerase GmhA (alternative name - LpcA) and its homologues in other bacterial species (Taylor *et al.*, 2008; Harmer, 2010; Do *et al.*, 2015). GmhA catalyzes isomerization of D-sedoheptulose-7-phosphate (S7P) into D-glycero-D-manno-heptose-7-phosphate (M7P), which constitutes a step in the pathway of lipopolysaccharide (LPS) synthesis – a part of the outer membrane of gram-negative bacteria (Kneidinger *et al.*, 2002; Taylor *et al.*, 2008). Interestingly, some bacteria encode only a single GmhA homologue, like for instance *P. aeruginosa* whose GmhA contains amino acid residues that were proven crucial for DiaA-DnaA interaction in *E. coli* (Keyamura *et al.*, 2007; Taylor *et al.*, 2008). This suggests that such proteins could join GmhA and DiaA functions. Binding of S7P or M7P by DiaA could regulate its activity with respect to DnaA and couple metabolism to DNA replication. Future effort in studies on cell cycle and size control should focus on clarification of a crosstalk between major processes: replication, cell envelope, metabolism and cell division.

REFERENCES

Adiciptaningrum A, Osella M, Moolman M, Lagomarsino M, Tans S Stochasticity and homeostasis in the *E. coli* replication and division cycle. *Sci Rep* **5**: 18261

Amir A (2014) Cell size regulation in bacteria. *Phys Rev Lett* **112**: 208102. https://doi.org/10.1103/PhysRevLett.112.208102

Badrinarayanan A, Le TBK, Laub MT (2015) Bacterial chromosome organization and segregation. *Annu Rev Cell Dev Biol* **31**: 171–199. https://doi.org/10.1146/annurev-cellbio-100814-125211

Barańska S, Glinkowska M, Herman-Antosiewicz A, Maciag-Dorszyńska M, Nowicki D, Szalewska-Palasz A, Wegrzyn A, Wegrzyn G (2013) Replicating DNA by cell factories: Roles of central carbon metabolism and transcription in the control of DNA replication in microbes, and implications for understanding this process in human cells. *Microb Cell Fact* **12**: https://doi.org/10.1186/1475-2859-12-55

Barber F, Ho P-Y, Murray AW, Amir A (2017) Details Matter: noise and model structure set the relationship between cell size and cell cycle timing. **5**: 1–16. https://doi.org/10.3389/fcell.2017.00092

Bosdriesz E, Molenaar D, Teusink B, Bruggeman FJ (2015) How fast-growing bacteria robustly tune their ribosome concentration to approximate growth-rate maximization. *FEBS J* **282**: 2029–2044. https://doi.org/10.1111/febs.13258

Brown A, Fernandez IS, Gordiyenko Y, Ramakrishnan V (2016) Ribosome-dependent activation of stringent control. *Nature* **534**: 277–280. https://doi.org/10.1038/nature17675

Campos M, Surovtsev I V, Kato S, Paintdakhi A, Beltran B, Ebmeier SE, Jacobs-Wagner C (2014) A constant size extension drives bacterial cell size homeostasis. *Cell* **159**: 1433–1446. https://doi.org/10.1016/j.cell.2014.11.022

Le Chat L, Espéli O (2012) Let's get 'Fisical' with bacterial nucleoid. *Mol Microbiol* **86**: 1285–1290. doi:10.1111/mmi.12073.

Chien A-C, Hill NS, Levin PA (2012) Cell size control in bacteria. *Curr Biol* **22**: R340-9. https://doi.org/10.1016/j.cub.2012.02.032

Cooper S, Helmstetter CE (1968) Chromosome replication and the division cycle of *Escherichia coli* B/r. *J Mol Biol* **31**: 519–540. https://doi.org/10.1016/0022-2836(68)90425-7

Cornet F, Jacobs-Wagner C, Dobihal GS, Campos M, Irnov I, Govers SK (2018) Genomewide phenotypic analysis of growth, cell morphogenesis, and cell cycle events in *Escherichia coli*. *Mol Syst Biol* **14**: e7573. https://doi.org/10.15252/msb.20177573

Crozat E, Rousseau P, Fournes F, Cornet F (2014) The FtsK family of DNA translocases finds the ends of circles. *J Mol Microbiol Biotechnol* **24**: 396–408. https://doi.org/10.1159/000369213

Dalmais B, Bolotin A, Monnier A-F, Kanga S, Canceill D, Titok M, Ehrlich SD, Jannière L, Chapuis J, Lestini R, Chatelier E Le, Suski C (2007) Genetic evidence for a link between glycolysis and DNA replication. *PLoS One* **2**: e447. https://doi.org/10.1371/journal.pone.0000447

Deforet M, Ditmarsch D van, Xavier J Cell-size homeostasis and the incremental rule in a bacterial pathogen. *Biophys J* **109**: 521–528

Dennis PP, Ehrenberg M, Bremer H (2004) Control of rRNA Synthesis in. **68**: 639–668. https://doi.org/10.1128/MMBR.68.4.639

Do H, Yun J-S, Lee CW, Choi YJ, Kim H-Y, Kim Y-J, Park H, Chang JH, Lee JH (2015) Crystal structure and comparative sequence analysis of GmhA from *Colwellia psychrerythraea* Strain 34H provides insight into functional similarity with DiaA. *Mol Cells* **38**: 1086–1095. https://doi.org/10.14348/molcells.2015.0191

Donachie WD (1968) Relationship between cell size and time of initiation of DNA replication. *Nature* **219**: 1077–1079. https://doi.org/10.1038/2191077a0

Donachie WD, Blakely GW (2003) Coupling the initiation of chromosome replication to cell size in *Escherichia coli*. *Curr Opin Microbiol* **6**: 146–150. https://doi.org/10.1016/S1369-5274(03)00026-2

Erickson HP, Anderson DE, Osawa M (2010) FtsZ in bacterial cytokinesis: cytoskeleton and force generator all in one. *Microbiol Mol Biol Rev* **74**: 504–528. https://doi.org/10.1128/MMBR.00021-10

Erzberger JP, Pirruccello MM, Berger JM (2002) The structure of bacterial DnaA: implications for general mechanisms underlying DNA replication initiation. *EMBO J* **21**: 4763–4773. https://doi.org/10.1093/emboj/cdf496.

Flåtten I, Fossum-Raunehaug S, Taipale R, Martinsen S, Skarstad K (2015) The DnaA protein is not the limiting factor for initiation of replication in *Escherichia coli*. *PLoS Genet* **11**: 1–22. https://doi.org/10.1371/journal.pgen.1005276.

von Freiesleben U1, Krekling MA, Hansen FG, Løbner-Olesen A (2000) The eclipse period of *Escherichia coli*. *Embo J* **19**: 6240–6248. https://doi.org/10.1093/emboj/19.22.6240

Fujimitsu K, Senriuchi T, Katayama T (2009) Specific genomic sequences of E. coli promote replicational initiation by directly reactivating ADP-DnaA. *Genes Dev* **23**: 1221–1233. https://doi.org/10.1101/gad.1775809

Funnell BE (2016) ParB Partition proteins: complex formation and spreading at bacterial and plasmid centromeres. *Front Mol Biosci* **3**: 44. https://doi.org/10.3389/fmolb.2016.00044

Gralla JD (2005) *Escherichia coli* ribosomal RNA transcription: Regulatory roles for ppGpp, NTPs, architectural proteins and a polymerase-binding protein. *Mol Microbiol* **55**: 973–977. https://doi.org/10.1111/j.1365-2958.2004.04455.x

Grant MA, Ferrari U, Sclavi B, Cosentino Lagomarsino M, Bassetti B, Saggioro C (2011) DnaA and the timing of chromosome replication in *Escherichia coli* as a function of growth rate. *BMC Syst Biol* **5**: 201. https://doi.org/10.1186/1752-0509-5-201

Guarné A, Brendler T, Zhao Q, Ghirlando R, Austin S, Yang W (2005) Crystal structure of a SeqA-N filament: Implications for DNA replication and chromosome organization. *EMBO J* **24**: 1502–1511. https://doi.org/10.1038/sj.emboj.7600634

Haeusser DP, Margolin W (2016) Splitsville: Structural and functional insights into the dynamic bacterial Z ring. *Nat Rev Microbiol* **14**: 305–319. https://doi.org/10.1038/nrmicro.2016.26

Hansen FG, Atlung T (2018) The DnaA Tale. In *Front Microbiol* **9**: 319. https://doi.org/10.3389/fmicb.2018.00319

Harashima H, Dissmeyer N, Schnittger A (2013) Cell cycle control across the eukaryotic kingdom. *Trends Cell Biol* **23**: 345–356. https://doi.org/10.1016/j.tcb.2013.03.002

Harmer NJ (2010) The Structure of sedoheptulose-7-phosphate isomerase from *Burkholderia pseudomallei* reveals a zinc binding site at the heart of the active site. *J Mol Biol* **400**: 379–392. https://doi.org/10.1016/j.jmb.2010.04.058

Harris LK, Theriot JA (2016) Relative rates of surface and volume synthesis set bacterial cell size. *Cell* **165**: 1479–1492. https://doi.org/10.1016/j.cell.2016.05.045

Harris LK, Theriot JA (2018) Surface area to volume ratio: A natural variable for bacterial morphogenesis. *Trends Microbiol* **26**: 815–832. https://doi.org/10.1016/j.tim.2018.04.008

Haschemi A, Kosma P, Gille L, Evans CR, Burant CF, Starkl P, Knapp B, Haas R, Schmid JA, Jandl C, Amir S, Lubec G, Park J, Esterbauer H, Bilban M, Brizuela L, Pospisilik JA, Otterbein LE, Wagner O (2012) The sedoheptulose kinase CARKL directs macrophage polarization through control of glucose metabolism. *Cell Metab* **15**: 813–826. https://doi.org/10.1016/j.cmet.2012.04.023

Hauryliuk V, Atkinson GC, Murakami KS, Tenson T, Gerdes K (2015) Recent functional insights into the role of (p)ppGpp in bacterial physiology. *Nat Rev Microbiol* **13**: 298–309. https://doi.org/10.1038/nrmicro3448

Hill NS, Kadoya R, Chattoraj DK, Levin PA (2012) Cell size and the initiation of DNA replication in bacteria. *PLoS Genet* **8**: e1002549. https://doi.org/10.1371/journal.pgen.1002549

Hiraga S, Kanaya S, Yamazoe M, Adachi S, Ohsumi K (2004) Sequential binding of SeqA protein to nascent DNA segments at replication forks in synchronized cultures of *Escherichia coli*. *Mol Microbiol* **55**: 289–298. https://doi.org/10.1111/j.1365-2958.2004.04389.x

Ho P-Y, Amir A (2015) Simultaneous regulation of cell size and chromosome replication in bacteria. *Front Microbiol* **6**: 662. https://doi.org/10.3389/fmicb.2015.00662

Ishida T, Akimitsu N, Kashioka T, Hatano M, Kubota T, Ogata Y, Sekimizu K, Katayama T (2004) DiaA, a novel DnaA-binding protein, ensures the timely initiation of *Escherichia coli* chromosome replication. *J Biol Chem* **279**: 45546–45555. https://doi.org/10.1074/jbc.M402762200

Jameson KH, Wilkinson AJ (2017) Control of initiation of DNA replication in *Bacillus subtilis* and *Escherichia coli*. *Genes (Basel)* **8**: https://doi.org/10.3390/genes8010022

Jin DJ, Cagliero C, Zhou YN (2012) Growth rate regulation in *Escherichia coli*. *FEMS Microbiol Rev* **36**: 269–287. https://doi.org/10.1111/j.1574-6976.2011.00279.x

Joshi MC, Bourniquel A, Fisher J, Ho BT, Magnan D, Kleckner N, Bates D (2011) *Escherichia coli* sister chromosome separation includes an abrupt global transition with concomitant release of late-splitting intersister snaps. *Proc Natl Acad Sci U S A* **108**: 2765–2770. https://doi.org/10.1073/pnas.1019593108

Jun S, Levin PA, Taheri-Araghi S, Bradde S, Hill NS, Vergassola M, Paulsson J, Sauls JT (2017) Cell-size control and homeostasis in bacteria. *Curr Biol* **27**: 1392. https://doi.org/10.1016/j.cub.2017.04.028

Jun S, Wright A (2010) Entropy as the driver of chromosome segregation. *Nat Rev Microbiol* **8**: 600–607. https://doi.org/10.1038/nrmicro2391

Kasho K, Fujimitsu K, Matoba T, Oshima T, Katayama T (2014) Timely binding of IHF and Fis to DARS2 regulates ATP-DnaA production and replication initiation. *Nucleic Acids Res* **42**: 13134–13149. https://doi.org/10.1093/nar/gku1051.

Kasho K, Katayama T (2013) DnaA binding locus datA promotes DnaA-ATP hydrolysis to enable cell cycle-coordinated replication initiation. *Proc Natl Acad Sci* **110**: 936–941. https://doi.org/10.1073/pnas.1212070110

Kasho K, Tanaka H, Sakai R, Katayama T (2017) Cooperative DnaA binding to the negatively supercoiled datA locus stimulates DnaA-ATP hydrolysis. *J Biol Chem* **292**: 1251–1266. https://doi.org/10.1074/jbc.M116.762815

Katayama T (2017) Initiation of DNA replication at the chromosomal origin of *E. coli*, oriC. *Adv Exp Med Biol* **1042**: 79–98. https://doi.org/10.1007/978-981-10-6955-0_4

Kato J, Katayama T (2001) Hda, a novel DnaA-related protein, regulates the replication cycle in *Escherichia coli*. *EMBO J* **20**: 4253–4262. https://doi.org/10.1093/emboj/20.15.4253

Kawakamii H, Keyamura K, Katayama T (2005) Formation of an ATP-DnaA-specific initiation complex requires DnaA arginine 285, a conserved motif in the AAA+ protein family. *J Biol Chem* **280**: 27420–27430. https://doi.org/10.1074/jbc.M502764200

Keyamura K, Abe Y, Higashi M, Ueda T, Katayama T (2009) DiaA dynamics are coupled with changes in initial origin complexes leading to helicase loading. *J Biol Chem* **284**: 25038–25050. https://doi.org/10.1074/jbc.M109.002717

Keyamura K, Fujikawa N, Ishida T, Ozaki S, Su'etsugu M, Fujimitsu K, Kagawa W, Yokoyama S, Kurumizaka H, Katayama T (2007) The interaction of DiaA and DnaA regulates the replication cycle in *E. coli* by directly promoting ATP DnaA-specific initiation complexes. *Genes Dev* **21**: 2083–2099. https://doi.org/10.1101/gad.1561207

Klumpp S, Hwa T (2014) Bacterial growth: Global effects on gene expression, growth feedback and proteome partition. *Curr Opin Biotechnol* **28**: 96–102. https://doi.org/10.1016/j.copbio.2014.01.001

Kneidinger B, Marolda C, Graninger M, Zamyatina A, McArthur F, Kosma P, Valvano MA, Messner P (2002) Biosynthesis pathway of ADP-L-glycero-beta-D-manno-heptose in *Escherichia coli*. *J Bacteriol* **184**: 363–369

Kurokawa K, Nishida S, Emoto A, Sekimizu K, Katayama T (1999) Replication cycle-coordinated change of the adenine nucleotide-bound forms of DnaA protein in *Escherichia coli*. *EMBO J* **18**: 6642–6652. https://doi.org/10.1093/emboj/18.23.6642

Leonard AC, Grimwade JE (2015) The orisome: structure and function. *Front Microbiol* **6**: 545

Magnan D, Bates D (2015) Regulation of DNA replication initiation by chromosome structure. *J Bacteriol* **197**: 3370–3377. https://doi.org/10.1128/jb.00446-15

Magnan D, Joshi MC, Barker AK, Visser BJ, Bates D (2015) DNA replication initiation is blocked by a distant chromosome-membrane attachment. *Curr Biol* **25**: 2143–2149. https://doi.org/10.1016/j.cub.2015.06.058

Micali G, Grilli J, Marchi J, Osella M, Cosentino Lagomarsino M (2018a) Dissecting the control mechanisms for DNA replication and cell division in *E. coli*. *Cell Rep* **25**: 761–771.e4. https://doi.org/10.1016/j.celrep.2018.09.061

Micali G, Grilli J, Osella M, Lagomarsino MC (2018b) C E L L B I O L O G Y Concurrent processes set *E. coli* cell division. 1–7

Michelsen O, Teixeira de Mattos MJ, Jensen PR, Hansen FG (2003) Precise determinations of C and D periods by flow cytometry in *Escherichia coli* K-12 and B/r. *Microbiology* **149**: 1001–1010. https://doi.org/10.1099/mic.0.26058-0

Murphy H, Potrykus K, Murphy H, Philippe N, Cashel M (2010) ppGpp is the major source of growth rate control in *E-coli* ppGpp is the major source of growth rate control in *E. coli*. **13**: 563–575. https://doi.org/10.1111/j.1462-2920.2010.02357.x

Nishida S, Fujimitsu K, Sekimizu K, Ohmura T, Ueda T, Katayama T (2002) A nucleotide switch in the *Escherichia coli* DnaA protein initiates chromosomal replication: evidnece from a mutant DnaA protein defective in regulatory ATP hydrolysis *in vitro* and *in vivo*. *J Biol Chem* **277**: 14986–14995. https://doi.org/10.1074/jbc.M108303200

Ortiz C, Natale P, Cueto L, Vicente M (2016) The keepers of the ring: regulators of FtsZ assembly. *FEMS Microbiol Rev* **40**: 57–67. https://doi.org/10.1093/femsre/fuv040

Osella M, Nugent E, Cosentino Lagomarsino M (2014) Concerted control of *Escherichia coli* cell division. *Proc Natl Acad Sci* **111**: 3431–3435. https://doi.org/10.1073/pnas.1313715111

Ozaki S, Katayama T (2012) Highly organized DnaA-oriC complexes recruit the single-stranded DNA for replication initiation. *Nucleic Acids Res* **40**: 1648–1665. https://doi.org/10.1093/nar/gkr832

Potrykus K, Cashel M (2008) (p)ppGpp: Still Magical? *Annu Rev Microbiol* **62**: 35–51. https://doi.org/10.1146/annurev.micro.62.081307.162903

Rowlett VW, Margolin W (2013) The bacterial Min system. *Curr Biol* **23**: R553-6. https://doi.org/10.1016/j.cub.2013.05.024

Rowlett VW, Margolin W (2015) The bacterial divisome: ready for its close-up. *Philos Trans R Soc Lond B Biol Sci* **370**: https://doi.org/10.1098/rstb.2015.0028

Rybenkov V V, Herrera V, Petrushenko ZM, Zhao H (2014) MukBEF, a chromosomal organizer. *J Mol Microbiol Biotechnol* **24**: 371–383. https://doi.org/10.1159/000369099

Sakiyama Y, Kasho K, Noguchi Y, Kawakami H, Katayama T (2017) Regulatory dynamics in the ternary DnaA complex for initiation of chromosomal replication in *Escherichia coli*. *Nucleic Acids Res* **45**: 12354–12373. https://doi.org/10.1093/nar/gkx914

Sand O, Gingras M, Beck N, Hall C, Trun N (2003) Phenotypic characterization of overexpression or deletion of the Escherichia coli crcA, cspE and crcB genes. *Microbiology* **149**: 2107–2117. https://doi.org/10.1099/mic.0.26363-0

Saxena R, Fingland N, Patil D, Sharma AK, Crooke E (2013) Crosstalk between DnaA protein, the initiator of *Escherichia coli* chromosomal replication, and acidic phospholipids present in bacterial membranes. *Int J Mol Sci* **14**: 8517–8537. https://doi.org/10.3390/ijms14048517

Schechter M, Maaloe O, Kjeldgaard NO (1958) Dependency on medium and temperature of cell size and chemical composition during balanced grown of Salmonella typhimurium. *J Gen Microbiol* **19**: 592–606. https://doi.org/10.1099/00221287-19-3-592

Scott M, Hwa T (2011) Bacterial growth laws and their applications. *Curr Opin Biotechnol* **22**: 559–565, https://doi.org/10.1016/j.copbio.2011.04.014.

Scott M, Klumpp S, Mateescu EM, Hwa T (2014) Emergence of robust growth laws from optimal regulation of ribosome synthesis. *Mol Syst Biol* **10**: 747–747. https://doi.org/10.15252/msb.20145379

Scott M, Mateescu EM, Zhang Z, Hwa T (2010) Interdependence of cell growth origins and consequences. *Science (80-)* **330**: 1099–1102. https://doi.org/10.1126/science.1192588

Shih Y-L, Zheng M (2013) Spatial control of the cell division site by the Min system in *Escherichia coli*. *Environ Microbiol* **15**: 3229–3239. https://doi.org/10.1111/1462-2920.12119

Si F, Li D, Cox SE, Sauls JT, Azizi O, Sou C, Schwartz AB, Erickstad MJ, Jun Y, Li X, Jun S (2017) Invariance of Initiation Mass and Predictability of Cell Size in Escherichia coli. *Curr Biol* **27**: 1278–1287. https://doi.org/10.1016/j.cub.2017.03.022

Skarstad K, Steen HB, Boye E (1983) Cell cycle parameters of slowly growing *Escherichia coli* B/r studied by flow cytometry. *J Bacteriol* **154**: 656–662

Speck C, Weigel C, Messer W (1999) ATP- and ADP-dnaA protein, a molecular switch in gene regulation. *EMBO J* **18**: 6169–6176. https://doi.org/10.1093/emboj/18.21.6169

Sperber AM, Herman JK (2017) Metabolism shapes the cell. *J Bacteriol* **199**: 1–14. https://doi.org/10.1128/jb.00039-17

Srivastava N, Cadart C, Sáez PJ, Grilli J, Terriac E, Attia R, Monnier S, Cosentino-Lagomarsino M, Piel M, Baum B (2018) Size control in mammalian cells involves modulation of both growth rate and cell cycle duration. *Nat Commun* **9**: https://doi.org/10.1038/s41467-018-05393-0

Stouf M, Fisher JK, Kleckner NE, Chatzi K, White MA (2018) Coordination of growth, chromosome replication/segregation, and cell division in *E. coli*. *Front Microbiol* **9**: 1–12. https://doi.org/10.3389/fmicb.2018.01469

Szwedziak P, Wang Q, Bharat TAM, Tsim M, Lowe J (2014) Architecture of the ring formed by the tubulin homologue FtsZ in bacterial cell division. *Elife* **3**: e04601. https://doi.org/10.7554/eLife.04601

Taheri-Araghi S, Bradde S, Sauls JT, Hill NS, Levin PA, Paulsson J, Vergassola M, Jun S (2015a) Cell-size control and homeostasis in bacteria. *Curr Biol* **25**: 385–391. https://doi.org/10.1016/j.cub.2014.12.009

Taheri-Araghi S, Bradde S, Sauls JT, Hill NS, Levin PA, Paulsson J, Vergassola M, Jun S (2015b) Cell-size control and homeostasis in bacteria – Supplemental Information. *Curr Biol* **25**: 385–391. https://doi.org/10.1016/j.cub.2014.12.009

Taylor PL, Blakely KM, De Leon GP, Walker JR, McArthur F, Evdokimova E, Zhang K, Valvano MA, Wright GD, Junop MS (2008) Structure and function of sedoheptulose-7-phosphate isomerase, a critical enzyme for lipopolysaccharide biosynthesis and a target for antibiotic adjuvants. *J Biol Chem* **283**: 2835–2845. https://doi.org/10.1074/jbc.M706163200

Vadia S, Levin PA (2015) Growth rate and cell size: A re-examination of the growth law. *Curr Opin Microbiol* **24**: 96–103. https://doi.org/10.1016/j.mib.2015.01.011

Waldminghaus T, Skarstad K (2009) The *Escherichia coli* SeqA protein. *Plasmid* **61**: 141–150. https://doi.org/10.1016/j.plasmid.2009.02.004

Wallden M, Fange D, Lundius EG, Baltekin O, Elf J (2016) The synchronization of replication and division cycles in individual *E. coli* cells. *Cell* **166**: 729–739. https://doi.org/10.1016/j.cell.2016.06.052

Wang X, Llopis PM, Rudner DZ (2013) Organization and segregation of bacterial chromosomes. *Nat Rev Genet* **14**: 191–203. https://doi.org/10.1038/nrg3375

Weart RB, Lee AH, Chien AC, Haeusser DP, Hill NS, Levin PA (2007) A metabolic sensor governing cell size in bacteria. *Cell* **130**: 335–347. https://doi.org/10.1016/j.cell.2007.05.043

Węgrzyn G, Szalewska-Pałasz A, Maciąg M, Nowicki D, Janniere L (2011) Genetic response to metabolic fluctuations: correlation between central carbon metabolism and DNA replication in *Escherichia coli*. *Microb Cell Fact* **10**: 19. https://doi.org/10.1186/1475-2859-10-19

Westfall CS, Levin PA (2017) Bacterial cell size: multifactorial and multifaceted. *Annu Rev Microbiol* **71**: 499–517. https://doi.org/10.1146/annurev-micro-090816-093803

Westfall CS, Levin PA (2018) Comprehensive analysis of central carbon metabolism illuminates connections between nutrient availability, growth rate, and cell morphology in *Escherichia coli*. *PLOS Genet* **14**: e1007205

Willis L, Huang KC (2017) Sizing up the bacterial cell cycle. *Nat Rev Microbiol* **15**: 606–620. https://doi.org/10.1038/nrmicro.2017.79

Zawadzki P, Stracy M, Ginda K, Zawadzka K, Lesterlin C, Kapanidis AN, Sherratt DJ (2015) The localization and action of topoisomerase IV in *Escherichia coli* chromosome segregation is coordinated by the SMC Complex, MukBEF. *Cell Rep* **13**: 2587–2596. https://doi.org/10.1016/j.celrep.2015.11.034

Zechiedrich EL, Khodursky AB, Cozzarelli NR (1997) Topoisomerase IV, not gyrase, decatenates products of site-specific recombination in *Escherichia coli*. *Genes Dev* **11**: 2580–2592. https://doi.org/10.1101/gad.11.19.2580

Wkład autorów – oświadczenia

Uniwersytet Gdański

mgr Joanna Morcinek-Orłowska
Katedra Genetyki Molekularnej Bakterii
Wydział Biologii
Uniwersytet Gdański

Gdańsk, 26.05.2025 r.

Oświadczenie o wkładzie w publikację

Oświadczam, że mój wkład w artykuł przeglądowy:

Morcinek-Orłowska J, Galińska J, Glinkowska MK. When size matters - coordination of growth and cell cycle in bacteria. Acta Biochim Pol. 2019 Apr 10;66(2):139-146. doi: 10.18388/abp.2018_2798. PMID: 30970043.

polegał na:

- przeglądzie literatury
- opracowaniu koncepcji artykułu przeglądowego
- napisaniu wstępnej wersji manuskryptu
- wprowadzeniu poprawek do ostatecznej wersji manuskryptu
- zaplanowaniu i wykonaniu rycin
- kierowaniu projektem Preludium 12, z którego sfinansowano wydanie publikacji

Joanna Morcinek-Orłowska

Wdział Biologii
Uniwersytetu Gdańskiego
Katedra Genetyki
Molekularnej Bakterii

tel. +48 58 523 60 65
e-mail: mol.KGB@ug.edu.pl

ul. Wita Stwosza 59
80-309 Gdańsk

www.ug.edu.pl

mgr Justyna Galińska
Cebertowicza 4/32
80-809 Gdańsk
e-mail: justyna.galinska95@gmail.com

Gdańsk, 26.05.2025

Oświadczenie o wkładzie w publikację

Oświadczam, że mój wkład w artykuł przeglądowy:

Morcinek-Orłowska J, Galińska J, Glinkowska MK. When size matters - coordination of growth and cell cycle in bacteria. Acta Biochim Pol. 2019 Apr 10;66(2):139-146. doi: 10.18388/abp.2018_2798. PMID: 30970043.

polegał na:

- uczestnictwie w przeglądzie literatury i przygotowaniu bibliografii
- uczestnictwie w przygotowaniu rycin

26.05.2025
Justyna Galińska

Uniwersytet Gdański

dr hab. Monika Glinkowska, prof. UG
Katedra Genetyki Molekularnej Bakterii
Wydział Biologii
Uniwersytet Gdański

Gdańsk, 26.05.2025 r.

Oświadczenie o wkładzie w publikację

Oświadczam, że mój wkład w artykuł przeglądowy:

Morcinek-Orłowska J, Galińska J, Glinkowska MK. When size matters - coordination of growth and cell cycle in bacteria. Acta Biochim Pol. 2019 Apr 10;66(2):139-146. doi: 10.18388/abp.2018_2798. PMID: 30970043.

polegał na:

- dyskusji zawartości artykułu i przedstawionych modeli regulacyjnych
- udziale w przygotowaniu ostatecznej wersji manuskryptu
- złożeniu manuskryptu do czasopisma oraz korespondencji z Edytorem i Recenzentami

Monika Glinkowska

Wdział Biologii
Uniwersytetu Gdańskiego
Katedra Genetyki
Molekularnej Bakterii

tel. +48 58 523 60 65
e-mail: mol.KGB@ug.edu.pl

ul. Wita Stwosza 59
80-309 Gdańsk

www.ug.edu.pl

Artykuł nr 2 (praca badawcza)

Morcinek-Orłowska J., Walter B., Forquet R., Cysewski D., Carlier M., Mozolewski M., Meyer S., Glinkowska M.

Interaction networks of *Escherichia coli* replication proteins under different bacterial growth conditions.

(2023) Scientific data. Vol. 10 No. 1:788.

IF (2023) = 5,91
Punktacja MNiSW (2023) = 140

scientific data

OPEN

DATA DESCRIPTOR

Interaction networks of *Escherichia coli* replication proteins under different bacterial growth conditions

Joanna Morcinek-Orłowska[1], Beata Walter[1], Raphaël Forquet[2], Dominik Cysewski[3], Maxime Carlier[2], Michał Mozolewski[1], Sam Meyer[2] & Monika Glinkowska[1]✉

In this work we analyzed protein-protein interactions (PPIs) formed by *E. coli* replication proteins under three disparate bacterial growth conditions. The chosen conditions corresponded to fast exponential growth, slow exponential growth and growth cessation at the stationary phase. We performed affinity purification coupled with mass spectrometry (AP-MS) of chromosomally expressed proteins (DnaA, DnaB, Hda, SeqA, DiaA, DnaG, HolD, NrdB), tagged with sequential peptide affinity (SPA) tag. Composition of protein complexes was characterized using MaxQuant software. To filter out unspecific interactions, we employed double negative control system and we proposed qualitative and quantitative data analysis strategies that can facilitate hits identification in other AP-MS datasets. Our motivation to undertake this task was still insufficient understanding of molecular mechanisms coupling DNA replication to cellular growth. Previous works suggested that such control mechanisms could involve physical interactions of replication factors with metabolic or cell envelope proteins. However, the dynamic replication protein interaction network (PIN) obtained in this study can be used to characterize links between DNA replication and various cellular processes in other contexts.

Background & Summary

Bacterial cell cycle consists of concurrent and interrelated processes: cell growth, chromosomal DNA replication and segregation culminated with cell division[1]. The essential processes of the cell cycle need to be coupled to nutrients availability to ensure safe and faithful transmission of genetic material to progeny cells. Under poor nutritional conditions or in slowly growing bacterial species, subsequent cell cycle events occur linearly, similar to eucaryotic cells. However, for fast-growing bacteria, in rich media, the time needed for synthesis of the full chromosomal copy exceeds the interval between subsequent divisions. To cope with that, at high growth rates all cell cycle stages occur simultaneously and, as a result, bacterial cells contain several replicating chromosomes at different replication stages. Nevertheless, irrespective of growth rate, DNA replication in *E. coli* and many other bacterial species starts at a defined cell volume/chromosomal origin ratio. All origins of replication (*oriC*), present in the cell at that time, fire simultaneously, once per division cycle[2–4]. However, molecular mechanism behind that size-dependent control remain uncertain.

The key component of the mentioned regulatory principles is certainly the DnaA protein. Its active, ATP-bound form accumulates at the entry to replication round and initiates a sequence of events at *oriC* leading to replication complex formation. Other crucial control elements encompass the DnaA protein regulators - DiaA, Hda and SeqA, of which the two former ones make a direct interaction with the replication initiator[5].

Interestingly, multiple connections of replication control mechanisms to metabolism have been shown over the last years for bacteria with disparate cell cycle control, like *E. coli*, *Bacillus subtilis*, and *Caulobacter crescentus*[6–11]. It seems likely that those links can operate through physical interaction of the replication proteins with metabolites or metabolic enzymes and that those interactions may change under conditions supporting fast and slow

[1]Department of Bacterial Molecular Genetics, Faculty of Biology, University of Gdansk, Gdansk, 80-308, Poland. [2]Univ Lyon, Université Claude Bernard Lyon 1, INSA-Lyon, Lyon, CNRS, UMR5240 MAP, F-69622, France. [3]Mass Spectrometry Laboratory, Institute of Biochemistry and Biophysics, PAS, Warsaw 02-106, Warszawa, Poland. ✉e-mail: monika.glinkowska@ug.edu.pl

growth rates. Moreover, a connection of DNA replication control to cell envelope synthesis has been suggested by showing that SeqA interacts with the outer membrane protein fraction and this association is temporally regulated through the cell cycle[12]. This increases potential DNA replication protein interaction network beyond metabolic enzymes. Exact molecular mechanisms underlying the links between replication and the mentioned processes remain largely unknown. Uncovering changes in the replication protein interaction networks (PIN) throughout different growth conditions may therefore foster identification of particular mechanisms employed by bacterial cells to coordinate the cell cycle with nutrient availability. Moreover, DNA-related processes, like transcription, DNA repair, and modification need to be coordinated with DNA replication. Those mechanisms are essential for genome stability from one generation to another and underscore its plasticity over evolutionary time scales.

Coordination of various processes in cells often takes form of direct protein-protein interactions between proteins belonging to distinct functional modules[13]. Therefore, the potential of replication factors dynamic PINs goes beyond information on growth rate-dependent control of replication initiation, and they can be used to study other aspects of bacterial chromosome biology.

The aim of this work was to investigate the composition of protein complexes formed by the main factors involved in DNA replication in *E. coli* under three disparate growth conditions. We selected 8 bait replication proteins, including main DNA replication regulators (initiator protein DnaA, regulatory proteins DiaA, Hda and SeqA)[5]. Other baits encompassed replication complex components (DNA helicase DnaB, DNA primase DnaG, ψ subunit of DNA polymerase III HolD)[14]. We also included NrdB, a ribonuclotide reductase (RNR) subunit, the enzyme producing deoxyribonucleotides, experimentally suggested to associate with the replication complex and influencing its activity[15,16]. We have affinity-tagged the chosen bait genes at the native chromosomal positions in wild type (MG1655, K12 derivative) genetic strain, using sequential affinity purification (SPA) tag sequence[17,18]. This left them under control of their native promoters, to ensure near-endogenous levels of the replication proteins used as baits in our experiment. To assess protein-protein interactions of selected replication proteins, we used AP-MS according to the adjusted protocol published previously by Butland and coworkers[18,19], followed by the identification of purified components using MaxQuant software environment[20] (the whole experimental pipeline is depicted in Fig. 1). Replication machinery interactome was probed in the late exponential phase (OD_{600} ~ 0.6–1.0) during fast bacterial growth in rich, undefined medium (referred as LB log) and in defined synthetic medium, supporting slow growth rate, with acetate as a sole carbon source (referred as M9 0.2% ac ON); we also tested the PPI profile upon cell culture entry to stationary phase for LB-grown cultures (referred as LB ON). This way, we could subsequently compare changes within the replication proteins PPI network between fast and slow growth conditions, and after bacterial growth had ceased.

Large-scale analyses of PPI using SPA-tagged protein baits have been described before for well-known and orphan ORFs[19,21] as well as cell envelope proteins[22]. However, they all were performed in standard laboratory conditions (rich medium, stationary growth phase) and with the use of DY330 (λ-Red recombination proficient) strain whose proteome might differ from wild type *E. coli*. Our dataset provides for the first time the insight of growth-dependent PIN dynamics of DNA replication proteins in wild-type *E. coli* strain. Moreover, we applied double-control system to filter out non-specific interactions with chromatography resins and SPA-tag and provided an easy-to-use, qualitative and quantitative data processing strategies that can be reused for other AP-MS datasets.

Methods

Strains, primers, and plasmids. List of all *E. coli* strains used in this study is presented in Table 1. Plasmids and primers are listed in Tables 2 and 3, respectively. All primers used to amplify linear DNA fragment used for λ-Red recombination-mediated SPA-tag integration contain constant sequences at their 3′ ends:

F: 5′-overhang-TCCATGGAAAAGAGAAG-3′

R:5′-overhang- CATATGAATATCCTCCTTAG-3′

Thus, only variable 5′-terminal sequences (overhangs) of the primers described as 'integration' primers are presented in Table 3.

Cloning of pUC19-pIVSK was performed using restriction-free cloning procedure, as described in[23].

Bacterial cultures and media. LB Lennox medium (0.5% yeast extract, 1% tryptone, 0.5% NaCl) and M9 acetate medium (1x M9 minimal salts, 2 mM MgSO4, 0.1 mM CaCl2, 0.05% thiamine, 25 μg/ml uridine, 0.2% sodium acetate) components were purchased from either Roth GmbH or Sigma-Aldrich. All overnight cultures were grown in LB Lennox medium. If needed, ampicilin (Sigma-Aldrich) or kanamycin (Sigma-Aldrich) were added to the final concentration of 50 μg/ml.

Large-scale bacterial cultures for protein complexes purification were prepared in 2 liters of medium and inoculated with 20 ml of an overnight culture. Large-scale cultures were grown at 37 °C to late exponential phase (OD_{600} = 0.6–1.0) (in the case of LB log and M9 acetate) or to stationary phase.

Construction of SPA-tagged *E. coli* strains. All strains used for isolation of bacterial protein complexes were based on MG1655 genetic background (Table 1). SPA-tagged strains were constructed by one-step integration of linear DNA fragment containing SPA-tag sequence and kanamycin resistance cassette using λ-Red recombination method[24] (Fig. 2). DNA fragments for integration were PCR-amplified with Phusion Flash DNA polymerase (Thermo Scientific) using genomic DNA of commercial, DY330 SPA-tagged strain as template. Primers used for PCR amplification consist of 20nt sequences specific to SPA-tag-kan^R and 50nt 5′-overhangs homologous to the chromosomal regions on either side of the integration site. PCR products were column-purified, eluted with ultra-pure distilled water and used for electroporation. Electrocompetent cells were prepared of MG1655 strain harboring pKD46 plasmid, expressing the λ-Red recombination proteins under the

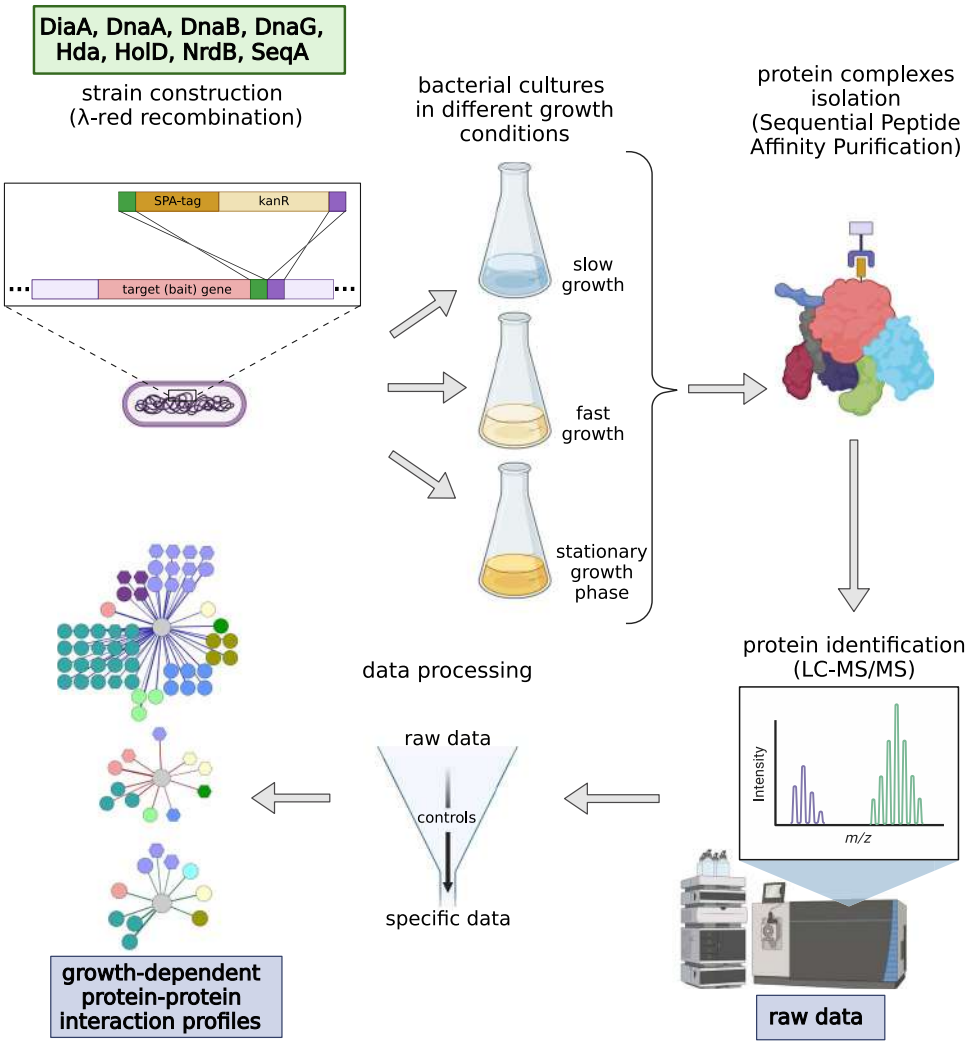

Fig. 1 Experimental pipeline of the AP-MS protein-protein interaction screen. 8 different *E. coli* strains with SPA-tagged bait proteins were cultured in three disparate growth conditions and subjected to protein complexes isolation. Isolated proteins were identified using LC-MS/MS. As a result of two distinct data processing strategies we ended up with growth-dependent PINs of *E. coli* crucial replication proteins.

control of arabinose promoter. The cells were grown in LB + amp at 30 °C to an OD_{600} of ~0.6, subsequently induced with 0.15% L-arabinose and grown for additional hour at 37 °C. Then the cells were pelleted and subjected to three rounds of washing and pelleting, twice with distilled water and once with 10% glycerol, both ice-cold. Finally, cells were concentrated 100-fold in 10% glycerol. For each transformation, 80 μl of competent cells was mixed with ~1 μg of PCR product. Electroporation was done with Eppendorf Eporator using 2500 V and 0,1 cm chambers. Electroporated cells were added to 1 ml LB, incubated for 3 h at 37 °C and spread onto LB plates with proper antibiotic. Positive transformants were PCR-verified, sequenced and subjected to FRT-FLP recombination to eliminate antibiotic resistance cassette, as described in[24].

Chromosome copy number assessment after replication runout. Wild type MG1655 strain grown in different media was subjected to rifampicin-cephalexin treatment (the whole procedure is described in details in[25]) at early exponential phase (OD_{600} ~ 0.15) to stop the following replication initiation round and cell division. As a result, bacterial cell contains the number of chromosome copies corresponding to the number of actively replicating origins at the moment of antibiotics treatment. The chromosome copy number was measured after DNA staining with Sytox green dye using BD FACS Calibur flow cytometer. We used four different media previously reported to ensure different growth rates[26], including minimal medium with acetate and LB medium (additionally supplemented with glucose), the conditions used in PPI screen presented in this work.

TEV protease expression and purification. TEV protease was overproduced in *E. coli* Rosetta (DE3) pLysS cells from pRK793 plasmid[27] in the form of an MBP fusion protein that cleaves itself *in vivo* to yield a TEV protease catalytic domain with an N-terminal His-tag and a C-terminal polyarginine tag. Overexpression was performed for 18 hours at 20 °C after addition of 1 mM isopropyl β-D-1-thiogalactopyranoside (IPTG). Cells were harvested, lysed by sonication in buffer A (50 mM Tris-HCl pH 8.0, 400 mM NaCl, 5% glycerol, 5 mM

strain	genotype	source
MG1655	K-12 F– λ– ilvG– rfb-50 rph-1	Laboratory collection
MG1655 DiaA-SPA kanR	K-12 F– λ– ilvG– rfb-50 rph-1 diaA::diaA-SPA:kanR	This study
MG1655 DnaA-SPA kanR	K-12 F– λ– ilvG– rfb-50 rph-1 dnaA::dnaA-SPA:kanR	This study
MG1655 DnaB-SPA kanR	K-12 F– λ– ilvG– rfb-50 rph-1 dnaB::dnaB-SPA:kanR	This study
MG1655 DnaG-SPA kanR	K-12 F– λ– ilvG– rfb-50 rph-1 dnaG::dnaG-SPA:kanR	This study
MG1655 Hda-SPA kanR	K-12 F– λ– ilvG– rfb-50 rph-1 hda::hda-SPA:kanR	This study
MG1655 HolD-SPA kanR	K-12 F– λ– ilvG– rfb-50 rph-1 holD::holD-SPA:kanR	This study
MG1655 NrdB-SPA kanR	K-12 F– λ– ilvG– rfb-50 rph-1 nrdB::nrdB-SPA:kanR	This study
MG1655 SeqA-SPA kanR	K-12 F– λ– ilvG– rfb-50 rph-1 seqA::seqA-SPA:kanR	This study
MG1655 DiaA-SPA FRT	K-12 F– λ– ilvG– rfb-50 rph-1 diaA::diaA-SPA:frt	This study
MG1655 DnaA-SPA FRT	K-12 F– λ– ilvG– rfb-50 rph-1 dnaA::dnaA-SPA:frt	This study
MG1655 DnaB-SPA FRT	K-12 F– λ– ilvG– rfb-50 rph-1 dnaB::dnaB-SPA:frt	This study
MG1655 DnaG-SPA FRT	K-12 F– λ– ilvG– rfb-50 rph-1 dnaG::dnaG-SPA:frt	This study
MG1655 Hda-SPA FRT	K-12 F– λ– ilvG– rfb-50 rph-1 hda::hda-SPA:frt	This study
MG1655 HolD-SPA FRT	K-12 F– λ– ilvG– rfb-50 rph-1 holD::holD-SPA:frt	This study
MG1655 NrdB-SPA FRT	K-12 F– λ– ilvG– rfb-50 rph-1 nrdB::nrdB-SPA:frt	This study
MG1655 SeqA-SPA FRT	K-12 F– λ– ilvG– rfb-50 rph-1 seqA::seqA-SPA:frt	This study
DY330 DnaA-SPA kanR	W3110 ΔlacU169 gal490 λCI857 Δ(cro-bioA) dnaA::dnaA-SPA:kanR	GE Healthcare Dharmacon
DH5a	*fhuA2 lac(del)U169 phoA glnV44 Φ80' lacZ(del)M15 gyrA96 recA1 relA1 endA1 thi-1 hsdR17*	Laboratory collection
Rosetta pLysS	F^- *ompT gal dcm lon hsdS*$_B$($r_B^-m_B^-$) λ(DE3 [*lac lacUV5-T7p07 ind1 sam7 nin5*]) [*malB*$^+$]$_{K\text{-}12}$(λ^S) pLysSRARE[*T7p20 ileX argU thrU tyrU glyT thrT argW metTleuW proL ori*$_{p15A}$](Cm^R)	Laboratory collection

Table 1. *Escherichia coli* strains used in this study.

plasmid	description	Source/reference
pUC19-pIVSK	pUC19 backbone with cloned mVenus-SPA sequence under the control of constitutive promoter placI.	This work
pKD46	Temperature-sensitive Red recombinase expression plasmid.	[24]
pCP20	Temperature-sensitive plasmid containing FLP gene to remove FRT-flanked antibiotic resistance cassette.	[24]
pRK793	Expression vector containing the gene encoding TEV protease. The induction of pRK793 with IPTG produces an MBP fusion protein that self-cleaves *in vivo* to generate a soluble His6-TEV protease.	[27]

Table 2. Plasmids used in this study.

β-mercaptoetanol, 15 mM imidazole) supplemented with 1.5 mM phenylmethanesulfonylfluoride (PMSF) and 1 tablet of Pierce™ Protease Inhibitors (Thermo Scientific, A32965). The lysate was cleared by centrifugation. The protein was purified from the soluble fraction of the lysate by Ni-affinity chromatography on a 5 ml HisTrap column (GE Healthcare) equilibrated with buffer A. The column was washed with buffer B (50 mM Tris-HCl pH 8.0, 1 M NaCl, 5% glycerol, 5 mM β-mercaptoetanol, 15 mM imidazole). Subsequently, the protein was eluted with buffer C (50 mM Tris-HCl pH 8.0, 400 mM NaCl, 5% glycerol, 5 mM β-mercaptoetanol, 500 mM imidazole) and dialyzed into buffer D (50 mM Tris-HCl pH 8.0, 200 mM NaCl, 10% glycerol, 2 mM β-mercaptoetanol). Protein concentration was estimated using NanoDrop Spectrophotometer (Thermo Scientific) at 280 nm and aliquots of purified protein were frozen in liquid nitrogen and stored at −70 °C.

Protein complexes purification. Isolation of SPA-tagged bacterial protein complexes was performed according to the detailed protocol published by Babu and coworkers[18], with several modifications, according to the scheme presented in Fig. 3. Briefly, cell pellets, harvested by centrifugation, were resuspended in 20–40 ml of sonication buffer (20 mM Tris pH 7.9, 100 mM NaCl, 0.2 mM EDTA, 10% glycerol, 0.1 mM DTT). The cell slurry was supplemented with 1 tablet of Pierce™ Protease Inhibitors (Thermo Scientific, A32965) per 50 ml of buffer and lysed by sonication. Cell debris was removed by centrifugation at 18000 rpm for 45 min. Cleared lysate was incubated with 50–75 U of Viscolase nuclease (A&A Biotechnology) for 30 min on ice. After degradation of nucleic acids, Triton X-100 was added to the lysate to the final concentration of 0.1%. The lysate was incubated with 250 μl of Sepharose® 4B-200 (Sigma-Aldrich), pretreated by washing with AFC buffer (10 mM Tris pH 7.9, 100 mM NaCl, 0.1% Triton X-100), for 1 h at 4 °C with gentle rotation (Fig. 3, step 1). This step was performed to decrease the amount of proteins sticking unspecifically to the resin. The beads were separated from the lysate, which was subsequently incubated with anti-FLAG Sepharose (Biotool, B23102), pretreated by washing with AFC buffer, for 3 h at 4 °C with gentle rotation (Fig. 3, step 2). The beads were subsequently collected by centrifugation at 4000 rpm for 15 min and transferred into mini-spin column. Beads were washed on column three times with

Primer name	sequence	description
diaA-SPAkan F	ATTGCCTGTGCGATCTGATCGATAACACGCTTTTCCCTCACCAGGATGAT	SPA-tag integration
diaA-SPAkan R	AGCGCGGAAATAAGGACTGCGATTGGCGATAATGCCTTCATGTATTCTCC	
dnaA-SPAkan F	GCCACGATATCAAAGAAGATTTTTCAAATTTAATCAGAACATTGTCATCG	
dnaA-SPAkan R	GTTGTAGCGGTTTTAATAAATGCTCACGTTCTACGGTAAATTTCATAGGT	
dnaB-SPAkan F	GTCAATGGTCGCGCTTCGACAACTATGCGGGGCCGCAGTACGACGACGAA	
dnaB-SPAkan R	GTGTTCCTTGATAAGTGTTTGCTTTAATTACCTAATTCATAAAATAATTA	
dnaG-SPAkan F	ACGAAGAACGCCTGGAGCTCTGGACATTAAACCAGGAGCTGGCGAAAAAG	
dnaG-SPAkan R	TGCGGCTGTCGGGGGCTTCCCGATCGCTCTTCGGCACTTAAGCCGTTAAA	
holD-SPAkan F	TATGGCAACAAATTTGCACATATGAACACGATTTCTTCCCTCGAAACGAC	
holD-SPAkan R	TCCACGGAAAGGCGTGGGCGCGTTGTTCAATGTGGTAAGCCGCCGGTAAA	
hda-SPAkan F	CCGCGCAACGTAAGCTGACCATTCCGTTTGTGAAAGAAATTCTGAAGTTG	
hda-SPAkan R	GCGTAGTTCGGATAAGGCGTTCGCGCCGCATCCGACAATAAACACCTTAT	
nrdB-SPAkan F	GGCAGATTGACTCGGAAGTGGACACCGACGATTTGAGTAACTTCCAGCTC	
nrdB-SPAkan R	ATCCTGGCACAGCAGTTGTGTGCCAGTGATGCGCAGGGTAACGCGGGCCA	
seqA-SPAkan F	AGTCGATGCAATTCCCGGCGGAATTGATTGAGAAGGTTTGCGGAACTATC	
seqA-SPAkan R	GGCCTGCACGATTGTGGATTGCCATTGCTTTGTCCTTTGTCTGCAACGTT	
S diaA F	TTGTTAGGGCCACAGGATGT	Recombinants screening
S diaA R	GACACTGCGTGGGTCAGTT	
S dnaA F	CTTCATGCCTGCCGTAAGAT	
S dnaA R	CGTACCGTCAGCAACCTGTA	
S dnaB F	AGGCATCGCGGAAATTATTA	
S dnaB R	ACCACCGCAACCATTTTACT	
S dnaG F	GAGCAAACCTTCACCGACTC	
S dnaG R	GCTGAAATCCAACGGTTGTT	
S holD F	ACAGTTGGCGGTTGGGTACT	
S holD R	ATTTTGCCGTTTTGCGTTA	
S hda F	TTTGAACTGCCGGAAGATGT	
S hda R	CCATCGCTAGTTGAAGCACA	
S nrdB F	GATCCCGTGGATCAACACTT	
S nrdB R	TCGCGACACTGGTACTCAAC	
S seqA F	GATGAACAAACGCTGCTGAA	
S seqA R	GTCAGTTGGGCGACGTTAAT	

Table 3. Primers used in this study.

250 µl of AFC buffer and twice with 250 µl of TEV cleavage buffer (50 mM Tris pH 7.9, 100 mM NaCl, 0.1% Triton X-100) to remove unbound proteins. 8 µl of in-house purified TEV protease (conc. ~5 mg/ml) in 250 µl of TEV cleavage buffer was added to the closed column and incubated overnight at 4 °C (Fig. 3, step 3). The next day supernatant containing cleaved proteins was collected, mixed with $CaCl_2$ to the final concentration of 1.5 mM and incubated for 3 h at 4 °C with gentle rotation with Calmodulin Sepharose (GE Healthcare, 17-0529-01), pretreated by washing with CBB buffer (10 mM Tris pH 7.9, 100 mM NaCl, 2 mM CaCl2, 0.1% Triton X-100) (Fig. 3, step 4). The protein-bound beads were transferred into a new mini-spin column, washed twice with 250 µl of CBB buffer and three times with 250 µl of CWB buffer (10 mM Tris pH 7.9, 100 mM NaCl, 0.1 mM CaCl2). Dried beads were stored at −20 °C and subjected directly to trypsin digestion prior to Liquid Chromatography coupled to tandem Mass Spectrometry (LC-MS/MS) (Fig. 3, steps 5 and 6). Each sample was prepared in three biological replicates.

Identification of proteins by LC-MS/MS. Dried beads were suspended in 50 µl of 100 mM NH4HCO3 and reduced with TCEP on a shaker at RT, alkylated with iodoacetamide in darkness for 45 min at RT on the shaker and digested overnight with 10 ng/µl trypsin. Digestion was stopped with 5%TFA to a final concentration of 0.1%, acetonitrile was added to a final concentration of 2%.

The resulting peptide mixtures were separated and measured at an online LC-MSMS setup. LC (Waters Accuity) RP-18 pre-columns (Waters), nano-UPLC RP-18 column (internal diameter: 75 µM, 250 mm long, Waters) using an acetonitrile gradient (2%–35% ACN in 180 min) in the presence of 0.1% trifluoroacetic acid at a flow rate of 250 nl/min. The column outlet was directly coupled to the ion source of an Orbitrap Elite mass spectrometer (Thermo Scientific). Measurements were conducted in positive polarity mode, with the capillary voltage set to 2.5 kV. The mass spectrometer was operated in a data-dependent mode. Higher-energy Collisional Dissociation (HCD) fragmentation was applied. Up to 10 MS/MS events were allowed per MS scan. Resolution of MS 30 000, MSMS 15 000, MS m/z range 300–2000, isolation width 3, normalized collision energy 32.0. Three blank washing runs were done between each sample to ensure the absence of cross-contamination from preceding samples. Analysis was performed at the Laboratory of Mass Spectrometry (IBB PAS, Warsaw). Data were analyzed using MaxQuant 1.6.3.4, referenced to *E. coli* proteome from UniProt database downloaded on

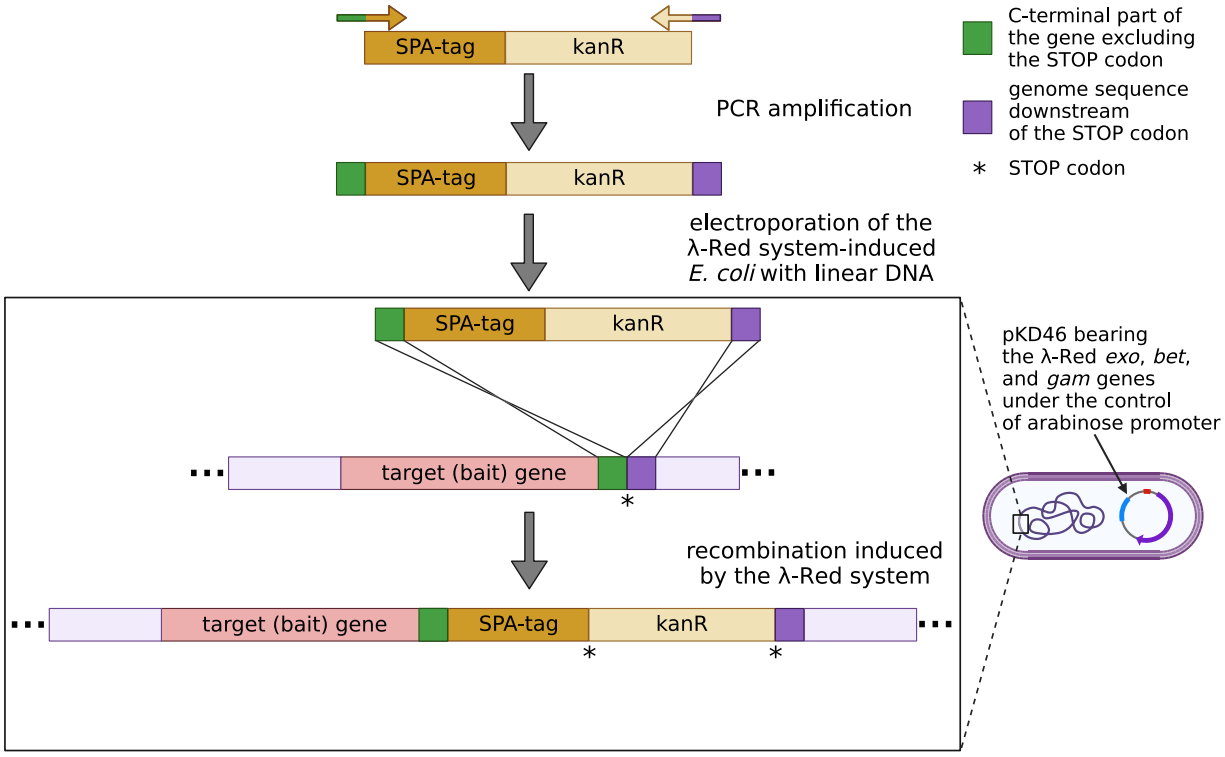

Fig. 2 Strain construction scheme for strains used in this study. DNA fragment with SPA-tag sequence and kanamycin resistance cassette was PCR-amplified using primers with overhangs specific to the chromosome integration site and electroporated into *E. coli* cells where the λ-Red system recombination genes were induced from pKD46 plasmid.

25.05.2020, 4391 entries. In total, 1600 proteins were identified (FDR 1%). The error ranges for the first and main searches were 20 ppm and 6 ppm, respectively, with 2 missed cleavages. Carbamidomethylation of cysteines was set as a fixed modification, and oxidation and protein N-terminal acetylation were selected as variable modifications for database searching. The minimum peptide length was set at 7 aa. Both peptide and protein identifications were filtered at a 1% false discovery rate and were thus not dependent on the peptide score. Enzyme specificity was set to trypsin, allowing cleavage of N-terminal proline. A 'common contaminants' database (incorporated in MaxQuant software) containing commonly occurring contaminations (keratins, trypsin etc.) was employed during MS runs.

Protein complexes - data processing. To determine unspecific interactants within our PPI screen, we included two types of control samples in our experiment. First control was based on untagged *E. coli* strain MG1655 (laboratory wild type strain), that is the genetic background of all the strains used in this study. It shows the proteins that unspecifically interact with the resins used during protein complexes isolation. Second control contains heterologous SPA-tagged protein (we used fluorescent protein mVenus) whose gene, under the control of constitutive lacI promoter, was delivered to MG1655 *E. coli* strain on high-copy plasmid pUC19-pIVSK. This control, in turn, enables to determine which proteins might unspecifically interact with the SPA-tag itself. Both control samples were subjected to the same purification procedure as the experimental ones, and were also prepared in three biological replicates.

After MaxQuant analysis, we processed the data in two distinct ways. Both processing strategies aim to filter out non-specific interactants, but the simple (qualitative) processing assumes that any protein that appears in at least one type of control should be rejected, whereas the complex (quantitative) strategy relies on intensity values and consider protein interactant as specific not only if absent in two control samples, but also if significantly more abundant in experimental than in control sample. The simple strategy uses mainly Protein List Comparator (ProLiC) in accession-based mode[28]. The complex data processing strategy, in turn, was done using custom Python script (version 3.7.6). Overall scheme of data processing is presented in Fig. 4. The detailed, consecutive steps in both types of processing are described below.

Simple (qualitative) data processing:

1. Sort intensity values from highest to lowest and keep only proteins with intensity >0
2. Prepare ProLiC input file of each sample replicate where the first column is protein accession ID, the second column is biomolecule type ('protein'), and the subsequent columns are gene name, protein description and intensity value.

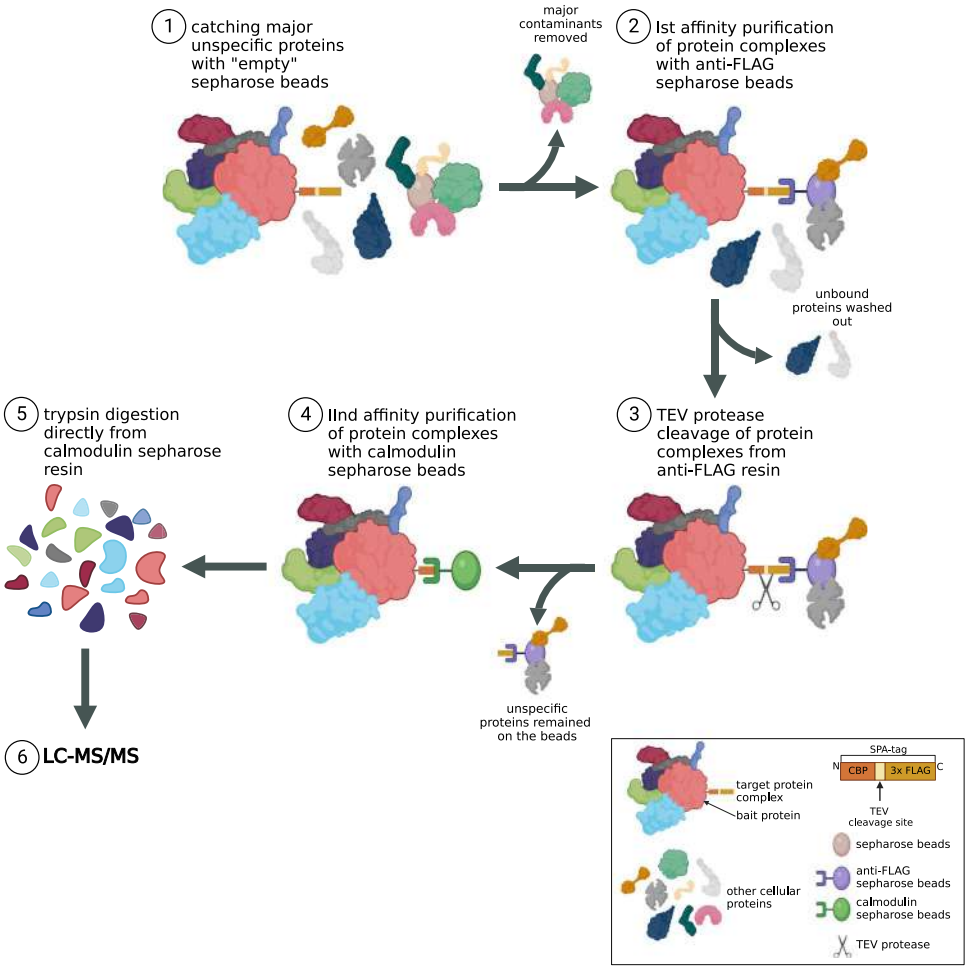

Fig. 3 Sequential Peptide Affinity (SPA) purification procedure. Soluble fraction of proteins was incubated with sepharose 4B resin to get rid of major contaminants unspecifically interacting with the beads (step 1). Protein complexes were subsequently immobilized on the anti-FLAG sepharose beads (step 2) and cleaved from the resin using TEV protease (step 3). Next, second affinity purification round with calmodulin sepharose beads was perfomed (step 4) followed by trypsin digestion directly from the resin (step 5) right before LC-MS/MS (step 6).

3. Compare three replicates of each experimental and control sample using ProLiC in accession-based mode. Keep only proteins common for all three sample replicates.
4. For each experimental and control sample of given growth condition, prepare ProLiC input file containing common-three replicates' proteins as described in step 2.
5. Compare each experimental sample from given growth condition with control 1 and control 2 using ProLiC in accession-based mode.
6. Consider protein as significant interactant if it appears only in the experimental samples and is absent in all replicates of both controls.

Complex (quantitative) data processing:

1. Normalize each protein intensity value per median intensity in the sample to reduce inter-sample variability. If intensity = 0 (protein absent in the sample replicate), replace the value with 1 (the value that gives 0 after log10 transformation).
2. Apply log10 transformation to the normalized intensity values (referred as 'intensity' in the next processing steps).
3. Calculate global variance and global standard deviation from all intensity values among all samples from given growth condition.
4. For each experimental and control sample, calculate average intensity value from three replicates of given growth condition (referred as 'av_intensity' in the next processing steps).
5. Compare each av_intensity value of experimental sample to the corresponding value of control 1. If the control av_intensity equals 0, consider protein as significant in relative to control 1 (protein absent in control 1). If not, go to the next step.

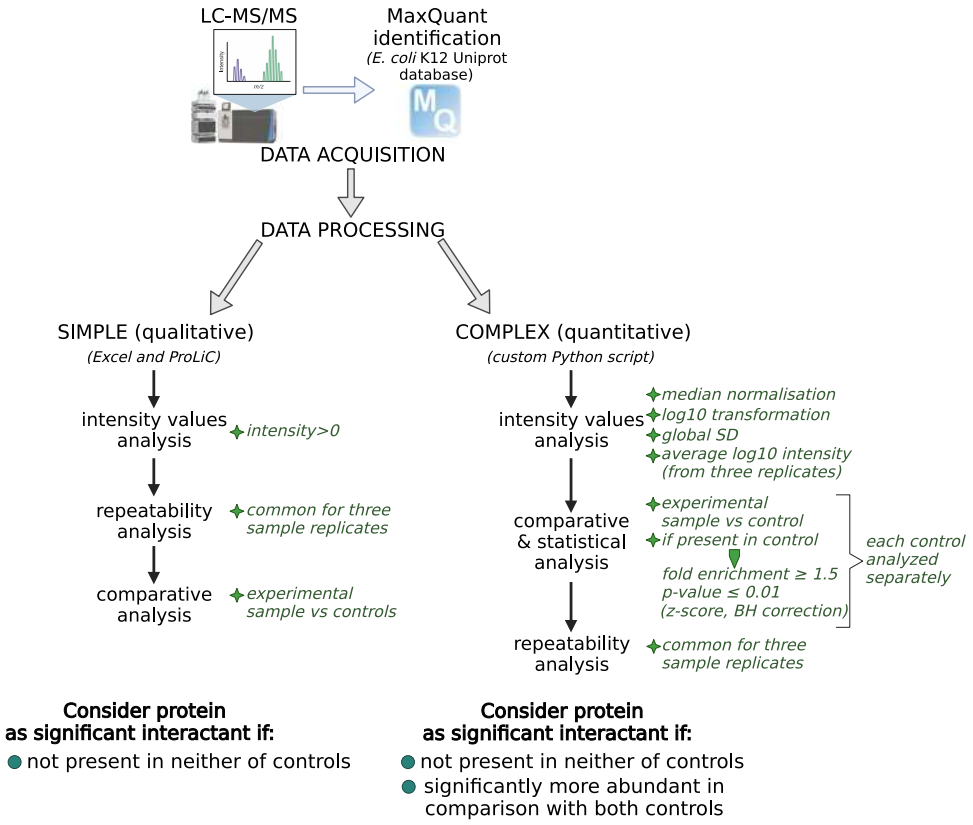

Fig. 4 Simple (qualitative) and complex (quantitative) processing strategies of raw MaxQuant data. Both strategies refer to the double control system, but the qualitative strategy is based solely on the presence/absence of interactant in both controls, whereas in the quantitative strategy the intensity values are compared between experimental and control samples, and statistical test is performed.

6. Compute the av_intensity log2 magnitude ratio between experimental and control sample. Keep only proteins with difference between control and experimental sample ≥ 1.5.
7. Assess the significance of the fold enrichment with a one-way z-score using global standard deviation. Adjust obtained p-value using Benjamini-Hochberg correction for multiple-testing. Keep only proteins with adjusted-pvalue ≤ 0.01.
8. Repeat steps 5–7 with control 2.
9. Check if proteins that meet the previous conditions are present in all three replicates of experimental sample.
10. Consider protein as significant interactant if it appears in all three experimental sample replicates and if it is absent or significantly enriched relative to both controls.

Data visualization and figures. Venn diagrams were made with a free online tool: http://bioinformatics.psb.ugent.be/webtools/Venn/. Protein interaction networks were analyzed and visualized using Cytoscape ver. 3.8.2. Volcano plots were made using VolcanoseR tool: https://goedhart.shinyapps.io/VolcaNoseR/. All Figures from the manuscript were prepared using https://biorender.com.

Data Records

The organization of our deposited data is depicted in Fig. 5. Briefly, as a result of MaxQuant identification of raw MS data, the raw MaxQuant protein lists were generated; these files served as input files to perform qualitative and quantitative data processing strategy. Raw MS data were deposited in Pride Repository under an entry PXD030113[29]. MaxQuant data (input files for our processing strategy), as well as quantitatively and qualitatively processed data, were deposited as protein lists in Excel files at Figshare Repository[30–32]. The coding of data samples included in this work is presented in Table 4 (short version containing MaxQuant datafiles' names) and Supplementary Table 1 (full version including corresponding raw MS datafiles' names).

Processed data are deposited as excel files containing protein lists along with the basic protein information such as ID, gene and protein name. Both data processing strategies contains 8 Excel files (one separate file for each bait protein), each with 3 sheets containing identified interactants for different growth conditions. Datafiles of each processing strategy are provided with metadata file, with the meaning of every column and a brief instruction about the table contents. Depending on the processing strategy, additional parameters included in

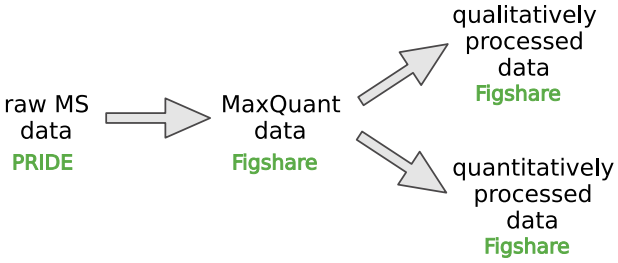

Fig. 5 A scheme depicting organization of raw MS data and processed data on PPI interactions between different files.

sample type (experimental(E)/control(C)): bait protein	growth condition		
	LB log	LB O/N	M9 0.2% ac O/N
E:**DiaA**	E1; I4; X6	I5; P1; X7	I6; T3; X5
E:**DnaA**	F2; U6; U7	F1; P2; X12	E3; I7; X11
E:**DnaB**	G4; W3; W4	G6; W5; W6	G2; W1; W2
E:**DnaG**	H1; J5; U9	C7; F6; H2	F7; H3; X15
E:**Hda**	C5; U8; X9	C6; P3; X10	I3; T4; X8
E:**HolD**	U1; U2; U3	F8; U11; X4	X1; X2; X3
E:**NrdB**	W7; W8; W9	F10; J4; U13	F9; J3; T10
E:**SeqA**	F4; X13; X14	F3; P4; U12	F5; T1; T2
C: MG1655 (**TYPE 1 CONTROL**)	T7; T8; T9	P5; U10; X17	T5; T6; X16
C:MG1655 (placI)mVenus-SPA-pUC19 (**TYPE 2 CONTROL**)	S1; S2; S3	O9; R4; R5	R1; R2; R3

Table 4. MaxQuant data sample coding.

the datafiles are different. In case of complex (quantitative) data processing[31], all calculations on the intensity value are present in the datafile as well as the statistical test's p-value and difference between the samples and both controls. Even though we did not consider intensity values during qualitative processing strategy[32], we have decided to leave the normalized intensity value also in the qualitatively processed datafiles to give the user an opportunity to sort and compare the data between samples if needed.

All Figures, tables and Appendix files were also uploaded to Figshare Repository[33]

Technical Validation

Experimental setup and data processing strategies. To assess if growth conditions chosen for the PPI screen indeed ensure different growth rates and replication frequency, changes in the bacterial cell cycle were confirmed using flow cytometry measurement of chromosome copy number after replication run-out. As expected, bacterial cells grown in LB medium exhibit overlapping replication cycles indicated by populations of 8 and 16 chromosome copies. In turn, growth in minimal medium supplemented with sodium acetate resulted in populations containing 1 or 2 copies of chromosomes, that is non-overlapping replication rounds (Supplementary Figure 1)[26]. Additionally, we tested growth rates of all constructed SPA-tagged strains in both microbial media used for our PPI screen and found no considerable differences from the wild-type strain, indicating that addition of the SPA-tag did not interfere considerably with strain physiology (Figs. 6 and 7 and Appendix files 1 and 2)[33].

Affinity-directed proteomics is often strongly biased with false-positive results. Proteins may interact unspecifically with affinity tags and chromatography resins used during isolation process which obscures subsequent identification of true interactants. This issue is partially solved during sequential purification procedure: pre-incubation with empty resin and cutting protein complexes after the first affinity binding with sequence-specific TEV protease should decrease the amount of unspecific proteins remained in subsequent steps (see Fig. 3). We also tested that the TEV protease batch used cleaved the bulk bait protein off the anti-FLAG resin (Supplementary Figure 2).

However, the level of unspecific interactants identified after MS is still significantly high, therefore, efficient system to separate the wheat from the chaff needs to be developed. To tackle this problem, we performed two types of control experiments. The first involved an untagged wild type strain (MG1655 *E. coli* strain – genetic background in our experiments) and the second - the wild type strain expressing a SPA-tagged fluorescent Venus protein from plasmid. Both types of control samples (in triplicates) were grown under identical conditions to those used for the strains expressing the tagged bait proteins and were subsequently subjected to identical purification procedure. In the first case, the control experiment enabled correction for proteins attaching unspecifically to the resins, in the second – for proteins binding to a random SPA-tagged protein or SPA-tag itself. The use of the two control types delimits abundance range of a protein that binds unspecifically, dependent on resin occupancy by a bait protein. Specifically, we made a presumption that the level of proteins binding unspecifically to the resin will be lower when the amount of bait protein and its interactants is high and thus, the resin beads

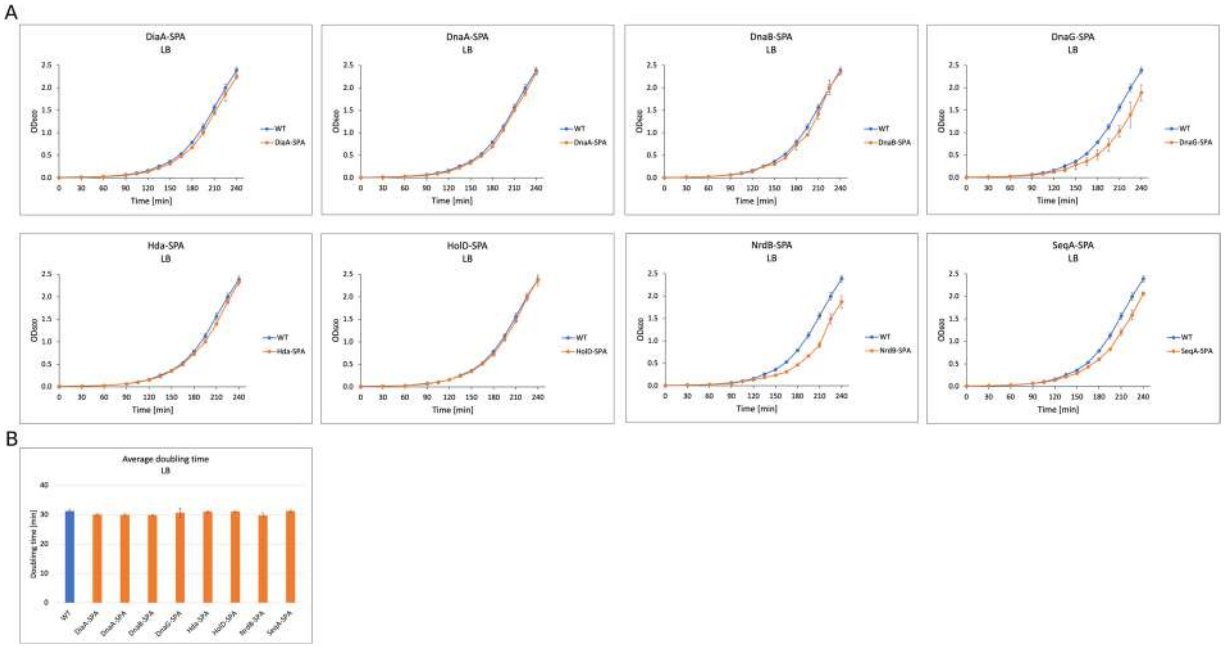

Fig. 6 Growth curves and generation time comparison for the wild type and SPA-tagged strains used in this study growing in LB medium.

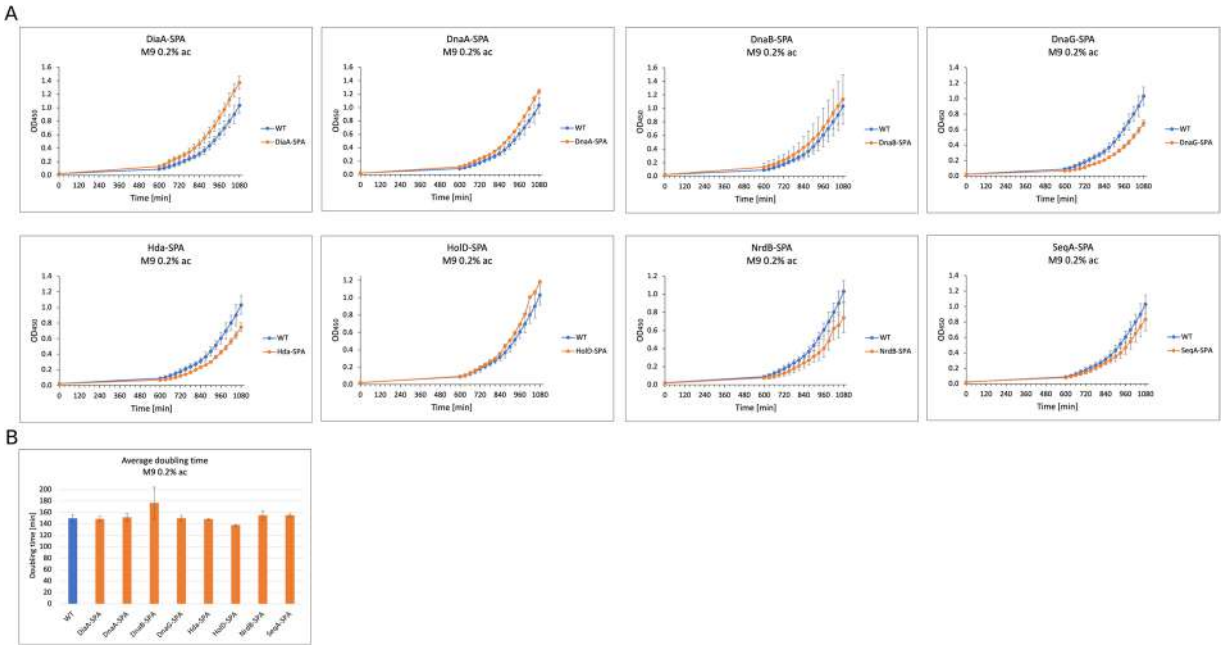

Fig. 7 Growth curves and generation time comparison for the wild type and SPA-tagged strains used in this study growing in M9 + 0.2% acetate medium.

are more occupied. The differences between resin occupancy among different bait proteins may result from different native protein expression levels as well as various tag surface exposition on the natively folded proteins.

Using very restrictive criteria for hits identification, the presence of a protein in at least one of the controls described above should disqualify it as a true-positive interactant. However, considering that MS is a sensitive technique, not every protein forming an interaction with the resins or SPA-tag itself should be automatically accounted for as a false-positive as long as it has been identified in significantly higher amount in experimental sample containing tagged bait protein. Therefore, we present the data processed with the same control samples, but using two different strategies, described in details in Methods section. Simple (qualitative) strategy is based only on the presence of protein hits in control samples, regardless of their intensity values, whereas complex (quantitative) strategy allows to calculate protein intensity enrichment value and assess its statistical

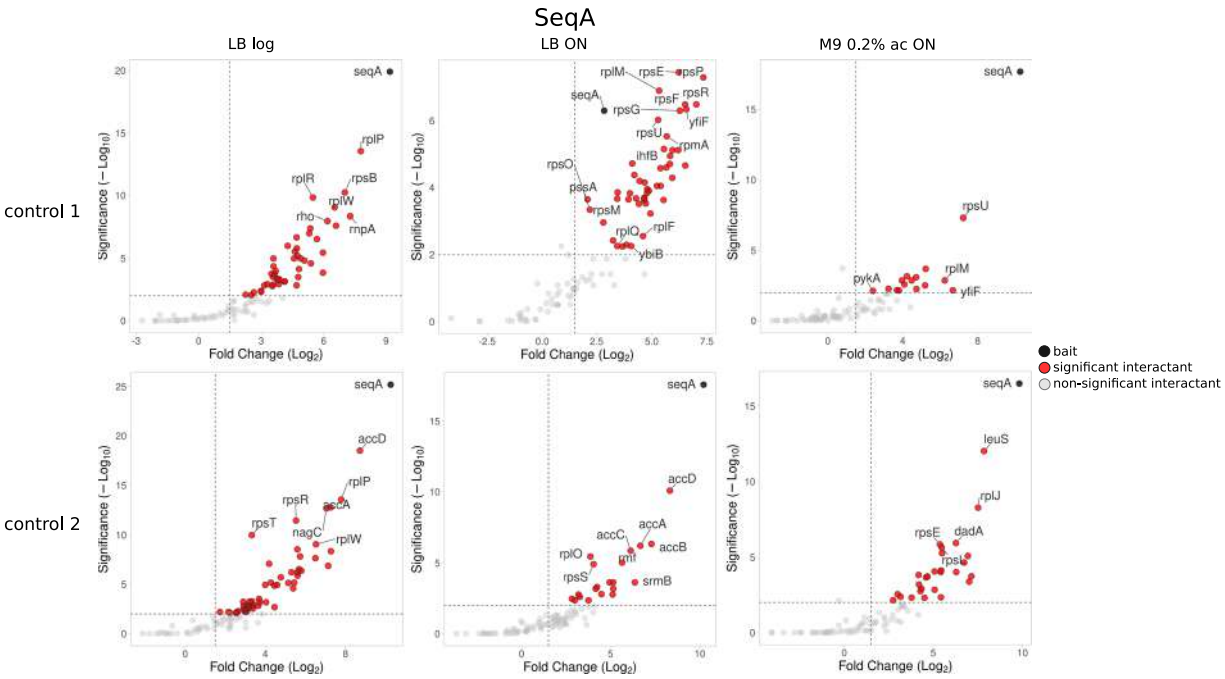

Fig. 8 Volcano plots depicting enrichment and statistical significance of uncovered interactions for one of the bait proteins - SeqA.

significance (Fig. 4). We also validated that the bait protein was in each case the most highly enriched one (Fig. 8, Supplementary Fig. 3A-G).

Data reproducibility. As a result of MaxQuant analysis (referenced to *E. coli* proteome from UniProt database containing 4391 different protein IDs), 1596 different protein IDs were identified within all the samples used for searching (FDR 1%)[29]. Depending on the growth condition, the average numbers of identified protein IDs in the samples (including experimental and control ones) were as follows: 250 (LB log), 212 (M9 0.2% ac ON) and 248 (LB ON). The bait protein intensity across different growth conditions was similar (Supplementary Figure 4). The data reproducibility between three sample replicates is presented on Venn diagrams (Fig. 9 and Appendix file 3)[33]. Protein IDs that appeared in all three replicates constituted 10.8–42.7% of all different protein IDs for a given bait. For downstream data processing we included only proteins that appeared in all three sample replicates. In qualitative processing strategy[32], we compared common-three replicates protein set of experimental and control samples. In turn, in quantitative strategy[31], we performed statistic tests for every common-three-replicates protein hit that appeared in at least one replicate of the control samples (Fig. 4). Statistic tests were performed separately for each control, and we further considered as hits only the interactions that were statistically significant with respect to both control types as well as preys that did not appear in any of the controls.

Importantly, the analysis of quantitatively processed data revealed that the set of interactants for every bait used in our screen changed drastically with growth conditions (Fig. 10). In general, the highest number of significant interactions was observed in samples obtained from bacteria during their exponential growth in rich medium, whereas the smallest – in samples grown in minimal medium with acetate. This difference in significant prey number can only partially be attributed to bait abundance in samples from different growth conditions (Supplementary Figure 4) since the intensity level of identified bait protein in different growth conditions is similar. Moreover, each of the queried replication proteins forms a unique constellation of contacts with the rest of the proteome with only small overlaps between baits (Fig. 11).

Data reliability. Our data confirmed previously found, well-known interactions between complex components of several replication proteins, namely these formed by DNA polymerase III subunits, ribonucleotide reductase complex or between Hda and β sliding clamp of DNA polymerase III[14,34,35]. These are stable complexes that were isolated under all tested conditions. Our results also recapitulated the interactions described previously as spatiotemporally regulated during the cell cycle (DnaB-DnaC, DiaA-DnaA, HolD-Ssb, topoisomerase III-HolD)[14,36,37] or performing special function, *i.e.* replication through highly transcribed regions (DnaB-Rep)[38]. These results confirm that the approach we used accurately identifies different types of complexes formed by the selected replication proteins.

Usage Notes

Navigating and visualizing the data. The goal of protein-protein interaction screens is often to determine which cellular processes are connected between each other. To test that, GO enrichment analysis are often performed. However, they are usually used to make specific conclusions rather than to organize the data. Here, we manually classified identified prey proteins into 10 functional categories (Table 5) to make navigating the data

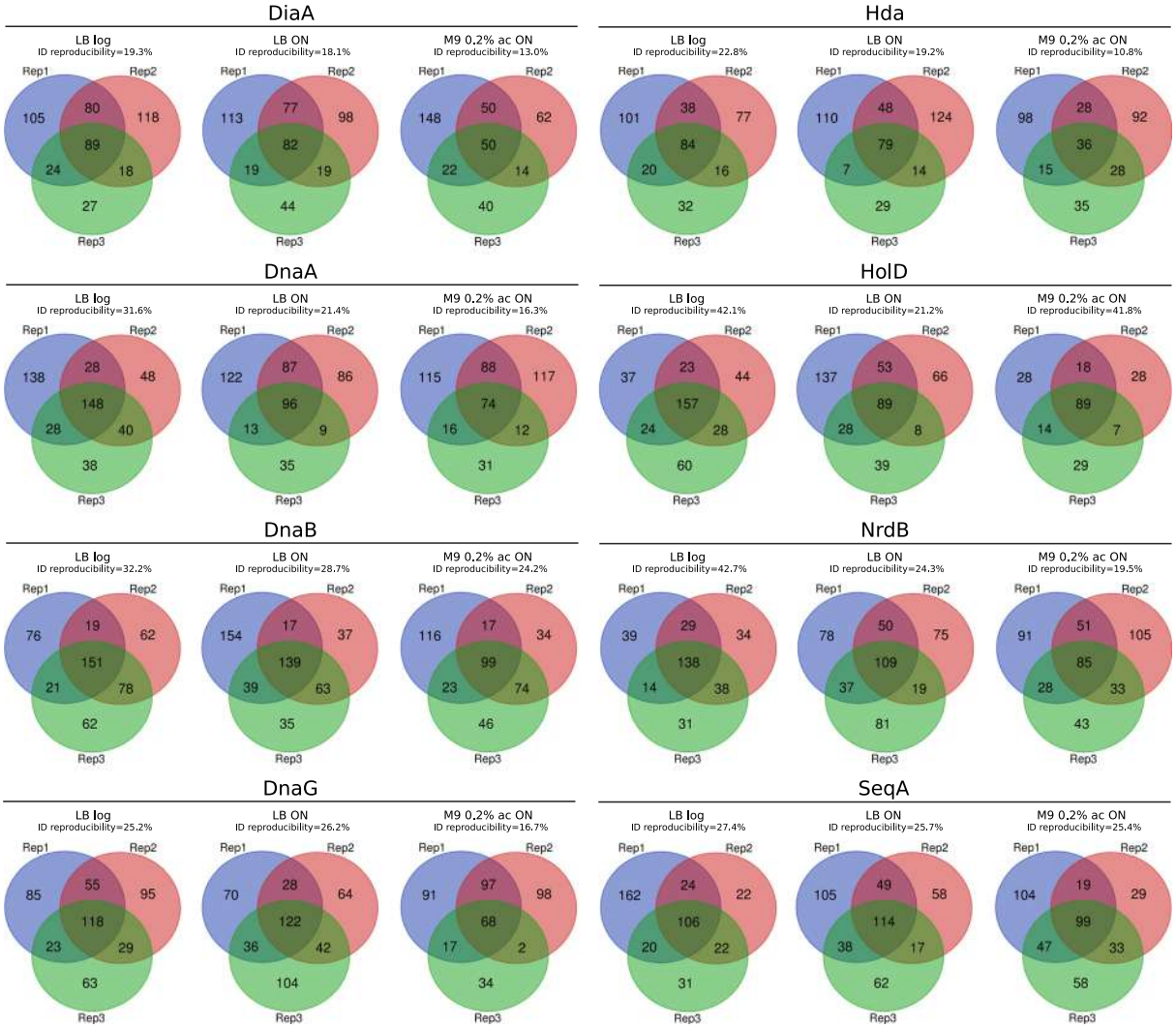

Fig. 9 Venn diagrams presenting the protein IDs overlap between three experimental replicates for each bait protein.

easier and let the user focus only on particular protein subgroups or notice the functional connections between replication and other processes, which can be an initial step for further functional studies. We are perfectly aware that such a classification is in many cases arbitral and might not reflect all the functions of proteins involved in different cellular processes (*i. e.* moonlighting enzymes), but anyway it may be useful when looking at the data from a wider perspective.

Apart from uploading the datafiles containing protein lists, we visualized our data as PINs (Supplementary Figure 5A-H). Basically, manually made functional categories were used to arrange the PIN layout. Proteins belonging to each category were given different node colour as presented on the example network in Supplementary Figure 6; significantly enriched preys were distinguished from preys absent in both controls by node shape. Each of three tested growth conditions has different edge colour, in case of quantitatively processed data the edge width reflects the fold enrichment value with control 2 (heterologous SPA-tagged protein). Thus, by looking at the network, the user will find numerous information about the protein-protein interactions. PINs of quantitatively and qualitatively processed data are deposited in the NDEX project (links below) in the interactive form, with every parameter easily accessible:

https://www.ndexbio.org/#/networkset/4555289d-18d6-11ed-ac45-0ac135e8bacf?accesskey=2986992b747495b613f833709fe92d5dce65cdf9c731b0b0a56af07ef01e023e

https://www.ndexbio.org/#/networkset/53cc0577-196e-11ed-ac45-0ac135e8bacf?accesskey=d136944dff0a03b5effb16643f21d07ab33d8d3e4bfad1f16a190d3d13959144

Reusing the data. In this work we present AP-MS dataset processed in two distinct ways. According to the established criteria, different proteins might be considered as specific interactants. Thus, one can reprocessed the data using different criteria. For example, in the case of qualitative data processing protein hits that appeared in at least two out of three replicates might also be considered. In the case of quantitative data processing, in turn, less

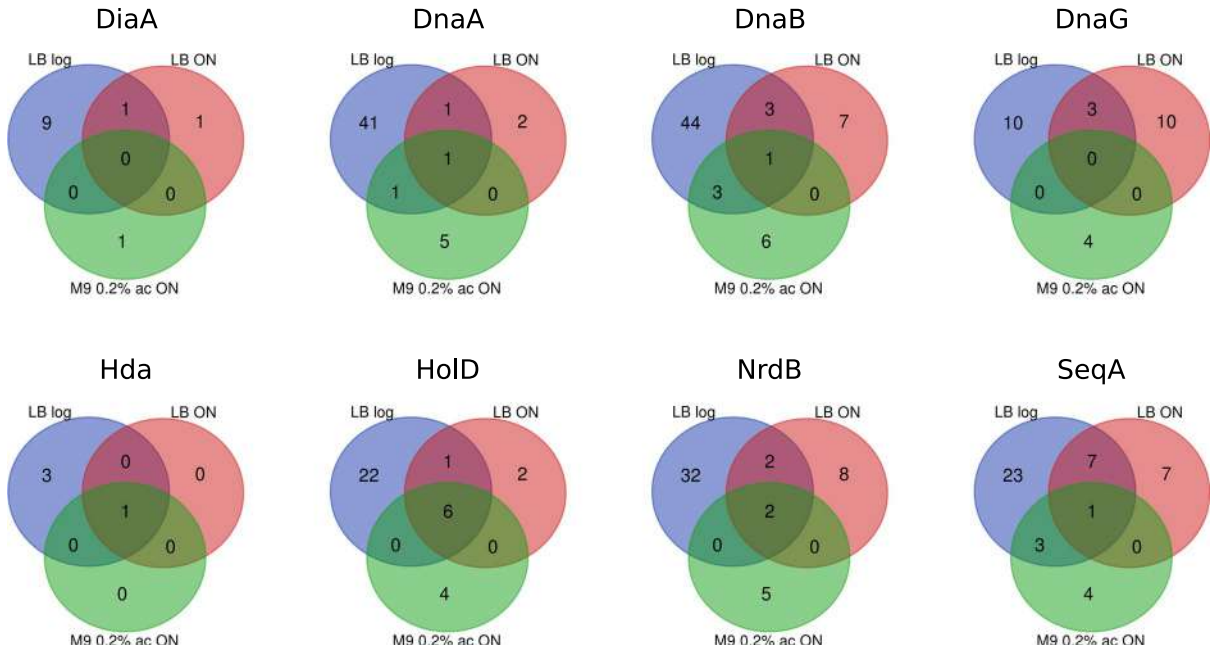

Fig. 10 Venn diagrams presenting the protein IDs overlap between three growth conditions for each bait protein (quantitative data processing).

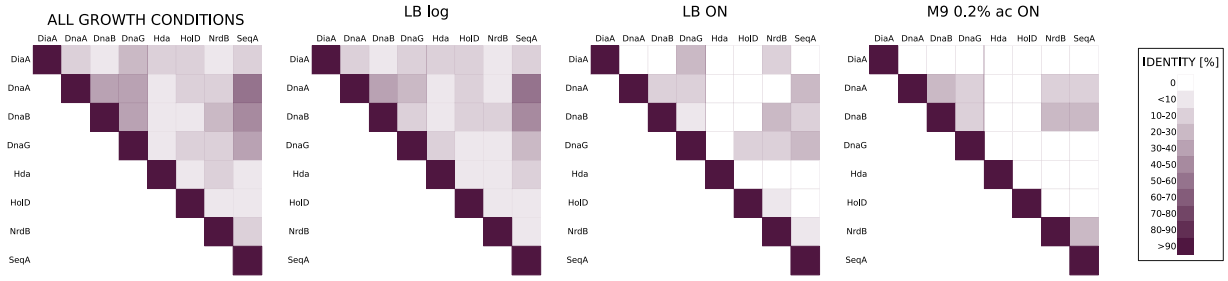

Fig. 11 Pairwise comparison of uncovered interaction profiles of 8 baits used in this work (quantitative data processing). Similarity matrices were made based on comparison of interaction profiles between each of 8 bait proteins used in PPI screen ('each with each' comparison). Percent of the same interactants between compared baits was calculated and this value was weighted-averaged to the number of all interactants identified in our PPI screen.

protein functional category	description
UNCHARACTERIZED/ORPHAN PROTEINS	proteins of undefined GO terms or uncharacterized biological function (experimentally)/orphan proteins
TRANSCRIPTION CONTROL PROTEINS	RNA polymerase subunits and transcription factors/transcription factors
RNA PROCESSING PROTEINS	RNA processing proteins (RNAses, proteins involved in RNA metabolism and modification, degradosome
RIBOSOMAL & TRANSLATION PROTEINS	ribosome biogenesis, ribosome subunits proteins, aa-tRNA ligases, translation proteins/ribosomal and translation proteins, rRNA/tRNA modifying proteins
METABOLIC & TRANSPORT PROTEINS	metabolic enzymes, transport proteins, secretion proteins, post-translational modification enzymes
CELL ENVELOPE PROTEINS	cell envelope proteins (proteins involved in synthesis/transport of cell membrane/cell wall components, membrane proteins)
DNA ARCHITECTURE/STRUCTURE PROTEINS	DNA binding proteins (not connected with transcription or not characterized), topoisomerases
DNA REPLICATION PROTEINS	DNA polymerase subunits, replication regulatory proteins, ssb protein
CHROMOSOME SEGREGATION & CELL DIVISION PROTEINS	FtsZ ring assembly proteins, FtsZ positioning system, chromosome segregation proteins
STRESS & STARVATION RESPONSE PROTEINS	DNA recombination, DNA recombinational repair, DNA repair, prophage integration, chaperone proteins, stres response, heat/cold/pH/starvation response proteins, DNA damage response, stringent response, SOS reponse etc.

Table 5. Custom functional categories of prey proteins used in this study.

restrictive (*i. e*. 0.05) p-value or different fold enrichment threshold may be chosen. Obviously, the user can also take the raw MaxQuant data[29] and process it in a totally different way.

The double-control system design as well as processing strategies presented in this work can be used with the data generated from other C-terminal SPA-tag *E. coli* strains of different genetic backgrounds as well as in other AP-MS datasets identified using MaxQuant environment. Complex data processing presented here may constitute a cheaper and easier alternative to quantitative AP-MS methods using isotope labelling.

Code availability

The code used to assess significance of the interactions was deposited under the following link: https://github.com/MaximeCarlier12/Interactome_proteins_ecoli.

The MIT license is available at: https://github.com/MaximeCarlier12/Interactome_proteins_ecoli/blob/master/LICENSE.

Received: 13 January 2023; Accepted: 30 October 2023;
Published online: 10 November 2023

References

1. Reyes-Lamothe, R. & Sherratt, D. J. The bacterial cell cycle, chromosome inheritance and cell growth. *Nat. Rev. Microbiol.* **17**, 467–478 (2019).
2. Si, F. *et al*. Invariance of Initiation Mass and Predictability of Cell Size in Escherichia coli. *Current Biology* **27**, 1278–1287 (2017).
3. Donachie, W. D. Relationship between cell size and time of initiation of DNA replication. *Nature* **219**, 1077–9 (1968).
4. Wallden, M., Fange, D., Lundius, E. G., Baltekin, O. & Elf, J. The synchronization of replication and division cycles in individual *E. coli* cells. *Cell* **166**, 729–739.
5. Katayama, T. Initiation of DNA Replication at the Chromosomal Origin of E. coli, oriC. *Adv. Exp. Med. Biol.* **1042**, 79–98 (2017).
6. Maciag-Dorszyńska, M., Ignatowska, M., Jannière, L., Wegrzyn, G. & Szalewska-Pałasz, A. Mutations in central carbon metabolism genes suppress defects in nucleoid position and cell division of replication mutants in Escherichia coli. *Gene* **503**, 31–35 (2012).
7. Nouri, H. *et al*. Multiple links connect central carbon metabolism to DNA replication initiation and elongation in Bacillus subtilis. *DNA Res.* **25**, 641–653 (2018).
8. Frandi, A. & Collier, J. Multilayered control of chromosome replication in Caulobacter crescentus. *Biochem. Soc. Trans.* **47**, 187–196 (2019).
9. Maciąg, M., Nowicki, D., Janniere, L., Szalewska-Pałasz, A. & Węgrzyn, G. Genetic response to metabolic fluctuations: correlation between central carbon metabolism and DNA replication in Escherichia coli. *Microb. Cell Fact.* **10**, 19 (2011).
10. Horemans, S. *et al*. Pyruvate kinase, a metabolic sensor powering glycolysis, drives the metabolic control of DNA replication. *BMC Biol.* **20**, 87 (2022).
11. Beaufay, F., Coppine, J. & Hallez, R. When the metabolism meets the cell cycle in bacteria. *Curr. Opin. Microbiol.* **60**, 104–113 (2021).
12. d'Alençon, E., Taghbalout, A., Kern, R. & Kohiyama, M. Replication cycle dependent association of SeqA to the outer membrane fraction of E. coli. *Biochimie* **81**, 841–846 (1999).
13. Typas, A. & Sourjik, V. Bacterial protein networks: Properties and functions. *Nat. Rev. Microbiol.* **13**, 559–572 (2015).
14. Schaeffer, P. M., Headlam, M. J. & Dixon, N. E. Protein-protein interactions in the eubacterial replisome. *IUBMB Life* **57**, 5–12 (2005).
15. Sánchez-Romero, M. A., Molina, F. & Jiménez-Sánchez, A. Organization of ribonucleoside diphosphate reductase during multifork chromosome replication in Escherichia coli. *Microbiology (N Y)* **157**, 2220–2225 (2011).
16. Ge, Z. *et al*. Manipulating the Bacterial Cell Cycle and Cell Size by Titrating the Expression of Ribonucleotide Reductase. *mBio* **8**, 6–11 (2017).
17. Zeghouf, M. *et al*. Sequential Peptide Affinity (SPA) System for the Identification of Mammalian and Bacterial Protein Complexes. *J. Proteome Res.* **3**, 463–468 (2004).
18. Babu, M. *et al*. Sequential peptide affinity purification system for the systematic isolation and identification of protein complexes from Escherichia coli. *Methods Mol. Biol.* **564**, 373–400 (2009).
19. Butland, G. *et al*. Interaction network containing conserved and essential protein complexes in Escherichia coli. *Nature* **433**, 531–537 (2005).
20. Cox, J. & Mann, M. MaxQuant enables high peptide identification rates, individualized p.p.b.-range mass accuracies and proteome-wide protein quantification. *Nat. Biotechnol.* **26**, 1367–1372 (2008).
21. Hu, P. *et al*. Global Functional Atlas of *Escherichia coli* Encompassing Previously Uncharacterized Proteins. *PLoS Biol.* **7**, 0929–0947 (2009).
22. Babu, M. *et al*. Genetic interaction maps in *Escherichia coli* reveal functional crosstalk among cell envelope biogenesis pathways. *PLoS Genet*. **7** (2011).
23. van den Ent, F. & Lowe, J. RF cloning: a restriction-free method for inserting target genes into plasmids. *J. Biochem. Biophys. Methods* **67**, 67–74 (2006).
24. Datsenko, K. A. & Wanner, B. L. One-step inactivation of chromosomal genes in *Escherichia coli* K-12 using PCR products. *Proc. Natl. Acad. Sci. USA* **97**, 6640–5 (2000).
25. Hawkins, M., Atkinson, J. & McGlynn, P. *Escherichia coli* Chromosome Copy Number Measurement Using Flow Cytometry Analysis. *Methods Mol. Biol.* **1431**, 151–159 (2016).
26. Stokke, C., Flåtten, I. & Skarstad, K. An easy-to-use simulation program demonstrates variations in bacterial cell cycle parameters depending on medium and temperature. *PLoS One* **7**, e30981 (2012).
27. Kapust, R. B. *et al*. Tobacco etch virus protease: mechanism of autolysis and rational design of stable mutants with wild-type catalytic proficiency. *Protein Engineering, Design and Selection* **14**, 993–1000 (2001).
28. Turewicz, M. *et al*. BioInfra.Prot: A comprehensive proteomics workflow including data standardization, protein inference, expression analysis and data publication. *J. Biotechnol.* **261**, 116–125 (2017).
29. Cysewski, D. & Glinkowska, M. *PRIDE*. https://identifiers.org/pride.project:PXD030113 (2022).
30. Morcinek-Orłowska, J. MaxQuant data. *Figshare* https://doi.org/10.6084/m9.figshare.24055632.v1 (2023).
31. Morcinek-Orłowska, J. Quantitative data processing, 20230829. *Figshare* https://doi.org/10.6084/m9.figshare.24050925.v1 (2023).
32. Morcinek-Orłowska, J. Qualitative data processing, 20230829. *Figshare* https://doi.org/10.6084/m9.figshare.24055629.v1 (2023).
33. Morcinek-Orlowska, J. Scientific data PPI article content, 20230830. *Figshare* https://doi.org/10.6084/m9.figshare.24061275.v1 (2023).
34. Kolberg, M., Strand, K. R., Graff, P. & Andersson, K. K. Structure, function, and mechanism of ribonucleotide reductases. *Biochim. Biophys. Acta* **1699**, 1–34 (2004).
35. Kurz, M., Dalrymple, B., Wijffels, G. & Kongsuwan, K. Interaction of the sliding clamp beta-subunit and Hda, a DnaA-related protein. *J. Bacteriol.* **186**, 3508–3515 (2004).

36. Lee, C. M., Wang, G., Pertsinidis, A. & Marians, K. J. Topoisomerase III acts at the replication fork to remove precatenanes. *J. Bacteriol.* **201**, 1–13 (2019).
37. Higashi, M., Katayama, T., Abe, Y., Keyamura, K. & Ueda, T. DiaA Dynamics Are Coupled with Changes in Initial Origin Complexes Leading to Helicase Loading. *Journal of Biological Chemistry* **284**, 25038–25050 (2009).
38. Guy, C. P. *et al*. Rep provides a second motor at the replisome to promote duplication of protein-bound DNA. *Mol. Cell* **36**, 654–666 (2009).

Acknowledgements

This work was supported by National Science Center (Poland) UMO-2014/13/B/NZ2/01139 (M.G.) and UMO-2016/23/N/NZ2/02378 (J.M-O).

Author contributions

Joanna Morcinek-Orłowska: performed the experiments, analysed and visualised the data, wrote the manuscript, obtained funding. Beata Walter: performed some of the experiments, revised the manuscript. Raphaël Forquet: analysed the data, contributed to manuscript writing, revised the manuscript. Dominik Cysewski: performed MS and MaxQuant analysis, contributed to manuscript writing. Maxime Carlier: analysed the data, wrote the code, contributed to manuscript writing. Michał Mozolewski: prepared part of the data for the initial manuscript and the revision. Sam Meyer: planned data analysis strategy. Monika Glinkowska: planned and supervised the research, obtained funding, wrote the manuscript.

Competing interests

The authors declare no competing interests.

Additional information

Supplementary information The online version contains supplementary material available at https://doi.org/10.1038/s41597-023-02710-1.

Correspondence and requests for materials should be addressed to M.G.

Reprints and permissions information is available at www.nature.com/reprints.

Publisher's note Springer Nature remains neutral with regard to jurisdictional claims in published maps and institutional affiliations.

Suplement

Interaction networks of *Escherichia coli* replication proteins under different bacterial growth conditions

Supplementary information

Table of contents:

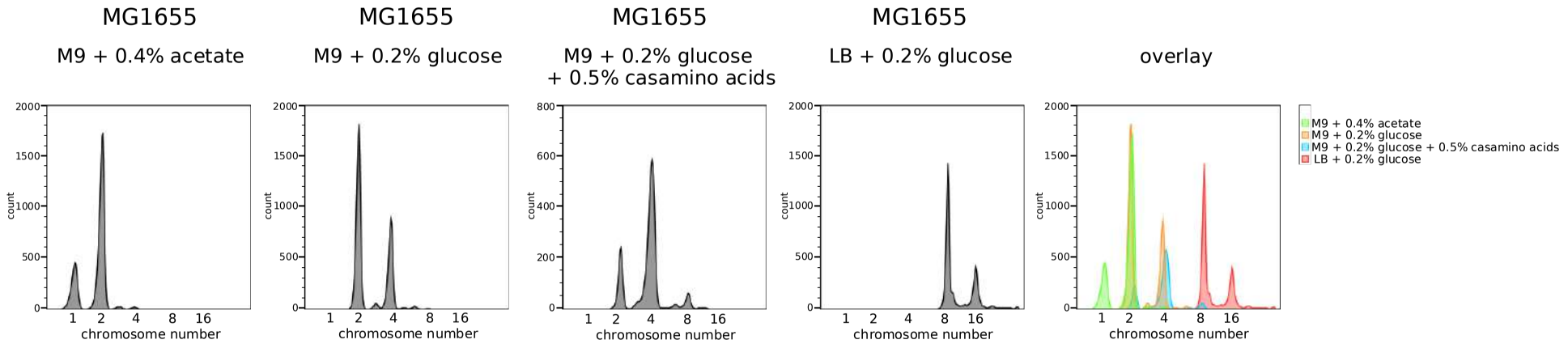

Supplementary figure 1
Flow cytometry histograms of MG1655 (genetic background) strain grown in 4 different growth conditions until early logarithmic growth phase (OD=0.15) and subjected to inhibition of new replication rounds as well as cell divisions. After completion of ongoing replication rounds the cells contain chromosome number equal to the number of origins present in the cell when inhibitors were added. Chromosomal DNA is then stained with a fluorescent dye and the DNA content is measured by flow cytometry. Cell populations contain particular chromosome number, depending on the growth rate.

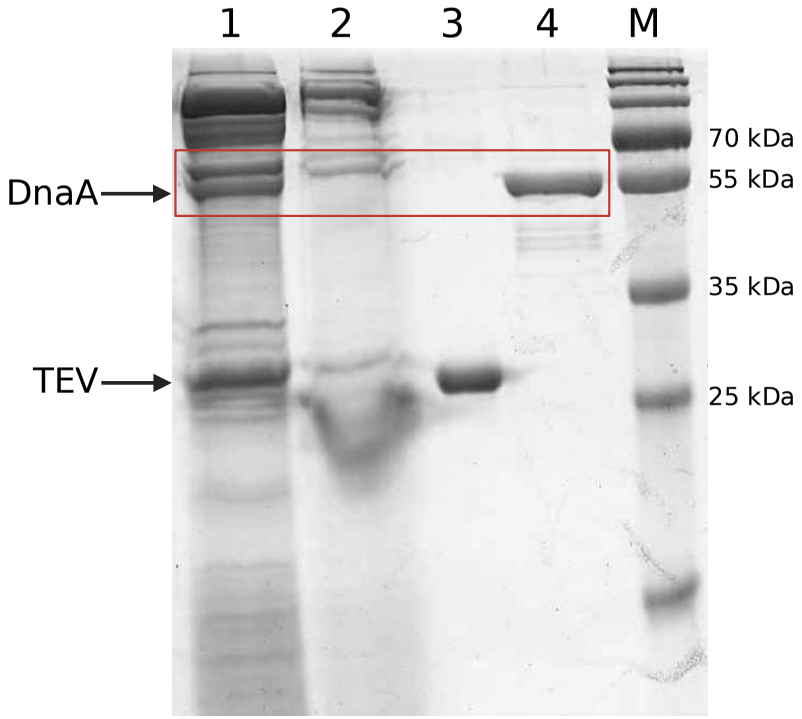

1 - elution sample after TEV cleavage from anti-FLAG affinity resin
2 - anti-FLAG affinity resin after TEV cleavage
3 - purified TEV
4 - purified DnaA
M - PageRuler™ Plus Prestained Protein Ladder

Supplementary figure 2
A test of TEV cleavage efficiency of the SPA-tagged DnaA protein bound to anti-FLAG resin. Samples were resolved in 10% SDS-PAGE gel, lane content was depicted in the picture. SPA-tagged DnaA was isolated from the respective strain according to the described protocol.

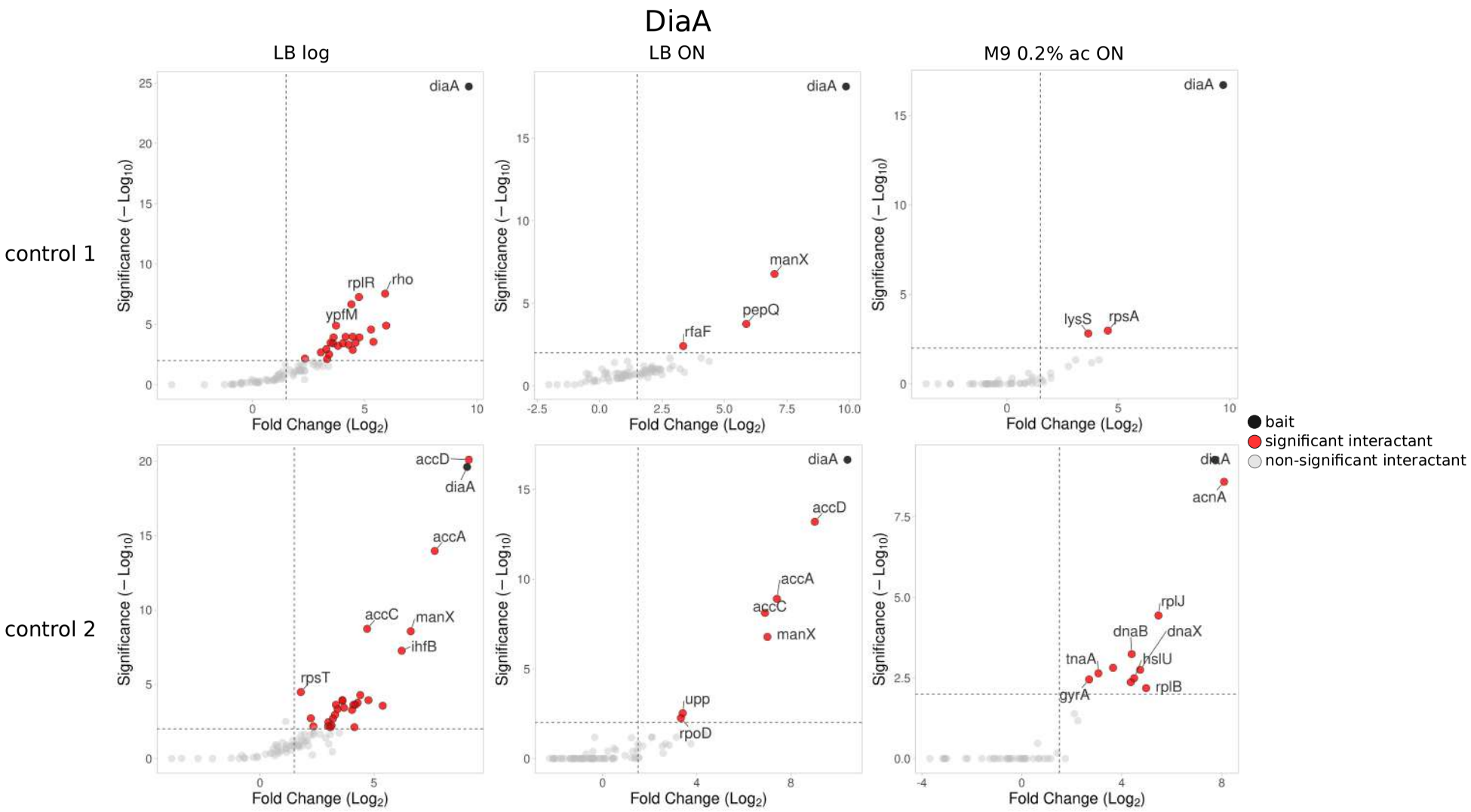

Supplementary figure 3A

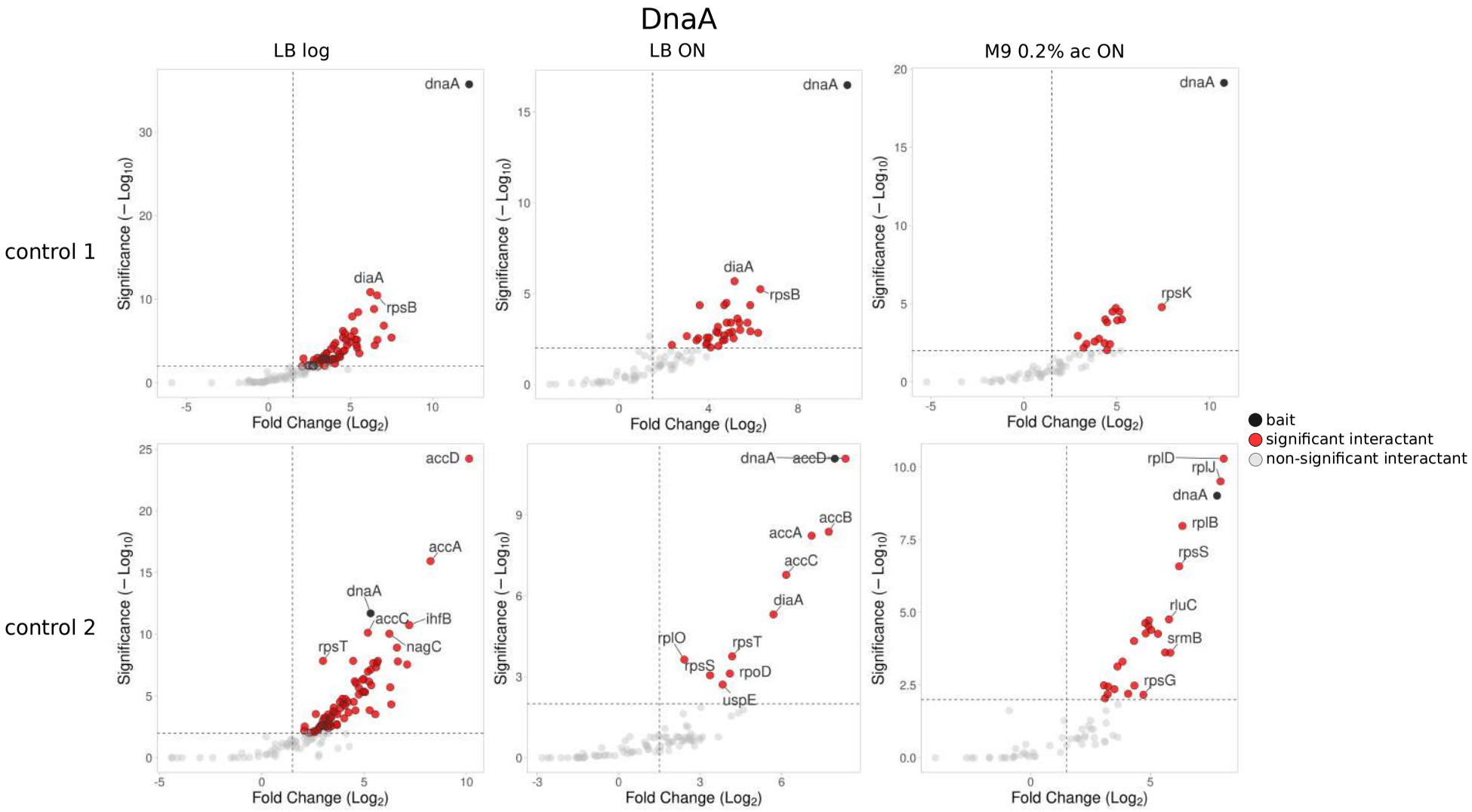

Supplementary figure 3B

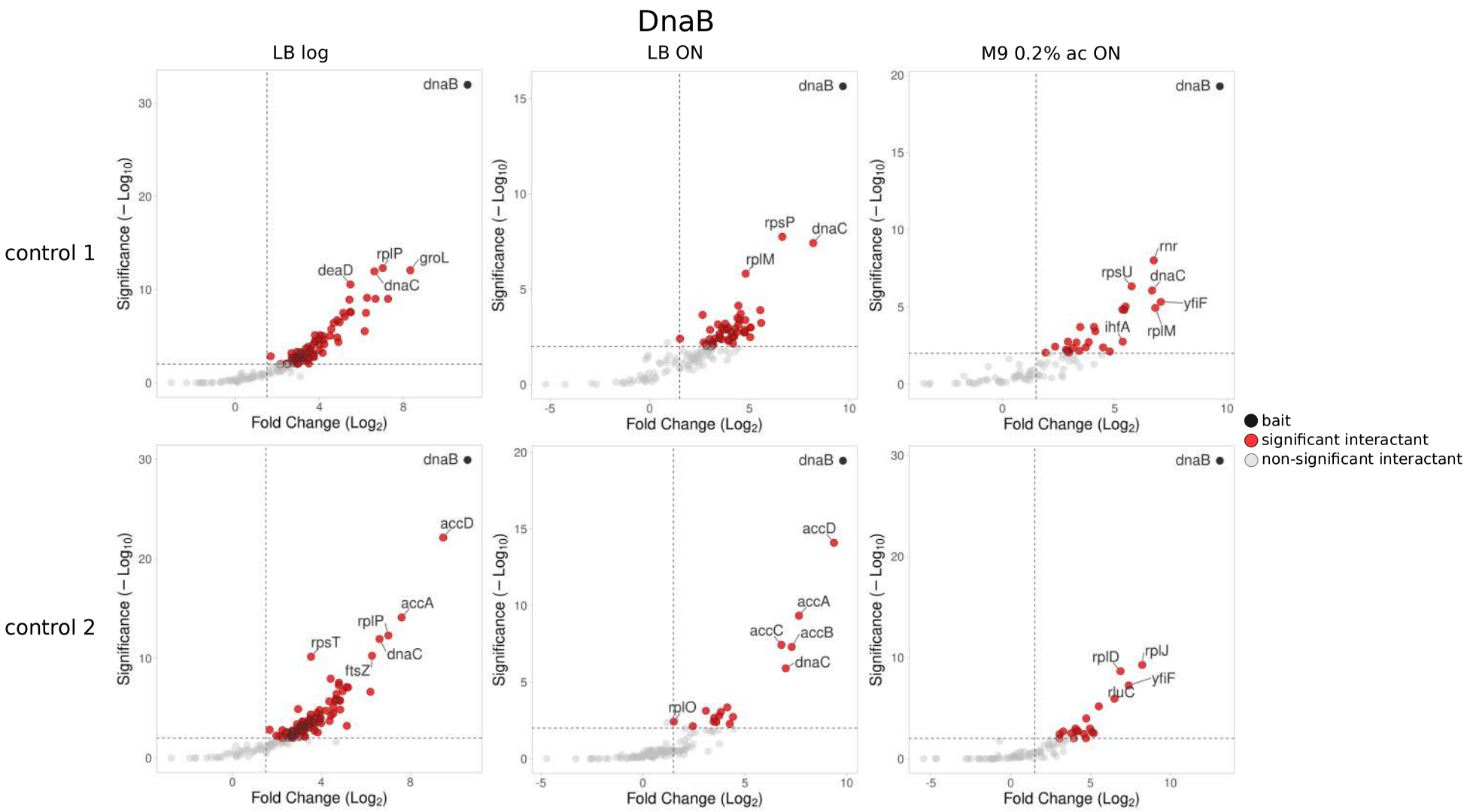

Supplementary figure 3C

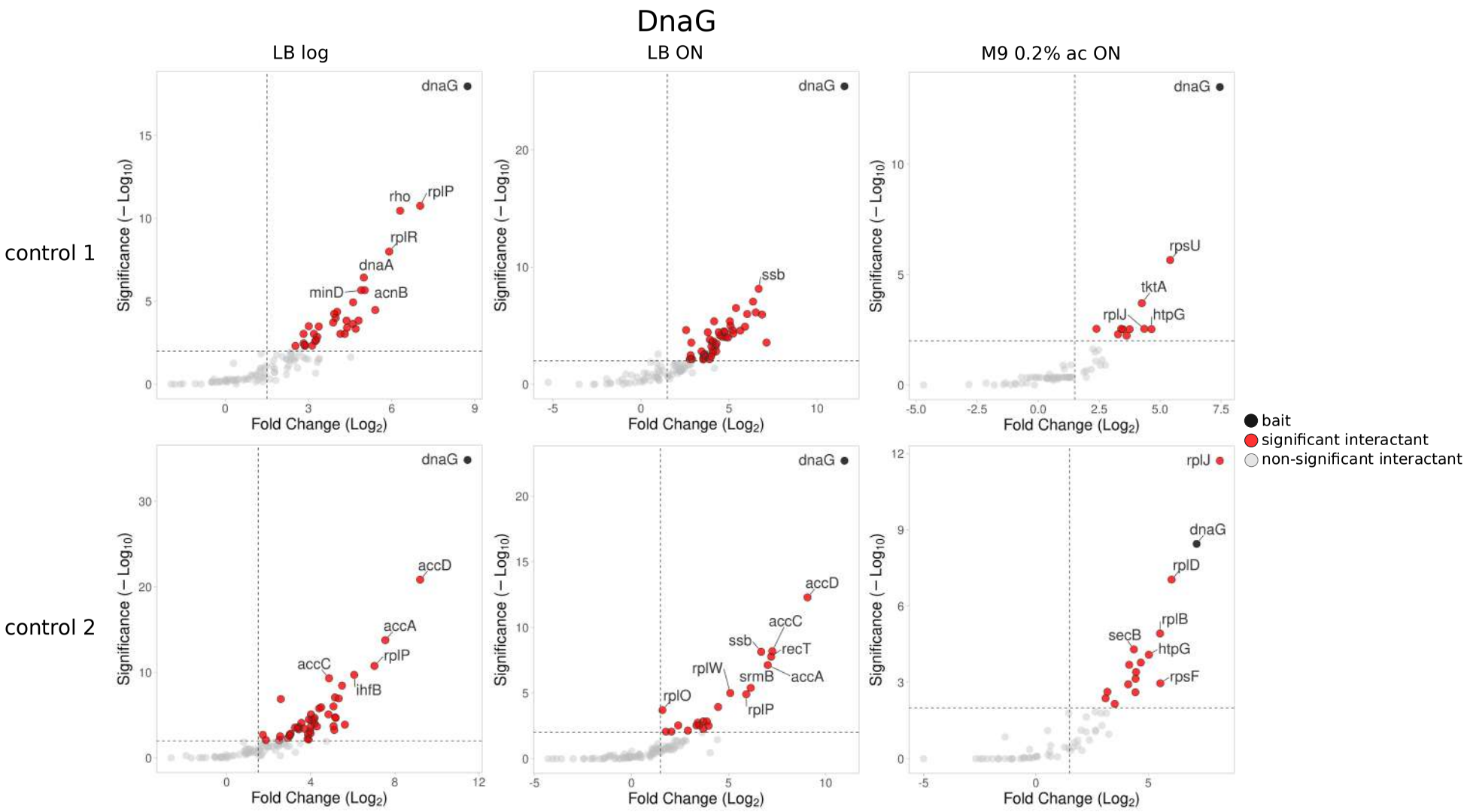

Supplementary figure 3D

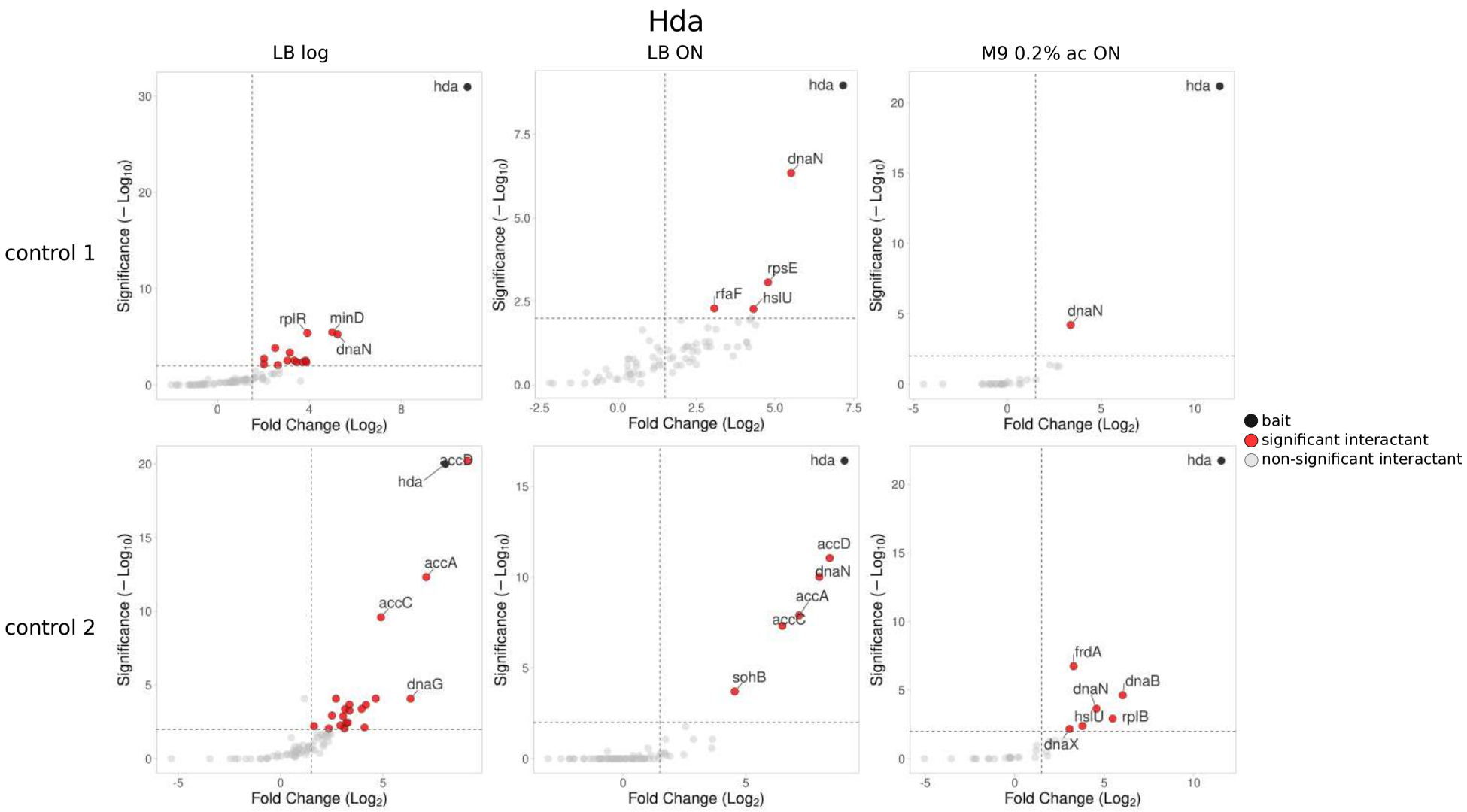

Supplementary figure 3E

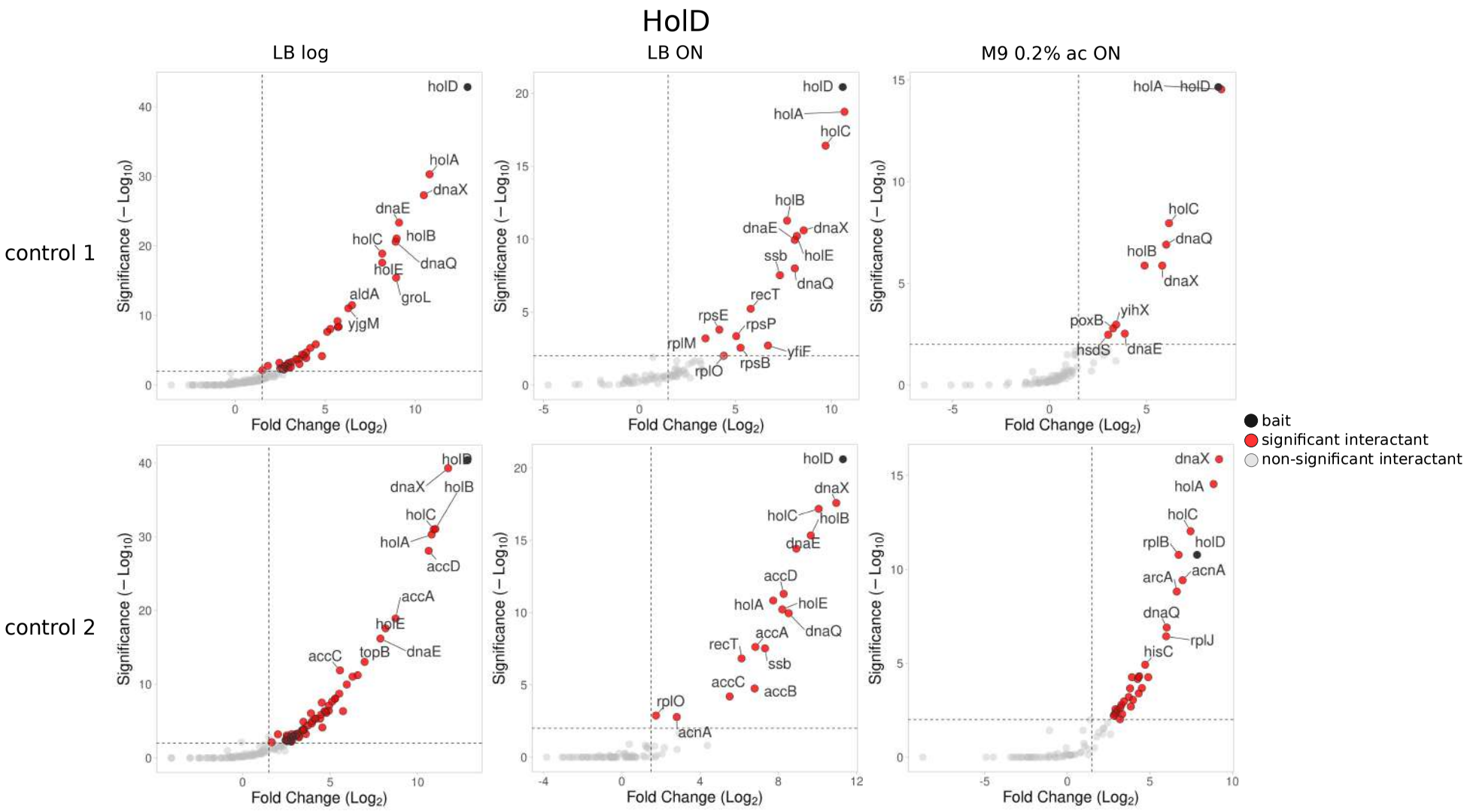

Supplementary figure 3F

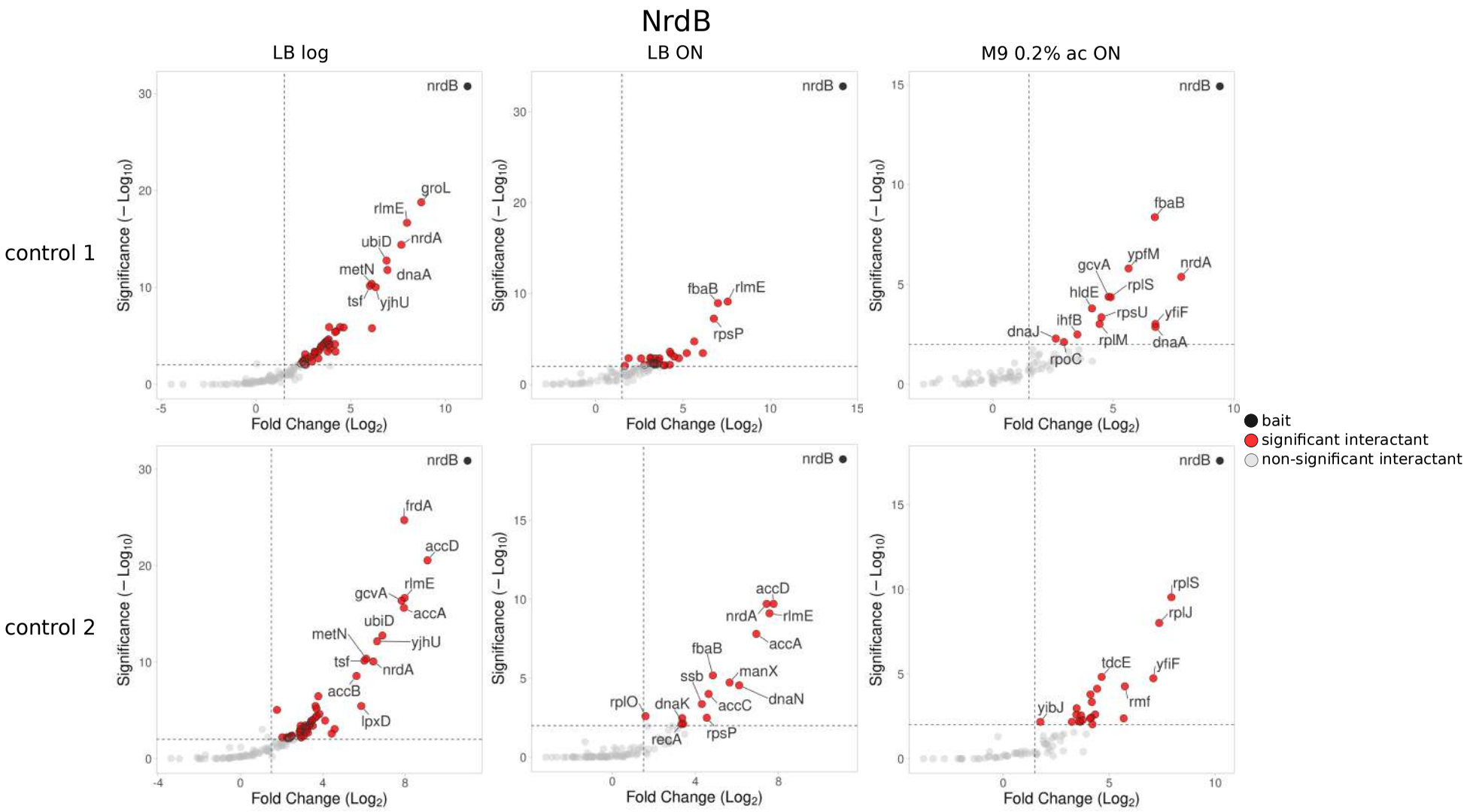

Supplementary figure 3G

Supplementary figure 3
Volcano plots depicting enrichment and statistical significance of uncovered interactions for various bait proteins:

A) DiaA
B) DnaA
C) DnaB
D) DnaG
E) Hda
F) HolD
G) NrdB

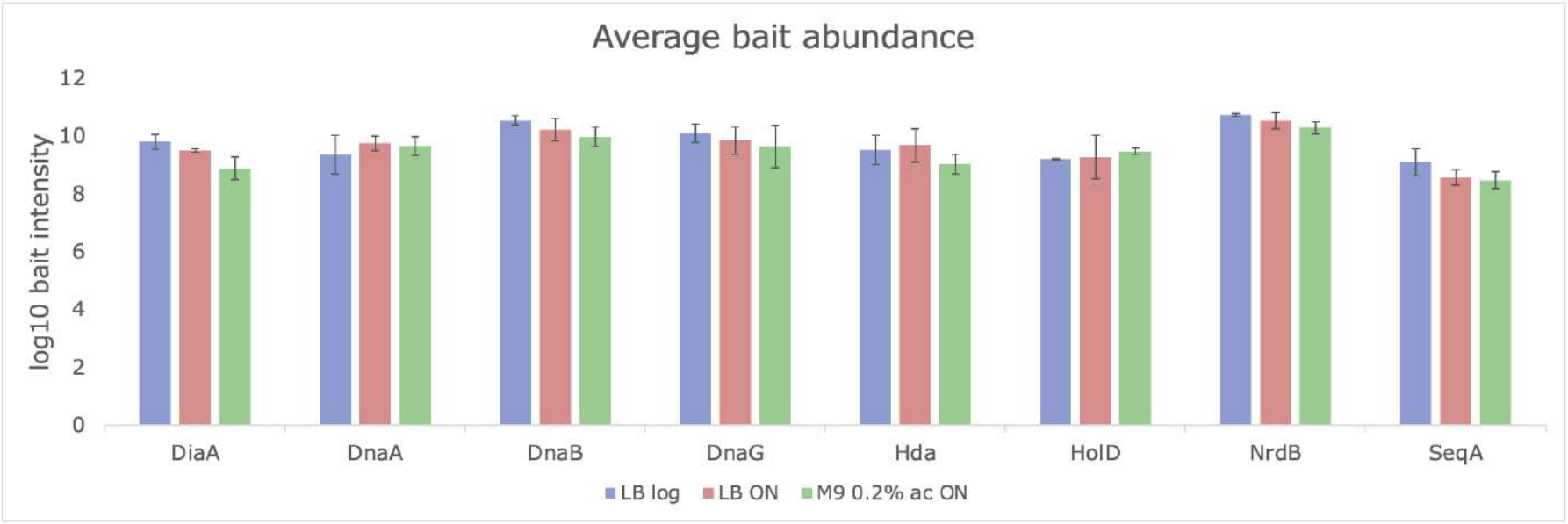

Supplementary figure 4
Average bait abundance shown as log10 of bait intensity value across different growth conditions of experimental samples.

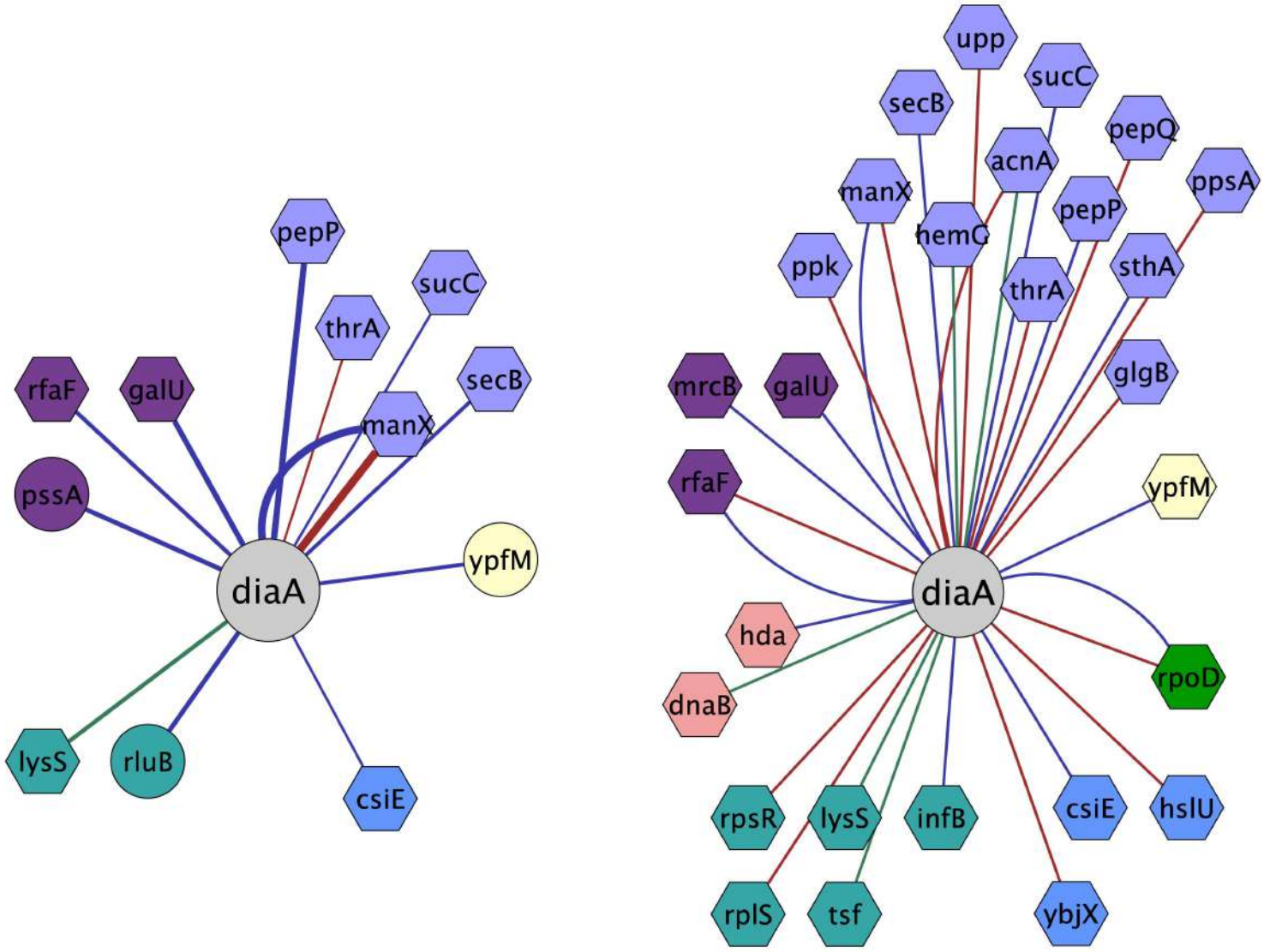

Supplementary figure 5A

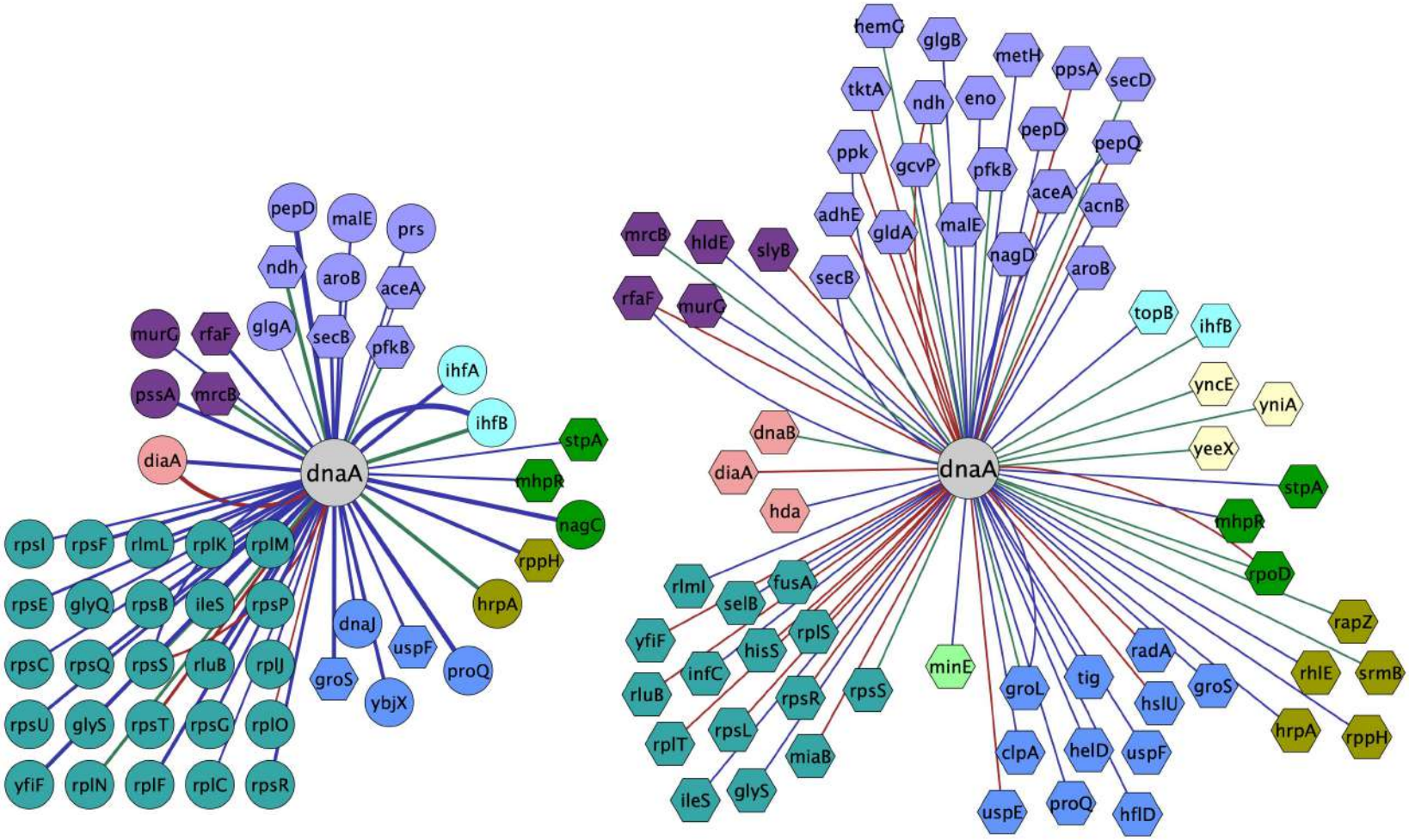

Supplementary figure 5B

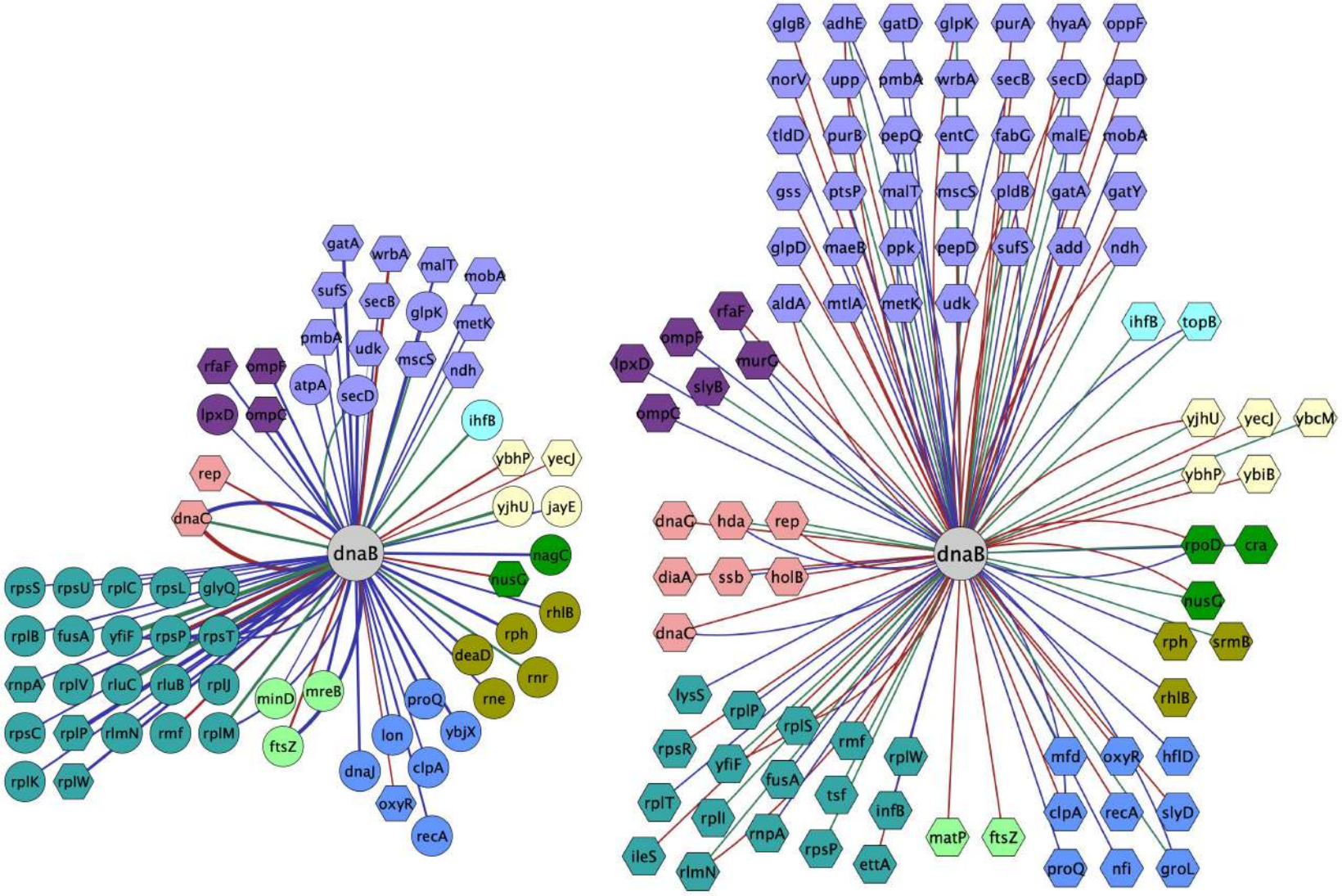

Supplementary figure 5C

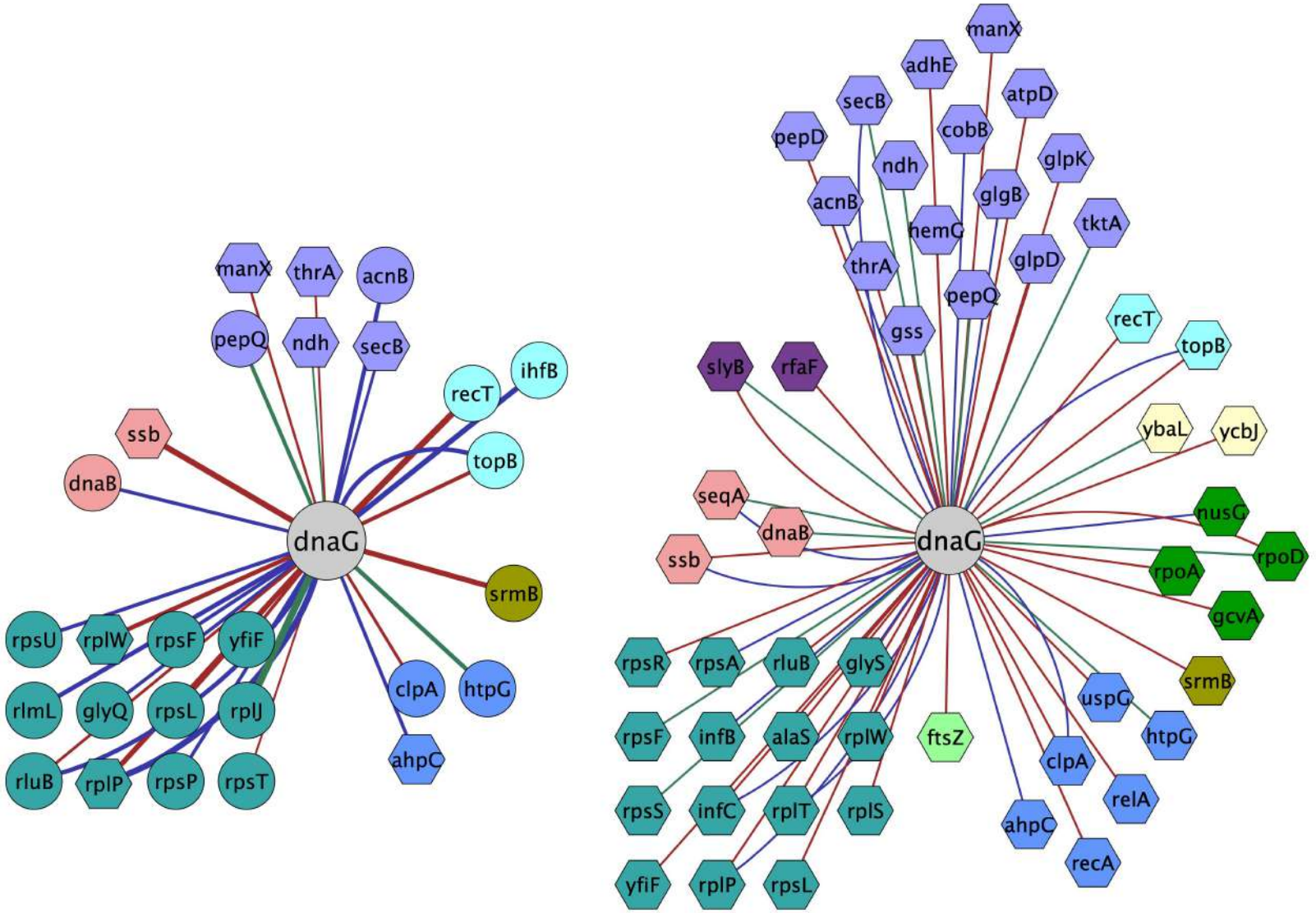

Supplementary figure 5D

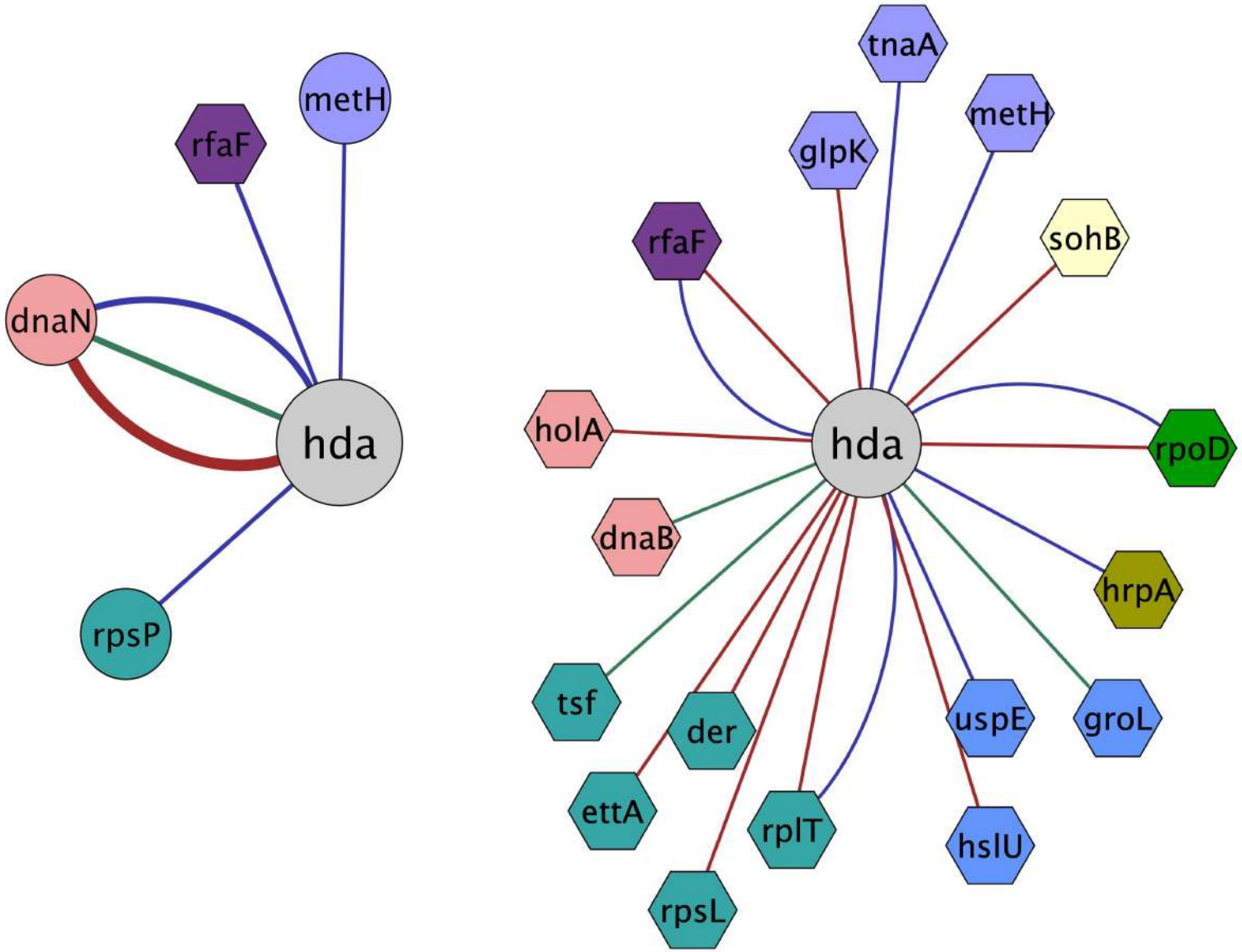

Supplementary figure 5E

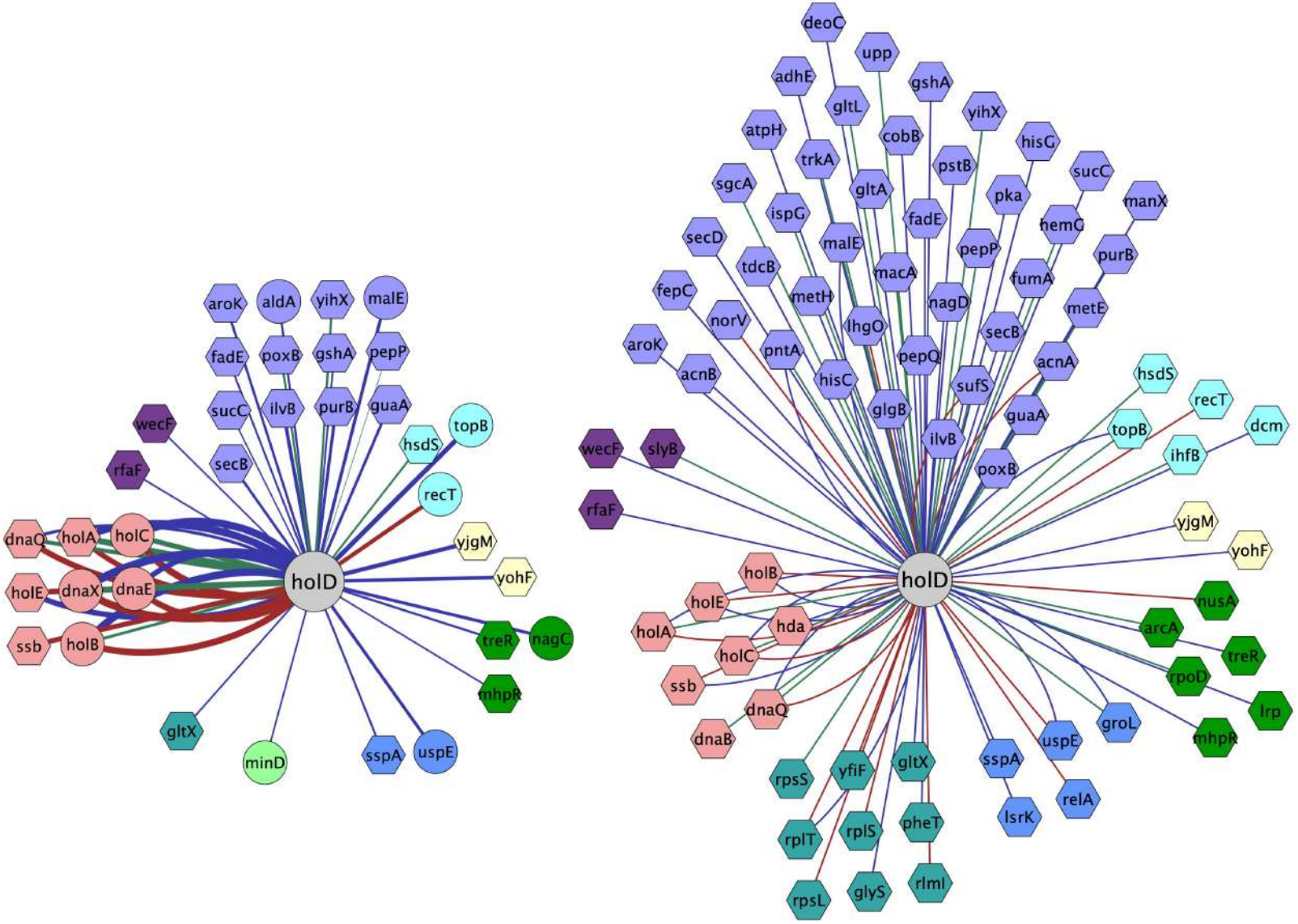

Supplementary figure 5F

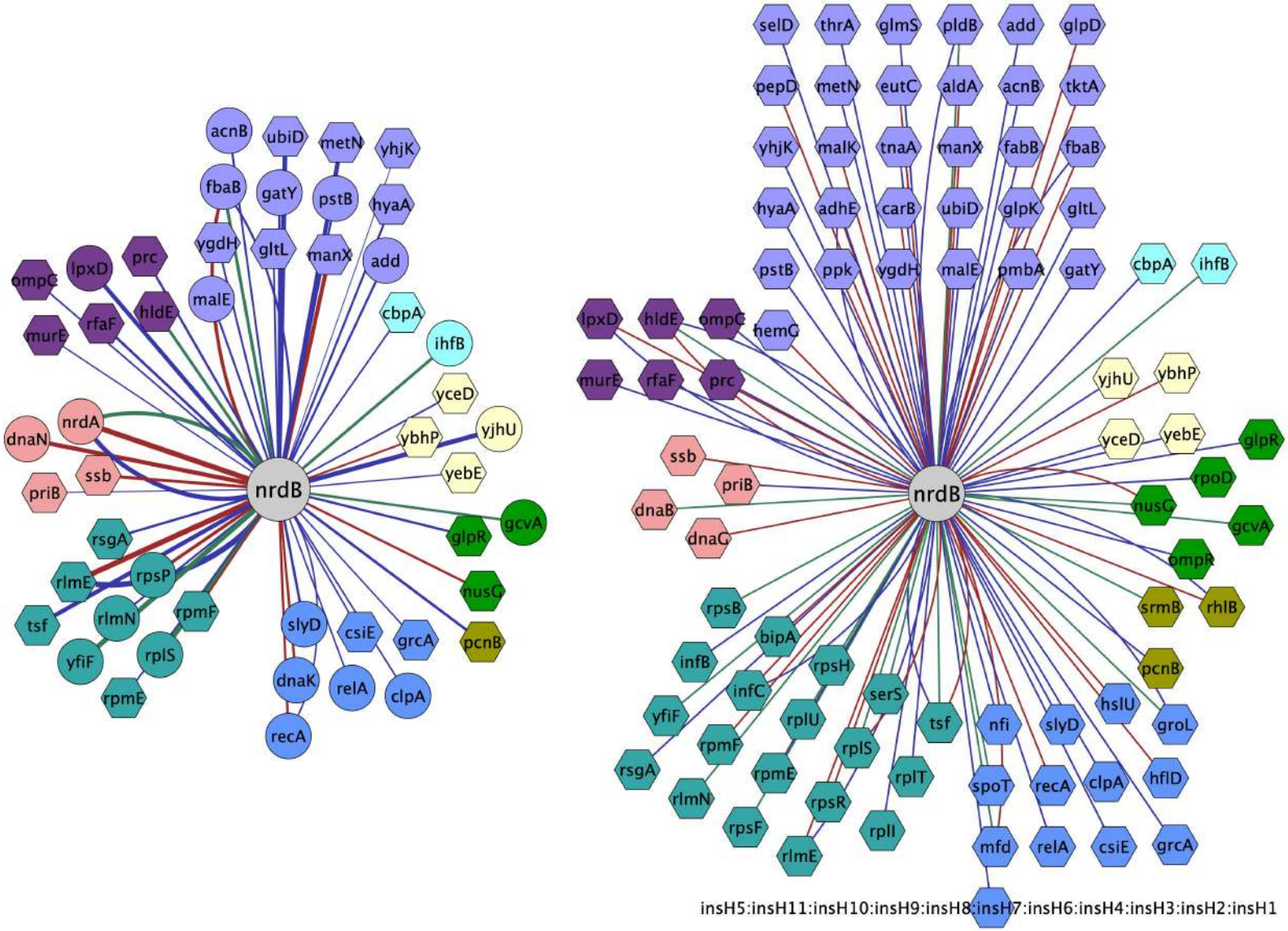

Supplementary figure 5G

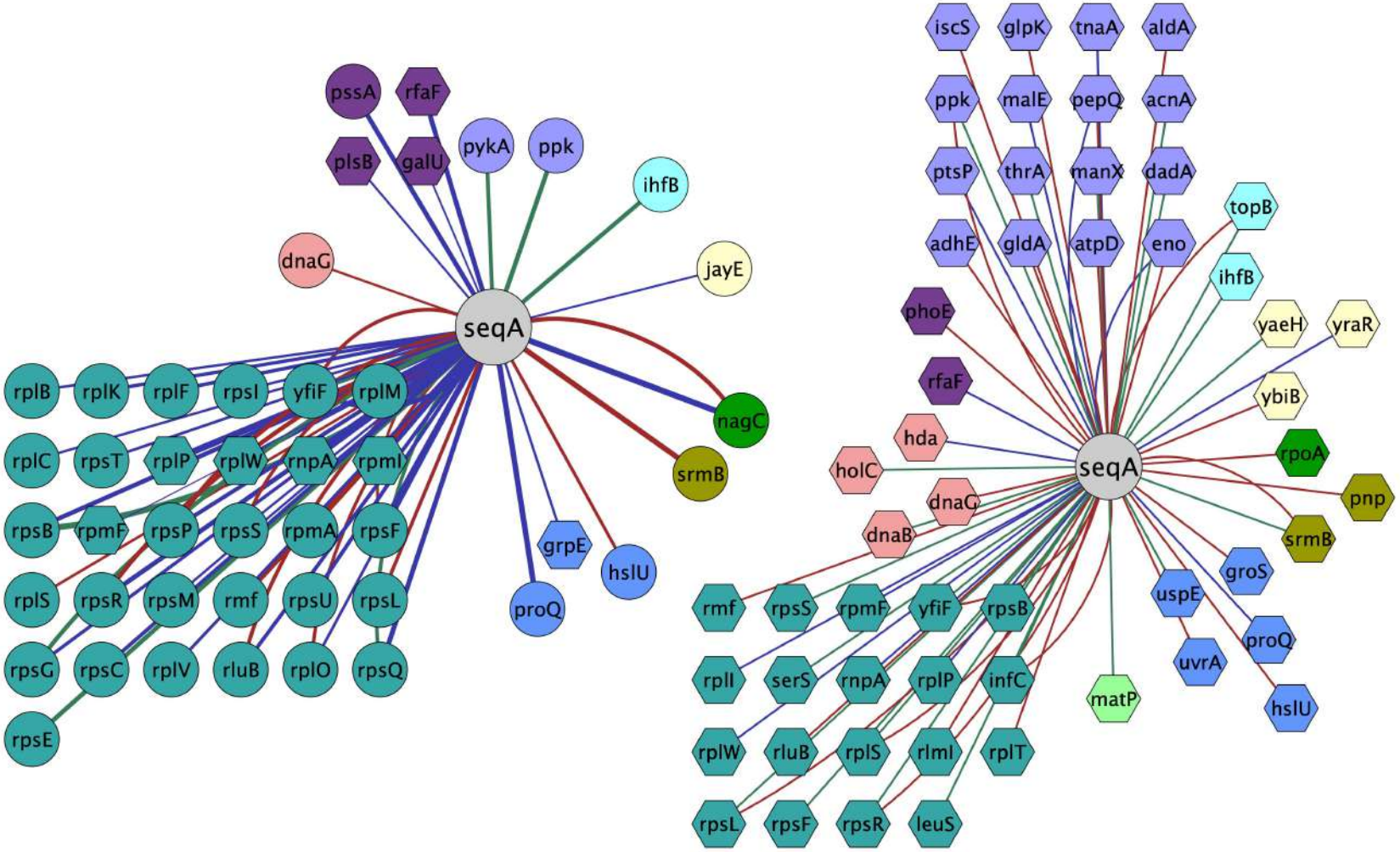

Supplementary figure 5H

Supplementary figure 5

A) PINs for DiaA - data processed quantitatively (left) and qualitatively (right).
B) PINs for DnaA - data processed quantitatively (left) and qualitatively (right).
C) PINs for DnaB - data processed quantitatively (left) and qualitatively (right).
D) PINs for DnaG - data processed quantitatively (left) and qualitatively (right).
E) PINs for Hda - data processed quantitatively (left) and qualitatively (right).
F) PINs for HolD - data processed quantitatively (left) and qualitatively (right).
G) PINs for NrdB - data processed quantitatively (left) and qualitatively (right).
H) PINs for SeqA - data processed quantitatively (left) and qualitatively (right).

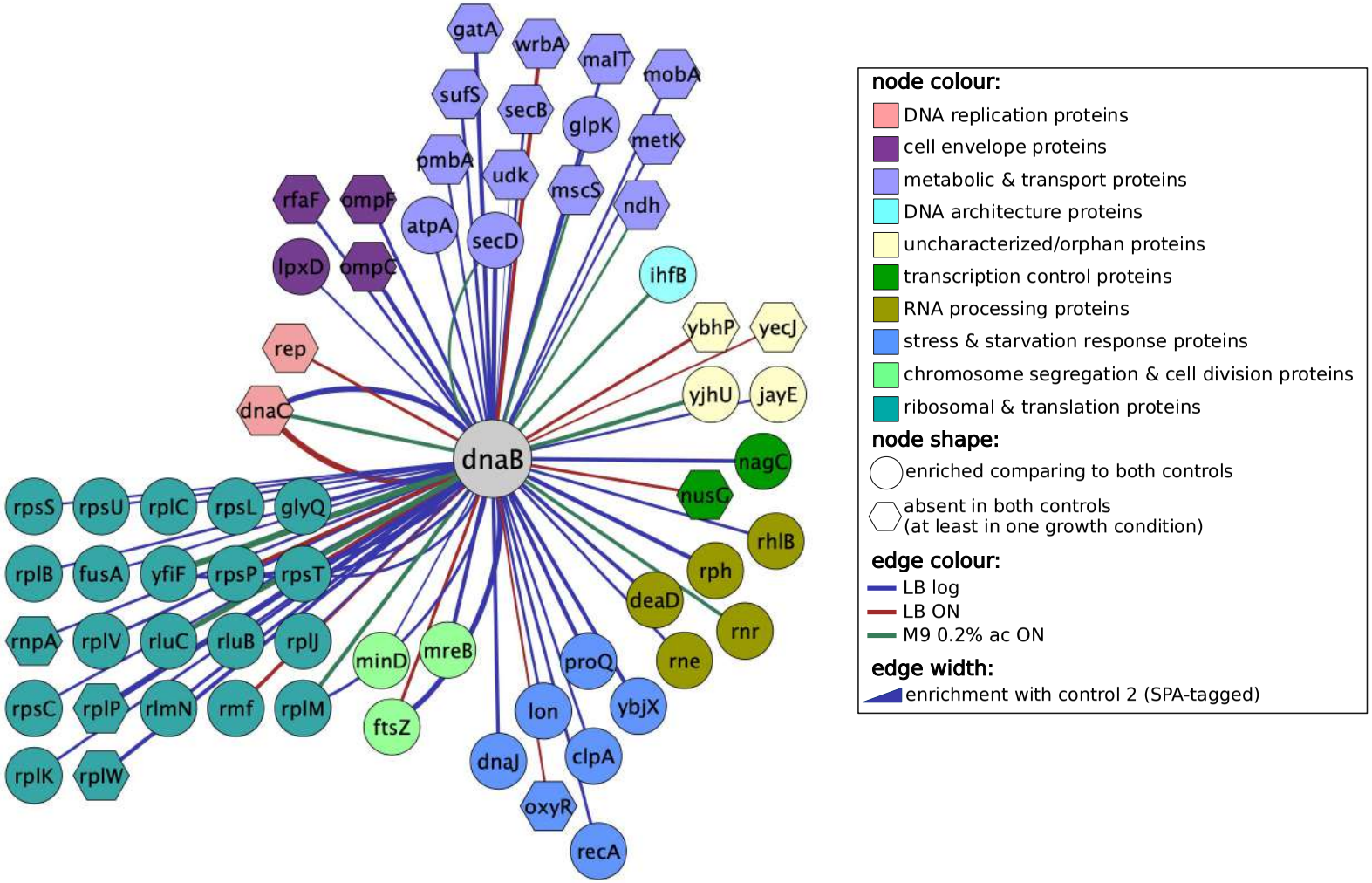

Supplementary figure 6
Example PIN along with the legend explaining how to read different nodes' and edges' parameters.

Supplementary Table 1
MaxQuant data sample coding along with corresponding raw MS datafiles' names

	MaxQuant data sample coding			raw MS data full file name in PRIDE		
sample type (experimental(E)/control(C)): bait protein	growth condition			growth condition		
	LB log	LB O/N	M9 0.2% ac O/N	LB log	LB O/N	M9 0.2% ac O/N
E:**DiaA**	E1; I4; X6	I5; P1; X7	I6; T3; X5	70408550glin_E1.raw; 709011793glin_I4.raw; 008131321glin_X6.raw	709011794glin_I5.raw; 908161515glin_P1.raw; 008131322glin_X7.raw	709011795glin_I6.raw; 911302356glin_T3.raw; 008131320glin_X5.raw
E:**DnaA**	F2; U6; U7	F1; P2; X12	E3; I7; X11	70524852glin_F2.raw; 912142457glin_U6.raw; 912142458glin_U7.raw	70524851glin_F1.raw; 908161516glin_P2.raw; 008131327glin_X12.raw	70408552glin_E3.raw; 709011796glin_I7.raw; 008131326glin_X11.raw
E:**DnaB**	G4; W3; W4	G6; W5; W6	G2; W1; W2	706281047glin_G4.raw; 00319348glin_W3.raw; 00319349glin_W4.raw	706281049glin_G6.raw; 00319350glin_W5.raw; 00319351glin_W6.raw	706281045glin_G2.raw; 00319346glin_W1.raw; 00319347glin_W2.raw
E:**DnaG**	H1; J5; U9	C7; F6; H2	F7; H3; X15	706281185glin_H1.raw; 710192290glin_J_5.raw; 912142460glin_U9.raw	611072350glin_C_7.raw; 70524856glin_F6.raw; 706281186glin_H2.raw	70524857glin_F7.raw; 706281187glin_H3.raw; 008131330glin_X15.raw
E:**Hda**	C5; U8; X9	C6; P3; X10	I3; T4; X8	611072348glin_C_5.raw; 912142459glin_U8.raw; 008131324glin_X9.raw	611072349glin_C_6.raw; 908161517glin_P3.raw; 008131325glin_X10.raw	709011792glin_I3.raw; 911302357glin_T4.raw; 008131323glin_X8.raw
E:**HolD**	U1; U2; U3	F8; U11; X4	X1; X2; X3	912142452glin_U1.raw; 912142453glin_U2.raw; 912142454glin_U3.raw	70524858glin_F8.raw; 912142462glin_U11.raw; 008131319glin_X4.raw	008131316glin_X1.raw; 008131317glin_X2.raw; 008131318glin_X3.raw

E:**NrdB**	W7; W8; W9	F10; J4; U13	F9; J3; T10	00319352glin_W7.raw; 00319353glin_W8.raw; 00319354glin_W9.raw	70524860glin_F10.raw; 710192289glin_J_4.raw; 912142464glin_U13.raw	70524859glin_F9.raw; 710192288glin_J_3.raw; 911302363glin_T10.raw
E:**SeqA**	F4; X13; X14	F3; P4; U12	F5; T1; T2	70524854glin_F4.raw; 008131328glin_X13.raw; 008131329glin_X14.raw	70524853glin_F3.raw; 908161518glin_P4.raw; 912142463glin_U12.raw	70524855glin_F5.raw; 911302354glin_T1.raw; 911302355glin_T2.raw
C: MG1655 **(TYPE 1 CONTROL**)	T7; T8; T9	P5; U10; X17	T5; T6; X16	911302360glin_T7.raw; 911302361glin_T8.raw; 911302362glin_T9.raw	908161519glin_P5.raw; 912142461glin_U10.raw; 008131332glin_X17.raw	911302358glin_T5.raw; 911302359glin_T6.raw; 008131331glin_X16.raw
C:MG1655 (placI)mVenus-SPA-pUC19 **(TYPE 2 CONTROL)**	S1; S2; S3	O9; R4; R5	R1; R2; R3	910182130glin_S1.raw; 910182131glin_S2.raw; 910182132glin_S3.raw	901043208glin_O9.raw; 909131890glin_R4.raw; 909131891glin_R5.raw	909131887glin_R1.raw; 909131888glin_R2.raw; 909131889glin_R3.raw

Wkład autorów – oświadczenia

Uniwersytet Gdański

mgr Joanna Morcinek-Orłowska
Katedra Genetyki Molekularnej Bakterii
Wydział Biologii
Uniwersytet Gdański

Gdańsk, 26.05.2025 r.

Oświadczenie o wkładzie w publikację

Oświadczam, że mój wkład w artykuł oryginalny:

Morcinek-Orłowska J, Walter B, Forquet R, Cysewski D, Carlier M, Mozolewski M, Meyer S, Glinkowska M. Interaction networks of Escherichia coli replication proteins under different bacterial growth conditions. Sci Data. 2023 Nov 10;10(1):788. doi: 10.1038/s41597-023-02710-1. PMID: 37949936; PMCID: PMC10638427.

obejmował:

- przeprowadzenie eksperymentów (konstrukcja szczepów *E. coli* oraz wektora plazmidowego, izolacja większości kompleksów białkowych, oczyszczenie proteazy TEV, kontrolne analizy metodą cytometrii przepływowej)
- analizę danych MS metodą jakościową
- uczestnictwo w analizie danych MS metodą ilościową
- wizualizację danych, przygotowanie rycin
- kierowanie projektem Preludium 12, w ramach którego sfinansowano część badań
- napisanie wstępnej oraz ostatecznej wersji manuskryptu wspólnie z dr hab. Moniką Glinkowską

Joanna Morcinek-Orłowska

Wdział Biologii
Uniwersytetu Gdańskiego
Katedra Genetyki
Molekularnej Bakterii

tel. +48 58 523 60 65
e-mail: mol.KGB@ug.edu.pl

ul. Wita Stwosza 59
80-309 Gdańsk

www.ug.edu.pl

dr Beata Walter
Zakład Biologii Strukturalnej
Międzyuczelniany Wydział Biotechnologii
Uniwersytetu Gdańskiego
i Gdańskiego Uniwersytetu Medycznego

Gdańsk, 26.05.2025 r.

Oświadczenie o wkładzie w publikację

Oświadczam, że mój wkład w artykuł oryginalny:

Morcinek-Orłowska J, Walter B, Forquet R, Cysewski D, Carlier M, Mozolewski M, Meyer S, Glinkowska M. Interaction networks of Escherichia coli replication proteins under different bacterial growth conditions. Sci Data. 2023 Nov 10;10(1):788. doi: 10.1038/s41597-023-02710-1. PMID: 37949936; PMCID: PMC10638427.

obejmował:

- przeprowadzenie części izolacji kompleksów białkowych
- rewizję ostatecznej wersji manuskryptu

Międzyuczelniany
Wydział Biotechnologii
Uniwersytetu Gdańskiego
i Gdańskiego Uniwersytetu
Medycznego

tel. +48 58 523 64 20
e-mail: beata.water@ug.edu.pl

ul. Abrahama 58
80-307 Gdańsk
www.biotech.ug.edu.pl

iMEAN

Raphaël Forquet, PhD
Life science modeller
+33 5 61 28 51 60
135 avenue de Rangueil, INSA Bâtiment 50
1077 Toulouse Cedex 4
imean-biotech.com

30/05/2025, Toulouse

Author contribution statement

I hereby declare that my contribution to the research article:

Morcinek-Orłowska J, Walter B, Forquet R, Cysewski D, Carlier M, Mozolewski M, Meyer S, Glinkowska M. Interaction networks of Escherichia coli replication proteins under different bacterial growth conditions. Sci Data. 2023 Nov 10;10(1):788. doi: 10.1038/s41597-023-02710-1. PMID: 37949936; PMCID: PMC10638427.

included:

- performing quantitative MS data analysis (contribution to the code writing and analyzing the data)
- participation in manuscript writing and revision

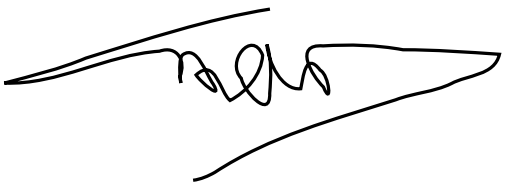

Dr Dominik Cysewski
Centrum Badań Klinicznych
Uniwersytet Medyczny w Białymstoku

Białystok 30.05.2025

Oświadczenie o wkładzie w publikację

Oświadczam, że mój wkład w artykuł oryginalny:

Morcinek-Orłowska J, Walter B, Forquet R, Cysewski D, Carlier M, Mozolewski M, Meyer S, Glinkowska M. Interaction networks of Escherichia coli replication proteins under different bacterial growth conditions. Sci Data. 2023 Nov 10;10(1):788. doi: 10.1038/s41597-023-02710-1. PMID: 37949936; PMCID: PMC10638427.

obejmował:

- identyfikację składu kompleksów białkowych poprzez tandemową spektrometrię mas poprzedzoną chromatografią cieczową oraz analizę widm za pomocą silnika przeszukiwania MaxQuant
- uczestnictwo w przygotowaniu wstępnej wersji manuskryptu oraz rewizji ostatecznej wersji manuskryptu

dr Dominik Cysewski

Asystent
Centrum Badań Klinicznych
Uniwersytet Medyczny w Białymstoku

INSTITUT NATIONAL DES SCIENCES APPLIQUÉES LYON

Sam Meyer
Assistant Professor, INSA Lyon
Microbiologie, Adaptation et Pathogénie,
UMR5240
Villeurbanne, France

Villeurbanne, June 4th, 2025

Author contribution statement

I hereby declare that my contribution to the research article:

Morcinek-Orłowska J, Walter B, Forquet R, Cysewski D, Carlier M, Mozolewski M, Meyer S, Glinkowska M. Interaction networks of Escherichia coli replication proteins under different bacterial growth conditions. Sci Data. 2023 Nov 10;10(1):788. doi: 10.1038/s41597-023-02710-1. PMID: 37949936; PMCID: PMC10638427.

included:

- planning of quantitative data analysis strategy
- supervising the data analysis

Sam Meyer

Uniwersytet Gdański

mgr Michał Mozolewski
Katedra Genetyki Molekularnej Bakterii
Wydział Biologii
Uniwersytet Gdański

Gdańsk, 26.05.2025 r.

Oświadczenie o wkładzie w publikację

Oświadczam, że mój wkład w artykuł oryginalny:

Morcinek-Orłowska J, Walter B, Forquet R, Cysewski D, Carlier M, Mozolewski M, Meyer S, Glinkowska M. Interaction networks of Escherichia coli replication proteins under different bacterial growth conditions. Sci Data. 2023 Nov 10;10(1):788. doi: 10.1038/s41597-023-02710-1. PMID: 37949936; PMCID: PMC10638427.

obejmował:

- przeprowadzenie części izolacji kompleksów białkowych
- przeprowadzenie części eksperymentów wymaganych podczas procesu recenzji artykułu

Michał Mozolewski

Wdział Biologii
Uniwersytetu Gdańskiego
Katedra Genetyki
Molekularnej Bakterii

tel. +48 58 523 60 65
e-mail: mol.KGB@ug.edu.pl

ul. Wita Stwosza 59
80-309 Gdańsk

www.ug.edu.pl

Uniwersytet Gdański

dr hab. Monika Glinkowska, prof. UG
Katedra Genetyki Molekularnej Bakterii
Wydział Biologii
Uniwersytet Gdański

Gdańsk, 26.05.2025 r.

Oświadczenie o wkładzie w publikację

Oświadczam, że mój wkład w artykuł oryginalny:

Morcinek-Orłowska J, Walter B, Forquet R, Cysewski D, Carlier M, Mozolewski M, Meyer S, Glinkowska M. Interaction networks of Escherichia coli replication proteins under different bacterial growth conditions. Sci Data. 2023 Nov 10;10(1):788. doi: 10.1038/s41597-023-02710-1. PMID: 37949936; PMCID: PMC10638427.

obejmował:

- zaplanowanie badań i koncepcji artykułu
- nadzorowanie przeprowadzonych eksperymentów oraz analizy danych
- kierowanie projektem Opus 7, w ramach którego sfinansowano większość badań
- przygotowanie wstępnej oraz ostatecznej wersji manuskryptu wspólnie z Joanną Morcinek-Orłowską
- złożenie manuskryptu do czasopisma oraz korespondencję z Edytorem i Recenzentami

Monika Glinkowska

Wdział Biologii
Uniwersytetu Gdańskiego
Katedra Genetyki
Molekularnej Bakterii

tel. +48 58 523 60 65
e-mail: mol.KGB@ug.edu.pl

ul. Wita Stwosza 59
80-309 Gdańsk

www.ug.edu.pl

Artykuł nr 3 (preprint pracy badawczej)

Morcinek-Orłowska J., Walter B., Forquet R., Cysewski D., Carlier M., Meyer S., Glinkowska M.

Protein interaction network analysis reveals growth conditions-specific crosstalk between chromosomal DNA replication and other cellular processes in *E. coli*.

(2021) bioRxiv 2021.12.08.471875.

Title: Protein interaction network analysis reveals growth conditions-specific crosstalk between chromosomal DNA replication and other cellular processes in *E. coli*

Authors: Joanna Morcinek-Orłowska[1], Beata Maria Walter[1], Raphaël Forquet[2], Dominik Cysewski[3,] Maxime Carlier[2], Sam Meyer[2] and Monika Glinkowska[1†]

1- Department of Bacterial Molecular Genetics, Faculty of Biology, University of Gdansk, Poland
2- Univ Lyon, Université Claude Bernard Lyon 1, INSA-Lyon, CNRS, UMR5240 MAP, F-69622, France
3- Institute of Biochemistry and Biophysics Polish Academy of Sciences, Warsaw, Poland

† - to whom correspondence should be addressed

Abstract

E. coli and many other bacterial species can alter their cell cycle according to nutrient availability. Under optimal conditions bacteria grow and divide very fast but they slow down the cell cycle when conditions deteriorate. This adaptability is underlined by mechanisms coordinating cell growth with duplication of genetic material and cell division. Several mechanisms regulating DNA replication process in *E. coli* have been described with biochemical details so far. Nevertheless we still don't fully understand the source of remarkable precision that allows bacterial cells to coordinate their growth and chromosome replication. To shed light on regulation of *E. coli* DNA replication at systemic level, we used affinity purification coupled with mass spectrometry (AP-MS) to characterize protein-protein interactions (PPIs) formed by key *E. coli* replication proteins, under disparate bacterial growth conditions and phases. We present the resulting dynamic replication protein interaction network (PIN) and highlight links between DNA replication and several cellular processes, like outer membrane synthesis, RNA degradation and modification or starvation response.

Importance

DNA replication is a vital process, ensuring propagation of genetic material to progeny cells. Despite decades of studies we still don't fully understand how bacteria coordinate chromosomal DNA duplication with cell growth and cell division under optimal and stressful conditions. At molecular level, regulation of processes, including DNA replication, is often executed through direct protein-protein interactions (PPIs). In this work we present PPIs formed by the key *E. coli* replication proteins under three different bacterial growth conditions. We show novel PPIs with confirmed impact on chromosomal DNA replication. Our results provide also alternative explanations of genetic interactions uncovered before by others for *E.coli* replication machinery.

Introduction

At molecular level, most of biological functions are performed by proteins. Composite cellular activities are usually carried out by various sets of proteins organized into protein complexes, rather than by proteins acting alone. Formation of a complex, which is mediated by protein-protein interactions between their components, ensures coordination of processes and channeling of substrates. Often, protein assemblies gain additional features in comparison to their individual units, so that ultimately a protein complex means more than a simple sum of its parts. The entirety of protein-protein interactions in a cell constitutes a protein interaction network (1, 2). Recent studies on protein network properties revealed their general characteristics like connectivity, modularity and dynamics (3). It was shown that most proteins (nodes) within a network form limited number of connections (edges), but relatively small number of proteins form highly connected nodes called hubs. Moreover, proteins responsible for certain autonomous cellular activities are organized into well connected modules, typically forming few interactions between each other (1). Those intramodular connections may play a pivotal role in coordinating various cellular functions or in concerted response of cells to external stimuli. However, protein-protein interactions are also differentiated with respect to affinity of interactants and assembly on/off rate, ranging from very stable to transient ones. Hence, protein complexes are usually understood as stable multimolecular machines that act at the same time and place, whereas modules contain proteins that participate in a particular process, but their interactions are spatiotemporally regulated (4–6). Dynamics of proteins and PPIs underlies transformations of PINs under different conditions and reflects cellular responses to environmental cues, cell cycle or developmental stages. When conditions change, certain functional modules may continue, change composition, dissipate or fuse, forming additional connections (7–10). Uncovering dynamics of such condition-specific protein sub-networks dedicated to a certain process can facilitate understanding of their regulation at systemic level.

Bacterial cell cycle is a sequence of events directed by spatiotemporally regulated protein complexes. It consists of concurrent and interrelated processes: cell growth, chromosomal DNA replication and segregation culminated with cell division (11). For fast-growing bacteria like *E. coli*, the time needed for synthesis of full chromosomal copy exceeds the interval between subsequent divisions and, to cope with that, all cell cycle stages occur simultaneously (Fig. 1A)(12). Thus, bacterial cell may contain several replicating chromosomes at different replication stages, however still one initiation of replication per cell

cycle rule is held (12). Coordination of DNA replication with cell growth and cell division in bacteria is still insufficiently understood. It is widely accepted that DNA replication starts at a certain cell volume/chromosomal origin ratio and that all origins of replication (*oriC*) present in the cell fire simultaneously (Fig. 1B)(13–15), but molecular mechanism behind this dependence remains uncertain. The key components of the mentioned control principles are certainly the DnaA protein that initiates a sequence of events at *oriC* leading to replication complex formation, as well as its regulators DiaA, Hda and SeqA(16). However, it seems that cell cycle regulatory mechanism may differ under conditions supporting fast and slow growth rates. As fast growth, we assume here doubling times of 20-30 min with multiple overlapping replication rounds, whereas as slow growth rate – doubling times exceeding 70 min with single, complete chromosome duplication round. In addition to adhering to those general principles, preservation of genomic integrity during the cell cycle requires solving many particular problems by bacterial cells, for instance handling replication-transcription conflicts or coordinating DNA modification, structure and repair with chromosome duplication and segregation. Changes in growth rate and doubling time, as well as their underlying molecular mechanisms, are part of bacterial adaptation and stress responses, which are crucial for their thriving in the environment across evolutionary time scales. Uncovering changes in the replication protein interaction network may foster identification of particular mechanisms employed by bacterial cells to coordinate the cell cycle under various conditions. In this work, we took up a proteomics-based approach to test changes of replication proteins sub-network under three disparate growth conditions. We show that interactions formed by each of the eight chosen proteins change dramatically with growth conditions, except those responsible for assembly of stable complexes, like DNA polymerase III (DNA Pol III) (17), Hda-DnaN(18), NrdA-NrdB(19)and DnaB-DnaC (Fig. 1C) (20). We suggest that this remodeling may be crucial for regulation of DNA replication under different environmental conditions. Results of our screen imply also a link between DNA replication and other cellular processes, like RNA modification and degradation or synthesis of lipopolysaccharide (LPS). Moreover, they also provide alternative explanation for a few previously observed interactions made by replication proteins-encoding genes. In addition, we suggest functional relations for several unannotated genes.

Materials and methods

Strains, primers, and plasmids

List of all *E. coli* strains used in this study is shown in Supplementary table 1. Plasmids and primers used in this study are listed in Supplementary tables 2 and 3, respectively. Cloning of pUC19-pIVSK was performed using restriction-free cloning procedure, as described in (21).

Bacterial cultures and media

LB Lennox medium (0.5% yeast extract, 1% tryptone, 0.5% NaCl) and M9 acetate medium (1x M9 minimal salts, 2 mM MgSO4, 0.1 mM CaCl2, 0.05% thiamine, 25 μg/ml uridine, 0.2% sodium acetate) were purchased from either Carl Roth GmbH or Sigma-Aldrich (now Merck). Overnight cultures were grown in LB Lennox medium. Ampicilin (Sigma-Aldrich) or kanamycin (Sigma-Aldrich) were added to the final concentration of 50 μg/ml where aplicable.

Bacterial cultures for protein complexes purification were inoculated with 20 ml of an overnight culture into 2 l of media and grown at 37°C to late exponential phase (OD_{600}=0.6-1.0) (in case of LB log and M9 acetate) or to stationary phase.

Construction of SPA-tagged *E. coli* strains and deletion mutants.

All strains used for isolation of bacterial protein complexes were based on MG1655 genetic background (Supplementary table 1). SPA-tagged strains were constructed by one-step integration of linear DNA fragment containing SPA-tag sequence and kanamycin resistance cassette using λ-Red recombination method (22). DNA fragments for integration were PCR-amplified using genomic DNA of commercial SPA-tagged strain as template and primers that consist of 20nt sequences specific to SPA-tag-kan^R and 50nt 5'-overhangs homologous to the chromosomal regions on either side of the integration site. Deletion strains were also constructed using λ-Red recombination method (22) relying on gene replacement with kanamycin or chloramphenicol resistance cassettes. Antibiotic resistance cassettes were PCR-amplified using pKD3 or pKD13 plasmids and primers containing 50nt 5'-overhangs homologous to the region upstream and downstream of the targeted gene. PCR products were column-purified, eluted with ultra-pure distilled water and used for electroporation of MG1655 strain harboring pKD46 plasmid, expressing the λ-Red recombination proteins.

Electrocompetent cells were prepared from MG1655/pKD46 strain grown in LB+amp at 30°C to an OD_{600} ~0.6, followed by induction with 0.15% L-arabinose and further growth for an additional one hour at 37°C. The cells were further pelleted and washed twice with ice-cold distilled water and once with ice-cold 10% glycerol. Cells were resuspended in 10 % glycerol at 100-fold concentration. For transformation, 80 µl of competent cells was mixed with ~1 µg of PCR product. Electroporation was done with Eppendorf Eporator using 2500 V and 0,1 cm chambers. Electroporated cells were added to 1 ml LB, incubated for 3h at 37°C and plated on LB with an appropriate antibiotic. Positive transformants were PCR-verified, sequenced and subjected to FRT-FLP recombination to remove antibiotic resistance cassette, as described in (22).

Protein complexes purification

Isolation of SPA-tagged bacterial protein complexes was performed according to protocol published by Babu and coworkers (23), with several modifications. Briefly, cell pellets harvested by centrifugation were resuspended in 20-40 ml of sonication buffer (20 mM Tris pH 7.9, 100 mM NaCl, 0.2 mM EDTA, 10% glycerol, 0.1 mM DTT, supplemented with 1 tablet of Pierce™ Protease Inhibitors (Thermo Scientific, A32965) per 50 ml of buffer) and lysed by sonication. Cell debris was removed by centrifugation at 18000 rpm for 45 min. Cleared protein lysate was incubated with 50-75 U of Viscolase nuclease (A&A Biotechnology) for 30 min on ice. After nucleic acids degradation, Triton X-100 was added to final concentration of 0.1%. The lysate was further incubated with 250 µl of prewashed in AFC buffer (10 mM Tris pH 7.9, 100 mM NaCl, 0.1% Triton X-100) Sepharose® 4B-200 (Sigma-Aldrich), for 1h at 4°C with gentle rotation. This step was performed to decrease unspecific resin binding. The lysate was cleared from Sepharose® 4B-200 and further incubated with prewashed anti-FLAG Sepharose (Biotool, B23102), for 3h at 4°C with gentle rotation. The anti-FLAG Sepharose was collected by centrifugation at 4000 rpm for 15 min and transferred into mini-spin column. The resin was washed three times with 250 µl AFC buffer and twice with 250 µl TEV cleavage buffer (50 mM Tris pH 7.9, 100 mM NaCl, 0.1% Triton X-100). Eight µl of in-house purified TEV protease (conc. ~5 mg/ml) was added in 250 µl of TEV cleavage buffer on a column, sealed and incubated overnight at 4°C. Further, the supernatant containing cleaved proteins was collected, and $CaCl_2$ was added to a final concentration of 1.5 mM. The proteins were loaded on a column with prewashed in CBB buffer (10 mM Tris pH 7.9, 100 mM NaCl, 2 mM CaCl2, 0.1% Triton X-100) Calmodulin

Sepharose (GE Healthcare, 17-0529-01) and incubated for 3h at 4°C with gentle rotation. . The protein-bound resin was washed twice with 250 µl of CBB buffer and three times with 250 µl of CWB buffer (10 mM Tris pH 7.9, 100 mM NaCl, 0.1 mM CaCl2). Dried resin was stored at -20°C prior trypsin digestion for Liquid Chromatography coupled to tandem Mass Spectrometry (LC-MS/MS).

Identification of proteins by LC-MS/MS

Dried resin was resuspended in 50 µl of 100 mM NH_4HCO_3, reduced with TCEP and alkylated with iodoacetamide for 45 min at RT in dark, followed by overnight digestion with 10 ng/µl trypsin. Digestion was stopped with 5%TFA to a final concentration of 0.1%, followed by addition of acetonitrile to a final concentration of 2%. The resulting peptide mixtures were separated and measured at an online LC-MSMS setup. LC (Waters Accuity) RP-18 pre-columns (Waters), nano-HPLC RP-18 column (internal diameter: 75 µM, Waters) using an acetonitrile gradient (2%–35% ACN in 180 min) in the presence of 0.1% trifluoroacetic acid at a flow rate of 250 nl/min. The column outlet was directly coupled to the ion source of an Orbitrap Elite mass spectrometer (Thermo Scientific). Three-blank-washing runs were done between each sample to ensure the absence of cross-contamination from preceding samples. The mass spectrometer was operated in a data-dependent mode.

Analysis was performed at the Laboratory of Mass Spectrometry (IBB PAS, Warsaw). Data were analyzed using MaxQuant 1.6.3.4, referenced to *E.coli* proteome from UniProt database downloaded on 25.05.2020, 4391 entries. In total, 1600 proteins were identified (FDR 1%). The error ranges for the first and main searches were 20 ppm and 6 ppm, respectively, with 2 missed cleavages. Carbamidomethylation of cysteines was set as a fixed modification, and oxidation and protein N-terminal acetylation were selected as variable modifications for database searching. The minimum peptide length was set at 7 aa. Both peptide and protein identifications were filtered at a 1% false discovery rate and were thus not dependent on the peptide score. Enzyme specificity was set to trypsin, allowing cleavage of N-terminal proline. A ‘common contaminants’ database (incorporated in MaxQuant software) containing commonly occurring contaminations (keratins, trypsin etc.) was employed during MS runs.

Data were deposited in Pride Repository under an entry PXD030113.

Protein complexes - data analysis

To filter out non-specific interactants, i.e., prey proteins that are more abundant in the negative controls than in the specific experiments, statistical analyses were carried out using a

custom Python script (version 3.7.6). First, based on protein intensity values, median normalization was performed for each sample to reduce inter-sample variability, followed by log10 transformation. Proteins not identified in a sample with 0 intensity value, were replaced with intensity value=1 to enable logarythmic transformation of the data.

For each prey protein record, the ratio magnitude between an experimental sample and negative control was computed and its significance was assessed using a one-way z-scorewith mean standard error computed from all proteins and samples, to increase statistical power. A protein was considered to be significantly more abundant in a specific experiment than in the negative control if the ratio magnitude between the two sets was >= 1.5, and its FDR (False Discovery Rate) adjusted-pvalue was <= 0.05 (Benjamini-Hochberg correction for multiple-testing).

Venn diagrams were made with a free online tool: http://bioinformatics.psb.ugent.be/webtools/Venn/. Protein interaction networks were analyzed and done using Cytoscape ver. 3.8.2. Functional enrichment analysis was done using a free web tool - GSEA (24).

Chromosomal DNAreplication analysis with flow cytometry

Chromosome number measurements were performed as described in Hawkins and coworkers, with several modifications (25). Briefly, cells weregrown with aeration at 37°C until OD600=0.15 in LB medium supplemented with 0.2% glucose (fast growth) or AB medium (15.1mM $(NH_4)_2SO_4$, 42.3 mM Na_2HPO_4, 22 mM KH_2PO_4, 51.3 mM NaCl, 0.1 mM $CaCl_2$, 1 mM $MgCl_2$, 0.003 mM $FeCl_3$, 10 µg/ml thiamine, and 25 µg/ml uridine) supplemented with 0.4% sodium acetate (slow growth). Threeml samples were collected, treated with 150 µg/ml rifampicin, and 10 µg/ml cephalexin and incubated for 4 h at 37^{o}C with mixing. Incubation with antibiotics results in cells containing an integral number of chromosomes, corresponding to the number of replication origins at the time of drug treatment. Subsequently, cells were harvested, washed with TBS (20 mM Tris-HCl pH 7.5, 130 mM NaCl) and fixed with cold 70% ethanol overnight or longer. Additional 3 mL sample at OD_{600}=0.15 was collected without antibiotic treatment and fixed as above. After sample collection, bacterial culture was grown up to early stationary phase with OD_{600} measurements to determine doubling time of bacterial population.

Prior to flow cytometry analysis, cells were resuspended in 50 mM sodium citrate followed by RNA digestion with RNase A for 4 h. Chromosomal DNA was stained with 2 mM Sytox Green (Invitrogen) and DNA content per cell was measured with BD FACSCalibur at 488 nm Argon Ion laser. MG1655 (WT) strain grown in AB medium containing one of the following carbon sources: 0.4% sodium acetate, 0.2% glucose, 0.2% glucose + 0.5% casamino acids or in LB medium with 0.2% glucose, treated with antibiotics, fixed and stained as above was usedas a standard for each flow cytometry measurement, indicating cells containing 1/2 , 2/4, 4/8 or 8/16 chromosomes, respectively.

Flow cytometry data were analyzed using FlowJo ver. 10.8.0. To determine cell volume, fixed exponentially growing cells (collected without antibiotic treatment) were micro photographed using Leica DM500 microscope. Cell length and width were measured in ImageJ and cell volume was calculated with cylinder volume equation ($\pi r^2 h$) where r – half of cell width and h – cell length.

Figures

All figures from the manuscript were prepared using https://biorender.com.

Results

Experimental setup and data analysis of the replication proteins interaction network and its dynamics under different bacterial growth conditions

The rationale behind our experimental plan was that protein modules responsible for chromosome duplication may undergo substantial remodeling as conditions change, underlying growth rate and/or condition-dependent control of DNA replication. Therefore, we aimed to investigate the composition of protein complexes formed by the main DNA replication regulators (DnaA, DiaA, Hda, SeqA)(16) and key replication complex components (DnaB, DnaG, HolD)(17) in chosen, disparate conditions. In our analysis, we included also NrdB, a ribonuclotide reductase (RNR) subunit, the key enzyme producing deoxyribonucleotides. Experimental evidence suggests that RNR may be associated with the replication complex (26), with its activity dictating the length of the C period (27). We used AP-MS according to the protocol published previously by Butland and coworkers (23, 28) to assess protein-protein interactions of selected replication proteins. Replication machinery

interactome was probed during fast bacterial growth in rich, undefined medium (LB) and in defined synthetic medium, supporting slow growth rate, with acetate as a sole carbon source. In both cases, protein complexes were investigated in the late exponential phase (OD_{600} ~ 0.6-1.0) and for LB-grown cultures also upon cell culture entry to stationary phase. This way, we could subsequently compare changes within the replication proteins PPI network between fast and slow growth conditions, and after bacterial growth had ceased. For each protein queried, we prepared a strain producing its SPA-tagged version. We constructed C-terminally tagged translational fusions of the cognate genes, under control of their native promoters, in the MG1655 genetic background. Using such a setup we wanted to ensure near-endogenous levels of the replication proteins used as baits in our experiment, to minimize spurious interactions. Following isolation by tandem AP, composition of proteins co-purified with the baits was assessed by mass spectrometry and analyzed quantitatively using MaxQuant (29). A critical issue in AP-MS experiments is elimination and identification of protein impurities that interact either with resins or bound proteins unspecifically and obscure subsequent identification of true interactants. On the other hand, not every protein forming an interaction with the resins or SPA-tag itself should be automatically accounted for as a false-positive when analyzing samples containing tagged baits and therefore protein enrichment should be calculated in such cases. To tackle this problem, we performed two types of control experiments for each growth condition tested, which further allowed to set threshold criteria for unspecific protein binding and filter interactions characterized by substantial prey enrichment and low False Discovery Rate (FDR adjusted p-values < 0.01). Controls were composed of an untagged MG1655 strain and an MG1655 strain expressing a SPA-tagged fluorescent Venus protein, both grown under identical conditions to those used for the strains expressing the tagged bait proteins. In the first case, the control experiment enabled correction for proteins attaching unspecifically to the resins, in the second – for proteins binding to a random SPA-tagged protein or SPA-tag itself. The use of the two control types delimits abundance range of a protein that binds unspecifically, dependent on resin occupancy by a bait protein. Specifically, we made a presumption that the level of proteins binding unspecifically to the resin will be lower when the amount of bait protein and its interactants is high and thus, the resin beads are more occupied. The differences between resin occupancy among different bait proteins may result from different native protein expression levels as well as various tag surface exposition on the natively folded proteins. Considering reproducibility of the results, for further statistical analysis we took into account only protein hits that were identified in each of three sample replicates (Supplementary figure 1A-H and

Supplementary file 1). However, we performed statistic tests for every protein hit that appeared in at least one replicate of the control samples. Statistic tests were performed separately for each control. We further considered as hits only the interactions that were statistically significant with respect to both control types as well as preys that did not appear in any of the controls. In similar proteomics analysis published previously, authors considered as potential hits also the proteins that appeared in both three and at least two sample replicates. We did not perform statistical analysis for the latter cases, but we selected those proteins which appear in at least two sample replicates but are not present in either of the controls and listed them in the Supplementary file 2. Moreover, we did not perform any manual curation of the data, leaving also all recovered ribosomal proteins in our dataset. Although ribosomal proteins constitute frequent contaminants in AP-MS experiments, their profile changed significantly for each protein tested and for HolD, DiaA, NrdB and Hda the fraction of ribosomal protein preys was much less abundant than for DnaA, SeqA, DnaB and DnaG. Therefore, some of the co-purified ribosomal components may represent true interactants. For instance, such direct interaction has been previously reported between DnaA and the ribosomal protein L2 (30).

Screen results recapitulate well-known replication proteins contacts and provide possible explanations for several previously observed genetic interactions

As expected, results of the screen confirmed well-known connections between complex components of several replication proteins, like these formed by DNA polymerase III subunits, ribonucleotide reductase complex or between Hda and β sliding clamp of DNA polymerase III (Fig. 1C). These are stable complexes that were isolated under all tested conditions. Our results also recapitulated the interactions described previously as spatiotemporally-regulated during the cell cycle (DnaB-DnaC, DiaA-DnaA, HolD-Ssb, topoisomerase III-HolD) (Fig. 1C, 2) (17, 31, 32) or performing special function, i.e. replication through highly transcribed regions (DnaB-Rep)(33) (Fig. 2). These results confirm that the approach we used accurately identifies different types of complexes formed by the selected replication proteins. Moreover, our data also corroborates some of the experimentally supported interactions present in the STRING database (Fig. 2). Though, the majority of the identified interactions have not been reported in the STRING database before (Supplementary file 3). On the other hand, our screen has not captured all of the experimentally confirmed interactions found in the STRING database. This is however not surprising as most of the missing interactions were previously identified based on assays consisting of purified proteins

or the yeast two-hybrid system (Supplementary table 4). In those assays, both protein partners are provided at relatively high amounts at the same time and space. Those conditions may not be recapitulated under bacterial growth conditions used in our study and instead those protein assemblies may be specific to certain physiological sates of bacterial cells or represent less prominent cellular protein complexes.

Interestingly, among significantly enriched preys, we have found examples of proteins which had been previously implicated in an interplay with the *E. coli* replication machinery by genetic screens (Supplementary file 2, Fig. 3). Namely, SspA protein was isolated as an interactant of HolD, whereas RlmE was found in complex with NrdB. Previously, a deletion of *sspA* has been shown to suppress growth defect of a *ΔholD* strain (34). SspA is a transcription factor required for stress and starvation responses, therefore the mechanism of suppression was suggested to be indirect and operate through changes in gene expression in a *ΔsspA* strain (35). Another study revealed that SspA may in fact be needed to solve transcription-replication conflicts (36). RlmE, on the other hand, is a 23S rRNA methyltransferase responsible for methylation of the 2'-O ribose position at the conserved U2552 nucleotide. Growth of *ΔrlmE* strains was found sensitive to hydroxyurea, a well-known inhibitor of ribonucleotide reductase (37). This sensitivity was attributed to increased membrane stress of cells devoid of RlmE, due to perturbed translation and the resultant elevated incorporation of misfolded proteins to their cell membrane. However, in light of our results, in both cases, the observed genetic interactions may have more complex cause and arise from direct protein-protein contacts of RlmE and SspA with the replication machinery. Those results show that the data produced by our screen provide meaningful results, supporting reliability of previously uncharacterized protein-protein interactions identified in this work.

Interaction networks are specific for each replication protein and bacterial growth condition

Results of the PPIs analysis revealed that each of the queried replication proteins forms a unique constellation of contacts with the rest of the proteome (Fig. 3, Supplementary file 4). For simplicity, preys identified in the screen were classified into arbitrary single functional categories, although some proteins could be ascribed to more than one cellular function. Nevertheless, as described in the preceding paragraphs, our screen confirmed previously found interactions among the replication proteins. In AP-MS experiments, it is possible that the identified preys do not form a direct contact with the bait, but rather with some of true

primary interactants. Those preys may still be a part of a larger complex formed by the bait or comprise alternative complexes formed by the interactant. However, a small overlap between sets of preys co-purified with baits that interact with each other suggests that the selected preys, at least in part, represent direct interactions (Fig. 4). Interestingly, DnaA regulators Hda and DiaA formed a small number of interactions, whereas proteins associated with replication forks progression (HolD, NrdB, DnaB, SeqA) and DnaA formed large but distinct networks. For instance, HolD displayed many statistically significant connections with various metabolic proteins but none with the ribosomal ones, contrary to SeqA, which interacted with only two metabolic enzymes. One of them was polyphosphate kinase (Ppk), being also a component of *E. coli* RNA degradosome (38), as described in more detail in the next sections, could also be classified as a RNA modification machinery member. In general, similarity of the PPI network (percentage of the same preys) was the highest for DnaA and SeqA and high also for DnaB and SeqA, although SeqA has not been found to interact directly with either DnaA or DnaB (Fig. 4). In both cases, however, high similarity stems from a large number of significantly enriched ribosomal proteins common between the three baits which are likely in part false-positives. Though, unlike DnaA, DnaB shares with SeqA ribosomal protein interactants L16 (RplP) and L23 (RplW) (LB, log phase) (Fig. 3) that were absent from all controls and thus are considered as hits. It is also worth noting that the two ribosomal proteins were identified as a part of the DnaG protein complex. Primase by itself co-purified with SeqA (LB, stationary phase; Fig. 3), indicating that the two proteins may interact. Such interaction hasn't been described before for the *E. coli* replication complex and its role remains unknown.

Importantly, the set of interactants for every bait used in our screen changed drastically with growth conditions (Fig. 5A). In general, the highest number of statistically significant interactions was observed in samples obtained from bacteria during their exponential growth in rich medium, whereas the smallest – in samples grown in minimal medium with acetate (Fig. 5A). This difference in statistically significant prey number can only partially be attributed to bait abundance in samples from different growth conditions (Fig. 5B). At the same time, stable complexes, like DNA Pol III, Hda-DnaN or DnaB-DnaC were isolated under all conditions, showing that the procedure provides meaningful results irrespective of the culture growth conditions. Those results suggest also that PPI modules comprising the tested replication proteins undergo significant reorganization as environmental conditions change.

Functional enrichment analysis of PPIs formed by different replication proteins

Functional enrichment analysis of PPIs formed by six of the tested replication proteins in all tested conditions revealed several interesting features (Fig. 6; Supplementary file 6). The number of interactants isolated with DiaA and Hda was too low to perform this kind of analysis. As mentioned earlier, HolD protein sub-network was enriched in metabolic enzymes (Fig. 6). Two of them (PurB and GuaA) are members of purine nucleotide synthesis pathways, suggesting possible coordination between nucleotides pool and DNA replication. Interestingly, four proteins were enriched in interactants with RNA-binding function (DnaB, DnaG, DnaA, SeqA). In addition, DnaB was enriched in preys with ribonuclease activity (Fig. 6). Closer examination of the data revealed that two of the above mentioned proteins (DnaB and SeqA) were co-purified with components of the *E. coli* degradosome (Fig. 3)(38). Specifically, DnaB pulled-down RNase E (Rne), RhlB and also Ppk (p-value = 0.01) in the samples from the exponential growth in LB, whereas SeqA was isolated with ppk. SeqA also pulled-down SrmB, which interacts directly with RNase E, in samples isolated from LB overnight culture. SrmB was also found as a prey in the case of DnaG. As mentioned earlier, DnaG and SeqA were found to co-purify with each other. However, statistical significance was found in the case of SeqA bait and DnaG prey in the samples isolated from LB overnight culture, whereas in the reversed experiment SeqA co-immunoprecipitated significantly with DnaG in the samples from exponential phase (p-value = 0.01). Those results suggest that DnaB and SeqA may both interact with the RNA degradosome, while SeqA interacts also with DnaG. All those interactions have not been described before.

Interestingly, our analysis recovered many connections between protein involved in cell envelope biogenesis and the replication proteins. Namely, DnaA was enriched in peptidoglycan synthesis proteins (MurG, MrcB) in the functional enrichment analysis. All other replication proteins tested have also shown conspicuous number of interactions with enzymes related to synthesis of the cell envelope precursors or cell envelope integral proteins, although GO term enrichment analysis did not show statistical significance in those cases. In particular, proteins engaged in the lipopolysacharide (LPS) synthesis (39) were purified with NrdB (RfaF, HldE, LpxD), DnaB (LpxD and RfaF), HolD (RfaF, WecF) and SeqA (RfaF). While RfaF was present as prey in many experimental samples (highly-enriched with DnaB and SeqA baits), it is worth mentioning that it was absent from all but one of the eighteen control samples (from all conditions), where it was identified in minute amounts. SeqA was also found to co-immunoprecipitate with PlsB, an enzyme engaged in a membrane

phosphlipids synthesis. Intriguingly, we have also found GalU, previously implicated in cell division control through its product (40), as prey of DiaA and to a lesser extent – SeqA. Those interactions seemed very specific as GalU was also present in very small amounts in only one of 18 control samples. A connection between cell envelope biogenesis and DNA replication has been suggested by many previous studies which we discuss in more detail below.

NrdB subunit of RNR, as expected, was enriched in DNA replication proteins – Ssb, PriB and DNA Pol III subunit DnaN. The latter may be the RNR contact point within the replication complex.

Interaction networks components have functional impact on replication timing in the E. coli cell cycle

While cell cycle stages of fast-growing bacteria occur simultaneously, it is crucial for the cell to provide precise timing of the replication initiation in each cell cycle as well as to couple each replication initiation with corresponding cell division according to 'one initiation of replication per cell cycle' rule (12) (Fig. 1A). The main conclusion of numerous research on the interplay between bacterial growth and cell cycle is that cells maintain growth rate-dependent size homeostasis and that the relationship between cell size, replication timing and thus the DNA content in the cell is precisely regulated (14, 15) (Fig. 1B). As a consequence, each change in DNA content under specific growth rate should be accompanied with changes in growth rate and/or cell size. If these relationships are disturbed, bacterial population exhibit deregulations in precise replication timing, namely the initiation might occur too early or too late in the cell cycle. Moreover, problems in proper replication timing may also lead to even more serious effect – origins present in the cell may not fire simultaneously which results in uneven distribution of genetic material to progeny cells.

Consequently, chromosome copy number measurement along with size and growth rate calculations can be used as a way to determine the replication timing in exponentially growing bacterial population. In this approach, centered on flow cytometry, chromosomal content in bacterial cells is assessed after the so-called replication runout performed with rifampicin and cephalexin treatment (25). Upon inhibition of the initiation of new rounds of chromosome replication and cell division with those antibiotics bacterial cells remain with the chromosome number corresponding to the number of origins present at the time of antibiotics addition. DNA content can be then measured with flow cytometry and correlated with microscopically-determined cell size and growth rate of bacterial population derived from OD measurements (25, 41). Since the chromosome number present in *E. coli* cells growing in

defined media has been well established before (41), the wild type strain can serve as a standard to compare with mutant strains.

To determine whether replication protein interactants recovered in this work can be functionally involved in replication regulation during the cell cycle, we constructed deletion mutants of chosen genes encoding those proteins and subjected them to the analysis described in the preceding paragraph. We chose genes from two different functional groups, namely: *rlmE*, gene encoding 23S rRNA methyltransferase found in complex with NrdB and *rfaD*, gene encoding ADP-L-glycero-D-mannoheptose 6-epimerase found in complex with SeqA (p-value = 0.01). RfaD is engaged in LPS synthesis and related in several ways to another significant interactant identified in our screen – RfaF. Namely, RfaD is responsible for the synthesis of substrate metabolite that is directly used for the reaction mediated by RfaF. Besides, rfaD and rfaF genes are transcriptionally co-regulated within a single operon. We chose to analyse RfaD, because the type of analysis described above was not possible with *ΔrfaF* mutant, since it does not grow in minimal medium with acetate as carbon source (data not shown).

Deletion mutants were grown in two different conditions, providing fast and slow growth rate and corresponding to the conditions used for the PPI screen. Cells in early logarithmic growth phase (OD600=0.15) were subjected to replication runout and total chromosome copy number was measured using flow cytometry. Results for *rlmE* and *rfaD* deletion mutants are presented in Figures 7 and 8, respectively. *E. coli* MG1655 (WT) strain cultured in different media served as a reference strain to make a standard curve depicting the relationship between chromosome number and cell volume as well as between chromosome number and doubling time (supplementary fig. 2 and supplementary file 7).

Our results suggest that both deletion strains exhibit disturbances in proper replication timing, especially under the conditions supporting fast bacterial growth rate. The majority of cells within the populations of Δ*rlmE* and Δ*rfaD* mutants grown in LB medium supplemented with 0.2% glucose contained 4 and 8 chromosomes (less than WT cells that had 8 and 16 chromosomes under these growth conditions), both mutant populations contained a fraction of cells where asynchronous replication events occurred. Slowly growing Δ*rlmE* cells (minimal medium +acetate) showed no differences in chromosome number comparing to WT strain, whereas *ΔrfaD* population encompassed a small fraction of cells with higher DNA content.

Measurements of cell size and doubling time revealed that Δ*rlmE* strain grew slower than WT in rich medium, with elongated cells and bigger cell volume (supplementary table

4). Δ*rfaD* deletion mutant, in turn, exhibited slightly smaller cell volume in both growth conditions whereas doubling time was much longer than in comparison to the WT strain only in the minimal medium (Supplementary table 5). These values plotted on standard curve graphs suggested that the relationship between cell volume and DNA content is significantly disturbed in Δ*rlmE* deletion mutant under the conditions supporting fast growth rate. The interplay between chromosome number and cell cycle duration (expressed as cell doublings per hour) is also deregulated in fast-growing Δ*rlmE* strain, but also in slowly growing rfaD deletion mutant. Those results suggest that RlmE and RfaD indeed have an impact on cell cycle regulation and their relation with RNR and SeqA remains to be established.

Discussion

Protein-protein interactions are crucial for execution and regulation of all cellular functions. Cell cycle is a particular example of process regulated by spatiotemporally resolved protein complexes. It is because complexes composition has to change at different cell cycle stages to enable performance of different biochemical functions required at different steps. At the same time, coordination of genome duplication with other DNA transactions, like chromosome segregation and transcription, has to be ensured. The latter may also mean that different solutions are needed under different gene expression programs. Some of the protein complexes operating at chromosome replication constitute stable multisubunit machines, others rely on transient protein-protein interactions. For regulation of molecular processes, it is important not only whether a complex is formed or not but also – if its more or less abundant and how this affects the possibility of formation of alternative complexes. Thus, to fully understand regulation of DNA replication in bacteria at different environmental regimes, it is important to qualitatively and quantitatively assess the dynamics protein interaction network under various conditions. The major driving force of changes in protein complexes and entire modules are alterations in protein abundance and hence - abundance of the alternative interaction partners of hub proteins. However, whereas expression of genes encoding components of stable complexes is usually coordinated, it is not necessarily true for transient interactions. Thus, transient interactions may be more difficult to predict from gene expression data alone. Some of the mechanisms responsible for such interactions are post-translational protein modifications. Already existing *E. coli* protein-protein interaction networks are usually static and do not provide any information on how composition of protein

complexes and protein modules changes under different conditions. The same is true for well-established components of the *E. coli* replication and pre-replication complexes. The crucial interactions (for instance DnaA-Hda, DnaA-DiaA, Hda-DnaN) (Fig. 1C) are characterized but it is not known whether they all play a role under various conditions and if additional factors may be operational. In this work we analyzed the PPI network of the key proteins involved in DNA replication in *E. coli*. For this proof of concept study we chose label-free quantitative proteomics approach. We have shown that the number of interactions formed by each tested replication protein changes significantly with growth conditions. Those results corroborate the hypothesis that the network of replication machinery interactions changes to accommodate variations in DNA replication itself and other processes occurring on DNA (Fig. 3). We demonstrate that some interactions appear and dissolve under different conditions. Absent interactions in our results do not necessarily mean that they do not exist under particular conditions at all, but that they are less abundant or less stable. Our results also suggest that the high-throughput studies on PPIs, performed on stationary phase cells provide a fragmentary picture on the interaction network formed by the replication proteins.

Our screen performed on exponential cultures revealed several interesting interactions. First of all, DnaB and also SeqA were co-purified with components of the RNA degradosome (Fig. 3, Supplementary file 2). While, to our knowledge, no evidence on cooperation between the replication machinery and RNA degradosome exists so far in *E. coli*, it has been found that the function of RNA surveillance machinery is required for stability of human mitochondrial genome (42). Activity of human RNA degradosome is required for prevention of harmful R-loop formation in the mitochondrial genome. As R-loops impede replication fork progression in *E. coli* (43), it is possible that such interaction would foster R-loop removal and ensure processivity of the replisome. Similarly, stress response transcription factor SspA has been previously suggested to play a role in resolving transcription-replication conflicts(36). Our results indicate that a direct protein-protein interaction of SspA with HolD, or indirect – with other HolD interactant – may play a role in this SspA function (Fig. 3, Supplementary file 2).

One of the overrepresented functional protein categories among the preys, belonging also to RNA-modifying enzymes, were RNA methyltranferases (RlmE, RlmL) (Fig 6). We paid particular attention to one of them – RlmE, due to high specificity of the interaction, its condition-dependence and previously described phenotypic relation to the cognate replication protein bait – RNR. We analyzed cell cycle parameters in *E. coli* cells devoid of the *rlmE* gene and found that its absence affected replication synchrony and the correlation between chromosome number, cell volume and growth rate under fast growth conditions (Fig. 7).

Secondly, our screen revealed many interactions of replication proteins with the cell envelope (inner membrane-peptidoglycan-outer membrane) proteins or enzymes directly engaged in the synthesis of cell envelope precursors (Fig. 3, Supplementary file 2). Some connections of the replication regulators DnaA and SeqA with the cell membrane and outer membrane have been suggested before, as summarized in Fig. 9A. Namely, an interaction between acidic phospolipids and DnaA has been shown to enhance the exchange rate of ATP/ADP nucleotide bound by DnaA (44) and inhibit DnaA binding to *oriC* (45). In addition, a depletion of PgsA, an enzyme necessary for synthesis of acidic phospholipids, has been demonstrated to result in cell cycle arrest (46). The mechanism of this arrest is still not fully understood but a large body of evidence suggests that it is dependent on a membrane-binding region of DnaA (47, 48). Moreover, the negative replication regulator SeqA has been found to be responsible for hemimethylated *oriC* binding by membrane fractions (49) and be by itself associated with the cell inner membrane (50). What is more, *ΔseqA* mutants have been shown to exhibit increased LPS phosporylation, contributing to elevated ori/ter ratio in these mutants (51). In addition, many of the nucleotide synthesis pathway enzymes (PurACDF, GuaB, Prs, NrdA), including deoxynucleotide-producing RNR, have been localized to the inner membrane in a recent study (50). The replication protein interactants related to cell envelope metabolism identified in this study (Fig. 9B) may contribute to the already described regulatory mechanisms or represent alternative connections between cell membranes biology and DNA replication. In this work we confirmed that the DNA replication profile is perturbed in a mutant strain encoding one of the SeqA interactants – RfaD (Fig. 8), localized to the cytoplasmic side of the inner membrane (50). The mechanism of rfaD impact on chromosomal DNA replication control and the reason for appearance of asynchronous origin firing remain to be established. It is also worth noting that one of the interactants of DiaA protein found in this study, GalU, is an enzyme responsible for synthesis of UDP-glucose (Fig. 3, Supplementary file 2). This nucleotide sugar is necessary for production of cell envelope components including the LPS core. Intriguingly, that metabolite has also been implicated in regulation of the major division protein FtsZ, by binding to a moonlighting enzyme OpgH, involved in synthesis of osmoregulated periplasmic glucans (40). This way, the level of UDP-glucose influences *E. coli* cell size. Considering our results, it is possible that UDP-glucose metabolism is also implicated in DNA replication control.

Several reports have also suggested more or less direct regulation of various DNA replication-related protein activities by metabolic enzymes of the central carbon metabolism (CCM)(52–57). Here, we observed several metabolic enzymes among replication protein interactants,

with FbaB-NrdB (all conditions) and PfkB-DnaA (growth on M9+acetate) seeming highly specific (Fig. 3, Supplementary file 2).

Further studies are needed to verify physiological role of the uncovered PPIs. Moreover, implementation of more sensitive methods is required to detect very weak interactions and accurately quantify PPI network dynamics. However, this study proves that protein complexes formed by the *E. coli* replication proteins undergo large reorganization under different conditions which (Fig. 3; Fig 5), very likely, largely contributes to coordination of DNA replication with other cellular processes.

Funding

National Science Center (Poland) UMO-2014/13/B/NZ2/01139 (M.G.) and UMO-2016/23/N/NZ2/02378 (J.M-O)

References

1. Typas,A. and Sourjik,V. (2015) Bacterial protein networks: Properties and functions. *Nat. Rev. Microbiol.*, **13**, 559–572.
2. Caufield,J.H., Abreu,M., Wimble,C. and Uetz,P. (2015) Protein Complexes in Bacteria. *PLoS Comput. Biol.*, **11**, 1–23.
3. Meng,X., Li,W., Peng,X., Li,Y. and Li,M. (2021) Protein interaction networks: centrality, modularity, dynamics, and applications. *Front. Comput. Sci.*, **15**, 0–17.
4. Nooren,I.M.A. and Thornton,J.M. (2003) Diversity of protein-protein interactions. *EMBO J.*, **22**, 3486–3492.
5. Przytycka,T.M., Singh,M. and Slonim,D.K. (2010) Toward the dynamic interactome: It's about time. *Brief. Bioinform.*, **11**, 15–29.
6. Ou-Yang,L., Dai,D.Q. and Zhang,X.F. (2015) Detecting Protein Complexes from Signed Protein-Protein Interaction Networks. *IEEE/ACM Trans. Comput. Biol. Bioinforma.*, **12**, 1333–1344.
7. Srihari,S. and Leong,H.W. (2012) Temporal dynamics of protein complexes in PPI networks: a case study using yeast cell cycle dynamics. *BMC Bioinformatics*, **13 Suppl 1**.
8. Lin,C.Y., Lee,T.L., Chiu,Y.Y., Lin,Y.W., Lo,Y.S., Lin,C.T. and Yang,J.M. (2015) Module

organization and variance in protein-protein interaction networks. *Sci. Rep.*, **5**, 1–12.

9. Chang,X., Xu,T., Li,Y. and Wang,K. (2013) Dynamic modular architecture of protein-protein interaction networks beyond the dichotomy of 'date' and 'party' hubs. *Sci. Rep.*, **3**, 1–8.
10. Celaj,A., Schlecht,U., Smith,J.D., Xu,W., Suresh,S., Miranda,M., Aparicio,A.M., Proctor,M., Davis,R.W., Roth,F.P., *et al.* (2017) Quantitative analysis of protein interaction network dynamics in yeast. *Mol. Syst. Biol.*, **13**, 934.
11. Reyes-Lamothe,R. and Sherratt,D.J. (2019) The bacterial cell cycle, chromosome inheritance and cell growth. *Nat. Rev. Microbiol.*, **17**, 467–478.
12. Cooper,S. and Helmstetter,C.E. (1968) Chromosome replication and the division cycle of Escherichia coli B/r. *J. Mol. Biol.*, **31**, 519–40.
13. W. D. Donachie (1968) Relationship between Cell Size and Time of Initiation of DNA Replication. *Nature*, **219**, 1077–1079.
14. Si,F., Li,D., Cox,S.E., Sauls,J.T., Azizi,O., Sou,C., Schwartz,A.B., Erickstad,M.J., Jun,Y., Li,X., *et al.* (2017) Invariance of Initiation Mass and Predictability of Cell Size in Escherichia coli. *Curr. Biol.*, **27**, 1278–1287.
15. Wallden,M., Fange,D., Lundius,E., Baltekin,O. and Elf,J. The synchronization of replication and division cycles in individual E. coli cells. *Cell*, **166**, 729–739.
16. Katayama,T. (2017) Initiation of DNA Replication at the Chromosomal Origin of E. coli, oriC. *Adv. Exp. Med. Biol.*, **1042**, 79–98.
17. Schaeffer,P.M., Headlam,M.J. and Dixon,N.E. (2005) Protein-protein interactions in the eubacterial replisome. *IUBMB Life*, **57**, 5–12.
18. Su'etsugu,M., Takata,M., Kubota,T., Matsuda,Y. and Katayama,T. (2004) Molecular mechanism of DNA replication-coupled inactivation of the initiator protein in Escherichia coli: interaction of DnaA with the sliding clamp-loaded DNA and the sliding clamp-Hda complex. *Genes Cells*, **9**, 509–522.
19. Kolberg,M., Strand,K.R., Graff,P. and Andersson,K.K. (2004) Structure, function, and mechanism of ribonucleotide reductases. *Biochim. Biophys. Acta*, **1699**, 1–34.
20. Bárcena,M., Ruiz,T., Donate,L.E., Brown,S.E., Dixon,N.E., Radermacher,M. and Carazo,J.M. (2001) The DnaB.DnaC complex: a structure based on dimers assembled around an occluded channel. *EMBO J.*, **20**, 1462–1468.
21. van den Ent,F. and Lowe,J. (2006) RF cloning: a restriction-free method for inserting target genes into plasmids. *J. Biochem. Biophys. Methods*, **67**, 67–74.
22. Datsenko,K.A. and Wanner,B.L. (2000) One-step inactivation of chromosomal genes in

Escherichia coli K-12 using PCR products. *Proc. Natl. Acad. Sci. U. S. A.*, **97**, 6640–5.

23. Babu,M., Butland,G., Pogoutse,O., Li,J., Greenblatt,J.F. and Emili,A. (2009) Sequential peptide affinity purification system for the systematic isolation and identification of protein complexes from Escherichia coli. *Methods Mol. Biol.*, **564**, 373–400.
24. Subramanian,A., Tamayo,P., Mootha,V.K., Mukherjee,S., Ebert,B.L., Gillette,M.A., Paulovich,A., Pomeroy,S.L., Golub,T.R., Lander,E.S., *et al.* (2005) Gene set enrichment analysis: A knowledge-based approach for interpreting genome-wide expression profiles. *Proc. Natl. Acad. Sci. U. S. A.*, **102**, 15545–15550.
25. Hawkins,M., Atkinson,J. and McGlynn,P. (2016) Escherichia coli Chromosome Copy Number Measurement Using Flow Cytometry Analysis. *Methods Mol. Biol.*, **1431**, 151–159.
26. Sánchez-Romero,M.A., Molina,F. and Jiménez-Sánchez,A. (2011) Organization of ribonucleoside diphosphate reductase during multifork chromosome replication in Escherichia coli. *Microbiology*, **157**, 2220–2225.
27. Ge,Z., Dai,X., Wang,Y.-P., Yang,M., Guo,W., Zhu,M. and Wang,H. (2017) Manipulating the Bacterial Cell Cycle and Cell Size by Titrating the Expression of Ribonucleotide Reductase. *MBio*, **8**, 6–11.
28. Butland,G., Peregrin-Alvarez,J.M., Li,J., Yang,W., Yang,X., Canadien,V., Starostine,A., Richards,D., Beattie,B., Krogan,N., *et al.* (2005) Interaction network containing conserved and essential protein complexes in Escherichia coli. *Nature*, **433**, 531–537.
29. Cox,J. and Mann,M. (2008) MaxQuant enables high peptide identification rates, individualized p.p.b.-range mass accuracies and proteome-wide protein quantification. *Nat. Biotechnol.*, **26**, 1367–1372.
30. Chodavarapu,S., Felczak,M.M. and Kaguni,J.M. (2011) Two forms of ribosomal protein L2 of Escherichia coli that inhibit DnaA in DNA replication. *Nucleic Acids Res.*, **39**, 4180–4191.
31. Keyamura,K., Abe,Y., Higashi,M., Ueda,T. and Katayama,T. (2009) DiaA dynamics are coupled with changes in initial origin complexes leading to helicase loading. *J. Biol. Chem.*, **284**, 25038–25050.
32. Lee,C.M., Wang,G., Pertsinidis,A. and Marians,K.J. (2019) Topoisomerase III acts at the replication fork to remove precatenanes. *J. Bacteriol.*, **201**, 1–13.
33. Guy,C.P., Atkinson,J., Gupta,M.K., Mahdi,A.A., Gwynn,E.J., Rudolph,C.J., Moon,P.B., van Knippenberg,I.C., Cadman,C.J., Dillingham,M.S., *et al.* (2009) Rep provides a second motor at the replisome to promote duplication of protein-bound DNA. *Mol. Cell*,

36, 654–666.

34. Sinha,A.K. (2017) The inactivation of rfaP , rarA or sspA gene improves the viability of the Escherichia coli DNA polymerase III holD mutant. **104**, 1008–1026.
35. Dutra,B.E., Sutera,V.A. and Lovett,S.T. (2006) RecA-independent recombination is efficient but limited by exonucleases. *Proc. Natl. Acad. Sci.*, **104**, 216–221.
36. Cooper,D.L., Harada,T., Tamazi,S., Ferrazzoli,A.E. and Lovett,S.T. (2021) The Role of Replication Clamp-Loader Protein HolC of Escherichia coli in Overcoming Replication/Transcription Conflicts. *MBio*, **12**, e00184-21.
37. Nakayashiki,T. and Mori,H. (2013) Genome-Wide screening with hydroxyurea reveals a link between nonessential ribosomal proteins and reactive oxygen species production. *J. Bacteriol.*, **195**, 1226–1235.
38. Kaberdin,V.R., Singh,D. and Lin-Chao,S. (2011) Composition and conservation of the mRNA-degrading machinery in bacteria. *J. Biomed. Sci.*, **18**, 23.
39. Sperandeo,P., Martorana,A.M. and Polissi,A. (2019) Lipopolysaccharide Biosynthesis and Transport to the Outer Membrane of Gram-Negative Bacteria Springer International Publishing.
40. Hill,N.S., Buske,P.J., Shi,Y. and Levin,P.A. (2013) A Moonlighting Enzyme Links Escherichia coli Cell Size with Central Metabolism. *PLoS Genet.*, **9**.
41. Stokke,C., Flåtten,I. and Skarstad,K. (2012) An easy-to-use simulation program demonstrates variations in bacterial cell cycle parameters depending on medium and temperature. *PLoS One*, **7**, e30981.
42. Silva,S., Camino,L.P. and Aguilera,A. (2018) Human mitochondrial degradosome prevents harmful mitochondrial R loops and mitochondrial genome instability. *Proc. Natl. Acad. Sci. U. S. A.*, **115**, 11024–11029.
43. Gan,W., Guan,Z., Liu,J., Gui,T., Shen,K., Manley,J.L. and Li,X. (2011) R-loop-mediated genomic instability is caused by impairment of replication fork progression. *Genes Dev.*, **25**, 2041–2056.
44. Castumas,C.E., Crooke,E. and Kornberg,A. (1993) Fluid Membranes with Acidic Domains Activate DnaA , the Initiator. *PoLAR*, **24**, 1–4.
45. Makise,M., Mima,S., Katsu,T., Tsuchiya,T. and Mizushima,T. (2002) Acidic phospholipids inhibit the DNA-binding activity of DnaA protein, the initiator of chromosomal DNA replication in Escherichia coli. *Mol. Microbiol.*, **46**, 245–256.
46. Xia,W. and Dowhan,W. (2006) In vivo evidence for the involvement of anionic

phospholipids in initiation of DNA replication in Escherichia coli. *Proc. Natl. Acad. Sci.*, **92**, 783–787.

47. Fingland,N., Flåtten,I., Downey,C.D., Fossum-Raunehaug,S., Skarstad,K. and Crooke,E. (2012) Depletion of acidic phospholipids influences chromosomal replication in Escherichia coli. *Microbiologyopen*, **1**, 450–466.
48. Saxena,R., Fingland,N., Patil,D., Sharma,A.K. and Crooke,E. (2013) Crosstalk between DnaA protein, the initiator of Escherichia coli chromosomal replication, and acidic phospholipids present in bacterial membranes. *Int. J. Mol. Sci.*, **14**, 8517–8537.
49. Slater,S., Wold,S., Lu,M., Boye,E., Skarstad,K. and Kleckner,N. (1995) E. coli SeqA protein binds oriC in two different methyl-modulated reactions appropriate to its roles in DNA replication initiation and origin sequestration. *Cell*, **82**, 927–936.
50. Sueki,A., Stein,F., Savitski,M.M., Selkrig,J. and Typas,A. (2020) Systematic Localization of Escherichia coli Membrane Proteins . *mSystems*, **5**.
51. Rotman,E., Bratcher,P. and Kuzminov,A. (2009) Reduced lipopolysaccharide phosphorylation in Escherichia coli lowers the elevated ori/ter ratio in seqA mutants. *Mol. Microbiol.*, **72**, 1273–1292.
52. Dalmais,B., Bolotin,A., Monnier,A.-F., Kanga,S., Canceill,D., Titok,M., Ehrlich,S.D., Jannière,L., Chapuis,J., Lestini,R., *et al.* (2007) Genetic Evidence for a Link Between Glycolysis and DNA Replication. *PLoS One*, **2**, e447.
53. Węgrzyn,G., Szalewska-Pałasz,A., Maciąg,M., Nowicki,D. and Janniere,L. (2011) Genetic response to metabolic fluctuations: correlation between central carbon metabolism and DNA replication in Escherichia coli. *Microb. Cell Fact.*, **10**, 19.
54. Maciag-Dorszyńska,M., Ignatowska,M., Jannière,L., Wegrzyn,G. and Szalewska-Pałasz,A. (2012) Mutations in central carbon metabolism genes suppress defects in nucleoid position and cell division of replication mutants in Escherichia coli. *Gene*, **503**, 31–35.
55. Nouri,H., Monnier,A.-F., Fossum-Raunehaug,S., Maciag-Dorszynska,M., Cabin-Flaman,A., Képès,F., Wegrzyn,G., Szalewska-Palasz,A., Norris,V., Skarstad,K., *et al.* (2018) Multiple links connect central carbon metabolism to DNA replication initiation and elongation in Bacillus subtilis. *DNA Res. an Int. J. rapid Publ. reports genes genomes*, **25**, 641–653.
56. Westfall,C.S. and Levin,P.A. (2018) Comprehensive analysis of central carbon metabolism illuminates connections between nutrient availability, growth rate, and cell morphology in Escherichia coli. *PLOS Genet.*, **14**, e1007205.

57. Tymecka-Mulik,J., Boss,L., Maciag-Dorszynska,M., Matias Rodrigues,J.F., Gaffke,L., Wosinski,A., Cech,G.M., Szalewska-Palasz,A., Wegrzyn,G. and Glinkowska,M. (2017) Suppression of the Escherichia coli dnaA46 mutation by changes in the activities of the pyruvate-acetate node links DNA replication regulation to central carbon metabolism. *PLoS One*, **12**, e0176050.

Figure legends

Figure 1. Bacterial cell cycle. A) Cell cycle stages during overlapping and non-overlapping cell cycles. B – period from cell birth to initiation of replication, C – period of time required for synthesis of daughter chromosomes, D – period required for cell division; B) DNA replication starts at a constant cell mass (volume) per replication origin irrespective of growth rate (initiation mass, invariant unit cell, IUC). Cell size increases with growth rate and overlapping replication rounds occur in fast-growing cells. Red dots represent replication origin. C) Experimentally confirmed protein-protein interactions during replication complex formation (left panel) and those recapitulated in this work (right panel)

Figure 2. Experimentally confirmed PPIs present in the STRING database for the eight replication proteins analyzed in this work. Baits used in the screen are marked with octagons. PPIs confirmed in this worked are presented with green edges. Proteins identified in the screen as interactants of other replication proteins than their partner in the STRING database are highlighted in bold.

Figure 3. Condition-dependent protein-protein interactions formed by the eight *E. coli* replication proteins selected for this study. Briefly, protein complexes were analyzed by AP-MS. Chromosomally expressed DnaA, DiaA, Hda, SeqA, DnaB, DnaG, HolD, NrdB were C-terminally tagged with SPA-tag in MG1655 genetic background. Bacteria were grown either to middle/late exponential phase in LB medium or M9+acetate as a carbon source, or to stationary phase in LB. Bacterial cells were lysed and protein complexes were subjected to sequential affinity purification according to the protocol published in (23), with minor modifications. Isolated protein complexes were digested with trypsin and their components were identified using LC-MS/MS. Proteins were quantified using MaxQuant(29). Threshold

for unspecific interactions was delimited according to results of control experiments with untagged MG1655 strain or the strain expressing moderate levels of SPA-tagged mVenus protein. Graphs present preys isolated with each of the bait proteins under all tested conditions. Edges are color-coded according growth conditions where interaction was identified and edge width is proportional to prey enrichment. Only interactions with corrected p-value < 0.01 were shown. Preys were grouped into functional classes, listed in the figure legend.

Figure 4. Pairwise comparison of uncovered interaction profiles of 8 baits used in this work. Similarity matrices were made based on comparison of interaction profiles between each of 8 bait proteins used in PPI screen ('each with each' comparison). Percent of common interactants between compared bait pairs was calculated and subsequently weighted average was calculated of the number of all interactants identified in our PPI screen.

Figure 5. Venn diagrams showing similarity of interaction profiles for each bait protein used in this study under different conditions (upper panel). Diagrams presenting bait abundancies in the AP-MS experiments, under different growth conditions (showed as log10 value of bait intensity) (lower panel). Protein intensities were calculated using MaxQuant.

Figure 6. Functional enrichment analysis of interactions formed by six of the eight bait proteins used in this work. Analysis was performed with web tool GSEA, described in(24). The entire statistically significant prey set (p-value < 0.01) of each bait protein, obtained from each of the tested growth conditions, was used as input for analysis.

Figure 7. **Cell cycle parameters of the *ΔrlmE* strain.** (A) Upper panel - flow cytometry histograms presenting cell populations containing particular chromosome number, lower panel – microphotographs of representative cells from the population. Chromosome number, present in *E. coli* cells grown in LB+glucose or AB medium + acetate, was calculated after replication run-out, Sytox Green staining and flow cytometry analysis. (B) Graphs show an interplay between chromosome number and cell volume (left) or doublings per hour (right). Cell volume was measured using ImageJ software after collecting cell images with light microscope and phase contrast. OD_{600} measurement of exponentially growing cultures served as basis of growth rate calculation. WT *E. coli* strain cell cyle parameters were set up as a standard curve to which mutant strains can be compared.

*p-value<0.05 (t test)

*** p-value<0.001 (t test)

Figure 8. Cell cycle parameters of the *ΔrfaD* strain.

(A) Upper panel - flow cytometry histograms presenting populations containing particular chromosome number, lower panel – microphotographs of representative cells from the population. Chromosome number, present in *E. coli* cells grown in LB+glucose or AB medium + acetate, was calculated after replication run-out, Sytox Green staining and flow cytometry analysis. (B) Graphs show an interplay between chromosome number and cell volume (left) or doublings per hour (right). Cell volume was measured using ImageJ software after collecting cell images with light microscope and phase contrast. OD_{600} measurement of exponentially growing cultures served as basis of growth rate calculation. WT *E. coli* strain cell cyle parameters were set up as a standard curve to which mutant strains can be compared.

*p-value<0.05 (t test)

*** p-value<0.001 (t test)

Figure 9. Functional connections between cell envelope biogenesis and DNA replication identified so far in E. coli (A). Cell envelope structure and genes engaged in biogenesis of particular layers (B). Proteins identified in this work as interactants of the replication proteins were highlighted in green.

Supplementary figure legends

Figure S1 A-H. Similarity of three biological repetitions performed under each growth conditions for the analyzed bait proteins.

Figure S2 Flow cytometry results and standard curves depicting relation of chromosome number with cell volume and growth rate for the WT *E. coli* strain.

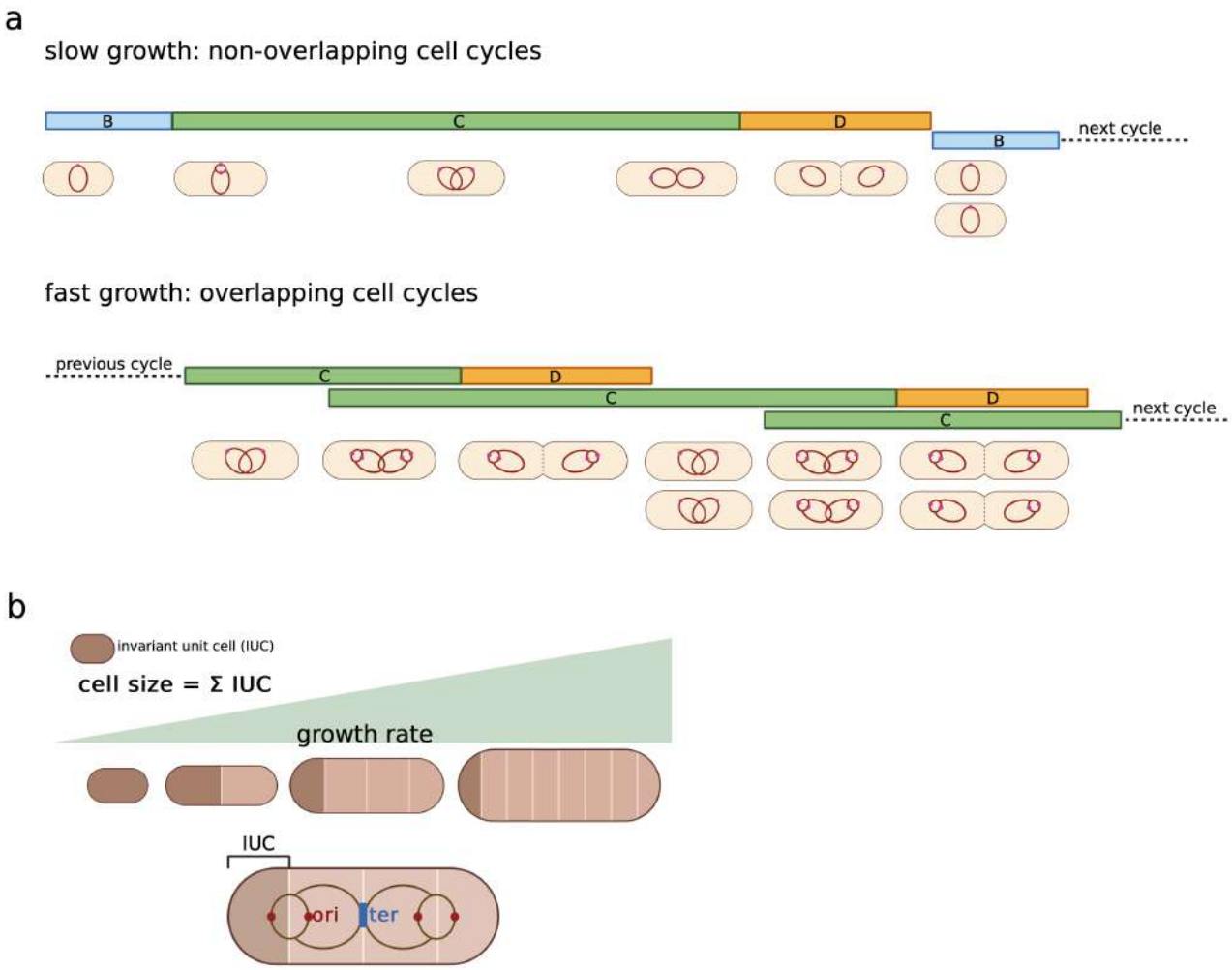

Figure 1. Bacterial cell cycle. (A) Cell cycle stages during overlapping and non-overlapping cell cycles. B – period from cell birth to initiation of replication, C – period of time required for synthesis of daughter chromosomes, D – period required for cell division; (B) DNA replication starts at a constant cell mass (volume) per replication origin irrespective of growth rate (initiation mass, invariant unit cell, IUC). Cell size increases with growth rate and overlapping replication rounds occur in fast-growing cells. Red dots represent replication origin.

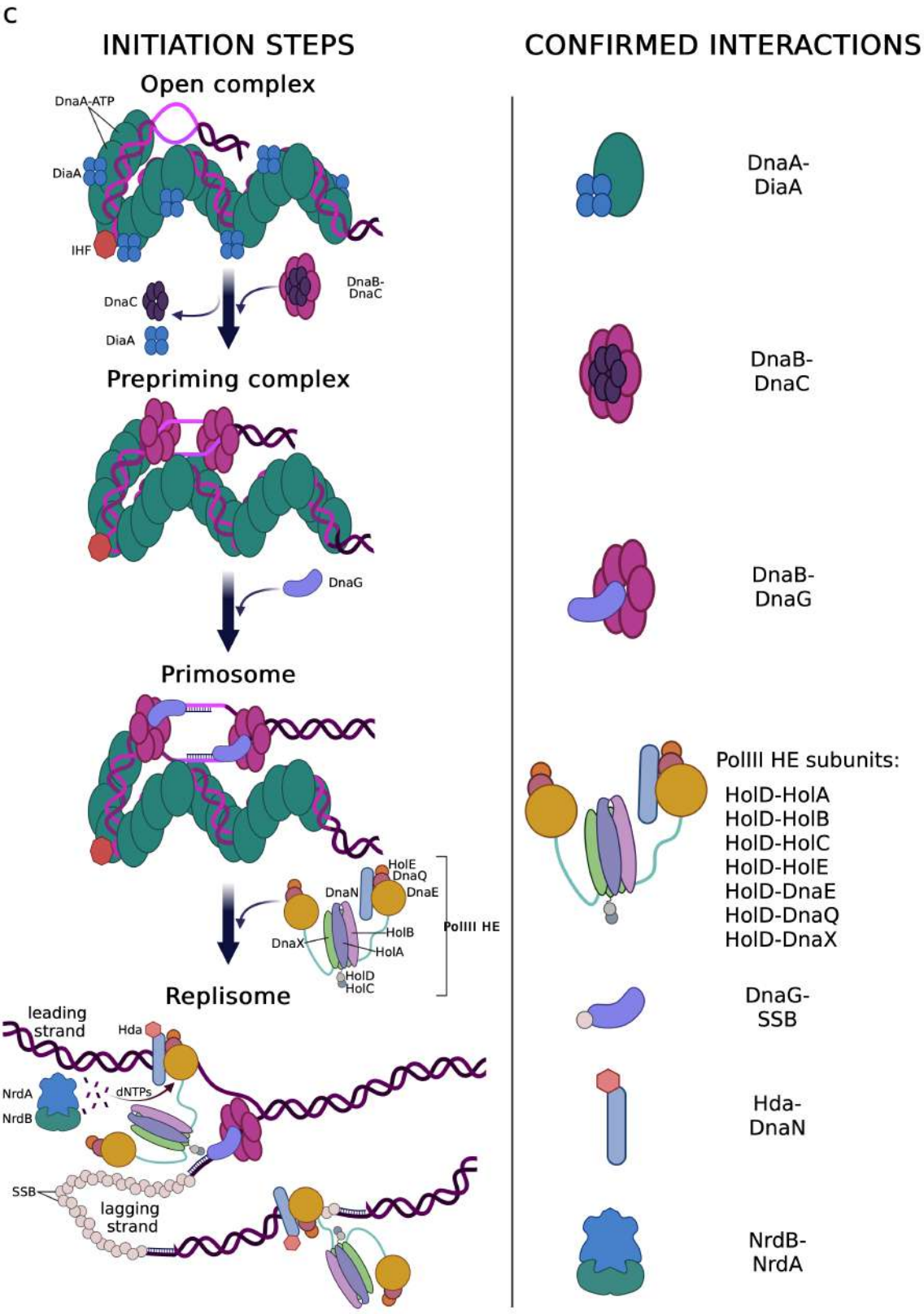

Figure 1. Bacterial cell cycle. (C) Experimentally confirmed protein-protein interactions during replication complex formation (left panel) and those recapitulated in this work (right panel).

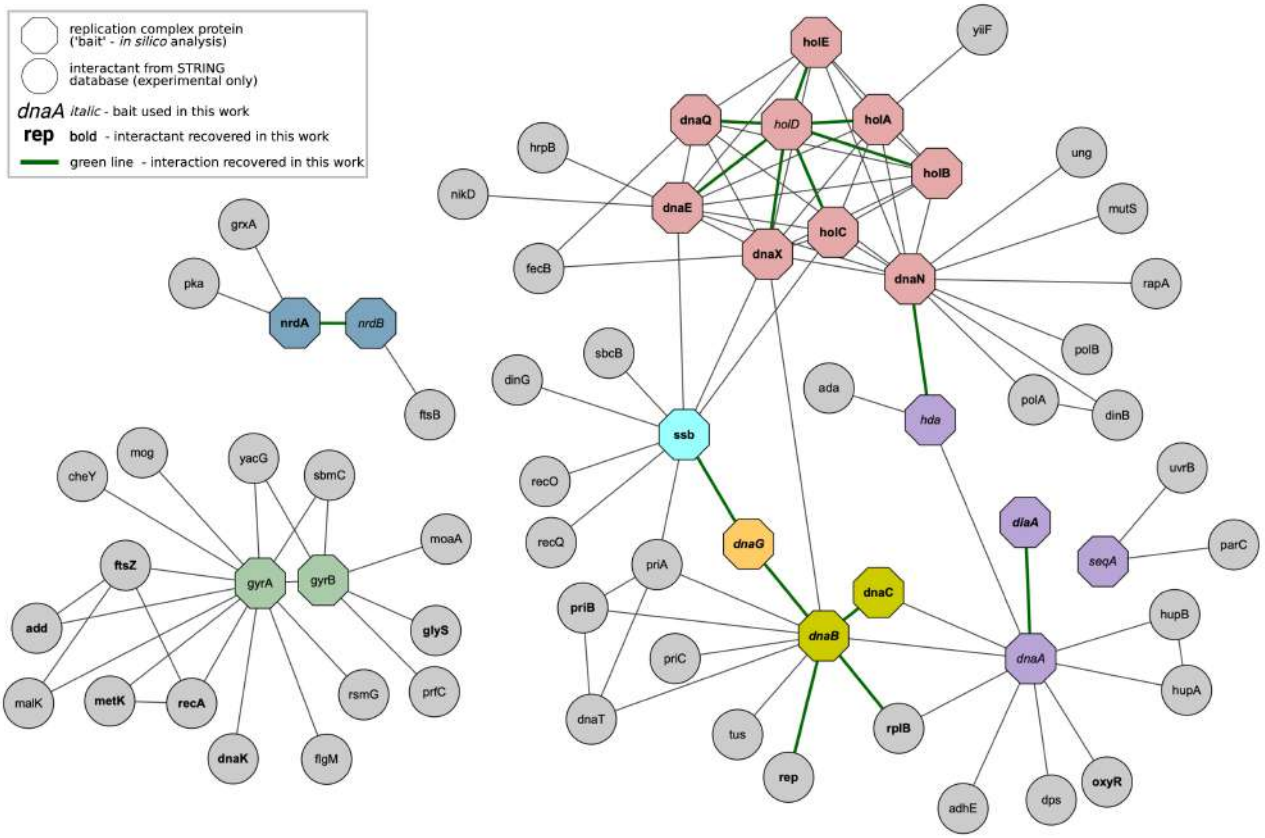

Figure 2. Experimentally confirmed PPIs present in the STRING database for the eight replication proteins analyzed in this work. Baits used in the screen are marked with octagons. PPIs confirmed in this worked are presented with green edges. Proteins identified in the screen as interactants of other replication proteins than their partner in the STRING database are highlighted in bold.

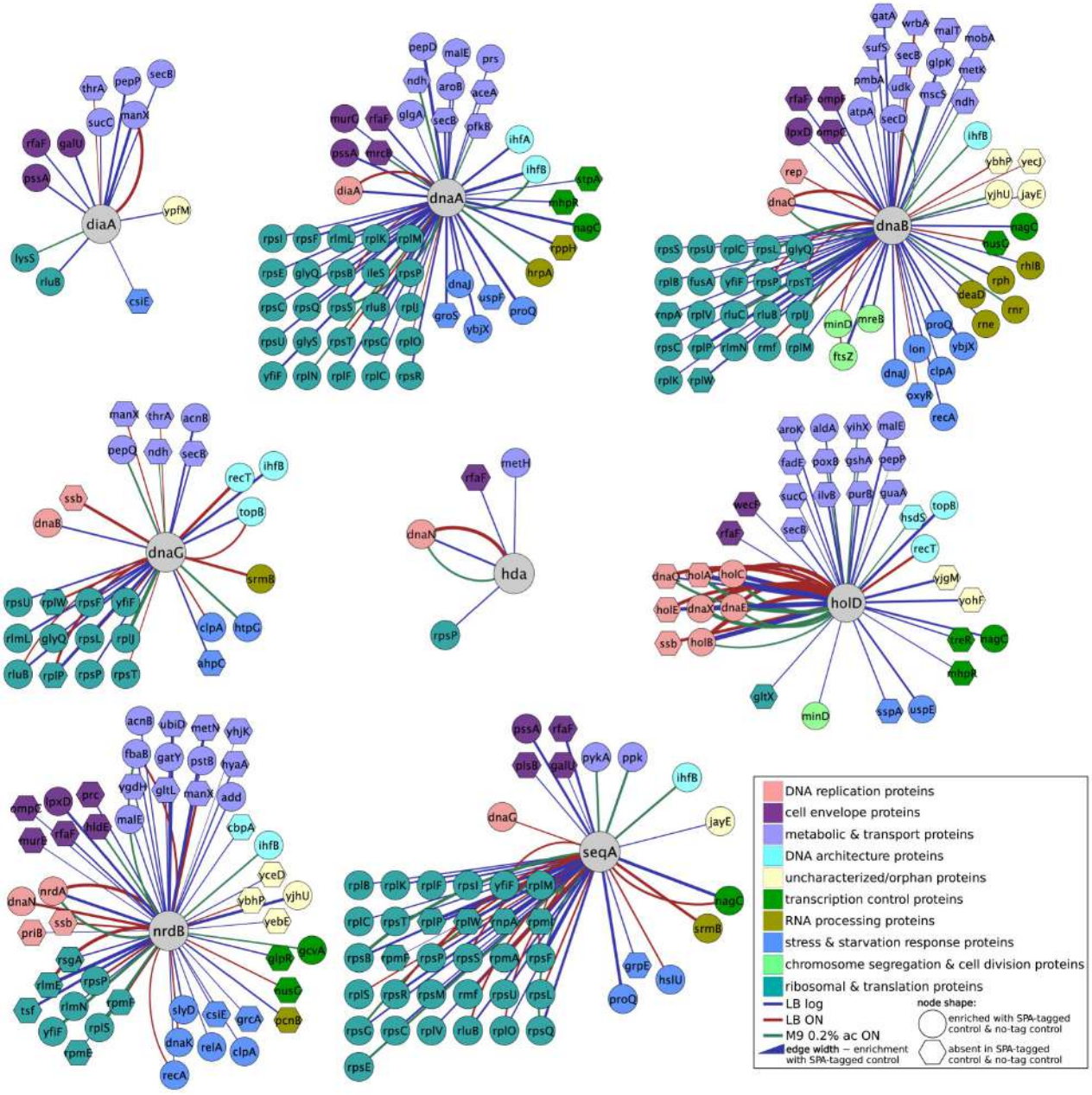

Figure 3. Condition-dependent protein-protein interactions formed by the eight *E. coli* replication proteins selected for this study. Briefly, protein complexes were analyzed by AP-MS. Chromosomally expressed DnaA, DiaA, Hda, SeqA, DnaB, DnaG, HolD, NrdB were C-terminally tagged with SPA-tag in MG1655 genetic background. Bacteria were grown either to middle/late exponential phase in LB medium or M9+acetate as a carbon source, or to stationary phase in LB. Bacterial cells were lysed and protein complexes were subjected to sequential affinity purification according to the protocol published in (23), with minor modifications. Isolated protein complexes were digested with trypsin and their components were identified using LC-MS/MS. Proteins were quantified using MaxQuant(29). Threshold for unspecific interactions was delimited according to results of control experiments with untagged MG1655 strain or the strain expressing moderate levels of SPA-tagged mVenus protein. Graphs present preys isolated with each of the bait proteins under all tested conditions. Edges are color-coded according growth conditions where interaction was identified and edge width is proportional to prey enrichment. Only interactions with corrected p-value < 0.01 were shown. Preys were grouped into functional classes, listed in the figure legend.

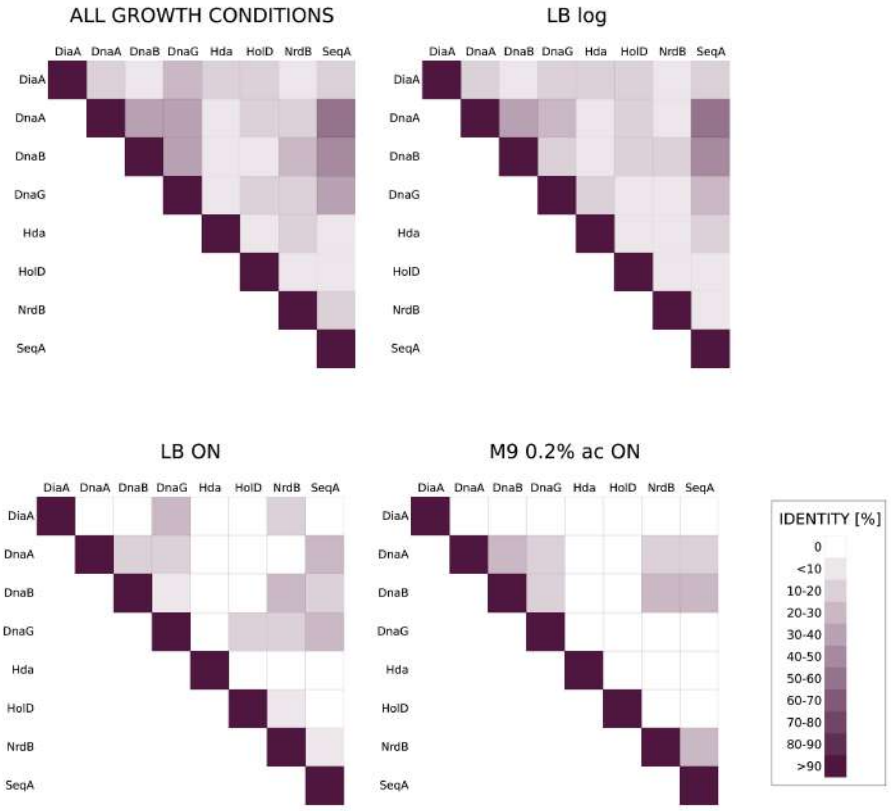

Figure 4. Pairwise comparison of uncovered interaction profiles of 8 baits used in this work. Similarity matrices were made based on comparison of interaction profiles between each of 8 bait proteins used in PPI screen ('each with each' comparison). Percent of common interactants between compared bait pairs was calculated and subsequently weighted average was calculated of the number of all interactants identified in our PPI screen.

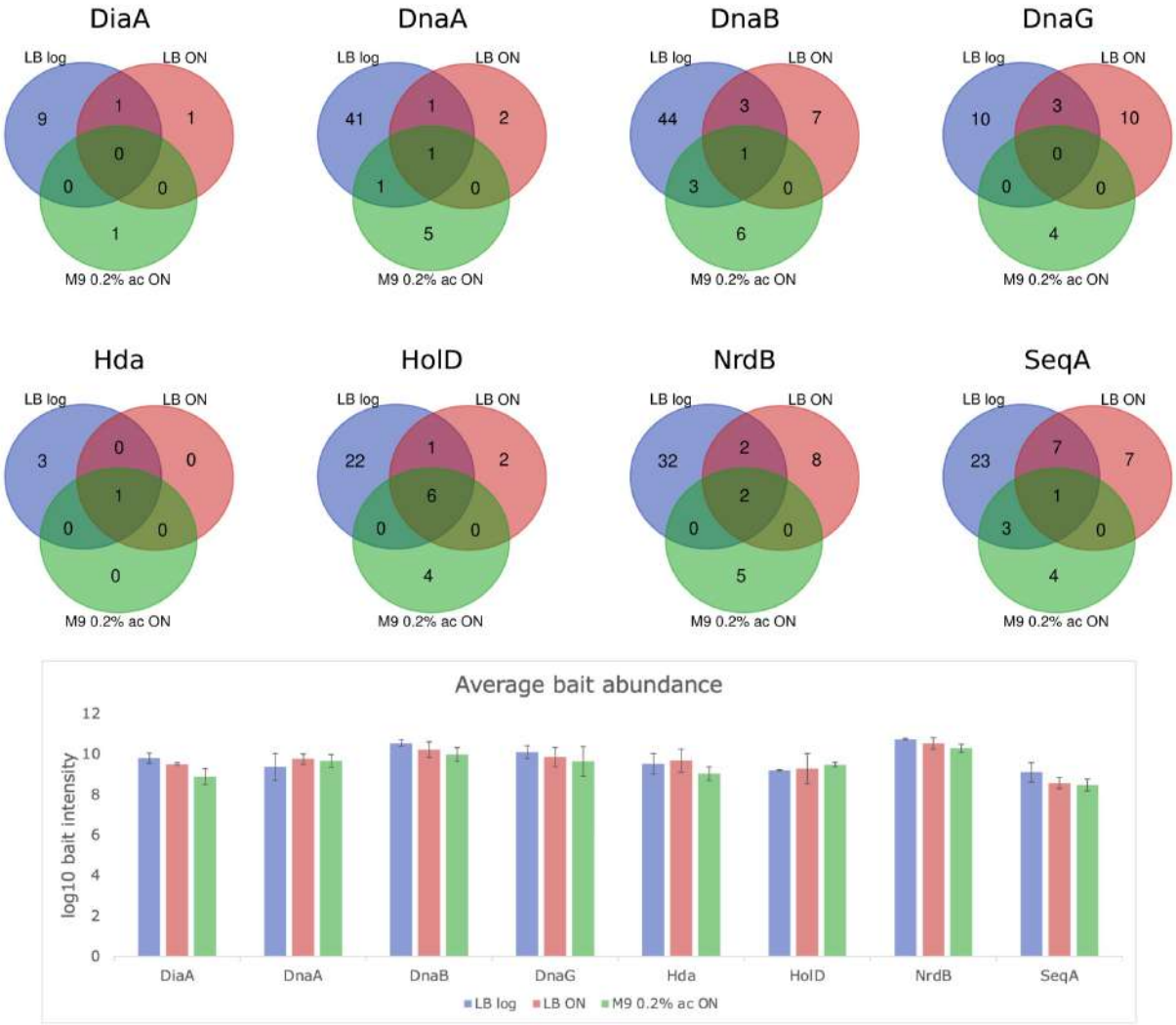

Figure 5. Venn diagrams showing similarity of interaction profiles for each bait protein used in this study under different conditions (upper panel). Diagrams presenting bait abundancies in the AP-MS experiments, under different growth conditions (showed as log10 value of bait intensity) (lower panel). Protein intensities were calculated using MaxQuant.

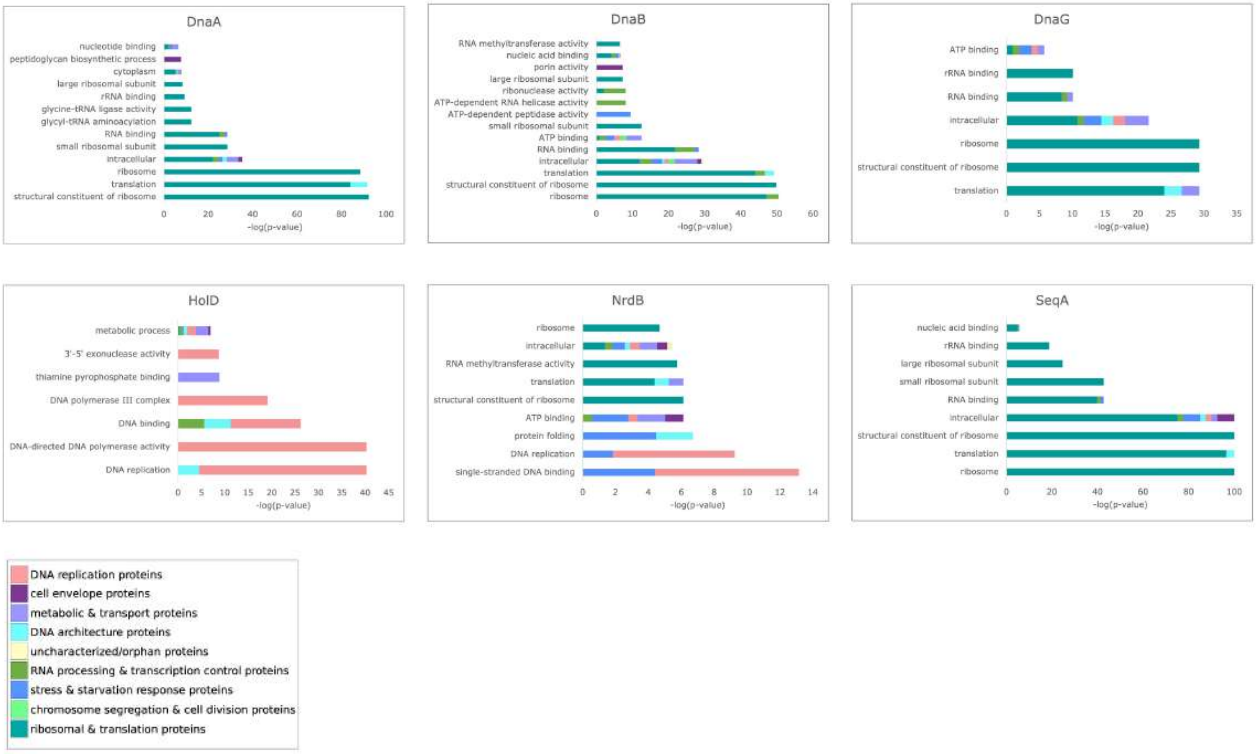

Figure 6. Functional enrichment analysis of interactions formed by six of the eight bait proteins used in this work. Analysis was performed with web tool GSEA, described in (24). The entire statistically significant prey set (p-value < 0.01) of each bait protein, obtained from each of the tested growth conditions, was used as input for analysis.

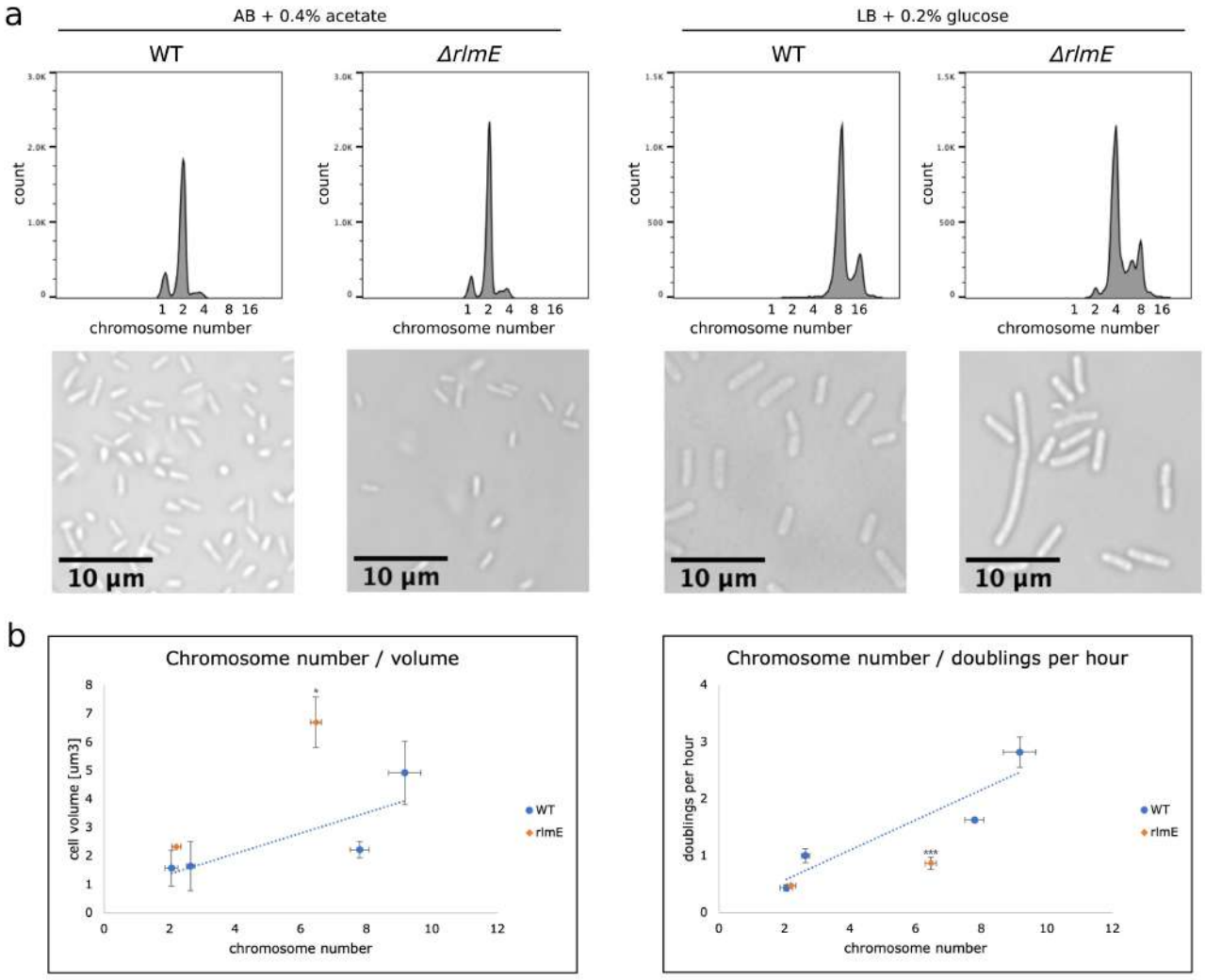

Figure 7. Cell cycle parameters of the ΔrlmE strain. (A) Upper panel - flow cytometry histograms presenting cell populations containing particular chromosome number, lower panel – microphotographs of representative cells from the population. Chromosome number, present in *E. coli* cells grown in LB+glucose or AB medium + acetate, was calculated after replication run-out, Sytox Green staining and flow cytometry analysis. (B) Graphs show an interplay between chromosome number and cell volume (left) or doublings per hour (right). Cell volume was measured using ImageJ software after collecting cell images with light microscope and phase contrast. OD600 measurement of exponentially growing cultures served as basis of growth rate calculation. WT *E. coli* strain cell cyle parameters were set up as a standard curve to which mutant strains can be compared. *p-value<0.05 (t test) *** p-value<0.001 (t test)

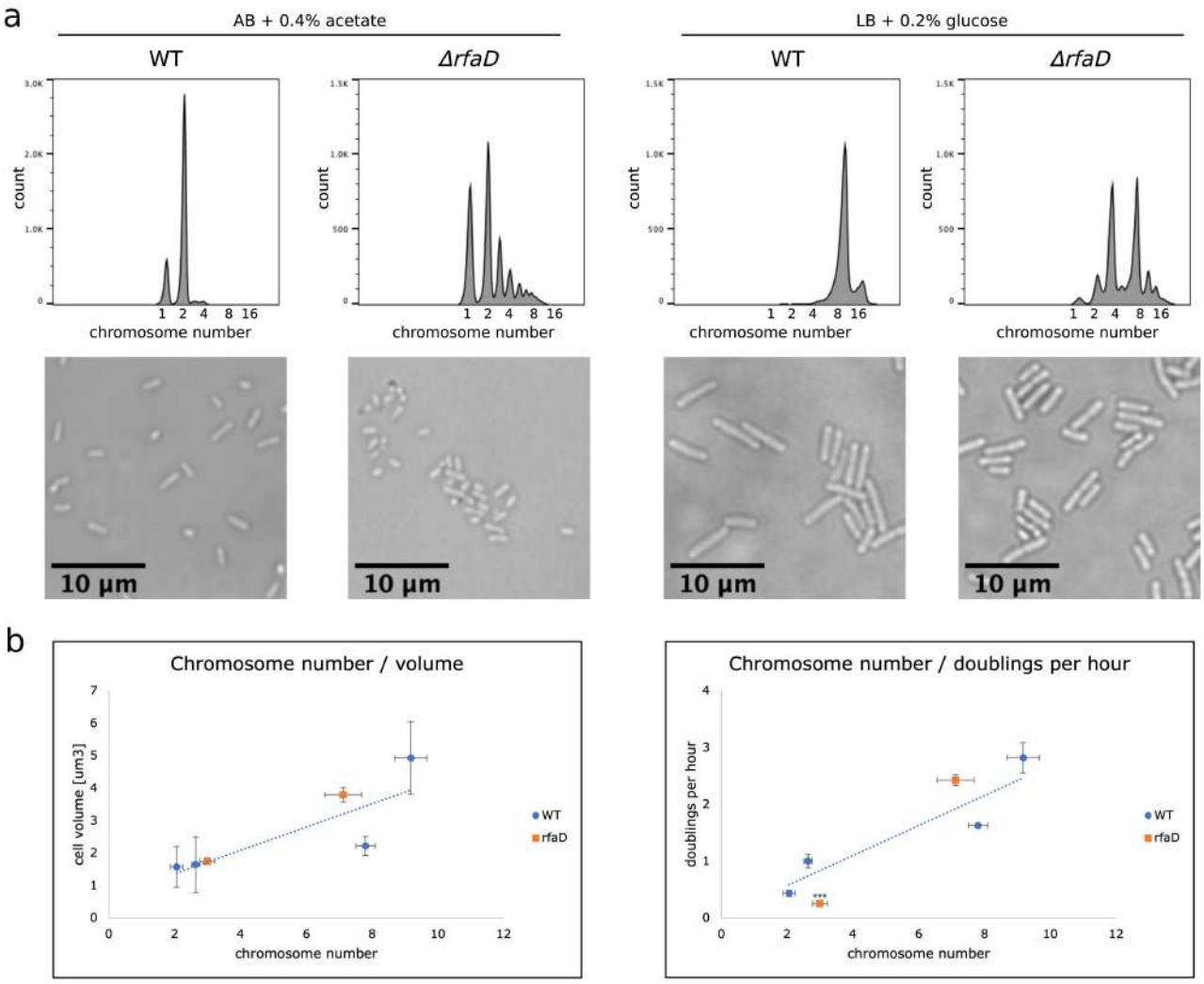

Figure 8. Cell cycle parameters of the ΔrfaD strain. (A) Upper panel - flow cytometry histograms presenting cell populations containing particular chromosome number, lower panel – microphotographs of representative cells from the population. Chromosome number, present in *E. coli* cells grown in LB+glucose or AB medium + acetate, was calculated after replication run-out, Sytox Green staining and flow cytometry analysis. (B) Graphs show an interplay between chromosome number and cell volume (left) or doublings per hour (right). Cell volume was measured using ImageJ software after collecting cell images with light microscope and phase contrast. OD600 measurement of exponentially growing cultures served as basis of growth rate calculation. WT *E. coli* strain cell cyle parameters were set up as a standard curve to which mutant strains can be compared. *p-value<0.05 (t test) *** p-value<0.001 (t test)

a

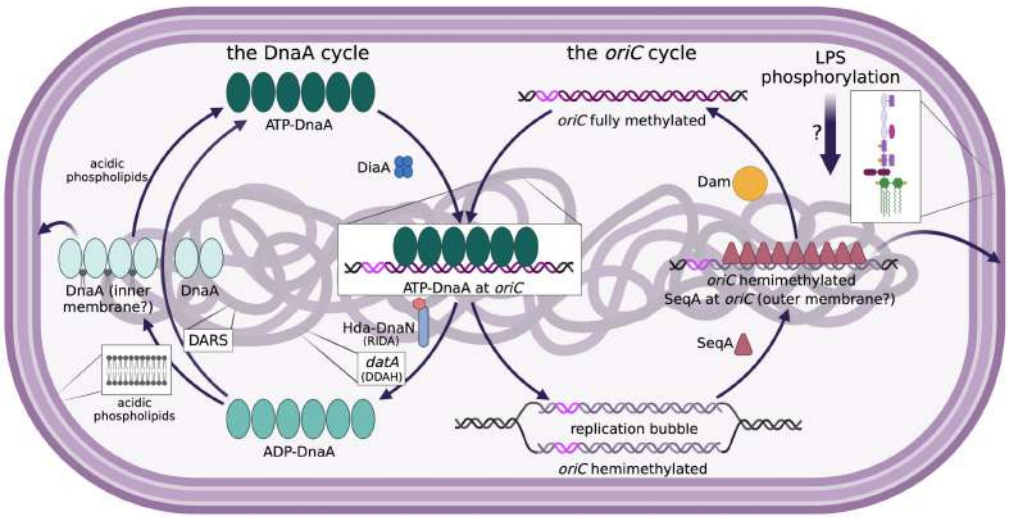

Figure 9. Functional connections between cell envelope biogenesis and DNA replication identified so far in *E. coli.* (A). The role of cell envelope structures in replication initiation control via two independent cycles – DnaA cycle and oriC cycle.

b

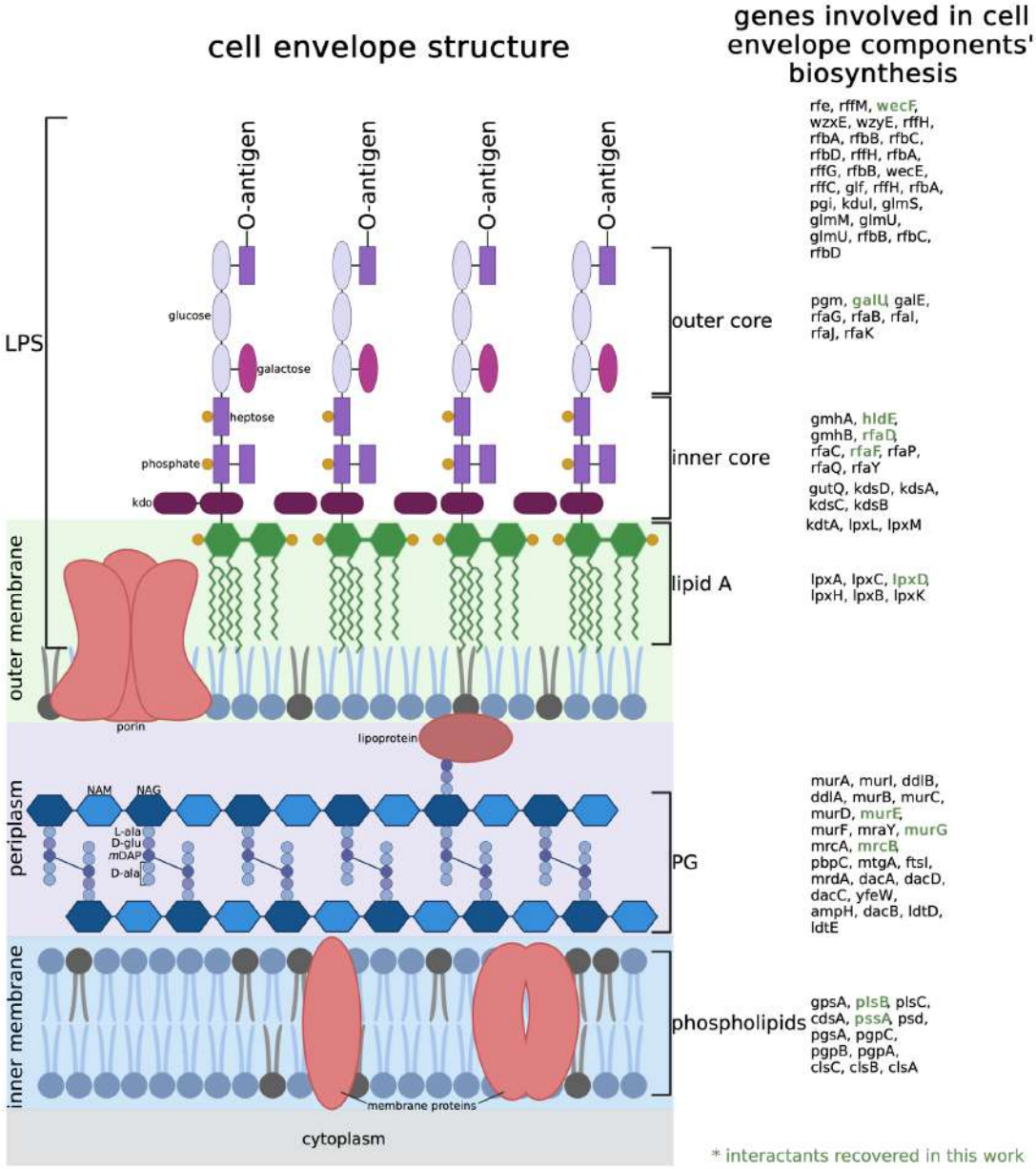

Figure 9. Functional connections between cell envelope biogenesis and DNA replication identified so far in *E. coli.* (B) Cell envelope structure and genes engaged in biogenesis of particular layers. Proteins identified in this work as interactants of the replication proteins were highlighted in green.

Suplement

Supplementary tables:

Supplementary table 1. *Escherichia coli* strains used in this study.

strain	genotype	source
MG1655	K-12 F– λ– ilvG– rfb-50 rph-1	Laboratory collection
MG1655 DiaA-SPA kanR	K-12 F– λ– ilvG– rfb-50 rph-1 diaA::diaA-SPA:kanR	This study
MG1655 DnaA-SPA kanR	K-12 F– λ– ilvG– rfb-50 rph-1 dnaA::dnaA-SPA:kanR	This study
MG1655 DnaB-SPA kanR	K-12 F– λ– ilvG– rfb-50 rph-1 dnaB::dnaB-SPA:kanR	This study
MG1655 DnaG-SPA kanR	K-12 F– λ– ilvG– rfb-50 rph-1 dnaG::dnaG-SPA:kanR	This study
MG1655 Hda-SPA kanR	K-12 F– λ– ilvG– rfb-50 rph-1 hda::hda-SPA:kanR	This study
MG1655 HolD-SPA kanR	K-12 F– λ– ilvG– rfb-50 rph-1 holD::holD-SPA:kanR	This study
MG1655 NrdB-SPA kanR	K-12 F– λ– ilvG– rfb-50 rph-1 nrdB::nrdB-SPA:kanR	This study
MG1655 SeqA-SPA kanR	K-12 F– λ– ilvG– rfb-50 rph-1 seqA::seqA-SPA:kanR	This study
MG1655 DiaA-SPA FRT	K-12 F– λ– ilvG– rfb-50 rph-1 diaA::diaA-SPA:frt	This study
MG1655 DnaA-SPA FRT	K-12 F– λ– ilvG– rfb-50 rph-1 dnaA::dnaA-SPA:frt	This study
MG1655 DnaB-SPA FRT	K-12 F– λ– ilvG– rfb-50 rph-1 dnaB::dnaB-SPA:frt	This study
MG1655 DnaG-SPA FRT	K-12 F– λ– ilvG– rfb-50 rph-1 dnaG::dnaG-SPA:frt	This study
MG1655 Hda-SPA FRT	K-12 F– λ– ilvG– rfb-50 rph-1 hda::hda-SPA:frt	This study
MG1655 HolD-SPA FRT	K-12 F– λ– ilvG– rfb-50 rph-1 holD::holD-SPA:frt	This study
MG1655 NrdB-SPA FRT	K-12 F– λ– ilvG– rfb-50 rph-1 nrdB::nrdB-SPA:frt	This study
MG1655 SeqA-SPA FRT	K-12 F– λ– ilvG– rfb-50 rph-1 seqA::seqA-SPA:frt	This study
DY330 DnaA-SPA kanR	W3110 ΔlacU169 gal490 λCI857 Δ(cro-bioA) dnaA::dnaA-SPA:kanR	GE Healthcare Dharmacon (template to PCR-amplify the SPA-tag-kanR fragment).
DH5α	*fhuA2 lac(del)U169 phoA glnV44 Φ80' lacZ(del)M15 gyrA96 recA1 relA1 endA1 thi-1 hsdR17*	Laboratory collection
MG1655 *ΔrlmE*	K-12 F– λ– ilvG– rfb-50 rph-1 rlmE::frt-catR-frt	This study
MG1655 *ΔrfaD*	K-12 F– λ– ilvG– rfb-50 rph-1 rfaD::frt-kanR-frt	This study

Supplementary table 2. Plasmids used in this study.

plasmid	description	source
pUC19-pIVSK	pUC19 backbone with cloned mVenus-SPA sequence under the control of constitutive promoter $p_{lacI.}$	This work
pKD46	Red recombinase expression plasmid.	Laboratory collection /Datsenko & Wanner 2000
pCP20	Temperature-sensitive plasmid containing FLP gene to remove FRT-flanked antibiotic resistance cassette.	Laboratory collection /Datsenko & Wanner 2000
pKD3	Source of FRT-flanked chloramphenicol resistance cassette.	Laboratory collection /Datsenko & Wanner 2000
pKD13	Source of FRT-flanked kanamycin resistance cassette.	Laboratory collection /Datsenko & Wanner 2000

Supplementary table 3. Primers used in this study.

All primers used to amplify linear DNA fragment used for lambda red recombination-mediated SPA-tag integration contain constant sequences at their 3’ ends:

F: 5’-overhang-TCCATGGAAAAGAGAAG-3’

R:5’-overhang- CATATGAATATCCTCCTTAG-3’

Thus, only variable 5’-end sequences (overhangs) of the primers described as ‘integration’ primers are presented in the table below.

Primer name	sequence	description
diaA-SPAkan F	ATTGCCTGTGCGATCTGATCGATAACACGCTTTTCCCTCACCAGGATGAT	Integration primers for diaA gene
diaA-SPAkan R	AGCGCGGAAATAAGGACTGCGATTGGCGATAATGCCTTCATGTATTCTCC	
dnaA-SPAkan F	GCCACGATATCAAAGAAGATTTTTCAAATTTAATCAGAACATTGTCATCG	Integration primers for dnaA gene
dnaA-SPAkan R	GTTGTAGCGGTTTTAATAAATGCTCACGTTCTACGGTAAATTTCATAGGT	
dnaB-SPAkan F	GTCAATGGTCGCGCTTCGACAACTATGCGGGGCCGCAGTACGACGACGAA	Integration primers for dnaB gene
dnaB-SPAkan R	GTGTTCCTTGATAAGTGTTTGCTTTAATTACCTAATTCATAAAATAATTA	
dnaG-SPAkan F	ACGAAGAACGCCTGGAGCTCTGGACATTAAACCAGGAGCTGGCGAAAAAG	Integration primers for dnaG gene
dnaG-SPAkan R	TGCGGCTGTCGGGGGCTTCCCGATCGCTCTTCGGCACTTAAGCCGTTAAA	

holD-SPAkan F	TATGGCAACAAATTTGCACATATGAACACGATTTCTTCCC TCGAAACGAC	Integration primers for holD gene
holD-SPAkan R	TCCACGGAAAGGCGTGGGCGCGTTGTTCAATGTGGTAAG CCGCCGGTAAA	
hda-SPAkan F	CCGCGCAACGTAAGCTGACCATTCCGTTTGTGAAAGAAA TTCTGAAGTTG	Integration primers for hda gene
hda-SPAkan R	GCGTAGTTCGGATAAGGCGTTCGCGCCGCATCCGACAAT AAACACCTTAT	
nrdB-SPAkan F	GGCAGATTGACTCGGAAGTGGACACCGACGATTTGAGTA ACTTCCAGCTC	Integration primers for nrdB gene
nrdB-SPAkan R	ATCCTGGCACAGCAGTTGTGTGCCAGTGATGCGCAGGGT AACGCGGGCCA	
seqA-SPAkan F	AGTCGATGCAATTCCCGGCGGAATTGATTGAGAAGGTTT GCGGAACTATC	Integration primers for seqA gene
seqA-SPAkan R	GGCCTGCACGATTGTGGATTGCCATTGCTTTGTCCTTTGT CTGCAACGTT	
S diaA F	TTGTTAGGGCCACAGGATGT	Screening primers for the diaA gene
S diaA R	GACACTGCGTGGGTCAGTT	
S dnaA F	CTTCATGCCTGCCGTAAGAT	Screening primers for the dnaA gene
S dnaA R	CGTACCGTCAGCAACCTGTA	
S dnaB F	AGGCATCGCGGAAATTATTA	Screening primers for the dnaB gene
S dnaB R	ACCACCGCAACCATTTTACT	
S dnaG F	GAGCAAACCTTCACCGACTC	Screening primers for the dnaG gene
S dnaG R	GCTGAAATCCAACGGTTGTT	
S holD F	ACAGTTGGCGGTTGGGTACT	Screening primers for the holD gene
S holD R	ATTTTGCCGTTTTGCGTTA	
S hda F	TTTGAACTGCCGGAAGATGT	Screening primers for the hda gene
S hda R	CCATCGCTAGTTGAAGCACA	
S nrdB F	GATCCCGTGGATCAACACTT	Screening primers for the nrdB gene
S nrdB R	TCGCGACACTGGTACTCAAC	
S seqA F	GATGAACAAACGCTGCTGAA	Screening primers for the seqA gene
S seqA R	GTCAGTTGGGCGACGTTAAT	
rlmE-del-cm F	TAAAAATTTACGCAATTGGTTACGATGAGTTATCCCCATG GGAAAGTTAATTGTGTAGGCTGGAGCTGCTTC	Deleton primers for the rlmE gene
rlmE-del-cm R	AGGATACTCTATATCCAGCATCTTTCAAACTTTCGTCTGA AATCTCCCGGcatgggaattagccatggtc	
S del rlmE F	GTTCAATCTCGGCCAGCAC	Screening primers for the deletion of rlmE gene
S del rlmE R	CGTTGATACGCGCTTCAC	
rfaD-del-kan F	ACATTCGTGTCTGAGATTGTCTCTGACTCCATAATTCGAA GGTTACAGTTAATTCCGGGGATCCGTCGACC	Deletion primers for the rfaD gene
rfaD-del-kan R	ATGTCGCCAACCCAAGACGGGCCGATCACCAGTATTTTC ATGCAGAGCTCTGTAGGCTGGAGCTGCTTCG	
S del rfaD F	TGCAATTAGCATCCTTGCAC	Screening primers for the deletion of rfaD gene
S del rfaD R	GTGACCGAGAGGCATAGGAA	

Supplementary table 4. Experimentally confirmed interactions present in the STRING database, formed by the bait proteins used in this study. Assays used to determine the interactions were indicated and the interactions detected in this work were highlighted in red.

Bait	Prey	Assay demonstrating the interaction
DnaA	OxyR, AdhE, Dps	affinity chromatography, small scale
	HupA, HupB	ELISA, tandem affinity purification
	RplB	molecular sieving, tandem affinity purification
	DnaB	solid phase assay, coimmunoprecipitation, surface plasmon resonance
	DiaA	anti tag coimmunoprecipitation nuclear magnetic resonance
DnaB	DnaG	molecular sieving, affinity chromatography, fluorescence polarization spectroscopy
	DnaC	Crystal structure, two hybrid array, molecular sieving
	Rep	surface plasmon resonance
	Tus	two hybrid assay
	PriC	two hybrid assay, molecular sieving
	PriA	molecular sieving
	PriB	molecular sieving
	DnaT	molecular sieving
	RplB	pull-down, molecular sieving
	DnaX	surface plasmon resonance
DnaG	ssb	solid phase assay
	DnaB	molecular sieving, affinity chromatography, fluorescence polarization spectroscopy
Hda	DnaN	anti-tag coimmunoprecipitation, two hybrid array, ELISA, tandem affinity purification
	DnaA	Surface plasmon resonance, anti-tag coimmunoprecipitation
	Ada	two hybrid array, pull down
DiaA	DnaA	anti-tag coimmunoprecipitation nuclear magnetic resonance
SeqA	UvrB	two hybrid array, pull down
	ParC	two hybrid assay
NrdB	NrdA	crystal structure
HolD	HolC, DnaQ, HolA, HolB, HolE, DnaX, DnaE	
	Ssb	tandem affinity chromatography, cosedimentation in solution, pull down
	TopB	tandem affinity purification, two hybrid array
	RecQ	tandem affinity purification

Supplementary table 5. Quantitative data of cell cycle parameters (chromosome number, cell volume, and growth rate) of WT, *ΔrlmE*, and *ΔrfaD* strains corresponding to figures 7 and 8.

	AB + 0.4% acetate (slow growth)					
	WT		*ΔrfaD*		*ΔrlmE*	
	AV	SD	AV	SD	AV	SD
chromosome number	2.055	0.194	2.990	0.225	2.204	0.137
average volume [µm^3]	1.577	0.627	1.747	0.104	2.327	0.026
doublings per hour	0.435	0.054	0.253	0.045	0.472	0.010
chromosome number/ average volume	1.530	0.667	1.712	0.109	0.947	0.050
chromosome number/ doublings per hour	4.764	0.551	12.159	2.790	4.665	0.196
	LB + 0.2% glucose (fast growth)					
	WT		*ΔrfaD*		*ΔrlmE*	
	AV	SD	AV	SD	AV	SD
chromosome number	9.170	0.492	7.116	0.561	6.458	0.165
average volume [µm^3]	4.926	1.116	3.799	0.224	6.699	0.894
doublings per hour	2.822	0.266	2.427	0.095	0.867	0.107
chromosome number/ average volume	1.985	0.617	1.881	0.224	0.978	0.156
chromosome number/ doublings per hour	3.281	0.407	2.938	0.298	7.546	1.203

Supplementary files:

Supplementary files 1-7 are uploaded to FigShare Repository and can be found under the following link:

https://figshare.com/s/536b3d4f3431fb852292

Supplementary figures:

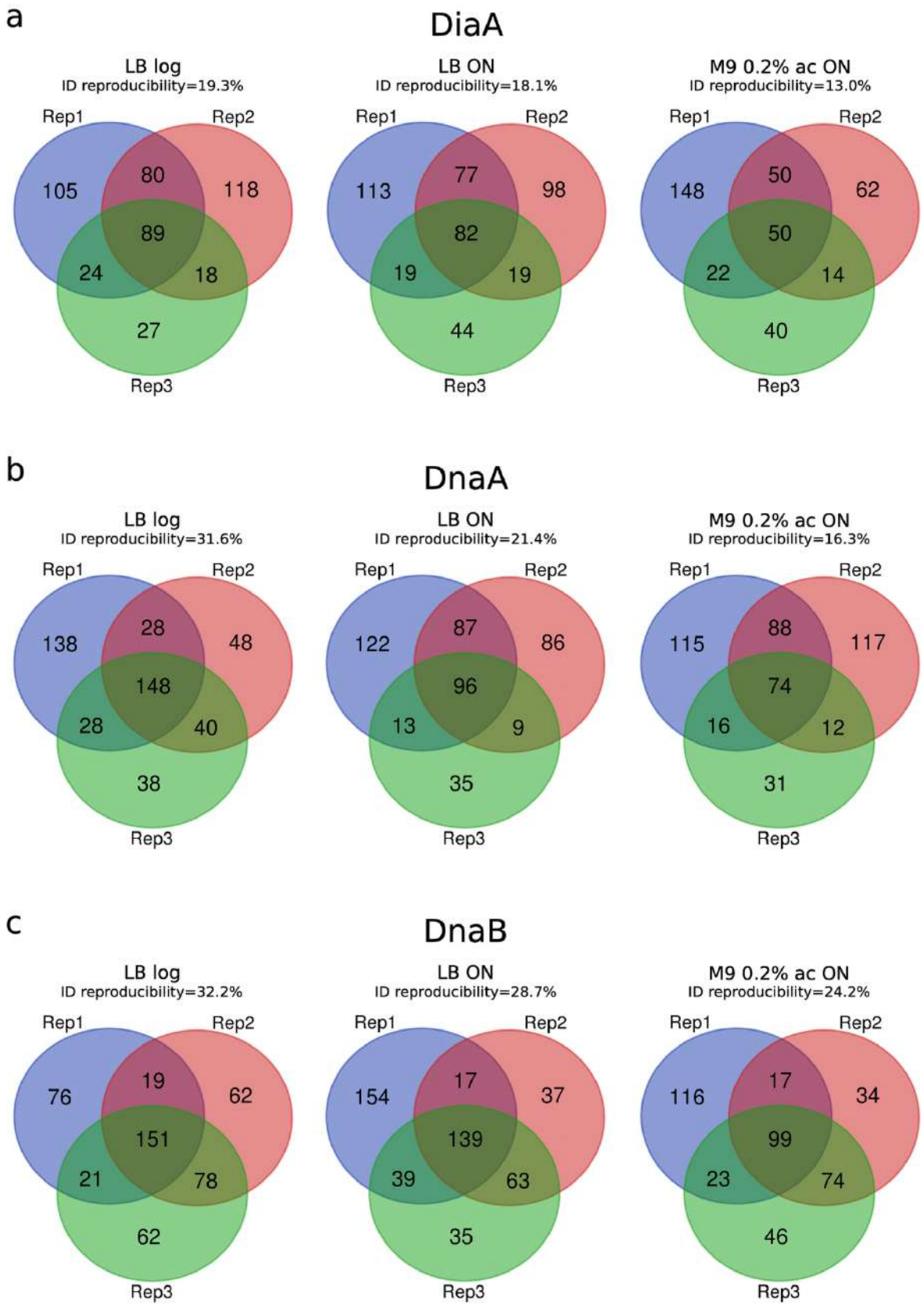

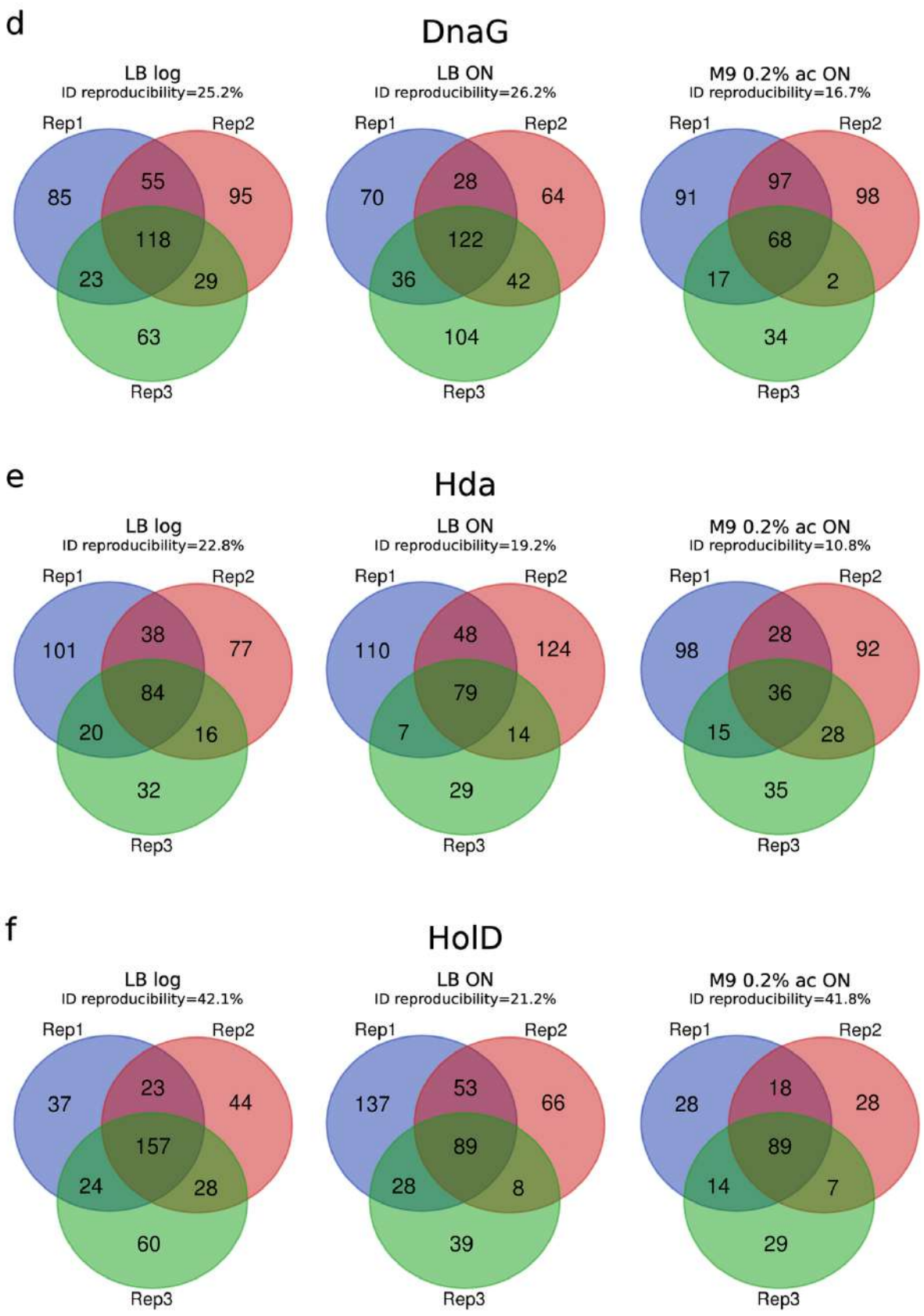
d
DnaG
LB log
ID reproducibility=25.2%
Rep1
Rep2
Rep3
85
55
95
118
23
29
63
LB ON
ID reproducibility=26.2%
70
28
64
122
36
42
104
M9 0.2% ac ON
ID reproducibility=16.7%
91
97
98
68
17
2
34
e
Hda
LB log
ID reproducibility=22.8%
101
38
77
84
20
16
32
LB ON
ID reproducibility=19.2%
110
48
124
79
7
14
29
M9 0.2% ac ON
ID reproducibility=10.8%
98
28
92
36
15
28
35
f
HolD
LB log
ID reproducibility=42.1%
37
23
44
157
24
28
60
LB ON
ID reproducibility=21.2%
137
53
66
89
28
8
39
M9 0.2% ac ON
ID reproducibility=41.8%
28
18
28
89
14
7
29

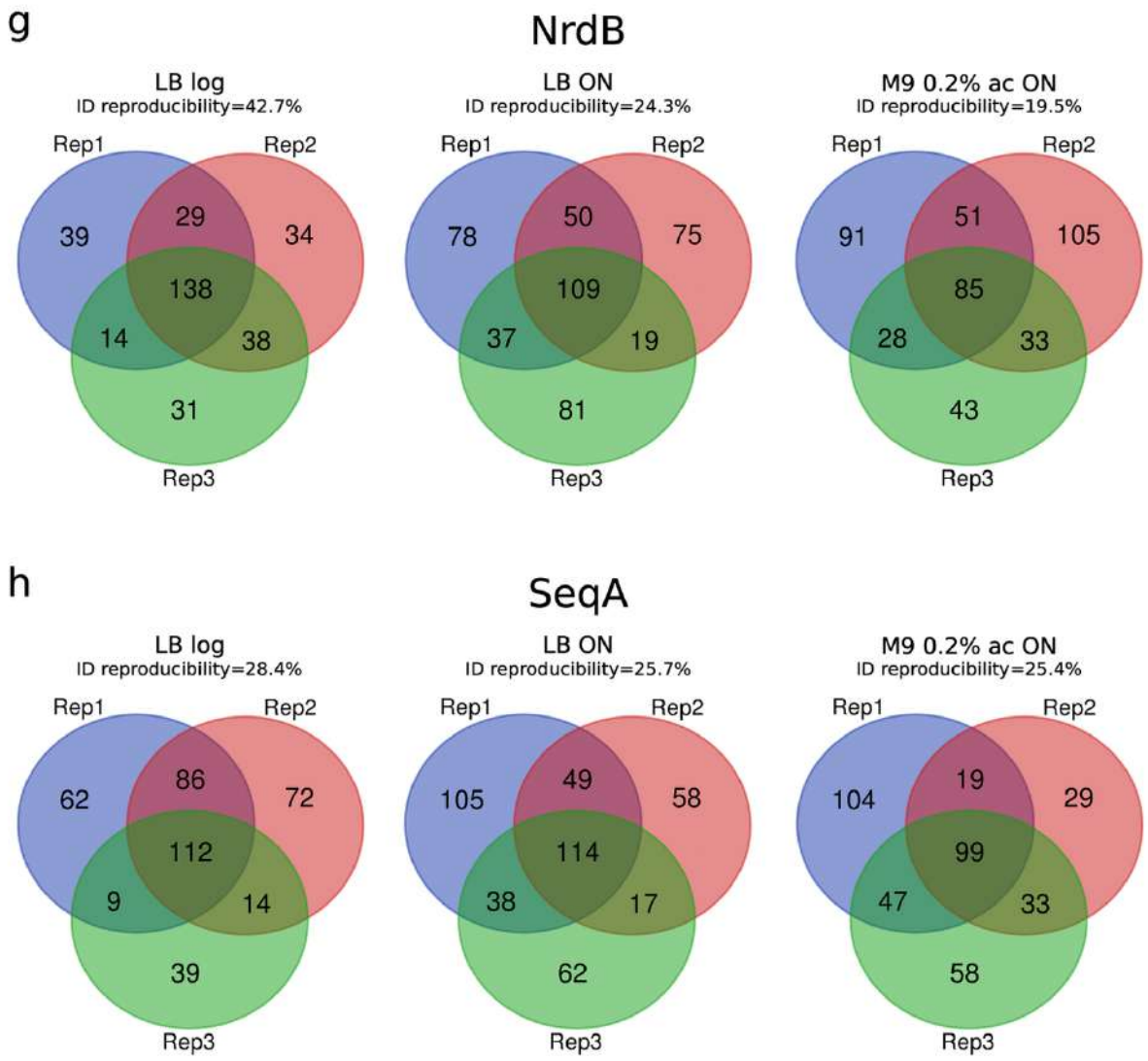

Figure S1. (A-H) Similarity of three biological repetitions performed under each growth conditions for the analyzed bait proteins.

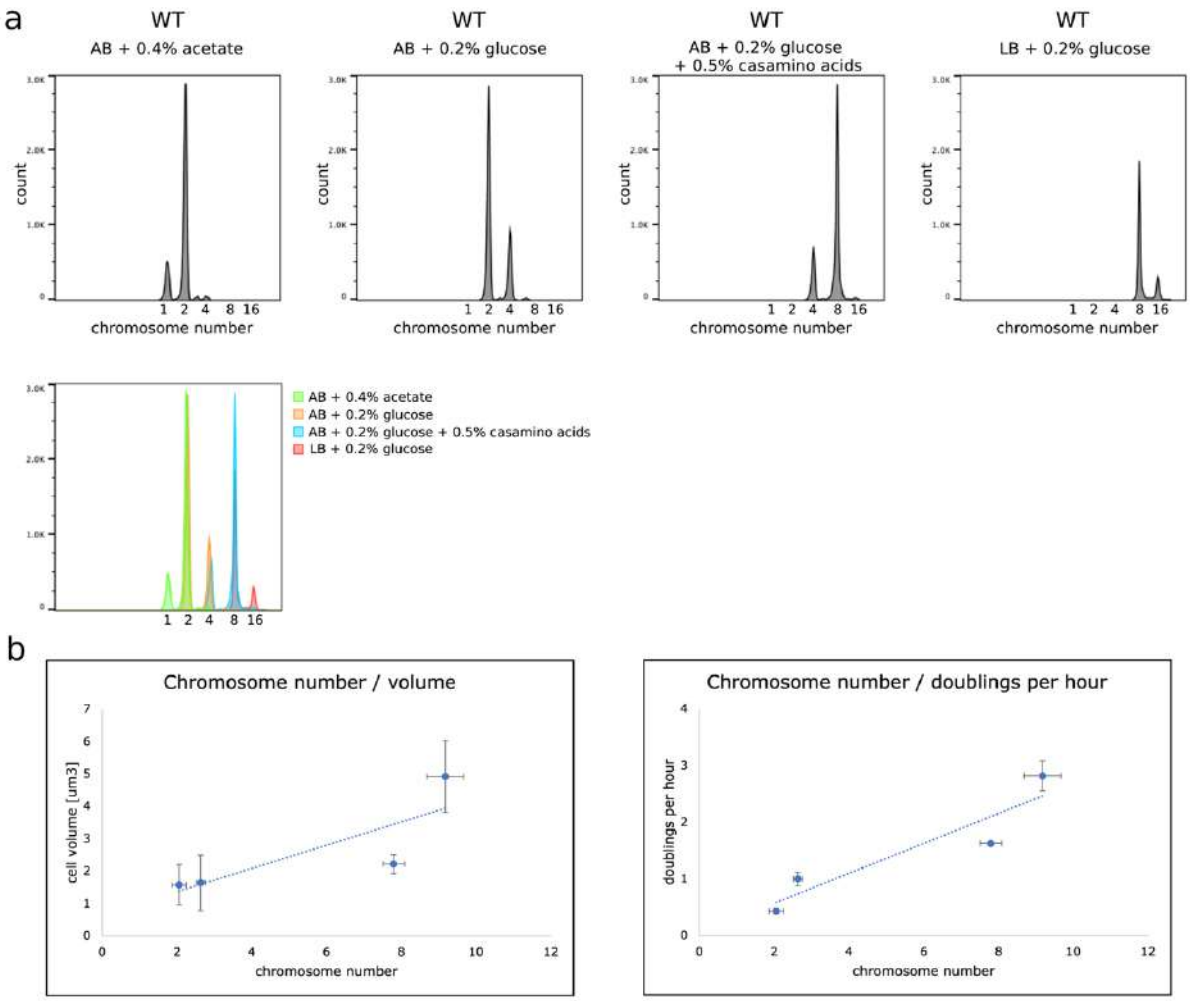

Figure S2. (A) Flow cytometry results and (B) standard curves depicting relation of chromosome number with cell volume and growth rate for the WT *E. coli* strain.

Wkład autorów – oświadczenia

Uniwersytet Gdański

mgr Joanna Morcinek-Orłowska
Katedra Genetyki Molekularnej Bakterii
Wydział Biologii
Uniwersytet Gdański

Gdańsk, 26.05.2025 r.

Oświadczenie o wkładzie w publikację

Oświadczam, że mój wkład w preprint artykułu oryginalnego:

Morcinek-Orłowska J, Walter B, Forquet R, Cysewski D, Carlier M, Meyer S, Glinkowska M. Protein interaction network analysis reveals growth conditions-specific crosstalk between chromosomal DNA replication and other cellular processes in E. coli. bioRxiv 2021.12.08.471875; doi: https://doi.org/10.1101/2021.12.08.471875

obejmował:

- przeprowadzenie eksperymentów (jak w artykule Sci Data. 2023;10(1):788, a ponadto: konstrukcja szczepów delecyjnych *E. coli*, ocena ilości chromosomów i czasu inicjacji replikacji w cyklu komórkowym metodą cytometrii przepływowej po zatrzymaniu replikacji)
- uczestnictwo w analizie danych MS metodą ilościową
- uczestnictwo w analizie funkcjonalnej zidentyfikowanych kompleksów białkowych
- wizualizację danych, przygotowanie rycin
- kierowanie projektem Preludium 12, w ramach którego sfinansowano część badań
- napisanie wstępnej oraz ostatecznej wersji manuskryptu wspólnie z dr hab. Moniką Glinkowską

Joanna Morcinek-Orłowska

Wdział Biologii
Uniwersytetu Gdańskiego
Katedra Genetyki
Molekularnej Bakterii

tel. +48 58 523 60 65
e-mail: mol.KGB@ug.edu.pl

ul. Wita Stwosza 59
80-309 Gdańsk

www.ug.edu.pl

dr Beata Walter
Zakład Biologii Strukturalnej
Międzyuczelniany Wydział Biotechnologii
Uniwersytetu Gdańskiego
i Gdańskiego Uniwersytetu Medycznego

Gdańsk, 26.05.2025 r.

Oświadczenie o wkładzie w publikację

Oświadczam, że mój wkład w preprint artykułu oryginalnego:

Morcinek-Orłowska J, Walter B, Forquet R, Cysewski D, Carlier M, Meyer S, Glinkowska M. Protein interaction network analysis reveals growth conditions-specific crosstalk between chromosomal DNA replication and other cellular processes in E. coli. bioRxiv 2021.12.08.471875; doi: https://doi.org/10.1101/2021.12.08.471875

obejmował:

- przeprowadzenie części izolacji kompleksów białkowych
- rewizję ostatecznej wersji manuskryptu

Międzyuczelniany Wydział Biotechnologii Uniwersytetu Gdańskiego i Gdańskiego Uniwersytetu Medycznego

tel. +48 58 523 64 20
e-mail: beata.water@ug.edu.pl

ul. Abrahama 58
80-307 Gdańsk
www.biotech.ug.edu.pl

iMEAN

Raphaël Forquet, PhD
Life science modeller
+33 5 61 28 51 60
135 avenue de Rangueil, INSA Bâtiment 50
1077 Toulouse Cedex 4
imean-biotech.com

30/05/2025, Toulouse

Author contribution statement

I hereby declare that my contribution to the research preprint:

Morcinek-Orłowska J, Walter B, Forquet R, Cysewski D, Carlier M, Meyer S, Glinkowska M. Protein interaction network analysis reveals growth conditions-specific crosstalk between chromosomal DNA replication and other cellular processes in E. coli. bioRxiv 2021.12.08.471875; doi: https://doi.org/10.1101/2021.12.08.471875

included:

- performing quantitative MS data analysis (contribution to the code writing and analyzing the data)
- participation in manuscript writing and revision

Dr Dominik Cysewski
Centrum Badań Klinicznych
Uniwersytet Medyczny w Białymstoku

Białystok 30.05.2025

Oświadczenie o wkładzie w publikację

Oświadczam, że mój wkład w preprint artykułu oryginalnego:

Morcinek-Orłowska J, Walter B, Forquet R, Cysewski D, Carlier M, Meyer S, Glinkowska M. Protein interaction network analysis reveals growth conditions-specific crosstalk between chromosomal DNA replication and other cellular processes in E. coli. bioRxiv 2021.12.08.471875; doi: https://doi.org/10.1101/2021.12.08.471875

obejmował:

- identyfikację składu kompleksów białkowych poprzez tandemową spektrometrię mas poprzedzoną chromatografią cieczową oraz analizę widm za pomocą silnika przeszukiwania MaxQuant
- uczestnictwo w przygotowaniu wstępnej wersji manuskryptu oraz rewizji ostatecznej wersji manuskryptu

dr Dominik Cysewski

Asystent
Centrum Badań Klinicznych
Uniwersytet Medyczny w Białymstoku

INSTITUT NATIONAL DES SCIENCES APPLIQUÉES LYON

Sam Meyer
Assistant Professor, INSA Lyon
Microbiologie, Adaptation et Pathogénie,
UMR5240
Villeurbanne, France

Villeurbanne, June 4th, 2025

Author contribution statement

I hereby declare that my contribution to the research preprint:

Morcinek-Orłowska J, Walter B, Forquet R, Cysewski D, Carlier M, Meyer S, Glinkowska M. Protein interaction network analysis reveals growth conditions-specific crosstalk between chromosomal DNA replication and other cellular processes in E. coli. bioRxiv 2021.12.08.471875; doi: https://doi.org/10.1101/2021.12.08.471875

included:

- planning of quantitative data analysis strategy and supervising the data analysis
- revision of original manuscript draft

Sam Meyer

Uniwersytet Gdański

dr hab. Monika Glinkowska, prof. UG
Katedra Genetyki Molekularnej Bakterii
Wydział Biologii
Uniwersytet Gdański

Gdańsk, 26.05.2025 r.

Oświadczenie o wkładzie w publikację

Oświadczam, że mój wkład w preprint artykułu oryginalnego:

Morcinek-Orłowska J, Walter B, Forquet R, Cysewski D, Carlier M, Meyer S, Glinkowska M. Protein interaction network analysis reveals growth conditions-specific crosstalk between chromosomal DNA replication and other cellular processes in E. coli. bioRxiv 2021.12.08.471875; doi: https://doi.org/10.1101/2021.12.08.471875

obejmował:

- zaplanowanie badań i koncepcji artykułu
- nadzorowanie przeprowadzonych eksperymentów oraz analizy danych
- zaplanowanie analizy funkcjonalnej zidentyfikowanych kompleksów białkowych
- kierowanie projektem Opus 7, w ramach którego sfinansowano większość badań
- przygotowanie wstępnej oraz ostatecznej wersji manuskryptu wspólnie z Joanną Morcinek-Orłowską

Monika Glinkowska

Wdział Biologii
Uniwersytetu Gdańskiego
Katedra Genetyki
Molekularnej Bakterii

tel. +48 58 523 60 65
e-mail: mol.KGB@ug.edu.pl

ul. Wita Stwosza 59
80-309 Gdańsk

www.ug.edu.pl

Artykuł nr 4 (preprint pracy badawczej)

Bryant J.A., Staunton K.A., Doherty H.M., Alao M.B., Ma X., **Morcinek-Orłowska J.**, Goodall E.C.A., Gray J., Milner M., Cole J.A., de Cogan F., Knowles T.J., Glinkowska M., Moradigaravand D., Henderson I.R., Banzhaf M.

Bam complex associated proteins in *Escherichia coli* are functionally linked to peptidoglycan biosynthesis, membrane fluidity and DNA replication.

(2024) eLife 13:RP99955.

Biochemistry and Chemical Biology

Bam complex associated proteins in *Escherichia coli* are functionally linked to peptidoglycan biosynthesis, membrane fluidity and DNA replication

Reviewed Preprint
v1 • September 3, 2024
Not revised

Jack A Bryant, Kara A Staunton, Hannah M Doherty, Micheal B Alao, Xuyu Ma, Joanna Morcinek-Orłowska, Emily CA Goodall, Jessica Gray, Mathew Milner, Jeffrey A Cole, Felicity de Cogan, Timothy J Knowles, Monika Glinkowska, Danesh Moradigaravand, Ian R Henderson, Manuel Banzhaf

Institute of Microbiology and Infection, School of Biosciences, University of Birmingham, Edgbaston, United Kingdom • School of Life Sciences, University of Nottingham, Nottingham, United Kingdom • Department of Biology, University of Gdańsk, Gdańsk, Poland • Institute for Molecular Bioscience, University of Queensland, St. Lucia, Australia • Laboratory for Infectious Disease Epidemiology, KAUST Smart-Health Initiative and Biological and Environmental Science and Engineering Division, King Abdullah University of Science and Technology, Makkah, Saudi Arabia • KAUST Computational Bioscience Research Center, King Abdullah University of Science and Technology, Makkah, Saudi Arabia • School of Pharmacy, University of Nottingham, Nottingham, United Kingdom • Newcastle University Biosciences Institute, Faculty of Medical Sciences, Newcastle University, Newcastle upon Tyne, UK

eLife assessment

This is a **useful** study that generated a rich inventory of genetic interactions with the potential to produce new insight into the molecular function of Bam-associated proteins. The interactions with genes of unknown function are of special interest as they may suggest experiments to find the functions of these genes. The overall data provided to support their conclusions is **solid**, but there is a major concern with known polar effects on certain mutations, which should be addressed by complementation.

https://doi.org/10.7554/eLife.99955.1.sa3

Abstract

Biogenesis of the bacterial outer membrane is key to bacterial survival and antibiotic resistance. Central to this is the β-barrel assembly machine (Bam) complex and its associated chaperones, which are responsible for transport, folding and insertion of outer membrane proteins (OMPs). The *Escherichia coli* Bam complex is composed of two essential subunits, BamA and BamD, and three non-essential accessory lipoproteins, BamB, BamC and BamE. Optimal Bam function is further dependent on the non-essential periplasmic chaperones

DegP, Skp and SurA. Despite intensive study, the specific function of these non-essential Bam-associated proteins remains unknown. Here, we analysed Δ*bamB*, Δ*bamC*, Δ*bamE*, Δ*surA*, Δ*skp* and Δ*degP* knockout strains by phenotypic screening, conservation analysis and high-throughput genetics. We reveal that Bam complex activity is impacted by changes in outer membrane lipid composition and that enterobacterial common antigen is essential in the absence of the chaperone SurA. We also show components of peptidoglycan are conditionally essential with Bam accessory lipoproteins and that DNA replication control is perturbed in the absence of specific OMP assembly components. Together, our data indicates potential mechanisms for coordination of OMP biogenesis with other cellular growth processes such as LPS and peptidoglycan biogenesis, and DNA replication control.

Introduction

The Gram-negative outer membrane is instrumental for virulence, antimicrobial resistance, and immune evasion. The outer membrane is an asymmetric lipid bilayer consisting of phospholipid on the inner leaflet, lipopolysaccharide (LPS) on the outer leaflet, integral outer membrane proteins (OMPs) and associated lipoproteins. Biogenesis of the outer membrane is completed by several multi-component proteinaceous machines. Central to this is the β-barrel assembly machine (Bam) complex, the essential protein machinery responsible for folding and insertion of OMPs into the outer membrane, which then act as transporters, porins, receptors, virulence factors, adhesins and enzymes [1, 2]. All OMPs are synthesised in the cytoplasm before being trafficked through the inner membrane to the periplasmic space by the Sec machinery. OMPs are prone to aggregation and must be maintained in an unfolded state during their translocation to the Bam complex [3]. Three quality control proteins that chaperone OMPs across the periplasm are SurA, Skp and DegP, the latter of which also serves as a protease to degrade misfolded OMPs in the periplasm. The double mutants Δ*surA*Δ*skp* and Δ*surA*Δ*degP* are not viable, which suggests that Skp, SurA and DegP might be functionally redundant [4]. The primary chaperone pathway to the Bam complex is thought to be SurA, while Skp and DegP are suggested to form a secondary pathway that is amplified in stress conditions [5]. However, single molecule studies with purified OmpC and Skp or SurA demonstrate that the two proteins recognise different conformations of the OMP and that while Skp is capable of dispersing aggregated OmpC, SurA is not [6]. In addition, the absence of SurA increases degradation of OMPs that have stalled on the Bam complex, whereas loss of Skp in this scenario has the opposite effect, enhancing their assembly [7]. This is potentially due to the role of Skp in recognising and removing stalled OMP substrates from the Bam complex before being degraded alongside the misfolded OMP by the protease DegP [8]. Together, these studies challenge the long-standing assumption that these pathways are redundant and suggests that Skp and SurA have specialised roles in maintaining OMPs in a folding competent state during periplasmic transit.

Following transport across the periplasmic space, OMPs are received at the outer membrane by the Bam complex. In *Escherichia coli*, the Bam complex is composed of two essential subunits, the outer membrane β-barrel BamA and the lipoprotein BamD, and three non-essential accessory lipoproteins, BamB, BamC and BamE [9, 10]. BamA is the central component of the complex and consists of a 16-stranded β-barrel and five periplasmically localised POlypeptide-TRansport-Associated (POTRA) domains that function to dock the accessory subunits [11, 12]. The POTRA domains are hypothesised to interact with incoming unfolded OMP substrates and feed them into the assembly machinery [13]. BamD is a lipoprotein composed of five tetratricopeptide repeat (TPR) domains that interact with POTRA 5 of BamA [9, 14, 15]. The remaining components of the complex are the accessory lipoproteins, BamB, BamC and BamE, which interact with BamA and BamD to form a functionally coordinated ring structure under the BamA barrel on the periplasmic face of the outer membrane [16–20].

The Bam complex accessory lipoproteins each contribute to full activity of the complex through a shared redundant function of coordinating efficient BamA/D interaction in OMP engagement and folding. Beyond this shared function, there is some limited information about specific roles of these proteins in the cell [10, 21]. For example, as part of the Rcs stress response signalling pathway, the outer membrane lipoprotein RcsF is threaded through an OMP during folding by the Bam complex. This process specifically requires BamE to directly interact with and coordinate BamA and BamD to enable completion of OMP folding around RcsF [22–24]. Lethal jamming of the Bam complex in the absence of BamE can be prevented by BamB [23, 25]. BamB has also been shown to be important in folding of high-flux substrates [26]. However, further information about the specific roles of BamB, BamC and BamE are lacking [21].

In this study, we provide evidence for specialised functions and show that changes to LPS structure lead to increased membrane fluidity and decreased Bam complex activity. We also identify that the cyclic form of enterobacterial common antigen (ECA), a periplasmic carbohydrate, is essential in the absence of the chaperone protein SurA. We demonstrate that the Bam accessory lipoproteins, including BamC, are essential in the absence of the peptidoglycan stem-peptide component *meso*-DAP, providing a strong phenotype for this poorly understood protein. Lastly, we show that loss of BamB causes the cells to over-initiate DNA replication, indicating potential coordination between OMP biogenesis and DNA replication. Together, our data indicate specialised roles for the Bam-associated proteins and highlights potential mechanisms for coordination of OMP biogenesis with processes such as outer membrane lipid biogenesis, peptidoglycan synthesis and DNA replication control.

Results

Loss of Bam-associated proteins leads to distinct phenotypes

We hypothesised that if the Bam-associated proteins have specialised roles in the cell it would be unlikely that they phenocopy each other. Therefore, we tested fitness of Δ*bamB*, Δ*bamC*, Δ*bamE*, Δ*surA*, Δ*skp* and Δ*degP* mutants of *E. coli* K-12 BW25113 compared to the parent strain under various stresses. We arrayed the strains in 384-well format on solid agar plates containing each stress or compound. Endpoint pictures were taken to quantify colony fitness based on size by the image analysis software Iris [27]. Fitness was scored using the chemical genomics analysis software ChemGAPP Small by comparing the mean colony size for the mutant in each condition to the mean colony size of that mutant in the LB agar condition, which was normalised to a fitness score of 1 [28]. Fitness scores below 1 represent decreased fitness, as a function of colony size compared to growth on LB agar, and scores above 1 indicate increased fitness in that condition.

The fitness of each mutant across all conditions identified that the Δ*bamB* and Δ*surA* mutants have the strongest fitness defects (**Fig 1**). Correlation between each mutant fitness profile pair was assessed by calculating the Pearson correlation coefficient. This demonstrated that Δ*bamB* and Δ*surA* have a similar phenotypic profile with a correlation coefficient of 0.74, the highest of all pairs of mutants (**Fig S1**). Similar decreased fitness scores were observed for both strains in the presence of bacitracin, carbenicillin, erythromycin, sodium dodecyl-sulfate (SDS), osmotic stress conditions due to varied salt concentrations, and vancomycin (**Fig 1**). This is unsurprising as SurA is the major chaperone pathway for OMPs to reach the Bam complex resulting in low fitness of Δ*bamB* and Δ*surA* when growing on LB at 37°C. However, they do not phenocopy in all conditions. For example, the Δ*bamB* strain grew better in the presence of the MreB inhibitor A22 with a fitness score of 1.59, but the Δ*surA* mutant was less fit in this condition (score of 0.51). They also had opposing fitness scores in the presence of doxycycline (Δ*bamB* – 1.65, Δ*surA* – 0.94) and hydroxyurea (Δ*bamB* – 0.68, Δ*surA* – 1.14) (**Fig 1**). The Δ*bamE* mutant mildly correlated to Δ*bamB* with a coefficient of 0.51 (**Fig S1**). However, both mutants were sensitive to vancomycin (Δ*bamB* – 0.06, Δ*bamE* – 0.66) and bacitracin (Δ*bamB* – 0.02, Δ*bamE* – 0.58) two antibiotics that

exceed the exclusion limit of outer membrane porins and to which sensitivity indicates damage to the permeability barrier. In contrast, Δ*bamC* has no strong phenotypes and correlated most strongly with the WT parent strain (**Fig 1** and **Fig S1**). Similarly to Δ*bamC*, the Δ*skp* mutant also has no strong phenotypes in our screen. The Δ*degP* strain was negatively correlated with the other periplasmic chaperone pathway group mutants Δ*skp* (-0.51) and Δ*surA* (-0.37) and with Δ*bamE* (-0.68) due to opposing fitness scores in a range of stresses (**Fig. 1** and **Fig S1**). Interpretation of this result is complicated by DegP not only functioning as a chaperone, but also as a protease that targets misfolded OMPs in the periplasm [29]. However, due to the role of DegP in degrading stalled OMPs that have been recognised by Skp, they might have been expected to correlate [8]. Together, the phenotypic profiling data indicate that while there are shared phenotypes between each knockout, we observe a broad range of unique, mutant specific phenotypes that suggests specialised roles beyond those observed previously.

TraDIS identifies unique synthetic lethal interactions for Bam-associated proteins

Considering that the Bam-associated proteins have specialised function, we sought to find their genetic interaction networks by using Transposon-Directed Insertion site Sequencing (TraDIS). When TraDIS libraries are generated in single gene deletion mutant backgrounds, the insertion frequencies of genes/regions compared to wild-type cells identifies genes that become more important for survival in the mutant backgrounds. These genes are termed conditionally essential, and help to identify co-dependencies of processes that the candidate gene might be involved in. The method can also identify mutants that are more fit in the given genetic background or condition [30–33]. Therefore, the parent strain (*E. coli* BW25113) and Δ*bamB*, Δ*bamC*, Δ*bamE*, Δ*surA*, Δ*skp*, or Δ*degP* mutants were transformed with a mini Tn5-kanamycin transposon and recovered on LB agar at 37°C. Transposon mutants were then pooled and transposon insertion sites identified by DNA sequencing as described previously [32]. The BioTraDIS pipeline was used for data analysis to classify genes as either essential or non-essential. Essential genes were then compared to the parent BW25113 TraDIS library to identify genes that became essential in the knockout strains (conditionally essential) (Table S1) [34]. For quality control, two independent replicates of each transposon library were sequenced over several sequencing runs. Individual sequencing runs had a high correlation coefficient of ≥0.93 between samples and generated >6 million TraDIS reads and >500,000 unique insertion sites for each strain (**Fig S2** and **S3**). Transposon insertion sites were evenly mapped throughout the genome, with the exception of an increased density around the origin of replication as expected due to gene dosage (**Fig S4**) [35].

These experiments are designed to identify novel genetic interactions, but this unbiased approach will also uncover known synthetic lethal gene pairs that allow benchmarking of our data. We confirmed known genetic interactions between *surA* and *skp* [4], *degP* and *surA* [4], *bamB* and *degP* [26] and *bamE* and *bamB* [25, 36] (**Fig S5**). The Δ*bamB*, Δ*bamC* and Δ*bamE* TraDIS libraries allowed identification of 93, 92 and 29 conditionally essential genes, respectively (**Fig 2A** and Table S1). This is particularly surprising as there are no known roles or dependencies for *bamC* and we did not observe strong phenotypes for Δ*bamC* in our phenotypic screen (**Fig 1**). Unfortunately, 54 of the genes identified as conditionally essential in the Δ*bamC* background are of unknown function, therefore providing no hypotheses for the role of BamC (Table S1). We then compared the conditionally essential gene lists to probe if they are involved in similar processes or contribute to the same function within the cell. In the case that all three Bam accessory proteins solely contribute to Bam function, we would expect to find significant overlap between mutants. However, we found many unique conditionally essential genes for each (62, 57 and 5 for Δ*bamB*, Δ*bamC* and Δ*bamE*, respectively), supporting the hypothesis that each has specialised roles in the cell (**Fig 2A**).

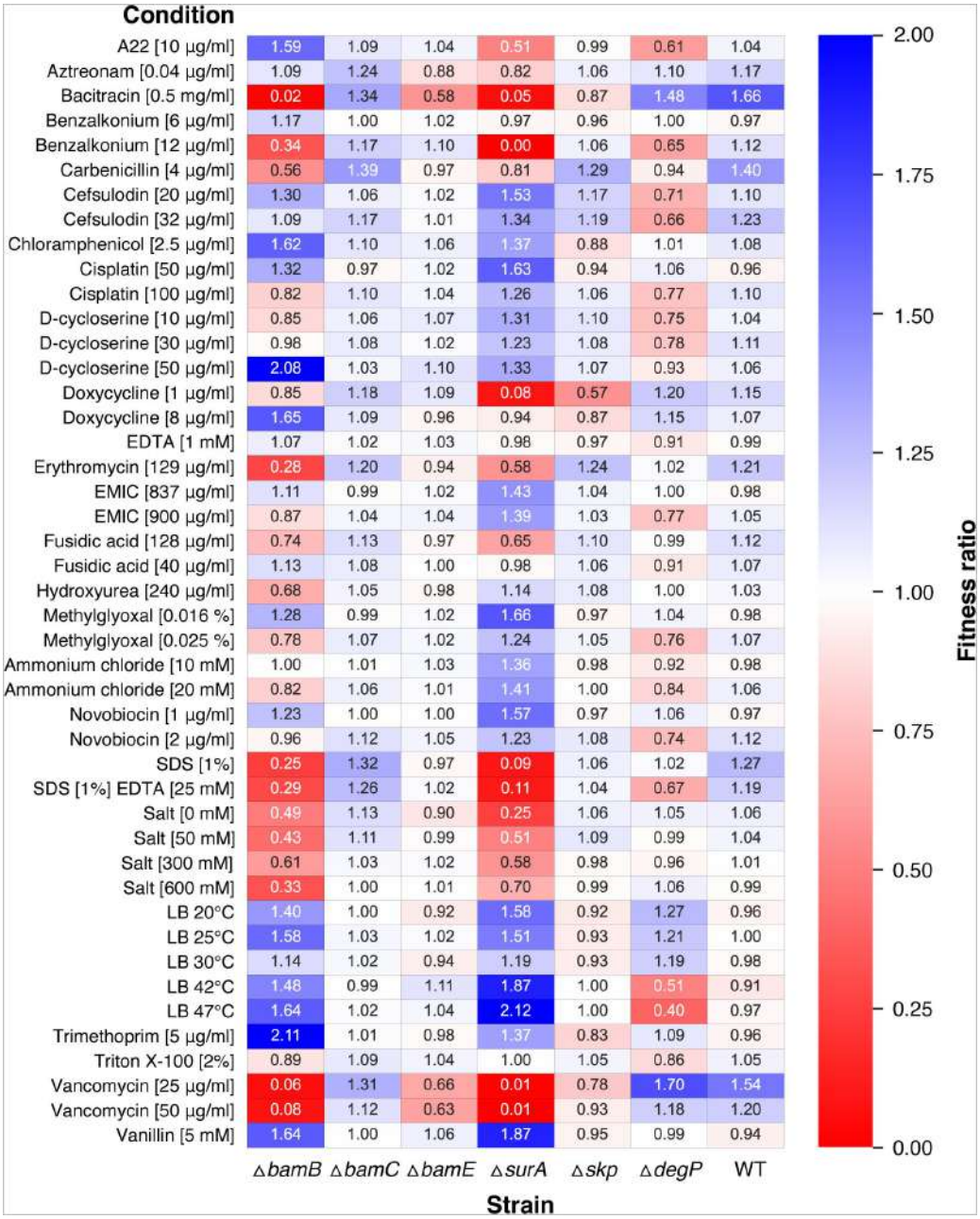

Figure 1

Phenotypic profiling of mutants lacking Bam-associated proteins

Heat map of fitness scores for the *E. coli* BW25113 parent strain and Δ*bamB*, Δ*bamC*, Δ*bamE,* Δ*surA*, Δ*skp*, or Δ*degP* mutants grown in various stress conditions. Colony size measurements for each condition were normalised by comparing to colony size of that strain when grown on LB medium at 37°C. Growth of each strain on LB is set to 1 and each condition normalised to this. Fitness scores above 1 represent better growth than the LB condition as measured by colony size and scores below 1 indicate smaller colony size than the LB condition. Some conditions are abbreviated due to space restrictions: EMIC - 1-Ethyl-3-methylimidazolium chloride, EDTA - Ethylenediaminetetraacetic acid, SDS – Sodium dodecyl sulfate.

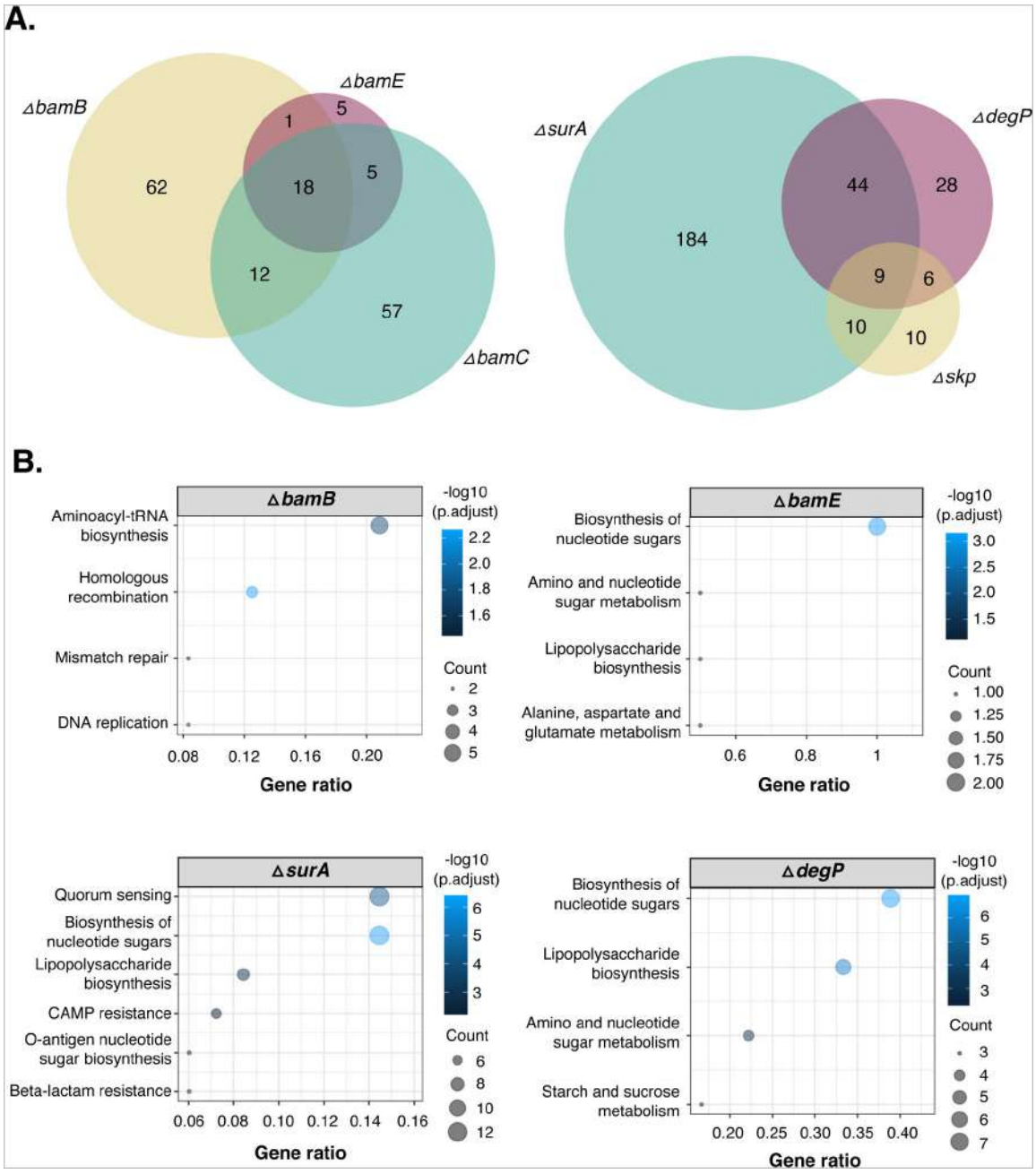

Figure 2

Genetic interaction analysis of Bam-associated genes by TraDIS

TraDIS libraries were constructed in the *E. coli* BW25113 parent strain and Δ*bamB*, Δ*bamC*, Δ*bamE,* Δ*surA*, Δ*skp*, or Δ*degP* mutants to identify genes that become essential in each knockout strain compared to the parent library (conditionally essential). **A.** Venn diagrams showing conditionally essential genes identified within the Δ*bamB*, Δ*bamC* and Δ*bamE* TraDIS libraries or the Δ*surA*, Δ*skp* and Δ*degP* libraries. **B.** Analysis of KEGG categories enriched in conditionally essential gene lists in the Δ*bamB*, Δ*bamE,* Δ*surA* and Δ*degP* TraDIS libraries, represented as bubble plots. No data is shown for the Δ*bamC* and Δ*skp* conditionally essential gene lists as there was no significant enrichment of any KEGG categories.

For the OMP chaperone pathway mutants we identified 247, 87 and 35 conditionally essential genes for the Δ*surA*, Δ*degP* and Δ*skp* mutants, respectively (**Fig 2A**). The Δ*surA* mutant had many strong phenotypes when probed against stresses (**Fig 1**), which could explain the large number of conditionally essential genes compared to the other OMP chaperone mutants (**Fig 2A**). Of the 87 conditionally essential genes in the Δ*degP* dataset, only 15 were also in the Δ*skp* background, despite DegP and Skp functioning together to degrade stalled OMP substrates [8]. This difference is also potentially due to the dual role of DegP as both a chaperone and a protease [29]. These results suggest that while there is functional redundancy between the SurA and DegP/Skp chaperone pathways, the function of the chaperones under specific chemical and genetic conditions is likely specialised (**Fig 1** and **2A**).To determine the functions and associated pathways of the conditionally essential genes identified in the mutant backgrounds, we completed GO and KEGG analyses. Enrichment analysis of KEGG pathways for the Δ*bamC* and Δ*skp* datasets resulted in no significant enrichment of any one category. However, genes involved in "Lipopolysaccharide biosynthesis" and "Biosynthesis of nucleotide sugars" were enriched in the Δ*surA*, Δ*degP* and Δ*bamE* conditionally essential gene lists and "O-antigen nucleotide sugar biosynthesis" was enriched in the Δ*surA* background (**Fig 2B** and Table S2). The most enriched KEGG pathway in the Δ*bamB* dataset was "Aminoacyl-tRNA biosynthesis", however these genes all encode tRNAs and are on average 75 bp in length. Visual inspection of these gene regions identified sparse insertion density within the local genomic area leading to a likely false positive for conditional essentiality. The Δ*bamB* dataset is also significantly enriched for three other KEGG pathways: "Homologous recombination", "Mismatch repair" and "DNA replication" (**Fig 2B** and Table S2). Together, the KEGG pathway enrichment analysis identifies the importance of LPS and ECA biosynthesis in these mutants as well as a potential link between OMP biogenesis and DNA replication. This directed our further investigations.

Genes required for heptose incorporation into LPS are synthetically lethal with *bamB, surA* and *degP*

We identified that fewer mutants were recovered with transposon insertions in genes involved in LPS assembly in the Δ*bamB*, Δ*surA* and Δ*degP* backgrounds than in the parent. In addition, genes involved in "Biosynthesis of nucleotide sugars" were significantly enriched, with genes identified being involved in the synthesis of heptose, a core component of LPS (**Fig 2B** and Table S2). Despite this category being enriched in the Δ*bamE* dataset, we found this was due to one gene in particular, *glmS*, and that the result was actually specific to the Δ*bamB*, Δ*surA* and Δ*degP* TraDIS libraries (**Fig 3A** and **Fig S6**). Synthesis of heptose consists of five main steps before it is incorporated into the LPS inner core (**Fig 3B**). In the Δ*surA* and Δ*degP* TraDIS libraries, all four genes involved in synthesis of heptose were essential: *gmhA*, *gmhB*, *hldE* and *waaD*. In the Δ*bamB* background all were essential except for *gmhB,* which is potentially because a Δ*gmhB* mutant is not completely devoid of heptose [37]. These data suggest that heptose production was functionally more important in Δ*degP* and Δ*surA* than in the Δ*bamB* mutant. The incorporation of heptose into the LPS structure was also functionally important. In Δ*degP* and Δ*surA* mutants, the genes *waaC* and *waaF* were conditionally essential, which are responsible for transfer of the first and second heptose onto the LPS inner core, respectively (**Fig 3A** and **3B**) [38, 39]. In contrast, in the Δ*bamB* mutant, *waaC* was conditionally essential whereas *waaF* was not. This implies that while Δ*degP* and Δ*surA* mutants are not able to tolerate having LPS with only one heptose residue, the Δ*bamB* mutant is.

LPS truncation increases membrane fluidity and decreases Bam complex activity

Increased outer membrane fluidity decreases Bam activity and modifications to LPS structure can lead to changes in membrane fluidity [40]. Thus, we hypothesised that changes in LPS core structure would affect membrane fluidity to differing degrees, which could affect Bam complex

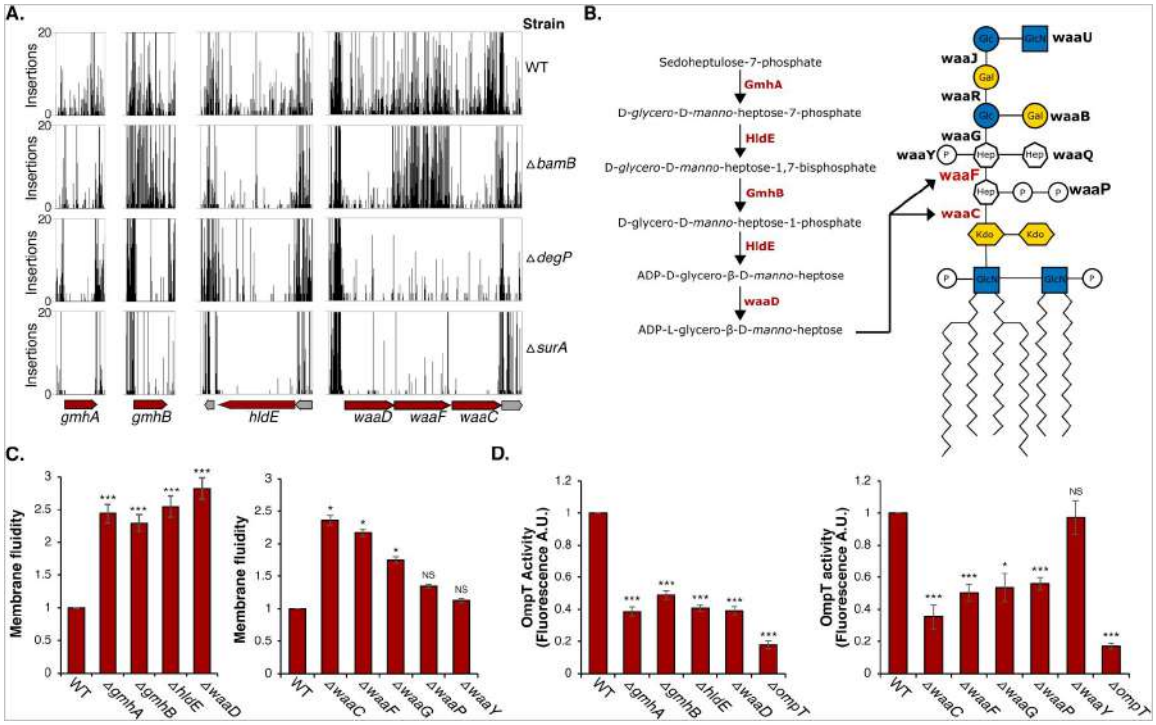

Figure 3

Incorporation of heptose into LPS is essential in Δ*bamB,* Δ*surA* and Δ*degP*

A. Transposon insertions in the genes *gmhA*, *gmhB*, *hldE, waaD, waaC,* and *waaF* in the parent, Δ*bamB,* Δ*surA* and Δ*degP* TraDIS libraries. Transposon cut-off is set to 20. Essential genes are represented as red arrows. **B**. Schematic of the heptose biosynthesis pathway and LPS structure in *E. coli* K-12 BW25113 with gene labels for LPS biosynthesis enzymes indicated next to the linkage they form or component they ligate. Enzymes identified as conditionally-essential are labelled in red text. **C.** Membrane fluidity was measured in Δ*gmhA,* Δ*gmhB,* Δ*hldE,* Δ*waaD,* Δ*waaC*, Δ*waaF*, Δ*waaG*, Δ*waaP* and Δ*waaY* mutants and compared to the parent strain by using pyrenedeconoic acid fluorescence. **D.** To determine the extent of Bam complex activity, successful folding and insertion of OmpT into the outer membrane was measured in the Δ*gmhA,* Δ*gmhB,* Δ*hldE,* Δ*waaD,* Δ*waaC*, Δ*waaF*, Δ*waaG*, Δ*waaP*, Δ*waaY* and Δ*ompT* mutants and compared to the parent strain. For panels C and D, experiments were performed in biological and technical triplicate with standard deviation represented by error bars. Two sample t-tests were used to assess statistical significance of differences from the WT strain with *** indicating p-values of <0.001, * indicating p-values of <0.05, and NS as not significant (p-value ≥ 0.05).

efficiency. To test this hypothesis we assessed membrane fluidity and Bam complex activity in strains lacking the genes encoding the heptose biosynthesis pathway (Δ*gmhA*, Δ*gmhB*, Δ*hldE*, and Δ*waaD*) and LPS core synthesis (Δ*waaC*, Δ*waaF*, Δ*waaP*, Δ*waaG* and Δ*waaY*) (**Fig 3**). There were no differences in transposon insertion index for the gene *waaY*, which encodes the enzyme responsible for phosphorylation of the second heptose in the LPS inner core. Therefore, Δ*waaY* should act as a control in this experiment [41]. In addition, Δ*waaP* and Δ*waaG*, which are responsible for phosphate addition to the first heptose, and incorporation of the first glucose, respectively [42], were included as a small decrease in the insertion indexes for these genes were observed in the Δ*surA* and Δ*degP* TraDIS datasets (**Fig S7**).

Fluidity of the membrane for each mutant was measured using the lipophilic pyrene probe, pyrene decanoic acid. The pyrene monomer can undergo excimer formation and demonstrates a shift in fluorescence, a process which is dependent on the ease of mobility within the membrane [43, 44]. Formation of the excimer was measured and compared to that of the parent strain (**Fig 3C**). The largest increase in membrane fluidity occurred in knockouts of genes required for heptose biosynthesis: Δ*gmhA*, Δ*gmhB*, Δ*hldE*, and Δ*waaD*. Of this group, the Δ*gmhB* mutant had the smallest increase in membrane fluidity and this gene was also not essential in the Δ*bamB* background (**Fig 3A** and **3C**). Of the genes required for LPS core biosynthesis, membrane fluidity was higher in Δ*waaC*, Δ*waaF* and Δ*waaG* than in the parent strain with the biggest change being in Δ*waaC* and the smallest in Δ*waaG*. However, there was no significant increase in fluidity in the Δ*waaP* mutant. Membrane fluidity of the Δ*waaF*, Δ*waaP* and Δ*waaG* mutants was intermediate between that of the heptoseless Δ*waaC* mutant and the parent, with the severity of the effect correlating to the severity of LPS core truncation. No significant change in membrane fluidity was measured in the Δ*waaY* mutant control (**Fig 3C**).

Next, we investigated whether impairment of heptose synthesis affected activity of the Bam complex, which was monitored by an *in vivo* OmpT fluorescence assay. The outer membrane protease OmpT requires the Bam complex for folding and insertion into the membrane and is able to cleave a fluorogenic peptide, which is monitored by increased fluorescence over time [10]. Except for Δ*waaY*, all mutants demonstrated a minimum 40% decrease in OmpT activity compared to the parent strain. The heptoseless Δ*waaC* mutant exhibited the greatest decrease in OmpT activity. The effect of Δ*waaF*, Δ*waaP* and Δ*waaG* mutations on OmpT activity levels was comparable to each other and intermediate between that of Δ*waaC* and the parent strain (**Fig 3D**). In summary, mutations that lead to heptoseless LPS had the biggest increase in membrane fluidity and the lowest levels of OmpT activity with a graded response based on the severity of LPS core truncations. This suggests there is a correlation between LPS core structure, membrane fluidity and Bam complex activity that leads to a variety of Bam complex activity levels depending on the form of LPS in the outer membrane.

Generation of cyclic ECA is essential in the absence of the chaperone SurA

Genes involved in 'Biosynthesis of nucleotide sugars' were significantly enriched as conditionally essential in the Δ*surA* mutant. The genes identified are involved in biosynthesis of ECA (**Fig 2B**), which is a highly conserved carbohydrate-derived molecule present on the external leaflet of the outer membrane and in the periplasm of Enterobacteriaceae [45, 46]. The ECA biosynthesis pathway genes were all conditionally essential with the exception of *wxyE*, which is required for survival of both the parent and the Δ*surA* mutant (**Fig 4A** and **4B**). In addition, fewer mutants were recovered with transposon insertions in the genes *rffH* and *rffG* than in the parent TraDIS library (**Fig 4A**). The gene products RffH and RffG catalyse the same enzymatic reaction and are homologous in sequence to the genes RfbA and RfbB, respectively. However, they form part of different operons and function in separate pathways despite *rffG* being able to complement an RfbB defective strain [47, 48]. This likely explains why *rffH* and *rffG* are not entirely essential in the Δ*surA* background.

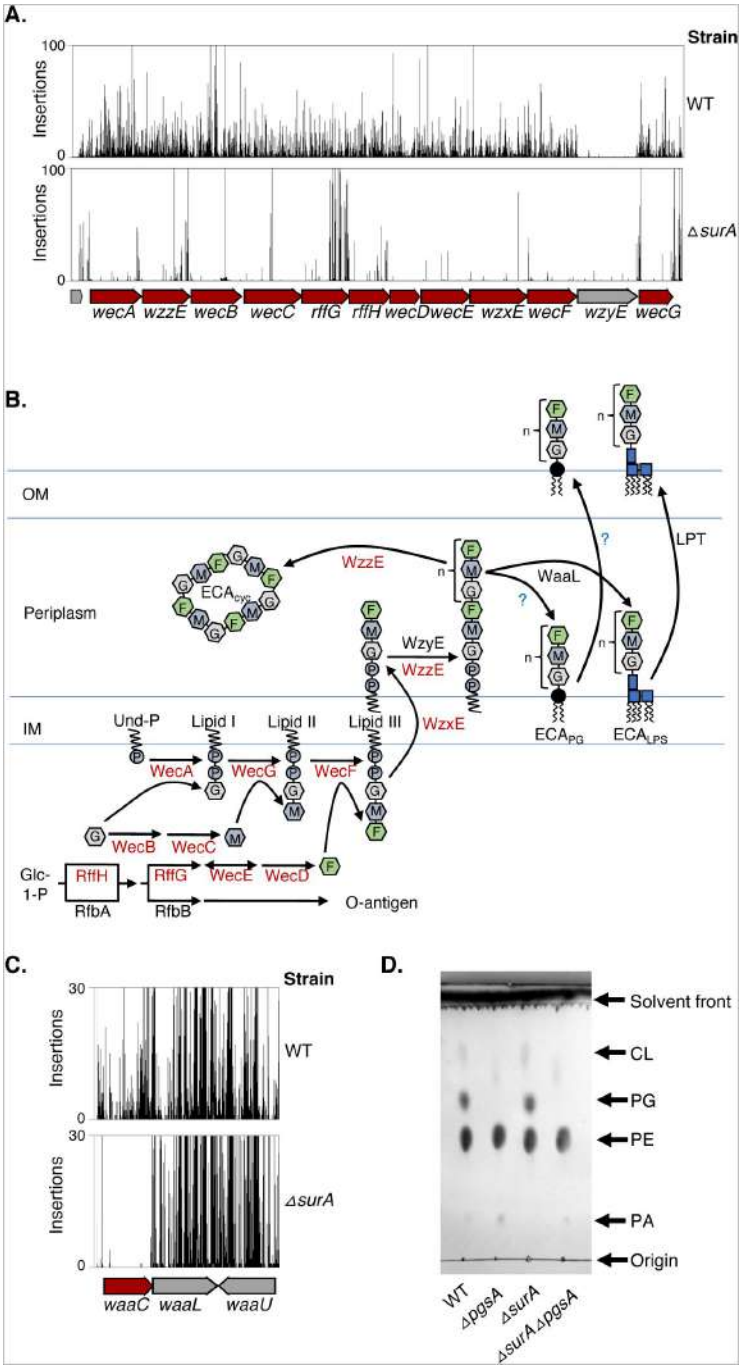

Figure 4

Synthesis of ECA is essential in the absence of the chaperone SurA

A. Transposon insertions in genes of the ECA biosynthesis pathway in the parent or Δ*surA* mutant TraDIS libraries. Transposon cut-off is set to 100. Essential genes are represented as red arrows. **B**. Schematic representation of the ECA biosynthesis pathway with the names of proteins labelled next to the reaction for which they are responsible. Conditionally essential proteins are labelled in red text. **C.** Transposon insertions in the *waaL* gene in either the parent or Δ*surA* mutant TraDIS libraries. Transposon cut-off is set to 100. **D.** Analysis of phospholipid content in the parent or Δ*surA* mutant with further mutations to disrupt synthesis of the major anionic phospholipids. The Δ*pgsA and* Δ*surA*Δ*pgsA* strains are also Δ*lpp*Δ*rcsF*. Phospholipid samples were separated and visualised by TLC using a solvent mixture of methanol/ chloroform/ water with a ratio of 2:2:1.8 before being visualised by phosphomolybdic acid and charring.

ECA exists in three forms that all share the same biosynthetic pathway: ECA that is covalently linked to LPS (ECA_{LPS}), covalently linked to diacylglycerol-phosphate (ECA_{PG}), or a cyclic form (ECA_{CYC}) that is localised to the periplasm as opposed to being surface exposed [45, 49]. We sought to determine which form of ECA is conditionally essential in Δ*surA*. Synthesis of ECA_{LPS} is facilitated by the O-antigen ligase WaaL, which is responsible for attaching the ECA molecule onto the LPS core [50, 51]. However, in the Δ*surA* TraDIS library, the gene *waaL* is non-essential (**Fig 4C**). This suggests that ECA_{LPS} is not essential in the Δ*surA* mutant. The formation of ECA_{PG} is completed by attachment of linear ECA chains to diacylglycerol by a phosphodiester bond through an unknown mechanism [50, 52]. To determine the essentiality of ECA_{PG} we targeted synthesis of the donor molecule for ECA_{PG}, the phospholipid phosphatidylglycerol [53]. The gene *pgsA* encodes phosphatidylglycerophosphate synthase, which catalyses the first committed step in biosynthesis of phosphatidylglycerol. However, loss of *pgsA* is lethal due to mislocalisation of Braun's lipoprotein, Lpp, to the inner membrane and activation of the Rcs stress system. These issues can be resolved by making an Δ*lpp*Δ*rcsF* mutant before constructing the Δ*pgsA* mutation [54–56]. The Δ*pgsA*Δ*surA*Δ*lpp*Δ*rcsF* quadruple mutant was viably constructed and the absence of phosphatidylglycerol was confirmed by phospholipid extraction and thin layer chromatography (**Fig 4D**). This confirmed that the phospholipid donor for synthesis of ECA_{PG} is not essential in the Δ*surA* mutant. Lastly, the gene *wzzE* is not required for the production of ECA_{LPS} or ECA_{PG}, but is required for production of ECA_{CYC} [50, 57, 58]. In the Δ*surA* TraDIS library, the gene *wzzE* contained a conditionally essential region indicating that ECA_{CYC} is likely to be the form of ECA that is conditionally essential in a Δ*surA* mutant (**Fig 4A**) [57].

meso-DAP is essential in the absence of BamB, BamC or BamE

The TraDIS data were searched for conditionally essential genes involved in cell envelope biogenesis pathways other than LPS and ECA biosynthesis. The gene *dapF* was identified as conditionally essential in Δ*bamB* and Δ*bamC* with visual inspection indicating decreased insertions in *dapF* in Δ*bamE* (**Fig 5A**). This was particularly surprising considering the lack of strong phenotypes in the Δ*bamC* background (**Fig 1**). DapF converts LL-diaminopimelate (LL-DAP) to *meso*-diaminopimelate (*meso*-DAP), which is then either decarboxylated to produce L-lysine by the enzyme LysA or is used in biosynthesis of peptidoglycan [59, 60]. The gene *lysA* was non-essential in all strains tested, suggesting the essentiality of *dapF* in these mutants is due to the requirement for *meso*-DAP in peptidoglycan (**Fig 5A** and **5B**). To validate the genetic interaction between Δ*dapF* and components of the Bam complex, the *dapF* gene was knocked out in the BW25113 parent strain, Δ*bamB,* Δ*bamC* or Δ*bamE* mutants. The double knockouts were selected in the presence of externally supplied *meso*-DAP, which alleviated the loss of *dapF*. Cells were then grown in liquid media in the presence of *meso*-DAP before being serially diluted in un-supplemented media and assayed for survival in the presence or absence of *meso*-DAP by efficiency of plating assay. All strains grew equally as well as the parent on LB agar supplemented with 1 mM *meso*-DAP, except for Δ*bamB*Δ*dapF* which showed a minor decrease in CFU and colony size (**Fig 5C**). However, in the absence of *meso*-DAP the single Δ*dapF* mutant demonstrated a decrease in survival and the double mutants were not viable (**Fig 5C**). Lastly, considering that loss of DapF will lead to a weaker peptidoglycan layer due to decreased crosslinks, we sought to negate the synthetic-lethal phenotype by growth in the presence of sucrose as an osmoprotectant [61, 62]. Unexpectedly, while the presence of 10% sucrose enabled survival of the single *dapF* mutant to levels comparable to the parent, this was insufficient to restore growth of the double mutant (**Fig 5C**). This data demonstrates that peptidoglycan structure is of increased importance in the absence of full Bam complex activity and that this may not simply be due to structural support for the envelope.

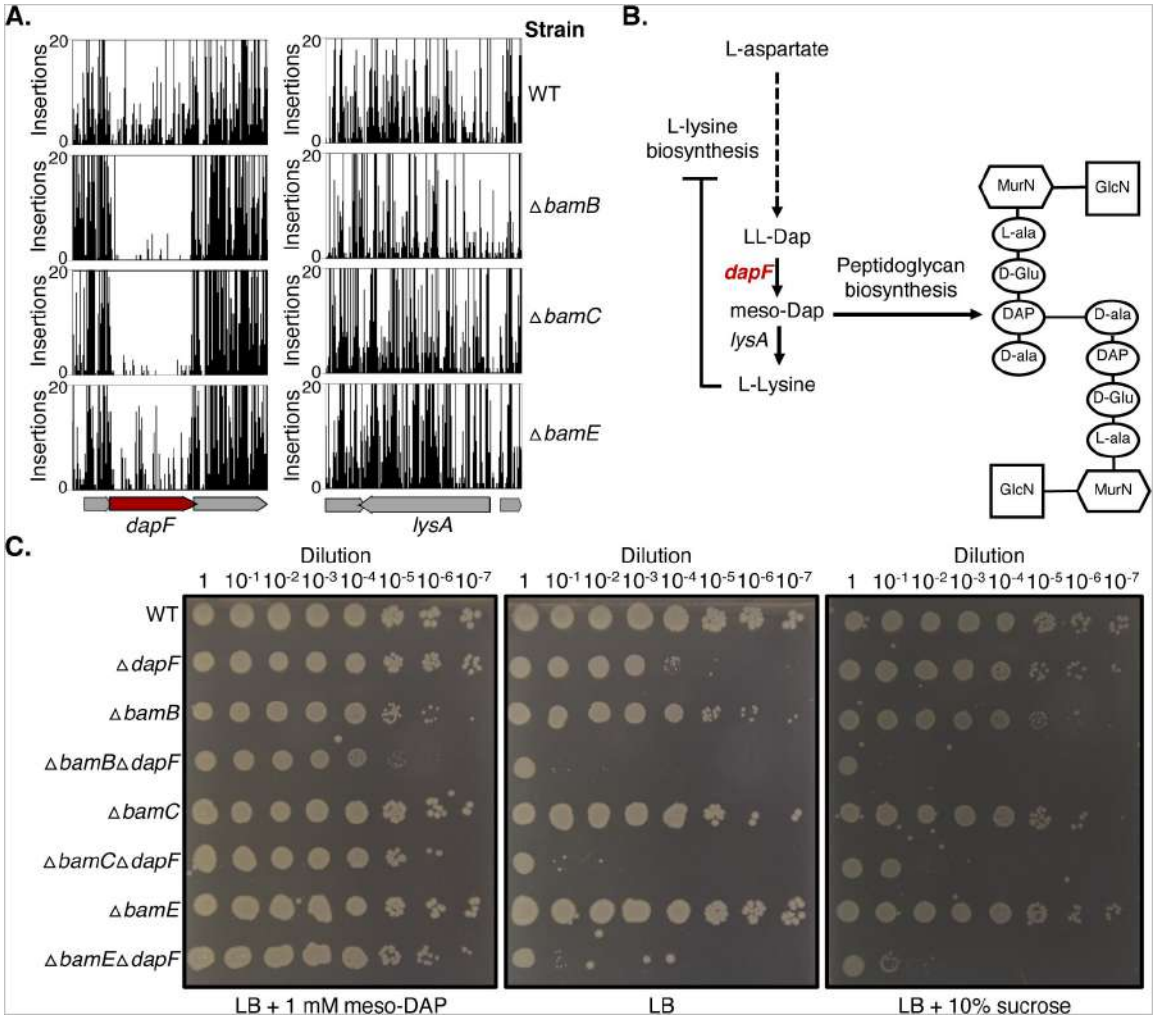

Figure 5

meso-DAP containing peptidoglycan is essential in the absence of Bam accessory lipoproteins

A. Transposon insertions in the genes *dapF* and *lysA* in the parent or Δ*bamB,* Δ*bamC,* Δ*bamE* mutant TraDIS libraries. Transposon cut-off is set to 20. Essential genes are represented as red arrows. **B**. Schematic representation of the L-lysine biosynthesis pathway with the names of proteins labelled next to the reaction for which they are responsible. Conditionally essential proteins are labelled in red text. A schematic structure of *E. coli* peptidoglycan is shown with the site of *meso*-DAP incorporation shown. **C.** Efficiency of plating assay showing survival of the Δ*dapF,* Δ*bamB,* Δ*bamC,* Δ*bamE,* Δ*dapF*Δ*bamB,* Δ*dapF*Δ*bamC, or* Δ*dapF*Δ*bamE* mutants grown on LB with or without 1 mM *meso*-DAP or 10 % sucrose. Cells were grown overnight in LB supplemented with 1 mM *meso*DAP before being normalised to OD_{600} = 1.00 and serially diluted 1:10 before 2 µl was spotted on agar plates and incubated at 37°C overnight.

Regulation of DNA replication initiation is disrupted in the absence of BamB

Our TraDIS experiment identified that in the Δ*bamB* dataset three KEGG pathways were significantly enriched: “Homologous recombination”, “Mismatch repair” and “DNA replication”. Bacterial DNA replication is mainly regulated at the initiation step by DnaA (**Fig 2A** and **6A**). The ATP-bound form of this protein binds to DnaA boxes present at the chromosomal origin of replication (*oriC*), with both high and low affinity, and directs replisome assembly [63]. Briefly, DnaA-ATP forms an oligomeric complex that facilitates unwinding of the DNA strands, which in turn enables assembly of the replisome: the complex responsible for replication of the bacterial chromosome. In *E. coli*, DnaA binding to its cognate DnaA boxes is modulated by regulatory proteins. Negative regulation is achieved by two proteins. The protein SeqA sequesters newly replicated origins, preventing premature reinitiation of replication [64–66]. The Hda protein works together with the β-sliding clamp to stimulate ATP hydrolysis of DnaA-ATP, which in the ADP-bound form is unable to promote initiation of DNA replication [64–68]. Positive regulation is facilitated by the DnaA initiator-associating factor, DiaA, which directly interacts with the N-terminal domain of DnaA to stimulate initiation at *oriC* [69, 70].

Analysis of the TraDIS data identified the genes *holC, holD, matP, seqA* and *hda* as conditionally essential in the Δ*bamB* mutant (Table S1). Within this set of genes, we chose to focus on those with the clearest conditional essentiality from the TraDIS data, *hda* and *seqA*. Insertions within the negative regulator encoding genes, *seqA* and *hda*, led to decreased survival of Δ*bamB*. In contrast, increased fitness of Δ*bamB* was observed for cells containing disruptions of the positive regulator gene *diaA* (**Fig 6B**). We confirmed the findings regarding the negative regulators by using CRISPRi. The *bamB::aph* allele was transferred into the dCas9 encoding strain *E. coli* LC-E18 and the kanamycin resistance marker was removed. The pSGRNA plasmid was used to express guide RNA targeting the *seqA* or *hda* genes in either the parent or Δ*bamB*. Expression of guide RNA targeting the *seqA* and *hda* genes led to significantly decreased survival of Δ*bamB* when compared to the parent strain, therefore confirming the observations made from TraDIS (**Fig 6C**). The positive genetic interaction between *bamB* and *diaA* was confirmed by measuring fitness of the Δ*bamB*Δ*diaA* mutant compared to both single deletion mutants. Fitness of the double mutant was greater than the expected fitness for this strain (**Fig 6D**).

Considering that loss of negative regulators of DNA replication initiation led to decreased fitness of Δ*bamB*, and loss of the positive regulator increases fitness, we hypothesised that the Δ*bamB* mutant may already have defective replication control. Therefore, we compared chromosomal content of the wild-type and Δ*bamB* strain by using an established replication run-out assay [71]. Both strains were grown to early exponential phase under conditions supporting fast cell growth (LB + 0.2% glucose), when cells contain multiple replicating chromosomes. We reasoned that dysfunction of replication control is usually exacerbated when cells grow with overlapping replication rounds. Next, cells were collected and treated with rifampicin to inhibit further rounds of DNA replication initiation, and with cephalexin to prevent cell division. Fixed cells were stained for DNA content with Sytox Green and analysed by flow cytometry. The comparison of chromosomal copy number revealed a higher proportion of cells with 16 chromosome copies for the Δ*bamB* mutant, which implies that initiation of replication occurs earlier during the cell cycle in this strain relative to the parent. Strikingly, a population of Δ*bamB* cells also displayed a number of chromosomes deviating from the normally observed 2^n, as manifested by an additional peak between the 8 and 16 chromosome peaks. This is a hallmark of asynchronous DNA replication events, when not all replication origins in the cell fire simultaneously (**Fig 6E**, S8-10). Analysis of the other Bam-accessory lipoprotein gene mutants and Δ*skp* by replication run-out assay revealed no significant changes from the parent pattern (**Fig S11**). Therefore, our results suggest that *E.*

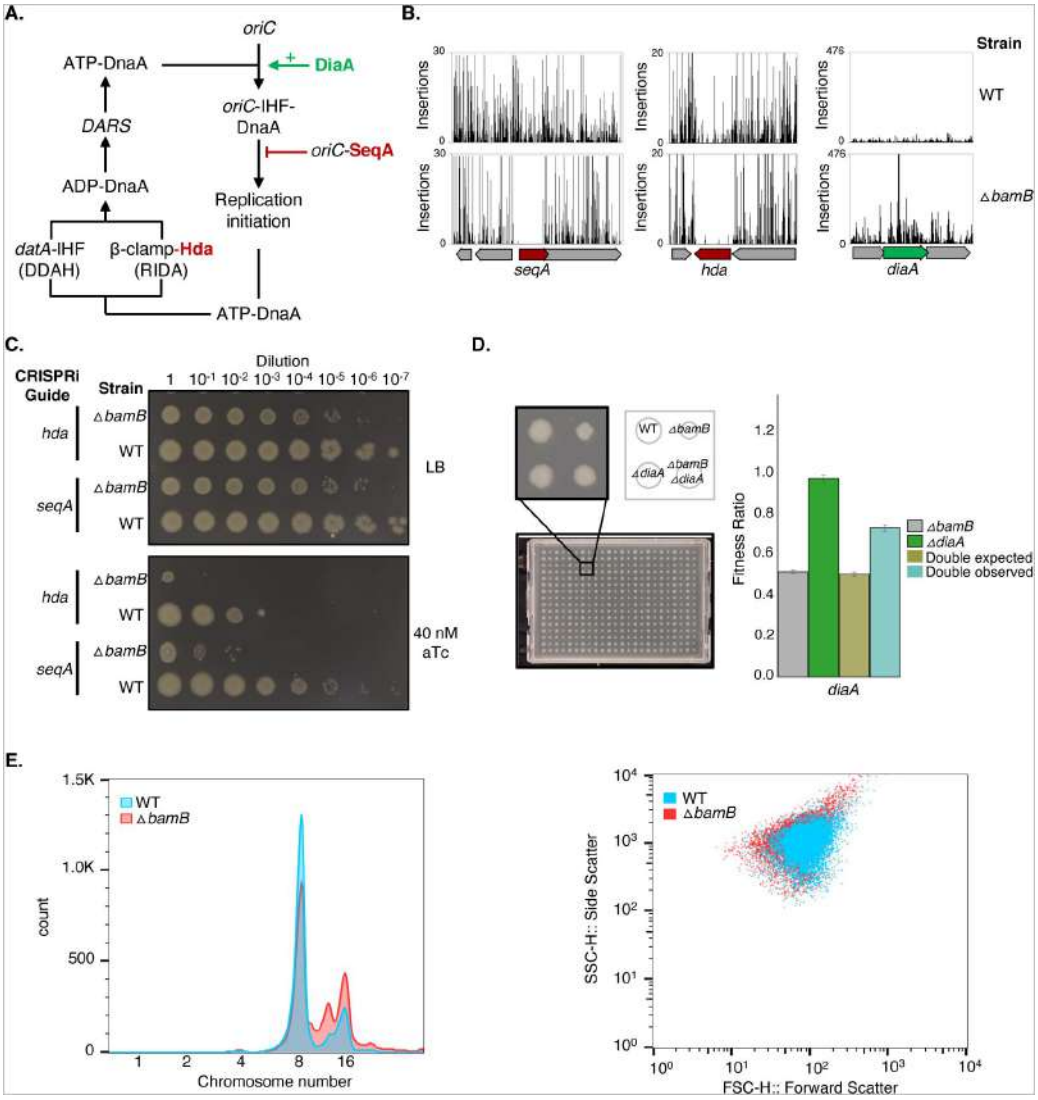

Figure 6

Loss of BamB leads to changes in DNA replication control

A. Schematic representing DNA replication control in *E. coli*. DiaA stimulates initiation at the origin of replication, *oriC*, by DnaA. SeqA prevents premature reinitiation of replication. Hda acts together with the β-sliding clamp to hydrolyse ATP-bound DnaA by regulatory inactivation of DnaA (RIDA). This can also occur through *datA*-dependent DnaA-ATP hydrolysis (DDAH). **B.** Transposon insertions in the genes *hda*, *seqA* and *diaA* in the parent or Δ*bamB* mutant TraDIS libraries. Conditionally-essential genes are represented as red arrows and genes that increase fitness are in green. **C.** Efficiency of plating assay showing survival of the parent dCas9 expressing strain LC-E18 (WT) or Δ*bamB* mutant derivatives carrying the pSGRNA plasmid, which encodes CRISPRi guide RNA targeting either *seqA* or *hda*. Cells were grown on LB with or without 40 nM anhydro-tetracycline (aTc) to induce guide RNA expression. **D**. The *E. coli* BW25113 parent strain, single, or double Δ*bamB* and Δ*diaA* mutants were spotted on LB agar in 384-well format, in triplicate, and grown overnight at 37°C before being imaged. Fitness was calculated based on colony size and fitness ratios generated relative to the WT parent. **E.** Flow cytometry of *E. coli* LC-E18 cells grown in LB followed by replication run-out assay. Forward scatter and side scatter are plotted with WT cell data indicated in blue and Δ*bamB* data points in red. Fluorescence is plotted and represents chromosomal content for each cell with chromosome numbers for each peak marked

coli over-initiates DNA replication in the absence of BamB. This is consistent with the observations that Δ*bamB* cells are more fit if they lose the positive regulator of DNA replication, DiaA, but have decreased fitness in the absence of the negative regulators SeqA and Hda.

OMP trafficking protein conservation varies throughout Gram-negative bacteria

The data presented here demonstrate that in *E. coli,* the Bam-associated proteins likely have specialised functions that are potentially coordinated with LPS structure, the presence and form of ECA, peptidoglycan biogenesis and DNA replication control. Considering these results, we revisited the evolutionary conservation of Bam complex subunits and the periplasmic chaperone pathway proteins [72]. Reference genomes for a diverse range of Gram-negative bacterial representative strains were used to search for sequences coding the Bam complex subunits (as observed in *E. coli*) or the chaperone pathway proteins SurA, Skp and DegP. A combination of Prokka annotation, hmmsearch, SignalP 6.0 [73] and manual curation were used to generate a neighbour joining tree with a heat map of gene counts in each organism (**Fig 7**). While we found broad conservation of all query proteins within the gamma- and beta-proteobacteria, there are some notable exceptions. The BamB and BamC lipoproteins are not conserved within two species of the aphid endosymbiont *Buchnera aphidicola* and the data confirm previous unpublished observations that a strain of *B. aphidicola*, (subspecies *Baizongia pistaciae*) appears to have entirely lost genes encoding the Bam complex [74]. Likely this is due to the strain containing only a few OMPs, therefore no longer requiring a dedicated OMP assembly machinery.

Outside of the gamma- and beta-proteobacteria, requirement for the Bam-associated proteins appears to be diverse. The lipoproteins BamB and BamC are largely absent in the alpha-proteobacteria, and the epsilon-proteobacteria only encode the core components BamA and BamD, demonstrating reductive evolution. This minimalist form of the Bam complex is sufficient for OMP insertion, which is likely due to reduced β-barrel complexity as observed in *Helicobacter pylori* [75] (**Fig 7**). While there is diversity in the presence or absence of these proteins in the organisms analysed, multiple copies of some components were also identified. We found that *Pseudomonas putida* encodes two copies of BamA, BamE and SurA. Outside of the gamma-proteobacteria there are numerous examples of species encoding multiple copies of BamA, particularly within the alpha-proteobacteria, such as the plant pathogen *Agrobacterium tumefaciens* (**Fig 7**). These copies may play specialised roles in folding and inserting specific cargo, or they may alleviate an increased requirement for OMP insertion in these organisms. Taken together, the diverse range of Bam complex subunit compositions within Gram-negative bacteria support the hypothesis that the Bam-associated proteins likely play specialised roles that vary in each organism.

Discussion

The Bam complex has been identified as a significant unrealised target for new antimicrobials, with several new inhibitors of this essential outer membrane biogenesis machine being identified recently [77, 78]. However, despite this focus as an important new avenue for drug discovery, and recent advances in understanding the mechanism by which the Bam complex folds and inserts OMPs into the outer membrane [79, 80], we still do not fully understand the roles of the Bam-associated proteins in *E. coli*. We also do not understand why the complex appears to be modular, with subunits being differentially conserved throughout Gram-negative bacteria as shown through our analysis and those done previously (**Fig 7**) [72]. Constituent parts of the outer membrane such as phospholipid species, type of LPS, O-antigen, ECA, lipoprotein content, and variety/flux of the unfolded OMP proteins can vary across bacterial species [81, 82]. Such variation would likely result in significant differences in the biophysical constraints of the membrane environment in which the Bam complex must operate. In addition, there is likely to be

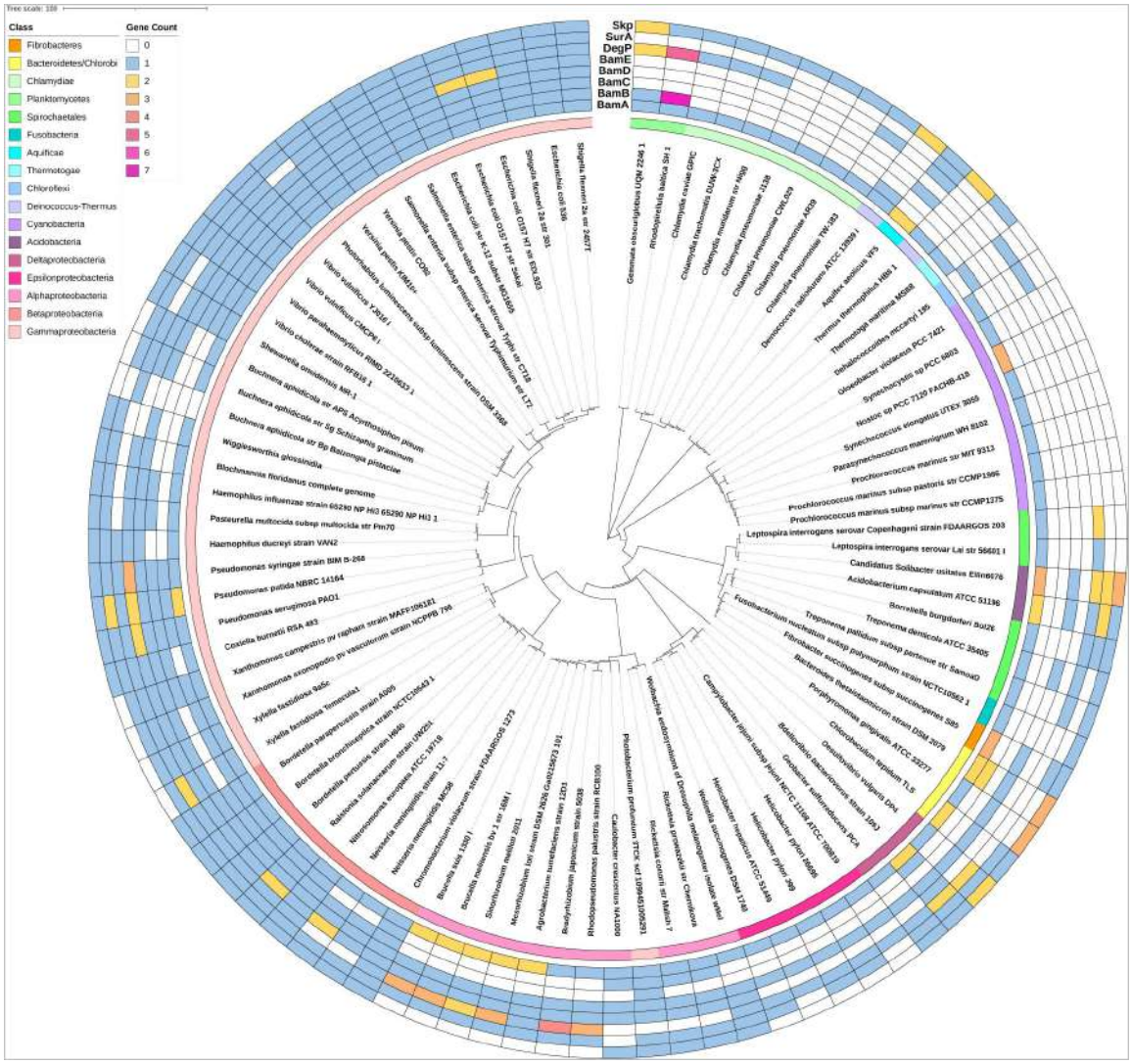

Figure 7

Conservation analysis of Bam-associated proteins in Gram-negative bacteria

Conservation of the BamB, BamC, BamE, SurA, DegP and Skp proteins among key Gram-negative bacterial species represented by a presence/absence map plotted onto a phylogenetic tree generated with iTOL [76]. Gene count in each species is represented by coloured boxes.

differing requirements for the chaperone pathway proteins depending on the pool of client OMPs. Considering that Skp and SurA have been shown to act on different unfolded states of OmpC, with Skp likely being more important during stress conditions, the environmental conditions experienced by each species could also dictate the requirement for each OMP chaperone [6]. Together, this strongly suggests that each accessory lipoprotein is likely to have specialised functions and that the chaperone proteins are unlikely to be truly functionally redundant. This is supported by our phenotypic profiling of knockout strains. Should each of the accessory lipoproteins merely contribute to overall activity of the Bam complex, and if there is true redundancy in the chaperone pathway, then we would expect that the knockout strains should phenocopy each other. However, we found this not to be the case (**Fig 1**). Our TraDIS analysis also supports this conclusion as we saw a large number of unique conditionally essential genes for each mutant (**Fig 2**).

Role of the outer membrane lipid environment for OMP insertion

The Bam complex must function within the constraints of the outer membrane lipid environment, therefore OMP biogenesis is likely to be affected by changes to outer membrane lipids. Indeed, we found conditional essentiality between genes involved in LPS inner core biogenesis and either *bamB*, *surA* or *degP*. Complete truncation of the LPS inner core by disruption of the last enzyme in the heptose biosynthesis pathway has previously been demonstrated to increase membrane fluidity and lead to decreased Bam complex activity [40]. We confirmed this observation and further demonstrate that the changes to membrane fluidity are of graded severity relating to the severity of LPS inner core truncation. This in turn leads to a graded impact on Bam complex activity (**Fig 3**). The Δ*bamB,* Δ*surA* and Δ*degP* knockout strains have the most severe phenotypes within the set of strains tested here (**Fig 1**). Also, loss of BamB, SurA or DegP each leads to OMP assembly defects, decreased numbers of folded OMPs in the outer membrane, and accumulation of unfolded OMPs in the periplasm [9, 26, 83–85]. We hypothesise that the negative effect of increased membrane fluidity on the Bam complex in combination with decreased levels of OMP assembly in the absence of BamB, SurA or DegP leads to OMP assembly levels that are too low to sustain cell viability. This is of particular significance when considering the variation in LPS structure seen between different strains, and the LPS modifications available, which could affect the level of Bam activity and influence the conservation of each Bam-associated protein [81, 82].

A role for ECA_{cyc} in amelioration of periplasmic protein folding stress?

The carbohydrate antigen ECA consists of three repeating sugars, is widely conserved amongst the *Enterobacterales*, and is produced in three forms that are either surface exposed (ECA_{LPS} and ECA_{PG}) or periplasmically localised (ECA_{CYC}). The invariant nature of the antigen suggests it has an important undiscovered function, however the role of ECA in outer membrane biology remains unknown [49]. We identified that ECA biogenesis becomes essential in the absence of the chaperone SurA (**Fig 4A**). Production of ECA requires the lipid carrier undecaprenyl phosphate (Und-P), which is limited in the cell and utilised in numerous metabolic reactions including the production of peptidoglycan, capsule, O-antigen and membrane-derived oligosaccharides. Disruption of ECA biogenesis can cause stress on these other pathways due to Und-P sequestration in ECA dead-end intermediates [49, 57, 86]. However, the first gene in the ECA pathway is conditionally essential in the absence of SurA (**Fig 4A**), therefore the effects are unlikely due to stress on the Und-P pool. Instead, we showed that the periplasmically localised form, ECA_{cyc}, is essential in the absence of SurA (**Fig 4**). It is possible that ECA_{cyc} might help stabilise the outer membrane of a Δ*surA* mutant, as it has been shown to suppress the envelope permeability defect of a Δ*yhdP* mutant. However, the molecular details of this suppression are yet to be discovered [57]. Alternatively, ECA_{cyc} could be performing a chaperone function directly, however this would require *in vitro* assays of protein aggregation with purified products for proof.

Coordination of OMP biogenesis with peptidoglycan biosynthesis

To ensure successful cell growth and division, activity of the Bam complex must be coordinated with biogenesis of the peptidoglycan layer. Our TraDIS analysis identified that in the Δ*bamB*, Δ*bamC* and Δ*bamE* mutants, the gene *dapF* was essential (**Fig 5A**). The DapF enzyme is responsible for synthesis of the peptidoglycan stem-peptide component *meso*-DAP. The single and double mutants could be rescued by exogenous *meso*-DAP, however only the single *dapF* mutant could be rescued by the osmo-protectant sucrose, which is sufficient to allow survival during disruption of peptidoglycan biogenesis (**Fig 5B**) [61]. Loss of *meso*-DAP in the single *dapF* mutant leads to accumulation of LL-DAP, which is incorporated into peptidoglycan and leads to decreased crosslinking [59, 62]. In the Δ*dapF* mutant the peptidoglycan layer would be able to withstand less mechanical load due to decreased crosslinking. This decreased mechanical strength, in combination with the reduced capacity for load bearing by the outer membrane in the Bam complex mutants, means that the cells are unlikely to withstand osmotic stress [87]. However, while this may be true for Δ*bamB* and Δ*bamE* mutants, there are no strong phenotypic effects for Δ*bamC* (**Fig 1**) [88]. Also, the loss of BamC has only a slight effect on the membrane permeability barrier, no detectable changes to the outer membrane proteome, and no effect on OMP folding in an *in vitro* assay [9, 89]. Consequently, the synthetic lethality between *dapF* and *bamC* is unlikely to be due to osmotic stress tolerance, as could be the case for the other mutants.

It has recently been demonstrated that the Bam complex preferentially inserts OMPs at the cell division site and that this is coordinated by interaction with the peptidoglycan layer [90]. While all of the Bam complex proteins were shown to interact with peptidoglycan *in vitro*, only BamA and BamC were found to interact with peptidoglycan in whole cells when analysed by crosslinking and pull-down assays [90]. Considering the interaction of mature peptidoglycan with BamC and the altered peptidoglycan structure in the Δ*dapF* strain [59, 62], we hypothesise that BamC might facilitate coordination between the Bam complex and peptidoglycan biosynthesis, however this requires further investigation.

Link between OMP biogenesis and DNA replication control

Not only must envelope biogenesis processes be coordinated with each other, but synthesis of the envelope must be coordinated with cell growth and cell division. Experimental evidence suggests that both DNA replication control [91, 92] and the rate of cell surface synthesis are coupled to cell volume [93]. This provides the rationale for existence of mechanisms that modulate DNA replication rate in response to cell envelope synthesis perturbation. Here we demonstrated that in the absence of BamB, cells over-initiate DNA replication and that synchrony of replication initiation at multiple origins is compromised (**Fig 6E**). Also, our phenotypic screen revealed that Δ*bamB* has increased fitness at sub-optimal growth temperatures. This would lead to slower growth, a factor that is known to alleviate some DNA replication control defects, such as those arising from loss of SeqA [64]. In addition, we found that the Δ*bamB* mutant is sensitive to hydroxyurea, which specifically inhibits ribonucleotide reductase and leads to depletion of the cellular dNTPs pool, replication fork arrest and genomic instability (**Fig 1**) [94, 95]. Similarly to Δ*bamB*, mutants that over-initiate replication, such as *seqA* mutants, are also sensitive to hydroxyurea [96].

Led by our TraDIS results, we confirmed that *seqA* and *hda* are essential in the Δ*bamB* mutant (**Fig 6**) and that this is likely due to over-initiation of DNA replication, which can be caused by all three of these mutations [64, 66, 97]. SeqA is required to prevent premature re-initiation of replication through sequestration of newly replicated GATC sites within oriC, whereas Hda prevents re-initiation of replication through regulatory inactivation of DnaA (RIDA), in combination with the β-sliding clamp of DNA polymerase [64, 98]. Interestingly, we also identified that two components of the β-sliding clamp loader complex, HolC and HolD, become

essential in the Δ*bamB* mutant (Table S1). These proteins contribute towards activity of the clamp loader. Therefore, the synthetic lethality could be due to decreased RIDA and over-initiation of DNA replication, as observed for the *hda* mutant [68, 99].

This is the first link between the Bam complex and DNA replication control, however links between the envelope and DNA replication have been observed previously. In order to initiate DNA replication, the DnaA protein must be in the ATP-bound form and regeneration of DnaA-ATP from the ADP-bound form is facilitated by interaction with phospholipids. [100, 101]. DNA replication control and envelope biogenesis are also linked by the SeqA protein, which has been associated to the purified outer membrane fraction in a cell-cycle dependent manner, however the mechanism remains unclear [102]. In addition, disrupted origin/terminus ratios in *seqA* mutant strains are suppressed by mutations in the *waaG*, *waaQ* and waa*P* genes, which are responsible for addition of the outer core of LPS, heptose III addition to the inner core and phosphorylation of heptose II of the LPS inner core, respectively [81, 103]. Interestingly, the Δ*bamB* mutant is also sensitive to changes in membrane fluidity brought about by LPS modifications that map to the inner core (**Fig 3**).

We also identified that insertions in the *diaA* gene, which encodes a positive regulator of DNA replication initiation, can suppress Δ*bamB*. The *diaA* gene is part of a conserved four gene cluster that also encodes LpoA - a regulator of peptidoglycan biogenesis, YraN - a protein of unknown function, and DolP - a cell-division site localised outer membrane lipoprotein shown to interact with the Bam complex [104, 105]. The genes in this cluster all appear to be linked to regulating cellular growth processes such as peptidoglycan biogenesis, OMP insertion into the outer membrane and DNA replication. This is of particular interest considering our data demonstrate potential coordination of these processes, which is essential to ensure efficient growth and survival during cell division.

Together, our data demonstrate that the Bam-associated proteins have specialised roles in the cell and highlights potential future targets to understand these roles. We provide further evidence that OMP transport, folding and insertion is affected by, and potentially coordinated with, peptidoglycan and LPS structure. We also show that Bam function is correlated with DNA replication control and highlight the BamB lipoprotein, outer membrane fluidity and LPS structure as a potential route through which this could occur. This provides a strong direction for further study to understand this coordination.

Materials and methods

Bacterial strains and culture conditions

For TraDIS experiments and phenotypic profiling, the parent strain was *E. coli* K-12 BW25113. The *E. coli* Δ*bamB*, Δ*bamC*, Δ*bamE*, Δ*surA*, Δ*skp* and Δ*degP* mutants were generated by transferring the relevant allele from the Keio library [106] into the clean parent strain by P1 transduction [107]. The kan^Rcassette was then removed by using the pCP20 plasmid [108] to leave a small in-frame 34 amino acid peptide consisting of residues from the FRT scar and the first amino acid and last seven of the target gene. These strains were then used for construction of transposon libraries and phenotypic profiling. The same approach was used for construction of the *E. coli* Δ*wecA*::*aph*, Δ*wecD*::*aph*, Δ*wecF*::*aph*, Δ*ompT*::*aph*, Δ*dapF*::*aph* and Δ*diaA*::*aph* mutants. The *diaA*::*aph* allele was also transferred into the Δ*bamB* derivative of *E. coli* BW25113 to generate the Δ*bamB*Δ*diaA*::*aph* double mutant. The *dapF*::*aph* allele was also transferred from the Keio library into Δ*bamB*, Δ*bamC*, Δ*bamE*, Δ*surA*, Δ*skp* and Δ*degP* mutants in the presence of 1 mM *meso*-diaminopimelate in order to generate double mutants. The Δ*rcsF*Δ*lpp*Δ*pgsA*Δ*surA* mutant was generated by transfer of alleles from the Keio library and subsequent removal of the kan^R cassette by use of the pCP20 plasmid before incorporation of the next allele by P1 transduction. The *E. coli*

Δ*bamB*, Δ*bamC*, Δ*bamE*, Δ*surA*, Δ*skp* and Δ*degP* mutants were generated by transferring the relevant allele from the Keio library [106] into the clean parent strain by P1 transduction [107]. The kan^Rcassette was then removed by using the pCP20 plasmid [108] to leave a small in-frame 34 amino acid peptide consisting of residues from the FRT scar and the first amino acid and last seven of the target gene. These strains were then used for construction of transposon libraries and phenotypic profiling. The same approach was used for construction of the *E. coli* Δ*wecA*::*aph*, Δ*wecD*::*aph*, Δ*wecF*::*aph*, Δ*ompT*::*aph*, Δ*dapF*::*aph* and Δ*diaA*::*aph* mutants. The *diaA*::*aph* allele was also transferred into the Δ*bamB* derivative of *E. coli* BW25113 to generate the Δ*bamB*Δ*diaA*::*aph* double mutant. The *dapF*::*aph* allele was also transferred from the Keio library into Δ*bamB*, Δ*bamC*, Δ*bamE*, Δ*surA*, Δ*skp* and Δ*degP* mutants in the presence of 1 mM *meso*-diaminopimelate in order to generate double mutants. The Δ*rcsF*Δ*lpp*Δ*pgsA*Δ*surA* mutant was generated by transfer of alleles from the Keio library and subsequent removal of the kan^R cassette by use of the pCP20 plasmid before incorporation of the next allele by P1 transduction. The *E. coli* Δ*gmhA*::*aph*, Δ*gmhB*::*aph*, Δ*hldE*::*aph*, Δ*waaD*::*aph*, Δ*waaC*::*aph*, Δ*waaF*::*aph*, Δ*waaP*::*aph*, Δ*waaG*::*aph*, Δ*waaY*::*aph* mutants were created by using λ-Red recombination, as previously described for single-step gene inactivation [109]. All mutants were confirmed by polymerase chain reaction and strains were routinely cultured on LB agar and LB broth. The dCas9 expressing strain *E. coli* LC-E18 and the pSGRNA plasmid was a gift from David Bikard (Addgene plasmid # 115924) and has been described previously [110]. The *E. coli* LC-E18 Δ*bamB* derivative was constructed as described for the BW25113 Δ*bamB* derivative with the kan^R cassette removed in order to allow selection of the pSGRNA plasmid in this background. All strains used in this study are listed in Table S3. Bacterial cultures were grown at 37°C unless otherwise stated. Where stated, the medium was supplemented with kanamycin (50 μg/ml), carbenicillin (100 μg/ml), and *meso*-DAP (1 mM). For micro-dilution survival assays, bacteria were grown in 5 ml LB medium at 37°C with aeration for ~16 hours. Cultures were normalised by optical density to OD_{600} = 1.00, 10-fold serially diluted in LB, and 2 μl of each dilution was inoculated onto LB agar plates.

Phenotypic screening

The *E. coli* K-12 BW25113 parent strain, Δ*bamB*, Δ*bamC*, Δ*bamE*, Δ*surA*, Δ*skp* and Δ*degP* mutants were screened against diverse stress conditions to phenotypically profile the mutants. Strains were arrayed in 384-well format and inoculated on 2% agar LB plates using a BM3-BC robot (S&P Robotic Inc.). In addition, the mutants and the wild type were subsequently inoculated on LB agar plates containing different stress conditions. The inoculated plates were incubated for 12 to 14 hours at 37°C before being imaged under controlled lighting with an 18-megapixel Canon rebelT3i (Canon) camera on the BM3-BC robot (S&P Robotic Inc.). Images of the plates were analysed using the software IRIS, which measured the size, opacity and circularity of each colony [27]. A total of 4 replica plates were generated for each stress condition. Fitness of the mutants was then scored and analysed using the ChemGAPP Small software [28]. Mean colony size for the mutant in each condition was compared to the mean colony size of that mutant in the LB agar condition, which was normalised to a fitness score of 1 [28]. Fitness scores below 1 represent decreased fitness, as a function of colony size compared to growth on LB agar, and scores above 1 indicate increased fitness in that condition. Each of the plates contained 56 replicates for the parent BW25113 strain (WT), Δ*bamB*, Δ*bamC*, Δ*bamE* and Δ*degP* strains with 52 replicates for Δ*surA* and Δ*skp* for plate space requirements. There were 4 replicate plates for each condition, all of which were treated as individual replicates and compared to their respective wild type parent replicates on each plate before the average was taken. The probability that the two means are equal across replicates was obtained by a one-way ANOVA. Correlation of fitness ratios for each strain was assessed by calculating the Pearson correlation coefficient for averaged fitness scores across replicates using Python before being plotted as a heatmap.

TraDIS library construction

The *E. coli* K-12 BW25113 parent strain, Δ*bamB*, Δ*bamC*, Δ*bamE*, Δ*surA*, Δ*skp* and Δ*degP* mutants were transformed with the EZ-Tn5™ <KAN-2> Tnp Transposome (Cambio) as previously described [32]. Approximately 1 million mutant colonies were pooled, thoroughly mixed and stored in LB supplemented with 15% glycerol at -80°C. DNA was extracted from at least two samples of each transposon library to generate independent sampling replicates for library generation.

Sequencing of TraDIS libraries

Cells from the pooled mutant library were harvested and genomic DNA was extracted for library preparation and sequencing as previously described [32]. Samples were sequenced using an Illumina MiSeq with a 150 cycle v3 cartridge.

TraDIS data analysis

Raw data were processed using a series of custom scripts as previously described [32]. The data were trimmed using Fastx barcode splitter and trimmer tools (Pearson *et al.*, 1997) and filtered based on inline indexes. The accuracy of the transposon sequences were checked in two steps: the first 22 bases, allowing for three nucleotide base mismatches and the last 10 bases of the transposon, allowing for up to one mismatch. Using Trimmomatic, sequences with less than 20 bases in length were removed (Bolger *et al.*, 2014). TraDIS data were then analysed using BioTraDIS (*https://sanger-pathogens.github.io/Bio-Tradis/*) [34] and aligned to the *E. coli* BW25113 reference genome CP009273.1, available from NCBI (Tatusova *et al.*, 2014). We used SMALT (*https://www.sanger.ac.uk/tool/smalt/*) as an aligner with zero value for mismatch threshold. We also set the parameter smalt_r, determining how to treat multi-mapping reads, to zero. This avoided repetitive elements to count as essential. We used the scripts *tradis_essentiality.R and tradis_comparison.R* as part of the package to produce the list of essentiality and then to compare the control and test libraries, respectively.

Membrane fluidity assay

Membrane fluidity was measured using the membrane fluidity kit (Abcam: ab189819), as previously described, but with minor modifications [104]. Bacterial strains were grown to mid-exponential phase (OD_{600} = ~0.4-0.6) in LB medium. Cells were harvested by centrifugation, washed with phosphate buffered saline (PBS) and incubated with labelling mix (10 µM pyrenedecanoic acid (PDA), 0.08% pluronic F-127, in PBS) in the dark for 20 min at 25°C with rocking. Cells were then washed twice in PBS and re-suspended in PBS prior to measuring fluorescence (excitation = 350 nm, emission = either 400 nm or 470 nm). Membrane fluidity was estimated by measuring the ratio of excimer (470 nm) to monomer (400 nm) fluorescence. The emission spectra were compared to unlabelled cells to confirm membrane incorporation and each experiment contained triplicate technical repeats and was then repeated three times. Membrane fluidity of the mutants of interest were expressed relative to the parent *E. coli* strain. Experiments were performed in technical triplicate and were repeated three times. Two sample t-tests were used to assess statistical significance of differences from the WT strain.

OmpT *in vivo* fluorescence assay

The OmpT assay for monitoring Bam activity was performed as described previously with minor modifications [10, 16, 40]. Bacterial strains were grown to mid-exponential phase (OD_{600} = ~0.4-0.6) in LB medium and were normalised to OD_{600} of 0.2 in growth media. The cell suspension (5 µl) was then added to 95 µl of 25 µM fluorogenic peptide, Abz-ARRAY(NO_2)-NH_2, diluted in PBS. Fluorescence emission was immediately measured (excitation = 325 nm, emission = 430 nm) over

a period of 5 h, with readings every 20 s. OmpT activity was expressed relative to the parent strain. Experiments were performed in technical triplicate and were repeated three times. Two sample t-tests were used to assess statistical significance of differences from the WT strain.

Phospholipid extraction and thin layer chromatography

Phospholipids were extracted using an adapted Bligh-Dyer method [111]. Bacterial cultures were grown overnight (~16 hours) at 37°C with shaking and cells were harvested by centrifugation. The bacterial cell pellets were resuspended and normalised to OD_{600} = 3 and mixed with methanol and chloroform (2:1). The cell suspension was incubated at 50°C for 30 min before additional chloroform and water was added to the samples to produce a final ratio 2:2:1.8 of methanol/chloroform/water. Following centrifugation, the phospholipid-containing phase was extracted and dried under nitrogen before being stored at -20°C. Samples were re-dissolved in chloroform before being separated by thin layer chromatography on silica gel membrane using a solvent system that consisted of chloroform, methanol, acetic acid (65:25:10). The plate was subsequently stained with phosphomolybdic acid (PMA) and warmed until the lipid species were visible.

Efficiency of plating assay

Efficiency of plating assays were completed as previously described [112]. Cells were grown overnight in LB (supplemented with 1 mM *meso*DAP where indicated) before being normalised to OD_{600} = 1.00 and serially diluted 1:10. Following dilution, 2 µl was spotted on agar plates containing supplements where indicated and incubated at 37°C for ~16 hours before being imaged.

Genetic interaction analysis

For genetic interaction analysis, overnight cultures were diluted 1/100 and then grown to OD_{600} = 0.8-1. Cultures were then spread on LB agar plates using sterile glass beads to create source plates, before being incubated for 12 to 14 hours at 37°C. Each strain was arrayed on LB agar plates, from the source plates, to form 384 colonies of 96 replicates for each strain using a BM3-BC robot (S&P Robotic Inc.). Plates were incubated at 37°C for 12 to 14 hours. The plate was then imaged under controlled lighting, with an 18-megapixel Canon rebelT3i (Canon) camera on the BM3-BC robot (S&P Robotic Inc.). Images were then analysed using the software called IRIS to measure the size, opacity and circularity of each colony on the plates [27]. Fitness of the mutants was then analysed and compared using the software ChemGAPP GI [28].

Flow cytometry analysis

Chromosome number measurements were performed as described previously, but with several modifications [71]. Briefly, cells were grown with aeration at 37°C until OD_{600}=0.15 in LB medium supplemented with 0.2% glucose. Samples were collected, treated with 150 µg/ml rifampicin, and 10 µg/ml cephalexin and incubated for 4 h at 37°C with mixing. Incubation with antibiotics results in cells containing an integral number of chromosomes, corresponding to the number of replication origins at the time of drug treatment. Subsequently, cells were harvested, washed with TBS (20 mM Tris-HCl pH 7.5, 130 mM NaCl) and fixed with cold 70% ethanol overnight. Additional samples were collected at OD_{600}=0.15 without antibiotic treatment and fixed as above.

Prior to flow cytometry analysis, cells were resuspended in 50 mM sodium citrate followed by RNA digestion with RNase A for 4 h. Chromosomal DNA was stained with 2 mM Sytox Green (Invitrogen) and DNA content per cell was measured with BD FACS Calibur at 488 nm Argon Ion laser. MG1655 (WT) strain grown in AB medium containing one of the following carbon sources: 0.4% sodium acetate, 0.2% glucose, 0.2% glucose + 0.5% casamino acids or in LB medium with 0.2%

glucose, treated with antibiotics, fixed and stained as above was used as a standard for each flow cytometry measurement, indicating cells containing 1/2 , 2/4, 4/8 or 8/16 chromosomes, respectively. Flow cytometry data was analyzed using FlowJo ver. 10.8.0.

Conservation analysis

Reference genomes were downloaded for each species from NCBI in fasta format and annotated using Prokka [113]. The 16s rRNA sequence for each species was then extracted from Prokka ffn files in fasta format. A Kmer based neighbour joining tree was produced via extracting a one-step sliding window of 8 base kmers from each 16s rRNA sequence. Following this, the number of unique kmers was counted for each species in order to produce a Kmer profile. The Jaccard similarity between each species Kmer profiles was then used to produce a distance matrix. This distance matrix was input into the R module ape::nj to produce the neighbour joining tree. The neighbour joining tree was reformatted as a nexus file and visualised within Figtree (*http://tree.bio.ed.ac.uk/software/figtree/*), where the tree was rooted at the midpoint and branches were transformed to become proportional.

To count the instances of the proteins BamA, BamB, BamC, BamD, BamE, DegP, SurA, and Skp, hmmsearch was used to extract proteins with the relevant domains from the Prokka annotated faa files. The Pfam domains used were PF01103, PF13360, PF06804, PF13525, PF04355, PF09312 and PF03938 for BamA, BamB, BamC, BamD, BamE, SurA, and Skp, respectively. For DegP, both PF00595 and PF13180 were used and the intersect taken. An e-value of 0.001 was used as a threshold for significant hits by hmmsearch. For BamA, hits annotated as the query protein were inputted into hmmscan and hits with at least one POTRA domain and an Omp85 domain were counted as true BamA hits. Hits containing a Tam-POTRA domain were excluded. Where a hit had only an Omp85 gene, the adjacent gene was checked for the POTRA domains. For BamB, any hmmsearch hits annotated as BamB or hypothetical proteins by Prokka were input into SignalP 6.0 [73] and hmmscan. Proteins assigned a LIPO (Sec/SPII) signal peptide within SignalP 6.0, with only one PQQ_2 domain within hmmscan were selected as true BamB hits. For BamC, all hits from hmmsearch were inputted into hmmscan to confirm the presence of the Lipoprotein-18 domain. Hits were also inputted into Phmmer and proteins with significant homology to BamC were counted as true hits. For BamD, hypothetical proteins and BamD hits were inputted into hmmscan and Phmmer and those with homology to BamD and a non-outcompeted YfiO domain counted as true hits. For BamE, hypothetical proteins and BamE hits were inputted into hmmscan and those with a singular SmpA_OmlA domain were counted as true hits. For DegP hypothetical proteins and DegP hits were inputted into hmmscan. If a hit had a PDZ type domain, Peptidase_M50 domain or Trypsin_2 domain then it was visualised on Pfam and manually assigned as DegP based on structure. If a DegP hit had any other type of domain, it was discounted. For SurA, all hits were run through hmmscan and Phmmer. Those with a SurA_N domain, Rotamase domain and a Rotamase_3 domain and homologous to SurA within Phmmer were counted. For Skp, all hits were run through Phmmer and only hits with only an OmpH domain and with homology to Skp counted as true hits. Finally, the neighbour-joining tree was edited in iTOL [76] to produce the heatmap of gene counts.

Acknowledgements

This work was supported by a UKRI Future Leaders Fellowship [MR/V027204/1] and a Springboard Award [SBF005\1112] to Manuel Banzhaf. The work was also funded by the National Science Centre Poland [UMO-2017/27/B/NZ2/00747] (awarded to Monika Glinkowska), the KAUST baseline fund [BAS/1/1108-01-01] awarded to Danesh Moradigaravand who is a member of the KAUST Smart-Health initiative, and the EU ITN Train2Target [721484] that funded training of Kara Staunton.

Supporting information

Supplemental Table 1

Supplemental Table 2

Supplemental Table 3

Note

This reviewed preprint has been updated to use the correct the funding information.

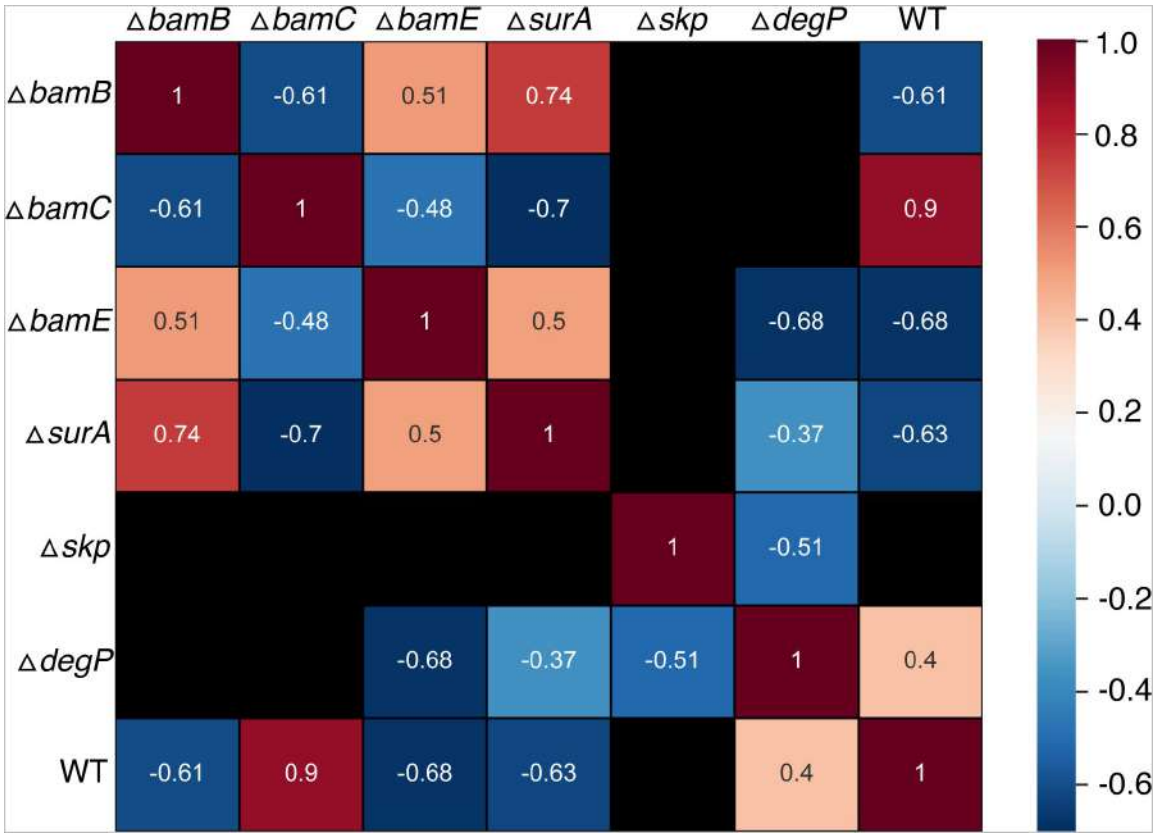

Figure S1

Correlation of phenotypic profiles

Heatmap of Pearson correlation coefficients for each pair of strain phenotypic profiles. Correlation of fitness ratios for each strain was assessed by calculating the Pearson correlation coefficient for averaged fitness scores across replicates using Python before being plotted as a heatmap. Black squares indicate a p-value ≥0.05 meaning the correlation coefficient achieved was not statistically significant.

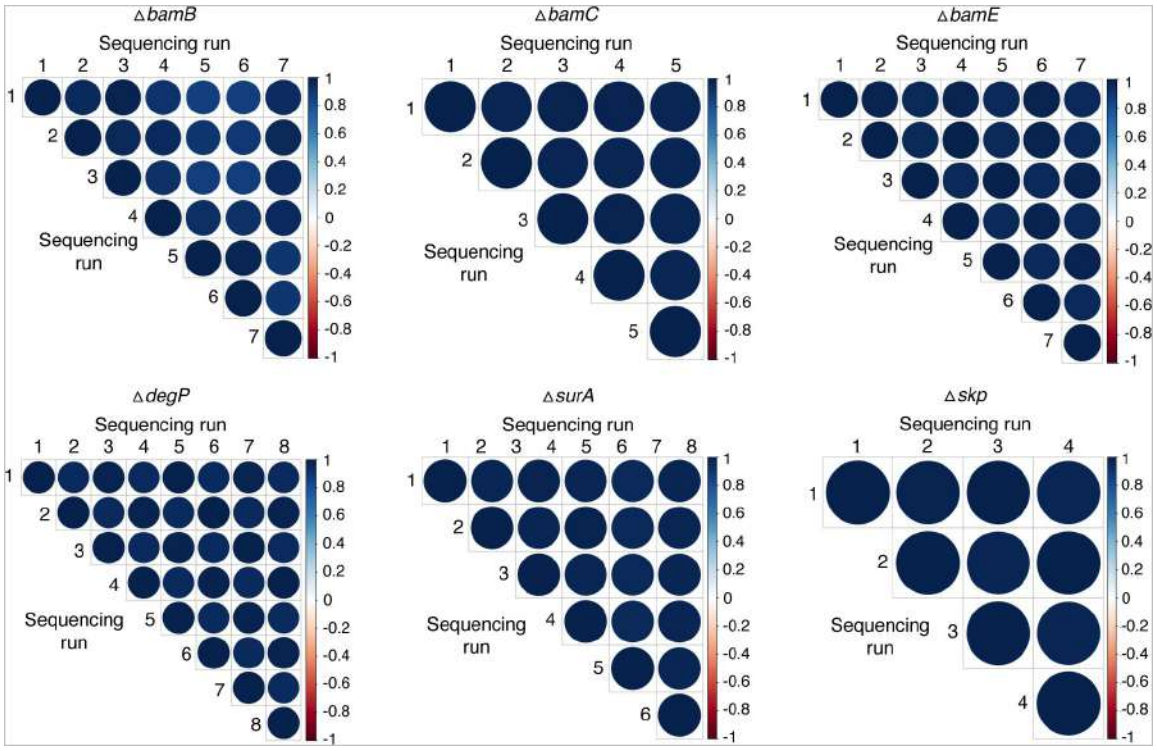

Figure S2

Reproducibility across TraDIS library sequencing runs

Correlogram of insertion indexes between individual sequencing runs for each TraDIS library. The colour and size of the bubbles correspond to the strength of the Pearson correlation coefficient between the indices for the same genes across the runs. The blue colour represents positive correlation.

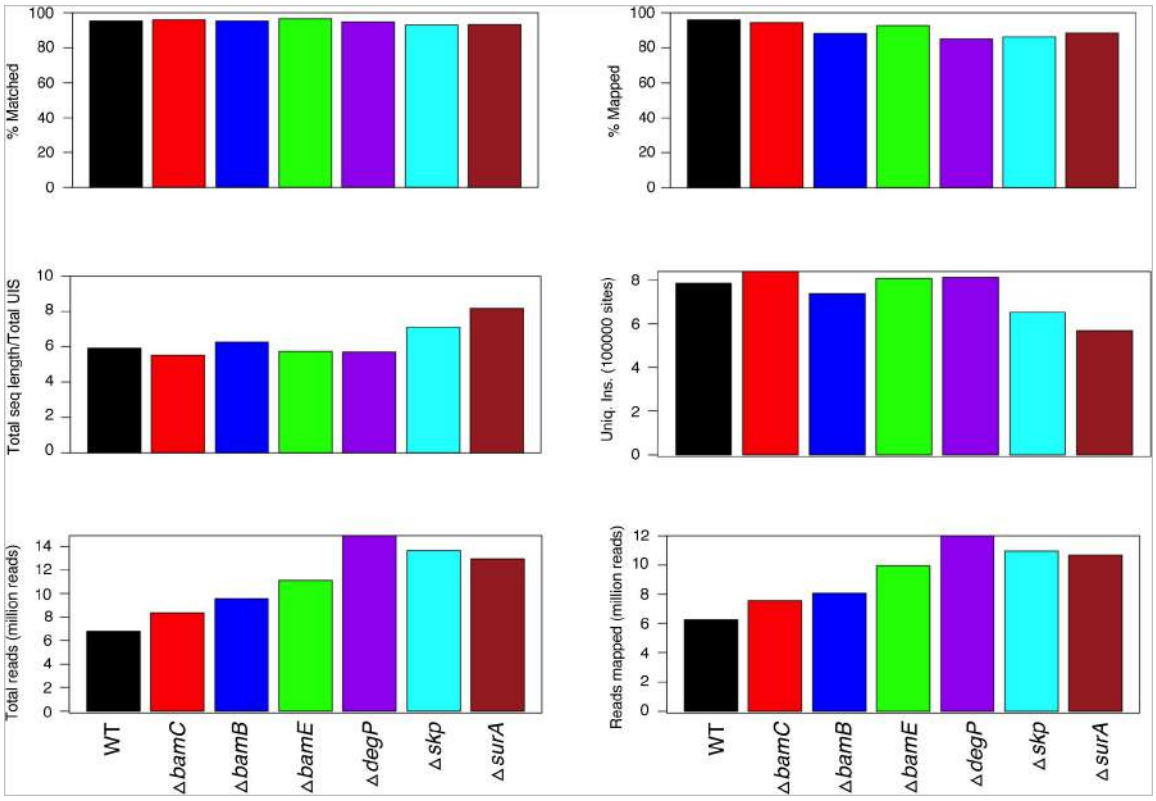

Figure S3

Transposon library construction metrics

TraDIS library construction metrics showing the percentage of sequencing reads that matched the transposon tag and that mapped to the chromosome. Total sequencing length as a function of total unique insertion sites, the total number of unique insertion sites for each sample, total number of sequencing reads, and the number of reads that mapped are also shown.

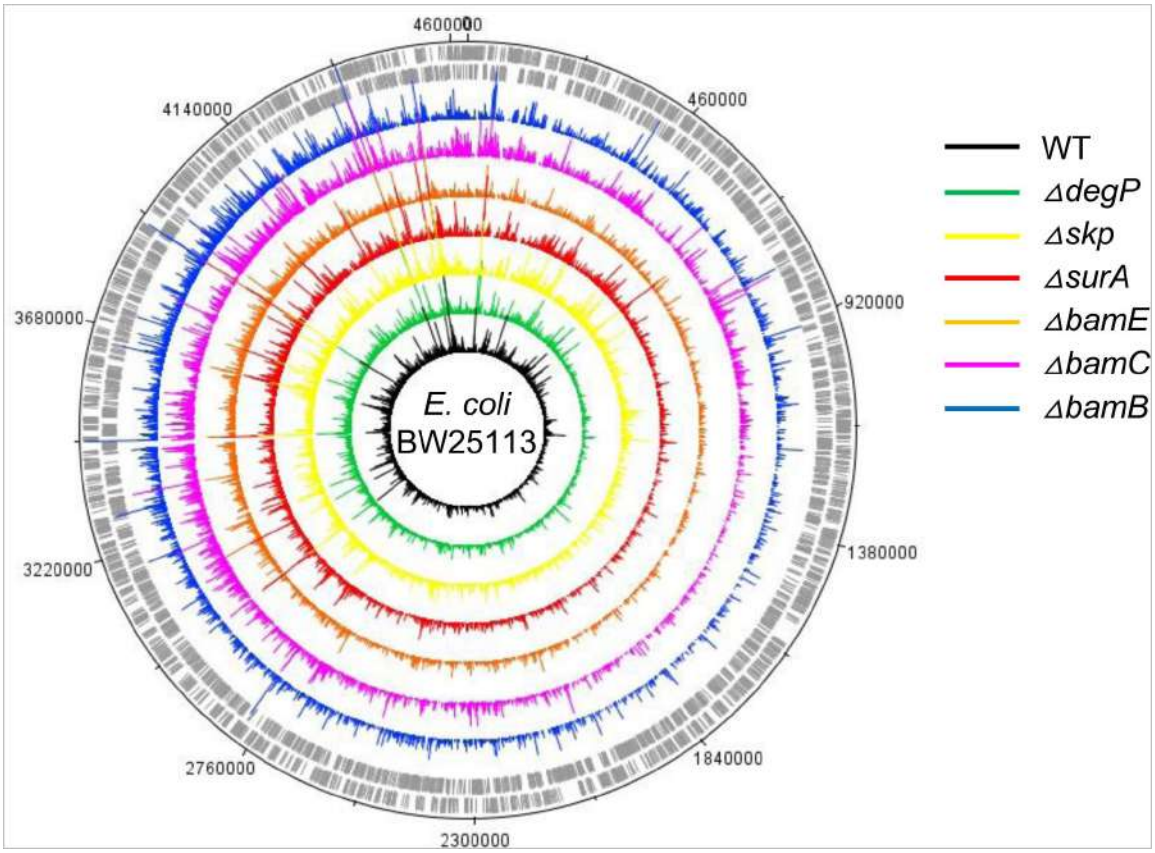

Figure S4

Circular plots of transposon insertion density in TraDIS libraries.

Circular plot of transposon insertion sites in the parent BW25113 (WT), Δ*degP,* Δ*skp,* Δ*surA,* Δ*bamE*, Δ*bamC*, Δ*bamB* TraDIS libraries, listed from innermost tracks outwards, generated using DNAPlotter. The outermost track marks the BW25113 genome in base pairs with the inner grey bar tracks corresponding to sense and antisense CDS.

Figure S5

Examples of known synthetic lethal interactions

Transposon insertions in the genes *degP*, *skp*, *bamB* or *bamE* in the WT parent strain, Δ*bamB*, or Δ*surA* mutant TraDIS libraries. Conditionally-essential genes are represented as red arrows, non-essential genes are represented by grey arrows. Transposon cut-off is set to 50.

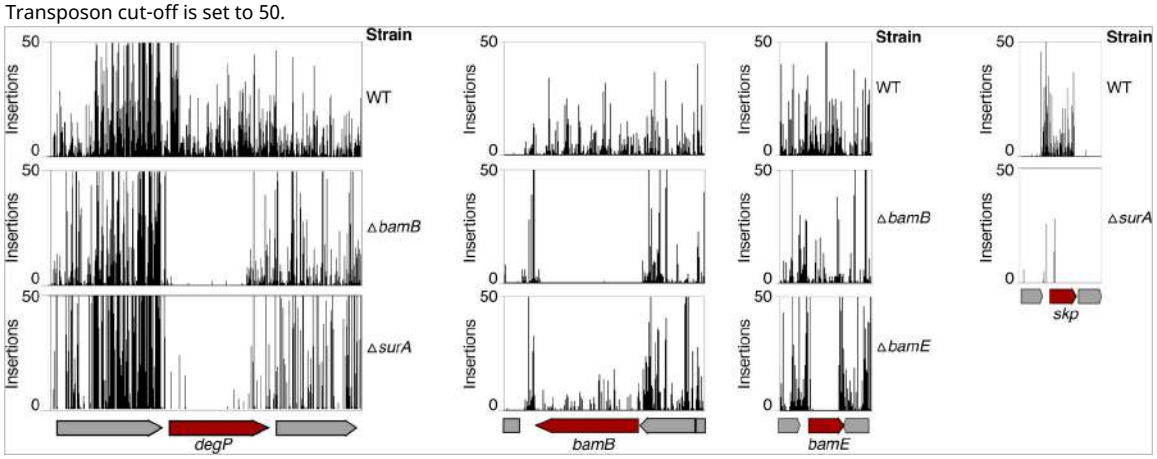

Figure S6

Transposon insertions in genes required for heptose biosynthesis in the Δ*bamC,* Δ*bamE* and Δ*skp* TraDIS libraries

Transposon insertions in the genes *gmhA*, *gmhB*, *hldE, waaD, waaC,* and *waaF* in the parent, Δ*bamC,* Δ*bamE* and Δ*skp* TraDIS libraries. Transposon cut-off is set to 20. Essential genes are represented as red arrows and non-essential genes are represented by grey arrows.

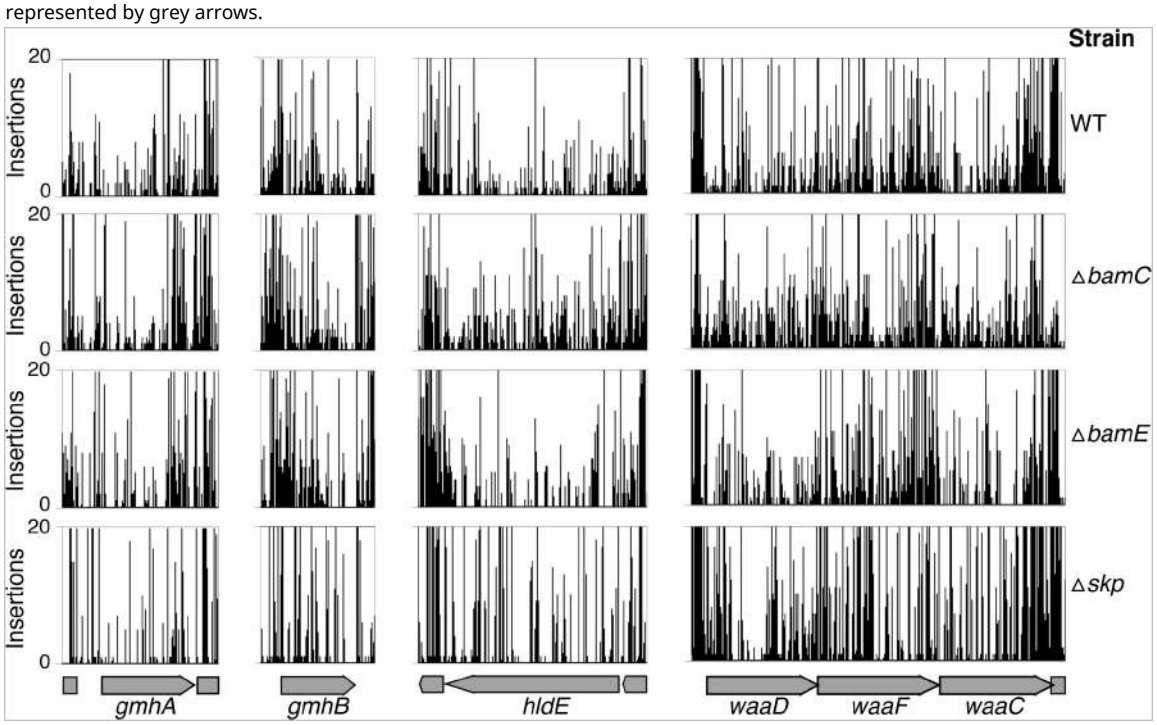

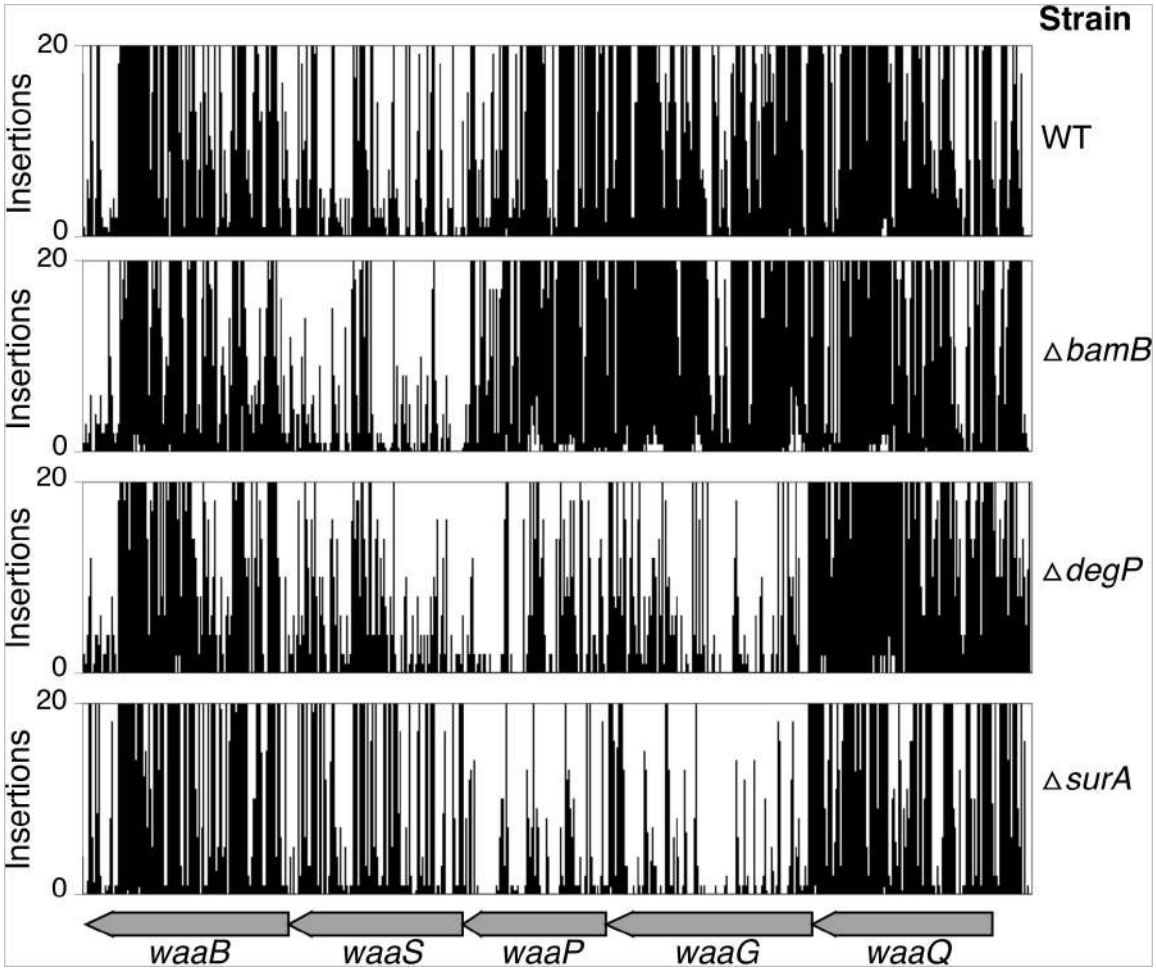

Figure S7

Transposon insertions in the *waaG* and *waaP* genes in the WT, Δ*bamB,* Δ*degP* and Δ*surA* TraDIS libraries

Transposon insertions in the genes *waaB, waaS, waaP, waaG* and *waaQ* in the parent, Δ*bamB,* Δ*degP* and Δ*surA* TraDIS libraries. Transposon cut-off is set to 20. Genes are represented by grey arrows.

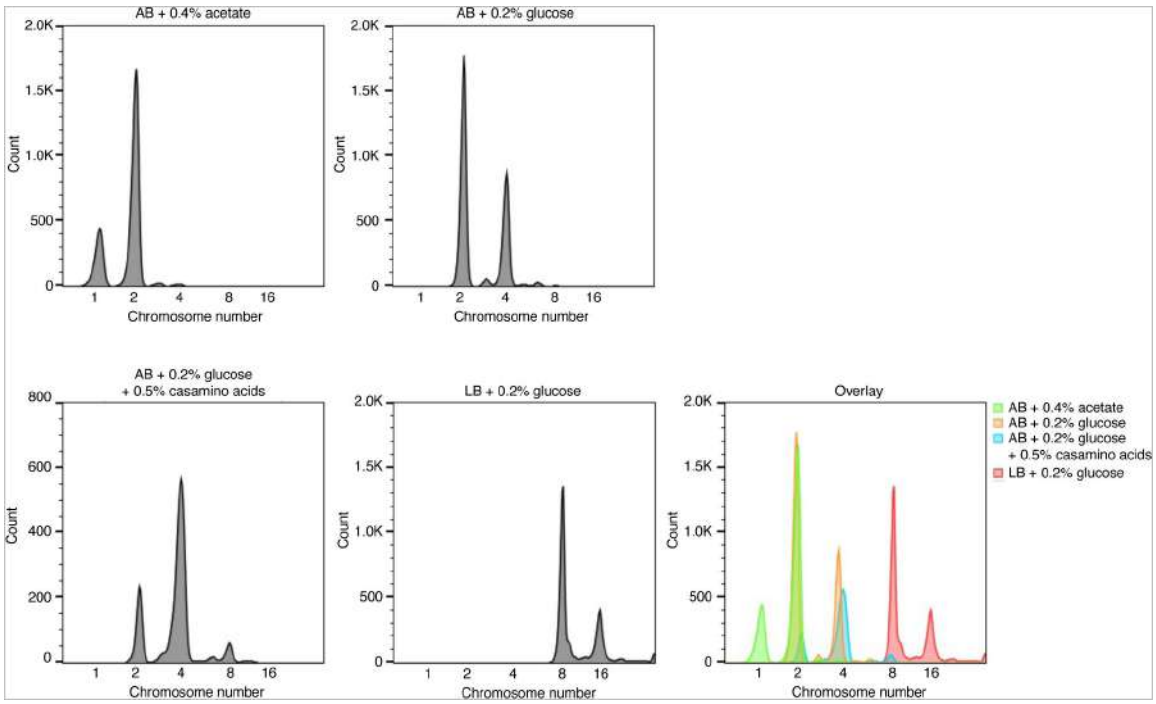

Figure S8

Replication run-out assay standards

Flow cytometry of *E. coli* MG1655 cells grown in media supporting different growth rates followed by replication run-out assay. Cells were grown in AB minimal medium supplemented with either 0.4% acetate, 0.2% glucose, or 0.2% glucose + 0.5% casamino acids, or LB supplemented 0.2% glucose at 37°C with aeration before being treated with rifampicin, cephalexin and stained with Sytox Green. Fluorescence is plotted and represents chromosomal content for each cell with chromosome numbers for each peak marked. An overlay of the separate data panels is presented.

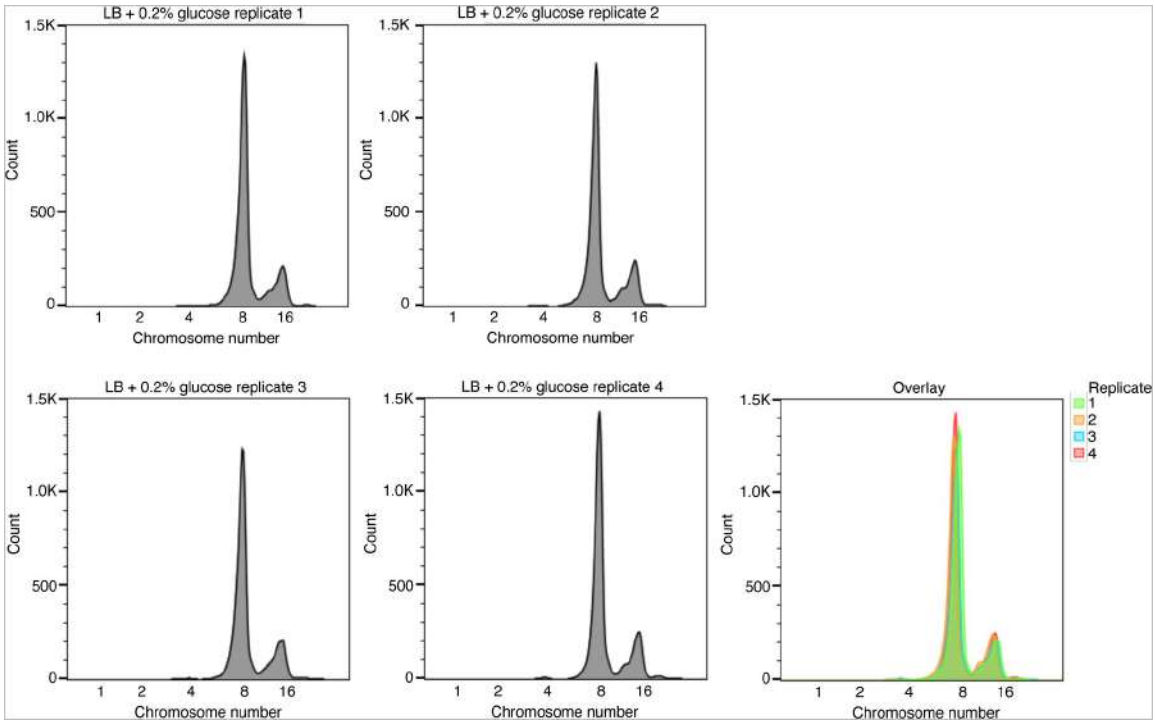

Figure S9

Reproducibility of replication run-out assays for the parent strain

Flow cytometry of *E. coli* LCE-18 cells grown in LB supplemented with 0.2% glucose at 37°C with aeration before being treated with rifampicin, cephalexin and stained with Sytox Green. Fluorescence is plotted and represents chromosomal content for each cell with chromosome numbers for each peak marked. Each experiment was repeated on 4 separate occasions and an overlay of the separate data panels is presented.

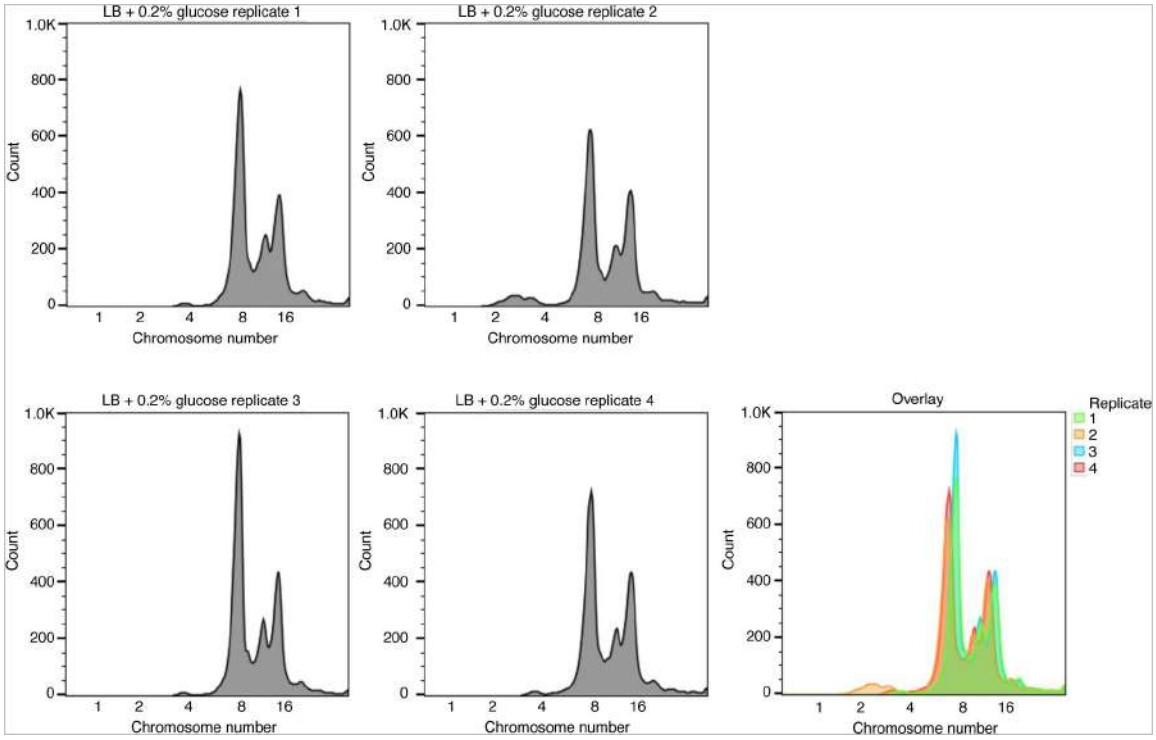

Figure S10

Reproducibility of replication run-out assays for the Δ*bamB* strain

Flow cytometry of *E. coli* LCE-18 Δ*bamB* cells grown in LB supplemented with 0.2% glucose at 37°C with aeration before being treated with rifampicin, cephalexin and stained with Sytox Green. Fluorescence is plotted and represents chromosomal content for each cell with chromosome numbers for each peak marked. Each experiment was repeated on 4 separate occasions and an overlay of the separate data panels is presented.

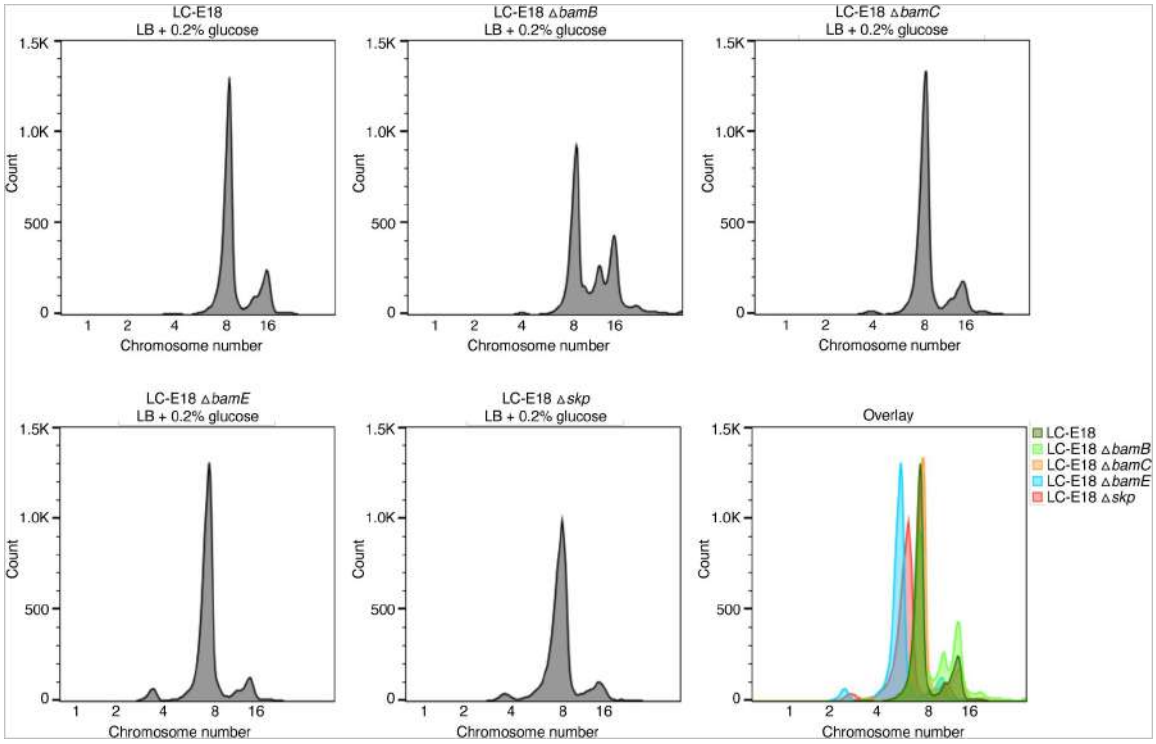

Figure S11

Replication run-out assays for the parent, Δ*bamB,* Δ*bamC,* Δ*bamE* and Δ*skp* strains

Flow cytometry of *E. coli* LCE-18 WT parent, Δ*bamB,* Δ*bamC,* Δ*bamE* or Δ*skp* cells grown in LB supplemented with 0.2% glucose at 37°C with aeration before being treated with rifampicin, cephalexin and stained with Sytox Green. Fluorescence is plotted and represents chromosomal content for each cell with chromosome numbers for each peak marked. An overlay of the separate data panels is presented.

References

1. Konovalova A, Kahne DE, Silhavy TJ (2017) **Outer Membrane Biogenesis** *Annu Rev Microbiol* **71**:539–56 https://doi.org/10.1146/annurev-micro-090816-093754

2. Rollauer SE, Sooreshjani MA, Noinaj N, Buchanan SK (2015) **Outer membrane protein biogenesis in Gram-negative bacteria** *Philos Trans R Soc Lond B Biol Sci* **370** https://doi.org/10.1098/rstb.2015.0023

3. Ruiz N, Kahne D, Silhavy TJ (2006) **Advances in understanding bacterial outer-membrane biogenesis** *Nat Rev Microbiol* **4**:57–66 https://doi.org/10.1038/nrmicro1322

4. Rizzitello AE, Harper JR, Silhavy TJ (2001) **Genetic evidence for parallel pathways of chaperone activity in the periplasm of Escherichia coli** *J Bacteriol* **183**:6794–800 https://doi.org/10.1128/jb.183.23.6794-6800.2001

5. Sklar JG, Wu T, Kahne D, Silhavy TJ (2007) **Defining the roles of the periplasmic chaperones SurA, Skp, and DegP in Escherichia coli** *Genes Dev* **21**:2473–84 https://doi.org/10.1101/gad.1581007

6. Li G, He C, Bu P, Bi H, Pan S, Sun R, et al. (2018) **Single-Molecule Detection Reveals Different Roles of Skp and SurA as Chaperones** *ACS Chem Biol* **13**:1082–9 https://doi.org/10.1021/acschembio.8b00097

7. Wang X, Peterson JH, Bernstein HD (2021) **Bacterial Outer Membrane Proteins Are Targeted to the Bam Complex by Two Parallel Mechanisms** *mBio* **12** https://doi.org/10.1128/mBio.00597-21

8. Combs AN, Silhavy TJ (2022) **The sacrificial adaptor protein Skp functions to remove stalled substrates from the β-barrel assembly machine** *Proc Natl Acad Sci U S A* **119** https://doi.org/10.1073/pnas.2114997119

9. Wu T, Malinverni J, Ruiz N, Kim S, Silhavy TJ, Kahne D (2005) **Identification of a multicomponent complex required for outer membrane biogenesis in Escherichia coli** *Cell* **121**:235–45 https://doi.org/10.1016/j.cell.2005.02.015

10. Hagan CL, Kim S, Kahne D (2010) **Reconstitution of outer membrane protein assembly from purified components** *Science* **328**:890–2 https://doi.org/10.1126/science.1188919

11. Sánchez-Pulido L, Devos D, Genevrois S, Vicente M, Valencia A (2003) **POTRA: a conserved domain in the FtsQ family and a class of beta-barrel outer membrane proteins** *Trends in biochemical sciences* **28**:523–6 https://doi.org/10.1016/j.tibs.2003.08.003

12. Gentle IE, Burri L, Lithgow T (2005) **Molecular architecture and function of the Omp85 family of proteins** *Mol Microbiol* **58**:1216–25 https://doi.org/10.1111/j.1365-2958.2005.04906.x

13. Knowles TJ, Jeeves M, Bobat S, Dancea F, McClelland D, Palmer T, et al. (2008) **Fold and function of polypeptide transport-associated domains responsible for delivering unfolded proteins to membranes** *Mol Microbiol* **68**:1216–27 https://doi.org/10.1111/j.1365-2958.2008.06225.x

14. Dong C, Hou HF, Yang X, Shen YQ, Dong YH (2012) **Structure of Escherichia coli BamD and its functional implications in outer membrane protein assembly** *Acta Crystallogr D Biol Crystallogr* **68**:95–101 https://doi.org/10.1107/s0907444911051031

15. Sandoval CM, Baker SL, Jansen K, Metzner SI, Sousa MC (2011) **Crystal structure of BamD: an essential component of the β-Barrel assembly machinery of gram-negative bacteria** *J Mol Biol* **409**:348–57 https://doi.org/10.1016/j.jmb.2011.03.035

16. Iadanza MG, Higgins AJ, Schiffrin B, Calabrese AN, Brockwell DJ, Ashcroft AE, et al. (2016) **Lateral opening in the intact beta-barrel assembly machinery captured by cryo-EM** *Nat Commun* **7**:12865 https://doi.org/10.1038/ncomms12865

17. Bakelar J, Buchanan SK, Noinaj N (2016) **The structure of the beta-barrel assembly machinery complex** *Science* **351**:180–6 https://doi.org/10.1126/science.aad3460

18. Gu Y, Li H, Dong H, Zeng Y, Zhang Z, Paterson NG, et al. (2016) **Structural basis of outer membrane protein insertion by the BAM complex** *Nature* **531**:64–9 https://doi.org/10.1038/nature17199

19. Browning DF, Bavro VN, Mason JL, Sevastsyanovich YR, Rossiter AE, Jeeves M, et al. (2015) **Cross-species chimeras reveal BamA POTRA and β-barrel domains must be fine-tuned for efficient OMP insertion** *Mol Microbiol* **97**:646–59 https://doi.org/10.1111/mmi.13052

20. Knowles TJ, Browning DF, Jeeves M, Maderbocus R, Rajesh S, Sridhar P, et al. (2011) **Structure and function of BamE within the outer membrane and the beta-barrel assembly machine** *EMBO Rep* **12**:123–8 https://doi.org/10.1038/embor.2010.202

21. Hart EM, Silhavy TJ (2020) **Functions of the BamBCDE Lipoproteins Revealed by Bypass Mutations in BamA** *J Bacteriol* **202** https://doi.org/10.1128/jb.00401-20

22. Konovalova A, Mitchell AM, Silhavy TJ (2016) **A lipoprotein/beta-barrel complex monitors lipopolysaccharide integrity transducing information across the outer membrane** *Elife* **5** https://doi.org/10.7554/eLife.15276

23. Tata M, Konovalova A (2019) **Improper Coordination of BamA and BamD Results in Bam Complex Jamming by a Lipoprotein Substrate** *mBio* **10** https://doi.org/10.1128/mBio.00660-19

24. Kumar S, Konovalova A (2023) **BamE directly interacts with BamA and BamD coordinating their functions** *Mol Microbiol* **120**:397–407 https://doi.org/10.1111/mmi.15127

25. Hart EM, Gupta M, Wühr M, Silhavy TJ (2019) **The Synthetic Phenotype of ΔbamB ΔbamE Double Mutants Results from a Lethal Jamming of the Bam Complex by the Lipoprotein RcsF** *mBio* **10** https://doi.org/10.1128/mBio.00662-19

26. Charlson ES, Werner JN, Misra R (2006) **Differential effects of yfgL mutation on Escherichia coli outer membrane proteins and lipopolysaccharide** *J Bacteriol* **188**:7186–94 https://doi.org/10.1128/jb.00571-06

27. Kritikos G, Banzhaf M, Herrera-Dominguez L, Koumoutsi A, Wartel M, Zietek M, et al. (2017) **A tool named Iris for versatile high-throughput phenotyping in microorganisms** *Nature microbiology* **2**:17014 https://doi.org/10.1038/nmicrobiol.2017.14

28. Doherty HM, Kritikos G, Galardini M, Banzhaf M, Moradigaravand D (2023) **ChemGAPP: a tool for chemical genomics analysis and phenotypic profiling** *Bioinformatics* **39** https://doi.org/10.1093/bioinformatics/btad171

29. Spiess C, Beil A, Ehrmann M (1999) **A temperature-dependent switch from chaperone to protease in a widely conserved heat shock protein** *Cell* **97**:339–47 https://doi.org/10.1016/s0092-8674(00)80743-6

30. Langridge GC, Phan MD, Turner DJ, Perkins TT, Parts L, Haase J, et al. (2009) **Simultaneous assay of every Salmonella Typhi gene using one million transposon mutants** *Genome Res* **19**:2308–16 https://doi.org/10.1101/gr.097097.109

31. Cain AK, Barquist L, Goodman AL, Paulsen IT, Parkhill J, van Opijnen T (2020) **A decade of advances in transposon-insertion sequencing** *Nat Rev Genet* **21**:526–40 https://doi.org/10.1038/s41576-020-0244-x

32. Goodall ECA, Isom GL, Rooke JL, Pullela K, Icke C, Yang Z, et al. (2021) **Loss of YhcB results in dysregulation of coordinated peptidoglycan, LPS and phospholipid synthesis during Escherichia coli cell growth** *PLoS Genet* **17**:e1009586 https://doi.org/10.1371/journal.pgen.1009586

33. Winkle M, Hernández-Rocamora VM, Pullela K, Goodall ECA, Martorana AM, Gray J, et al. (2021) **DpaA Detaches Braun's Lipoprotein from Peptidoglycan** *mBio* **12** https://doi.org/10.1128/mBio.00836-21

34. Barquist L, Mayho M, Cummins C, Cain AK, Boinett CJ, Page AJ, et al. (2016) **The TraDIS toolkit: sequencing and analysis for dense transposon mutant libraries** *Bioinformatics* **32**:1109–11 https://doi.org/10.1093/bioinformatics/btw022

35. Cooper S, Helmstetter CE (1968) **Chromosome replication and the division cycle of Escherichia coli B/r** *J Mol Biol* **31**:519–40

36. Sklar JG, Wu T, Gronenberg LS, Malinverni JC, Kahne D, Silhavy TJ (2007) **Lipoprotein SmpA is a component of the YaeT complex that assembles outer membrane proteins in Escherichia coli** *Proc Natl Acad Sci U S A* **104**:6400–5 https://doi.org/10.1073/pnas.0701579104

37. Kneidinger B, Marolda C, Graninger M, Zamyatina A, McArthur F, Kosma P, et al. (2002) **Biosynthesis pathway of ADP-l-glycero-β-d-manno-heptose in Escherichia coli** *J Bacteriol* **184**:363–9

38. Gronow S, Brabetz W, Brade H (2000) **Comparative functional characterization in vitro of heptosyltransferase I (WaaC) and II (WaaF) from Escherichia coli** *Eur J Biochem* **267**:6602–11 https://doi.org/10.1046/j.1432-1327.2000.01754.x

39. Kadrmas JL, Raetz CR (1998) **Enzymatic synthesis of lipopolysaccharide in Escherichia coli. Purification and properties of heptosyltransferase i** *J Biol Chem* **273**:2799–807 https://doi.org/10.1074/jbc.273.5.2799

40. Storek KM, Vij R, Sun D, Smith PA, Koerber JT, Rutherford ST (2019) **The Escherichia coli β-Barrel Assembly Machinery Is Sensitized to Perturbations under High Membrane Fluidity** *J Bacteriol* **201** https://doi.org/10.1128/jb.00517-18

41. Yethon JA, Heinrichs DE, Monteiro MA, Perry MB, Whitfield C (1998) **Involvement of waaY, waaQ, and waaP in the modification of Escherichia coli lipopolysaccharide and their role**

in the formation of a stable outer membrane *J Biol Chem* **273**:26310–6 https://doi.org/10.1074/jbc.273.41.26310

42. Parker CT, Kloser AW, Schnaitman CA, Stein MA, Gottesman S, Gibson BW (1992) **Role of the rfaG and rfaP genes in determining the lipopolysaccharide core structure and cell surface properties of Escherichia coli K-12** *J Bacteriol* **174**:2525–38 https://doi.org/10.1128/jb.174.8.2525-2538.1992

43. Kumar GS, Jagannadham MV, Ray MK (2002) **Low-temperature-induced changes in composition and fluidity of lipopolysaccharides in the antarctic psychrotrophic bacterium Pseudomonas syringae** *J Bacteriol* **184**:6746–9 https://doi.org/10.1128/jb.184.23.6746-6749.2002

44. Storek KM, Auerbach MR, Shi H, Garcia NK, Sun D, Nickerson NN, et al. (2018) **Monoclonal antibody targeting the β-barrel assembly machine of Escherichia coli is bactericidal** *Proc Natl Acad Sci U S A* **115**:3692–7 https://doi.org/10.1073/pnas.1800043115

45. Kuhn HM, Meier-Dieter U, Mayer H (1988) **ECA, the enterobacterial common antigen** *FEMS Microbiol Rev* **4**:195–222 https://doi.org/10.1111/j.1574-6968.1988.tb02743.x

46. Kunin CM (1963) **SEPARATION, CHARACTERIZATION, AND BIOLOGICAL SIGNIFICANCE OF A COMMON ANTIGEN IN ENTEROBACTERIACEAE** *J Exp Med* **118**:565–86 https://doi.org/10.1084/jem.118.4.565

47. Sivaraman J, Sauvé V, Matte A, Cygler M (2002) **Crystal structure of Escherichia coli glucose-1-phosphate thymidylyltransferase (RffH) complexed with dTTP and Mg2+** *J Biol Chem* **277**:44214–9 https://doi.org/10.1074/jbc.M206932200

48. Marolda CL, Valvano MA (1995) **Genetic analysis of the dTDP-rhamnose biosynthesis region of the Escherichia coli VW187 (O7:K1) rfb gene cluster: identification of functional homologs of rfbB and rfbA in the rff cluster and correct location of the rffE gene** *J Bacteriol* **177**:5539–46 https://doi.org/10.1128/jb.177.19.5539-5546.1995

49. Rai AK, Mitchell AM (2020) **Enterobacterial Common Antigen: Synthesis and Function of an Enigmatic Molecule** *mBio* **11** https://doi.org/10.1128/mBio.01914-20

50. Rai AK, Carr JF, Bautista DE, Wang W, Mitchell AM (2021) **ElyC and Cyclic Enterobacterial Common Antigen Regulate Synthesis of Phosphoglyceride-Linked Enterobacterial Common Antigen** *mBio* **12**:e0284621 https://doi.org/10.1128/mBio.02846-21

51. Schmidt G, Mannel D, Mayer H, Whang HY, Neter E (1976) **Role of a lipopolysaccharide gene for immunogenicity of the enterobacterial common antigen** *J Bacteriol* **126**:579–86 https://doi.org/10.1128/jb.126.2.579-586.1976

52. Kuhn HM, Neter E, Mayer H (1983) **Modification of the lipid moiety of the enterobacterial common antigen by the "Pseudomonas factor"** *Infection and immunity* **40**:696–700 https://doi.org/10.1128/iai.40.2.696-700.1983

53. Morris KN, Mitchell AM (2023) **Phosphatidylglycerol Is the Lipid Donor for Synthesis of Phospholipid-Linked Enterobacterial Common Antigen** *J Bacteriol* :e0040322 https://doi.org/10.1128/jb.00403-22

54. Rowlett VW, Mallampalli V, Karlstaedt A, Dowhan W, Taegtmeyer H, Margolin W, et al. (2017) **Impact of Membrane Phospholipid Alterations in Escherichia coli on Cellular Function**

and Bacterial Stress Adaptation *J Bacteriol* **199** https://doi.org/10.1128/jb.00849-16

55. Kikuchi S, Shibuya I, Matsumoto K (2000) **Viability of an Escherichia coli pgsA null mutant lacking detectable phosphatidylglycerol and cardiolipin** *J Bacteriol* **182**:371–6 https://doi.org/10.1128/jb.182.2.371-376.2000

56. Suzuki M, Hara H, Matsumoto K (2002) **Envelope disorder of Escherichia coli cells lacking phosphatidylglycerol** *J Bacteriol* **184**:5418–25 https://doi.org/10.1128/jb.184.19.5418-5425.2002

57. Mitchell AM, Srikumar T, Silhavy TJ (2018) **Cyclic Enterobacterial Common Antigen Maintains the Outer Membrane Permeability Barrier of Escherichia coli in a Manner Controlled by YhdP** *mBio* **9** https://doi.org/10.1128/mBio.01321-18

58. Kajimura J, Rahman A, Rick PD (2005) **Assembly of cyclic enterobacterial common antigen in Escherichia coli K-12** *J Bacteriol* **187**:6917–27 https://doi.org/10.1128/jb.187.20.6917-6927.2005

59. Richaud C, Higgins W, Mengin-Lecreulx D, Stragier P (1987) **Molecular cloning, characterization, and chromosomal localization of dapF, the Escherichia coli gene for diaminopimelate epimerase** *J Bacteriol* **169**:1454–9 https://doi.org/10.1128/jb.169.4.1454-1459.1987

60. Dewey DL, Work E (1952) **Diaminopimelic acid decarboxylase** *Nature* **169**:533–4 https://doi.org/10.1038/169533a0

61. Mickiewicz KM, Kawai Y, Drage L, Gomes MC, Davison F, Pickard R, et al. (2019) **Possible role of L-form switching in recurrent urinary tract infection** *Nat Commun* **10**:4379 https://doi.org/10.1038/s41467-019-12359-3

62. Mengin-Lecreulx D, Michaud C, Richaud C, Blanot D, van Heijenoort J (1988) **Incorporation of LL-diaminopimelic acid into peptidoglycan of Escherichia coli mutants lacking diaminopimelate epimerase encoded by dapF** *J Bacteriol* **170**:2031–9 https://doi.org/10.1128/jb.170.5.2031-2039.1988

63. Jameson KH, Wilkinson AJ (2017) **Control of initiation of DNA replication in Bacillus subtilis and Escherichia coli** *Genes* **8**:22

64. Lu M, Campbell JL, Boye E, Kleckner N (1994) **SeqA: a negative modulator of replication initiation in E. coli** *Cell* **77**:413–26 https://doi.org/10.1016/0092-8674(94)90156-2

65. Torheim NK, Skarstad K (1999) **Escherichia coli SeqA protein affects DNA topology and inhibits open complex formation at oriC** *Embo j* **18**:4882–8 https://doi.org/10.1093/emboj/18.17.4882

66. von Freiesleben U, Rasmussen KV, Schaechter M (1994) **SeqA limits DnaA activity in replication from oriC in Escherichia coli** *Mol Microbiol* **14**:763–72

67. Kato J, Katayama T (2001) **Hda, a novel DnaA-related protein, regulates the replication cycle in Escherichia coli** *Embo j* **20**:4253–62 https://doi.org/10.1093/emboj/20.15.4253

68. Katayama T, Kubota T, Kurokawa K, Crooke E, Sekimizu K (1998) **The initiator function of DnaA protein is negatively regulated by the sliding clamp of the E. coli chromosomal replicase** *Cell* **94**:61–71 https://doi.org/10.1016/s0092-8674(00)81222-2

69. Ishida T, Akimitsu N, Kashioka T, Hatano M, Kubota T, Ogata Y, et al. (2004) **DiaA, a novel DnaA-binding protein, ensures the timely initiation of Escherichia coli chromosome replication** *Journal of Biological Chemistry* **279**:45546–55

70. Keyamura K, Fujikawa N, Ishida T, Ozaki S, Su'etsugu M, Fujimitsu K, et al. (2007) **The interaction of DiaA and DnaA regulates the replication cycle in E. coli by directly promoting ATP–DnaA-specific initiation complexes** *Genes & development* **21**:2083–99

71. Hawkins M, Atkinson J, McGlynn P (2016) **Escherichia coli Chromosome Copy Number Measurement Using Flow Cytometry Analysis** *Methods Mol Biol* **1431**:151–9 https://doi.org/10.1007/978-1-4939-3631-1_12

72. Webb CT, Heinz E, Lithgow T (2012) **Evolution of the β-barrel assembly machinery** *Trends in microbiology* **20**:612–20 https://doi.org/10.1016/j.tim.2012.08.006

73. Teufel F, Almagro Armenteros JJ, Johansen AR, Gíslason MH, Pihl SI, Tsirigos KD, et al. (2022) **SignalP 6.0 predicts all five types of signal peptides using protein language models** *Nat Biotechnol* **40**:1023–5 https://doi.org/10.1038/s41587-021-01156-3

74. Malinverni JC, Silhavy TJ (2011) **Assembly of Outer Membrane β-Barrel Proteins: the Bam Complex** *EcoSal Plus* **4** https://doi.org/10.1128/ecosalplus.4.3.8

75. Webb CT, Chandrapala D, Oslan SN, Bamert RS, Grinter RD, Dunstan RA, et al. (2017) **Reductive evolution in outer membrane protein biogenesis has not compromised cell surface complexity in Helicobacter pylori** *Microbiologyopen* **6** https://doi.org/10.1002/mbo3.513

76. Letunic I, Bork P (2021) **Interactive Tree Of Life (iTOL) v5: an online tool for phylogenetic tree display and annotation** *Nucleic Acids Res* **49**:W293–w6 https://doi.org/10.1093/nar/gkab301

77. Steenhuis M, van Ulsen P, Martin NI, Luirink J (2021) **A ban on BAM: an update on inhibitors of the β-barrel assembly machinery** *FEMS Microbiol Lett* **368** https://doi.org/10.1093/femsle/fnab059

78. Theuretzbacher U, Blasco B, Duffey M, Piddock LJV (2023) **Unrealized targets in the discovery of antibiotics for Gram-negative bacterial infections** *Nat Rev Drug Discov* **22**:957–75 https://doi.org/10.1038/s41573-023-00791-6

79. Tomasek D, Rawson S, Lee J, Wzorek JS, Harrison SC, Li Z, et al. (2020) **Structure of a nascent membrane protein as it folds on the BAM complex** *Nature* **583**:473 https://doi.org/10.1038/s41586-020-2370-1

80. Doyle MT, Jimah JR, Dowdy T, Ohlemacher SI, Larion M, Hinshaw JE, et al. (2022) **Cryo-EM structures reveal multiple stages of bacterial outer membrane protein folding** *Cell* **185**:1143–56 https://doi.org/10.1016/j.cell.2022.02.016

81. Valvano MA (2022) **Remodelling of the Gram-negative bacterial Kdo(2)-lipid A and its functional implications** *Microbiology (Reading* **168** https://doi.org/10.1099/mic.0.001159

82. Simpson BW, Trent MS (2019) **Pushing the envelope: LPS modifications and their consequences** *Nat Rev Microbiol* **17**:403–16 https://doi.org/10.1038/s41579-019-0201-x

83. Krojer T, Sawa J, Schäfer E, Saibil HR, Ehrmann M, Clausen T (2008) **Structural basis for the regulated protease and chaperone function of DegP** *Nature* **453**:885–90 https://doi.org/10.1038/nature07004

84. Rouvière PE, Gross CA (1996) **SurA, a periplasmic protein with peptidyl-prolyl isomerase activity, participates in the assembly of outer membrane porins** *Genes Dev* **10**:3170–82 https://doi.org/10.1101/gad.10.24.3170

85. Lazar SW, Kolter R (1996) **SurA assists the folding of Escherichia coli outer membrane proteins** *J Bacteriol* **178**:1770–3 https://doi.org/10.1128/jb.178.6.1770-1773.1996

86. Jorgenson MA, Kannan S, Laubacher ME, Young KD (2016) **Dead-end intermediates in the enterobacterial common antigen pathway induce morphological defects in Escherichia coli by competing for undecaprenyl phosphate** *Mol Microbiol* **100**:1–14 https://doi.org/10.1111/mmi.13284

87. Rojas ER, Billings G, Odermatt PD, Auer GK, Zhu L, Miguel A, et al. (2018) **The outer membrane is an essential load-bearing element in Gram-negative bacteria** *Nature* **559**:617–21 https://doi.org/10.1038/s41586-018-0344-3

88. Nichols RJ, Sen S, Choo YJ, Beltrao P, Zietek M, Chaba R, et al. (2011) **Phenotypic landscape of a bacterial cell** *Cell* **144**:143–56 https://doi.org/10.1016/j.cell.2010.11.052

89. Thewasano N, Germany EM, Maruno Y, Nakajima Y, Shiota T (2023) **Categorization of Escherichia coli Outer Membrane Proteins by Dependence on Accessory Proteins of the β-barrel Assembly Machinery Complex** *Journal of Biological Chemistry* https://doi.org/10.1016/j.jbc.2023.104821

90. Mamou G, Corona F, Cohen-Khait R, Housden NG, Yeung V, Sun D, et al. (2022) **Peptidoglycan maturation controls outer membrane protein assembly** *Nature* **606**:953–9 https://doi.org/10.1038/s41586-022-04834-7

91. Wallden M, Fange D, Lundius EG, Baltekin Ö, Elf J (2016) **The Synchronization of Replication and Division Cycles in Individual E. coli Cells** *Cell* **166**:729–39 https://doi.org/10.1016/j.cell.2016.06.052

92. Si F, Li D, Cox SE, Sauls JT, Azizi O, Sou C, et al. (2017) **Invariance of Initiation Mass and Predictability of Cell Size in Escherichia coli** *Curr Biol* **27**:1278–87 https://doi.org/10.1016/j.cub.2017.03.022

93. Harris LK, Theriot JA (2016) **Relative Rates of Surface and Volume Synthesis Set Bacterial Cell Size** *Cell* **165**:1479–92 https://doi.org/10.1016/j.cell.2016.05.045

94. Davies BW, Kohanski MA, Simmons LA, Winkler JA, Collins JJ, Walker GC (2009) **Hydroxyurea induces hydroxyl radical-mediated cell death in Escherichia coli** *Mol Cell* **36**:845–60 https://doi.org/10.1016/j.molcel.2009.11.024

95. Nakayashiki T, Mori H (2013) **Genome-wide screening with hydroxyurea reveals a link between nonessential ribosomal proteins and reactive oxygen species production** *J Bacteriol* **195**:1226–35 https://doi.org/10.1128/jb.02145-12

96. Sutera VA, Lovett ST (2006) **The role of replication initiation control in promoting survival of replication fork damage** *Mol Microbiol* **60**:229–39 https://doi.org/10.1111/j.1365-2958.2006.05093.x

97. Camara JE, Breier AM, Brendler T, Austin S, Cozzarelli NR, Crooke E (2005) **Hda inactivation of DnaA is the predominant mechanism preventing hyperinitiation of Escherichia coli DNA replication** *EMBO Rep* **6**:736–41 https://doi.org/10.1038/sj.embor.7400467

98. Camara JE, Skarstad K, Crooke E (2003) **Controlled initiation of chromosomal replication in Escherichia coli requires functional Hda protein** *J Bacteriol* **185**:3244–8 https://doi.org/10.1128/jb.185.10.3244-3248.2003

99. Cooper DL, Harada T, Tamazi S, Ferrazzoli AE, Lovett ST (2021) **The Role of Replication Clamp-Loader Protein HolC of Escherichia coli in Overcoming Replication/Transcription Conflicts** *mBio* **12** https://doi.org/10.1128/mBio.00184-21

100. Sekimizu K, Kornberg A (1988) **Cardiolipin activation of dnaA protein, the initiation protein of replication in Escherichia coli** *J Biol Chem* **263**:7131–5

101. Garner J, Durrer P, Kitchen J, Brunner J, Crooke E (1998) **Membrane-mediated release of nucleotide from an initiator of chromosomal replication, Escherichia coli DnaA, occurs with insertion of a distinct region of the protein into the lipid bilayer** *J Biol Chem* **273**:5167–73 https://doi.org/10.1074/jbc.273.9.5167

102. d'Alençon E, Taghbalout A, Kern R, Kohiyama M. (1999) **Replication cycle dependent association of SeqA to the outer membrane fraction of E. coli** *Biochimie* **81**:841–6 https://doi.org/10.1016/s0300-9084(99)00212-6

103. Rotman E, Bratcher P, Kuzminov A (2009) **Reduced lipopolysaccharide phosphorylation in Escherichia coli lowers the elevated ori/ter ratio in seqA mutants** *Mol Microbiol* **72**:1273–92 https://doi.org/10.1111/j.1365-2958.2009.06725.x

104. Bryant JA, Morris FC, Knowles TJ, Maderbocus R, Heinz E, Boelter G, et al. (2020) **Structure of dual BON-domain protein DolP identifies phospholipid binding as a new mechanism for protein localisation** *Elife* **9** https://doi.org/10.7554/eLife.62614

105. Ranava D, Yang Y, Orenday-Tapia L, Rousset F, Turlan C, Morales V, et al. (2021) **Lipoprotein DolP supports proper folding of BamA in the bacterial outer membrane promoting fitness upon envelope stress** *Elife* **10** https://doi.org/10.7554/eLife.67817

106. Baba T, Ara T, Hasegawa M, Takai Y, Okumura Y, Baba M, et al. (2006) **Construction of Escherichia coli K-12 in-frame, single-gene knockout mutants: the Keio collection** *Mol Syst Biol* **2** https://doi.org/10.1038/msb4100050

107. Thomason LC, Costantino N, Court DL (2007) **E. coli genome manipulation by P1 transduction** *Curr Protoc Mol Biol* https://doi.org/10.1002/0471142727.mb0117s79

108. Cherepanov PP, Wackernagel W (1995) **Gene disruption in Escherichia coli: TcR and KmR cassettes with the option of Flp-catalyzed excision of the antibiotic-resistance determinant** *Gene* **158**:9–14

109. Datsenko KA, Wanner BL (2000) **One-step inactivation of chromosomal genes in Escherichia coli K-12 using PCR products** *Proc Natl Acad Sci U S A* **97**:6640–5 https://doi.org/10.1073/pnas.120163297

110. Cui L, Vigouroux A, Rousset F, Varet H, Khanna V, Bikard D (2018) **A CRISPRi screen in E. coli reveals sequence-specific toxicity of dCas9** *Nat Commun* **9**:1912 https://doi.org/10.1038/s41467-018-04209-5

111. Bligh EG, Dyer WJ (1959) **A rapid method of total lipid extraction and purification** *Can J Biochem Physiol* **37**:911–7 https://doi.org/10.1139/o59-099

112. Boelter G, Bryant JA, Doherty H, Wotherspoon P, Alodaini D, Ma X, et al. (2022) **The lipoprotein DolP affects cell separation in Escherichia coli, but not as an upstream regulator of NlpD** *Microbiology (Reading* **168** https://doi.org/10.1099/mic.0.001197

113. Seemann T (2014) **Prokka: rapid prokaryotic genome annotation** *Bioinformatics* **30**:2068–9 https://doi.org/10.1093/bioinformatics/btu153

Author information

Jack A Bryant[†]
Institute of Microbiology and Infection, School of Biosciences, University of Birmingham, Edgbaston, United Kingdom, School of Life Sciences, University of Nottingham, Nottingham, United Kingdom
ORCID iD: 0000-0002-7912-2144

For correspondence: jack.bryant@nottingham.ac.uk
[†]These authors contributed equally.

Kara A Staunton[†]
Institute of Microbiology and Infection, School of Biosciences, University of Birmingham, Edgbaston, United Kingdom

[†]These authors contributed equally.

Hannah M Doherty
Institute of Microbiology and Infection, School of Biosciences, University of Birmingham, Edgbaston, United Kingdom

Micheal B Alao
Institute of Microbiology and Infection, School of Biosciences, University of Birmingham, Edgbaston, United Kingdom

Xuyu Ma
Institute of Microbiology and Infection, School of Biosciences, University of Birmingham, Edgbaston, United Kingdom

Joanna Morcinek-Orłowska
Department of Biology, University of Gdańsk, Gdańsk, Poland

Emily CA Goodall
Institute for Molecular Bioscience, University of Queensland, St. Lucia, Australia

Jessica Gray
Institute for Molecular Bioscience, University of Queensland, St. Lucia, Australia

Mathew Milner
Institute of Microbiology and Infection, School of Biosciences, University of Birmingham, Edgbaston, United Kingdom, Laboratory for Infectious Disease Epidemiology, KAUST Smart-Health Initiative and Biological and Environmental Science and Engineering Division, King Abdullah University of Science and Technology, Makkah, Saudi Arabia, KAUST Computational Bioscience Research Center, King Abdullah University of Science and Technology, Makkah, Saudi Arabia

Jeffrey A Cole
Institute of Microbiology and Infection, School of Biosciences, University of Birmingham, Edgbaston, United Kingdom

Felicity de Cogan
School of Pharmacy, University of Nottingham, Nottingham, United Kingdom

Timothy J Knowles
Institute of Microbiology and Infection, School of Biosciences, University of Birmingham, Edgbaston, United Kingdom

Monika Glinkowska
Department of Biology, University of Gdańsk, Gdańsk, Poland

Danesh Moradigaravand
Laboratory for Infectious Disease Epidemiology, KAUST Smart-Health Initiative and Biological and Environmental Science and Engineering Division, King Abdullah University of Science and Technology, Makkah, Saudi Arabia, KAUST Computational Bioscience Research Center, King Abdullah University of Science and Technology, Makkah, Saudi Arabia
ORCID iD: 0000-0001-6652-5617

For correspondence: danesh.moradigaravand@kaust.edu.sa

Ian R Henderson
Institute for Molecular Bioscience, University of Queensland, St. Lucia, Australia

For correspondence: i.henderson@imb.uq.edu.au

Manuel Banzhaf
Institute of Microbiology and Infection, School of Biosciences, University of Birmingham, Edgbaston, United Kingdom, Newcastle University Biosciences Institute, Faculty of Medical Sciences, Newcastle University, Newcastle upon Tyne, UK

For correspondence: manuel.banzhaf@newcastle.ac.uk

Editors

Reviewing Editor
Ethel Bayer-Santos
The University of Texas at Austin, Austin, United States of America

Senior Editor
David Ron
University of Cambridge, Cambridge, United Kingdom

Reviewer #1 (Public Review):

Summary:

The overall goal of the manuscript is to delineate pathways that are conditionally essential with the Bam complex and associated chaperones. The Bam complex is made of several proteins, including BamA and BamD, which are essential. The protein complex works to insert proteins in the asymmetric outer membrane. Substrates are translated in the cytoplasm prior to transport across the cell envelope to the Bam complex. Transport includes non-essential periplasmic chaperones, SurA, Skp, and DegP. According to the authors, the pathways were assumed to be redundant. The Bam complex also includes non-essential components, BamBCE. These were thought to be accessory components that interact with BamA and BamD to coordinate optimal activity. While some roles have been assigned to BamE and BamB, a detailed understanding of the role of each accessory Bam protein is lacking. In this study, more specific roles for each non-essential Bam component are proposed.

Strengths:

The overall findings are intriguing and could advance our understanding as to how the Gram-negative cell envelope is assembled. These studies could provide new targets for antimicrobial treatment. In general, the manuscript was well-written.

Weaknesses:

While the overall findings are interesting, I had some concerns with the data analysis, presentation, and conclusions. Not all the conclusions are supported by data. The proposed revisions include experimental and editorial work. The manuscript is generally well-written and could provide impactful data to advance the field if the concerns are addressed.

Major concerns:

Overall Comments:

(1) The cutoffs the authors used to define "conditionally essential" mutants are not reported. The results also lack validation for lethality using a titratable system. It would be ideal to validate several genes in each dataset to determine cutoffs (i.e. 5-fold decrease in insertion mutants) for conditional lethality. It was not done (or described) here.

(2) Also, two mutations that both make the cells sick could provide an additive effect (i.e. dapF and BamB), which doesn't necessarily mean the pathways are linked. The authors should revise their wording. They have not shown genetic linkage in some cases.

(3) Mutations throughout the manuscript are not complemented. It would be ideal to add complementation data to show the gene-phenotype relationship is specific.

(4) Also, I would argue the term "conditionally essential genes" should be replaced with "synthetically lethal". Strains were compared in the same conditions but with different genetic backgrounds.

https://doi.org/10.7554/eLife.99955.1.sa2

Reviewer #2 (Public Review):

Summary:
Bryant et al. apply phenotypic profiling and saturating transposon mutagenesis to investigate the role of the non-essential lipoproteins BamB, BamC, and BamE, along with chaperones DegP, Skp, and SurA, in the biogenesis of the bacterial outer membrane. This generated a set of genetic interactions that revealed that changes in LPS and outer membrane fluidity impact Bam activity, and that the cyclic form of enterobacterial common antigen becomes essential in the absence of the chaperone surA. The study also uncovers that peptidoglycan crosslinking and DNA replication control are conditionally essential with the absence of certain Bam components, suggesting a coordination between outer membrane protein (OMP) biogenesis and other cellular processes such as lipid and peptidoglycan synthesis, as well as DNA replication.

Strengths:

(1) This is probably the first comprehensive analysis of genetic interactions involving Bam-associated proteins and should provide rich insight to refine the mechanistic understanding of this complex machine and the process of OM biogenesis.

(2) Good quality data and analysis. Well-presented manuscript.

Weaknesses:

(1) An important control in any genetic interaction study is to do complementation tests to demonstrate that the phenotype observed is indeed due to the missing gene under analysis. Although the Keio library was designed to avoid polar effects, it is impossible to predict other undesirable effects of the deletions (hitting of a non-annotated sRNA or RNA stability effects, for example). Thus, before one can safely conclude that a proposed genetic interaction is real, complementation tests should be carried out. This seems particularly important in the case of a new and surprising interaction, such as that between bamB and DNA replication and repair genes.

(2) Why not include the suppressor interactions in the work? There are probably plenty, and in principle, they should be as informative as the conditional essential (or synthetic lethal) ones. The only one highlighted in the paper is that between bamB and diaA, since it nicely fits with the synthetic lethal effects with initiation inhibitors seqA and hda. Even if the authors cannot make sense of the suppressor interactions, their inclusion in the paper should make the dataset richer and more valuable to the community.

(3) The enrichment analysis in Figure 2B deserves some clarification. What is the meaning of gene ratio? How can single genes of a pathway yield an enrichment signal? Why werenŕ seqA and hda included in the DNA replication class in 2B?

(4) The writing puts too much emphasis on demonstrating that bam lipoproteins and chaperones are specialized instead of fully redundant. However, I have the impression this is

a long-settled conclusion in the field, as the manuscript itself describes at several points when reviewing the literature.

https://doi.org/10.7554/eLife.99955.1.sa1

Reviewer #3 (Public Review):

In this work, Bryant, et al. investigate genetic interactions between non-essential members of the outer membrane protein biogenesis pathway and other genes in the genome using a transposon-directed insertion sequencing (TraDIS) approach in E. coli K-12. The authors identify interactions with other components of the envelope including LPS, peptidoglycan, and enterobacterial common antigen biogenesis, and they tie these interactions to specific members of the outer membrane biogenesis pathway. Although many of these interactions are known and have been previously investigated in the field, the study provides several synthetic phenotypes that could be useful for further investigations.

The strengths of the paper include their unbiased, TraDIS approach, and follow up on the interactions they observe. The interactions with genes of unknown function also are of interest as they may suggest experiments to find the functions of these genes. The largest weakness of this paper is the use of a gene deletion allele for bamB that is known to be polar leading to decreased expression of an essential gene. This largely invalidates all results related to DNA replication. In addition, it is a weakness that the paper does not adequately address its place in the field through discussion of existing results on the interactions they investigate.

https://doi.org/10.7554/eLife.99955.1.sa0

Author response:

We would like to thank the reviewers for their time and for their kind comments about our work. We expect that their comments will help us to improve the manuscript and so will plan the following experiments/revisions to address some of their comments:

> ***Reviewer 1 (Public Review):***
>
> *(1) The cutoffs the authors used to define "conditionally essential" mutants are not reported. The results also lack validation for lethality using a titratable system. It would be ideal to validate several genes in each dataset to determine cutoffs (i.e. 5-fold decrease in insertion mutants) for conditional lethality. It was not done (or described) here.*

We will report the cutoffs used when we generate the revised manuscript. Our experiments identified hundreds of lethal combinations and we have six datasets, validation of several genes from each would require generation of at least 20 depletion strains and subsequent testing of each. Validation using a depletion system would therefore be a significant undertaking and is typically not the standard when using these approaches. However, should time permit then we will attempt a subset of these experiments.

> *(2) Also, two mutations that both make the cells sick could provide an additive effect (i.e. dapF and BamB), which doesn't necessarily mean the pathways are linked. The authors should revise their wording. They have not shown genetic linkage in some cases.*

We will revise the text to address this.

> *(3) Mutations throughout the manuscript are not complemented. It would be ideal to add complementation data to show the gene-phenotype relationship is specific.*

We thank the reviewers for highlighting this and will complete the complementation experiments.

> *(4) Also, I would argue the term "conditionally essential genes" should be replaced with "synthetically lethal". Strains were compared in the same conditions but with different genetic backgrounds.*

We take the reviewers point and will revise the text accordingly.

> ***Reviewer 2 (Public Review):***
>
> *Weaknesses:*
>
> *(1) An important control in any genetic interaction study is to do complementation tests to demonstrate that the phenotype observed is indeed due to the missing gene under analysis. Although the Keio library was designed to avoid polar effects, it is impossible to predict other undesirable effects of the deletions (hitting of a non-annotated sRNA or RNA stability effects, for example). Thus, before one can safely conclude that a proposed genetic interaction is real, complementation tests should be carried out. This seems particularly important in the case of a new and surprising interaction, such as that between bamB and DNA replication and repair genes.*

We thank the reviewers for highlighting this and will complete the complementation experiments.

> *(2) Why not include the suppressor interactions in the work? There are probably plenty, and in principle, they should be as informative as the conditional essential (or synthetic lethal) ones. The only one highlighted in the paper is that between bamB and diaA, since it nicely fits with the synthetic lethal effects with initiation inhibitors seqA and hda. Even if the authors cannot make sense of the suppressor interactions, their inclusion in the paper should make the dataset richer and more valuable to the community.*

These data are available in supplementary table 1. However, we appreciate this is not obvious and so will make a new supplementary table and include a brief description of the data for the revised paper.

> *(3) The enrichment analysis in Figure 2B deserves some clarification. What is the meaning of gene ratio? How can single genes of a pathway yield an enrichment signal? Why weren t seqA and hda included in the DNA replication class in 2B?*

We apologise for the confusion caused and will include a description of the analysis in the methods section.

> *(4) The writing puts too much emphasis on demonstrating that bam lipoproteins and chaperones are specialized instead of fully redundant. However, I have the impression this is a long-settled conclusion in the field, as the manuscript itself describes at several points when reviewing the literature.*

We will revise the text to reduce this emphasis.

> ***Reviewer #3 (Public Review):***
>
> *In this work, Bryant, et al. investigate genetic interactions between non-essential members of the outer membrane protein biogenesis pathway and other genes in the genome using a transposon-directed insertion sequencing (TraDIS) approach in E. coli K-12. The authors identify interactions with other components of the envelope including LPS, peptidoglycan, and enterobacterial common antigen biogenesis, and they tie these interactions to specific members of the outer membrane biogenesis pathway. Although many of these interactions are known and have been previously investigated in the field, the study provides several synthetic phenotypes that could be useful for further investigations.*
>
> *The strengths of the paper include their unbiased, TraDIS approach, and follow up on the interactions they observe. The interactions with genes of unknown function also are of interest as they may suggest experiments to find the functions of these genes. The largest weakness of this paper is the use of a gene deletion allele for bamB that is known to be polar leading to decreased expression of an essential gene. This largely invalidates all results related to DNA replication. In addition, it is a weakness that the paper does not adequately address its place in the field through discussion of existing results on the interactions they investigate.*

We appreciate the reviewers' comments and concerns about the bamB allele, and we will address these concerns by completing complementation experiments for the CRISPRi depletion experiments and the run-out assays. However, despite the statement that it is known to be polar, several previous studies have also used the bamB Keio library strain. Many of these studies transfer the allele to a clean background and use the derivative in which the cassette has been removed as we have done here (Cox et al., 2017, Gunasinghe et al., 2018, Psonis et al., 2019, Storek et al., 2019, Ranava et al. 2021, Steenhuis et al., 2021, Thewasano et al., 2023). Therefore, we feel somewhat justified in our choice of strain.

We are unable to find a reference for the Keio bamB strain causing polar effects and would have appreciated the reviewers' guidance here. However, we believe the concern about polar effects stems from the observations of Ruiz et al., (2005), in which it was observed that a yfgL::ISE1 allele causes polar effects. This was hypothesised to be due to the ORF contained within the IS being transcribed in the opposite orientation to yfgL and the downstream der gene. They subsequently observed that a strain carrying a Tn5KAN-I-SceI insertion in yfgL (yfgL::kan) did not cause polar effects and this was hypothesised to be due to the kan cassette being co-oriented with yfgL. In addition, Charlson et al., 2006 generated a yfgL deletion by replacing the majority of the gene with a kan cassette in a manner similar to that of the Keio library that was subsequently flipped out. This study also found no evidence of polar effects on der. In theory, the strain used here, and in previous studies by other groups, should provide minimal disruption to transcription through generation of a mini-gene from the original bamB sequence to maintain operon expression. This is in contrast to the disruption caused by the yfgL::ISE1 allele.

While we do appreciate the concern, several pieces of evidence lend themselves to counter the statement that our strain choice largely invalidates the results. The der GTPase is essential, hence the concern about polar effects leading to the bamB phenotypes we see. However, depletion of der leads to cold sensitivity, whereas we find that the bamB strain used here actually performs better in colder temperatures. In addition, the der depletion is sensitive to doxycycline, whereas the bamB mutant has increased fitness in this condition (Fig 1) (Bharat and Brown, 2015, Hwang and Inouye, 2008). Hence, should the mutation lead to decreased expression of der then we would expect the bamB strain to phenocopy the der depletion, which it does not. Regardless of this information, we will still address these concerns by completing complementation experiments.

https://doi.org/10.7554/eLife.99955.1.sa4

Wkład autorów – oświadczenia

Uniwersytet Gdański

mgr Joanna Morcinek-Orłowska
Katedra Genetyki Molekularnej Bakterii
Wydział Biologii
Uniwersytet Gdański

Gdańsk, 01.06.2025 r.

Oświadczenie o wkładzie w publikację

Oświadczam, że mój wkład w preprint artykułu oryginalnego:

Bryant JA, Staunton KA, Doherty HM, Alao MB, Ma X, Morcinek-Orłowska J, Goodall ECA, Gray J, Milner M, Cole JA, de Cogan F Knowles TJ, Glinkowska M, Moradigaravand D, Henderson IR, Banzhaf M (2024) Bam complex associated proteins in Escherichia coli are functionally linked to peptidoglycan biosynthesis, membrane fluidity and DNA replication eLife 13:RP99955, https://doi.org/10.7554/eLife.99955.1

polegał na:

- wykonaniu części eksperymentów (ocena ilości chromosomów i czasu inicjacji replikacji w cyklu komórkowym metodą cytometrii przepływowej po zatrzymaniu replikacji).
- analizie i wizualizacji uzyskanych danych eksperymentalnych

Jednocześnie oświadczam, że mój wkład w powyższy artykuł jest znaczący i możliwy do wyodrębnienia.

Joanna Morcinek-Orłowska

Wydział Biologii
Uniwersytetu Gdańskiego
Katedra Genetyki
Molekularnej Bakterii

tel. +48 58 523 60 65
e-mail: mol.KGB@ug.edu.pl

ul. Wita Stwosza 59
80-309 Gdańsk

www.ug.edu.pl

University of Nottingham
UK | CHINA | MALAYSIA

School of Life Sciences
University of Nottingham
University Park
Nottingham
NG7 2RD

+44 (0)115 748 6784
jack.bryant@nottingham.ac.uk

20 June 2025

To whom it may concern,

I am writing to provide an author contribution statement for Joanna Morcinek-Orlowska in regard to our research article (reviewed preprint) outlined below:

Bryant JA, Staunton KA, Doherty HM, Alao MB, Ma X, Morcinek-Orłowska J, Goodall ECA, Gray J, Milner M, Cole JA, de Cogan F Knowles TJ, Glinkowska M, Moradigaravand D, Henderson IR, Banzhaf M (2024) Bam complex associated proteins in Escherichia coli are functionally linked to peptidoglycan biosynthesis, membrane fluidity and DNA replication eLife 13:RP99955, https://doi.org/10.7554/eLife.99955.1

As the first/corresponding author of the manuscript, I hereby confirm that the individual contribution of Joanna Morcinek-Orlowska to this publication is both substantial and clearly identifiable. We identified DNA replication control proteins as being synthetically lethal with the outer membrane protein biogenesis lipoprotein BamB. Joanna used a DNA replication run-out assay to analyse the parent *Escherichia coli* strain, Δ*bamB,* Δ*bamC,* Δ*bamE,* Δ*skp,* Δ*surA* and Δ*degP* strains to identify that the Δ*bamB* mutant over-initiates DNA replication during the cell cycle. This is a key result for the publication and confirmed our hypothesis that outer membrane biogenesis is coordinated with DNA replication control.

Yours sincerely,

Jack A. Bryant

Manuel Banzhaf
Senior Lecturer of Systems Microbiology
Tel: +44 (0)191 208 3219
email: manuel.banzhaf@newcastle.ac.uk

Microbes in Health and Disease
Newcastle University Bioscience Institute (NUBI)
Cookson Building
Newcastle University
Framlington Place
Newcastle upon Tyne
NE2 4HH
United Kingdom

3 July 2025

I hereby declare my contribution to the research article (reviewed preprint):

Bryant JA, Staunton KA, Doherty HM, Alao MB, Ma X, Morcinek-Orłowska J, Goodall ECA, Gray J, Milner M, Cole JA, de Cogan F Knowles TJ, Glinkowska M, Moradigaravand D, Henderson IR, Banzhaf M (2024) Bam complex associated proteins in Escherichia coli are functionally linked to peptidoglycan biosynthesis, membrane fluidity and DNA replication eLife 13:RP99955, https://doi.org/10.7554/eLife.99955.1

As the lead corresponding author of this study I contributed by conceptualising this work, providing funding and supervising my team.

Sincerely,

Dr. Manuel Banzhaf

UNIVERSITY OF BIRMINGHAM

Prof. Tim Knowles
Professor of Structural Biology
Programme Lead for Biochemistry

School of Biosciences
College Life and Environmental Sciences
Vincent Drive, Edgbaston
Birmingham B15 2TT
United Kingdom

Phone +44(0)121 414 5393
Email t.j.knowles@bham.ac.uk

Author contribution statement

To whom it may concern,

I hereby declare that my contribution to the research article (reviewed preprint):

Bryant JA, Staunton KA, Doherty HM, Alao MB, Ma X, Morcinek-Orłowska J, Goodall ECA, Gray J, Milner M, Cole JA, de Cogan F Knowles TJ, Glinkowska M, Moradigaravand D, Henderson IR, Banzhaf M (2024) Bam complex associated proteins in Escherichia coli are functionally linked to peptidoglycan biosynthesis, membrane fluidity and DNA replication eLife 13:RP99955, https://doi.org/10.7554/eLife.99955.1

includes:

Conceptualisation, Manuscript writing/revision, Supervision.

Sincerely,

Prof. Tim Knowles

THE UNIVERSITY OF QUEENSLAND
AUSTRALIA

Institute for Molecular Bioscience

18 November 2025

Author contribution statement

I hereby declare that my contribution to the research article (reviewed preprint):

Bryant JA, Staunton KA, Doherty HM, Alao MB, Ma X, Morcinek-Orłowska J, Goodall ECA, Gray J, Milner M, Cole JA, de Cogan F Knowles TJ, Glinkowska M, Moradigaravand D, Henderson IR, Banzhaf M (2024) Bam complex associated proteins in Escherichia coli are functionally linked to peptidoglycan biosynthesis, membrane fluidity and DNA replication eLife 13:RP99955, https://doi.org/10.7554/eLife.99955.1

included:

- Conceived project
- Secured funding
- Supervised students and staff
- Reviewed manuscript

Yours sincerely

Professor Ian Henderson
Executive Director
Institute for Molecular Bioscience

The University of Queensland
Brisbane QLD 4072 Australia
T +61 733462112
E director@imb.q.edu.au
W imb.uq.edu.au
ABN: 63 942 912 684
CRICOS Provider 00025B

Uniwersytet Gdański

dr hab. Monika Glinkowska, prof. UG
Katedra Genetyki Molekularnej Bakterii
Wydział Biologii
Uniwersytet Gdański

Gdańsk, 01.06.2025 r.

Oświadczenie o wkładzie w publikację

Oświadczam, że mój wkład w preprint artykułu oryginalnego:

Bryant JA, Staunton KA, Doherty HM, Alao MB, Ma X, Morcinek-Orłowska J, Goodall ECA, Gray J, Milner M, Cole JA, de Cogan F Knowles TJ, Glinkowska M, Moradigaravand D, Henderson IR, Banzhaf M (2024). Bam complex associated proteins in Escherichia coli are functionally linked to peptidoglycan biosynthesis, membrane fluidity and DNA replication. eLife 13:RP99955, https://doi.org/10.7554/eLife.99955.1

polegał na:

- optymalizacji warunków hodowli i metody cytometrii przepływowej po zatrzymaniu replikacji dla szczepów pozbawionych genów *bam*
- uczestnictwie w interpretacji wyników oraz przygotowaniu i rewizji manuskryptu

Monika Glinkowska

Wdział Biologii
Uniwersytetu Gdańskiego
Katedra Genetyki
Molekularnej Bakterii

tel. +48 58 523 60 65
e-mail: mol.KGB@ug.edu.pl

ul. Wita Stwosza 59
80-309 Gdańsk

www.ug.edu.pl

Artykuł nr 5 (manuskrypt pracy badawczej)

Bebel A.*, Morcinek-Orłowska J.*, Banzhaf M., Galińska J., Waldminghaus T., Zawilak-Pawlik A., Glinkowska M.

Interaction of the replication factor DiaA and primary metabolite sedoheptulose 7-phosphate regulates DNA replication in *Escherichia coli*.

* – wkład równorzędny

Interaction of the replication factor DiaA and primary metabolite sedoheptulose 7-phosphate regulates DNA replication in *Escherichia coli*

Aleksandra Bebel[1,2]*†, Joanna Morcinek-Orłowska[1*], Manuel Banzhaf[3], Justyna Galińska[1], Torsten Waldminghaus[4], Anna Zawilak-Pawlik[5] and Monika Glinkowska[1]†

1-Department of Bacterial Molecular Genetics, University of Gdansk, Gdansk, Poland

2 - Department of Biochemistry and Molecular Biology, University of Chicago, USA

3 - Institute of Microbiology & Infection and School of Biosciences, University of Birmingham, UK

4 - LOEWE Center for Synthetic Microbiology-SYNMIKRO, Philipps-Universität Marburg, Germany

5 - Hirszfeld Institute of Immunology and Experimental Therapy, Polish Academy of Sciences, Wroclaw, Poland

* - These authors contributed equally to this work

† - to whom correspondence should be addressed

Abstract

Bacteria coordinate DNA replication with cell growth, but the mechanism of this regulation remains unclear. Although biochemical mechanisms controlling the initiation of DNA replication in the model bacterium *Escherichia coli* are well characterized, it remains elusive what constitutes a signal for the growing cell to initiate the next round of chromosomal DNA replication. In this work, we present evidence that a primary metabolite sedoheptulose 7-phosphate (S7P) binds to a replication factor DiaA and affects its activity in promoting oligomerization of the DnaA initiator protein. Furthermore, our results show that the cellular level of S7P and the ability of DiaA to interact with the metabolite both influence DNA replication *in vivo*. S7P is an intermediate in the pentose phosphate pathway, providing building blocks for synthesis of nucleotides and a starting point for production of the outer membrane components. Consequently, the mechanism proposed in this work links DNA replication with cell growth through primary metabolism.

Introduction

DNA replication is a fundamental process occurring in cells of all prokaryotic and eukaryotic organisms. In order to assure correct copying and distribution of the cell's genetic material, the process of DNA replication is tightly controlled in terms of time, space, coupling to specific cell-cycle events, and abundance of necessary molecules. In bacterial cells, control of DNA replication is exerted mainly at the initiation step. The key player of that stage and a target of regulation by various factors is the initiator protein – DnaA. DnaA recognizes a single origin of replication (*oriC*) present in bacterial chromosomes and plays a role analogous to the

origin recognition complex (ORC) in Eukaryotes, directing the assembly of other replisome components (reviewed in [1,2]).

In *Escherichia coli*, DNA replication is initiated by a direct interaction of ATP-bound DnaA (DnaA-ATP) with specific DNA sequences at *oriC*, known as DnaA boxes. Several types of DnaA boxes exhibiting different affinities for DnaA are present within the *E. coli oriC* sequence, but only DnaA-ATP is able to interact efficiently with the low-affinity boxes [3]. Through a staged interaction with sequences of high and low affinity, DnaA-ATP forms an oligomeric complex of specific architecture that facilitates the unwinding of the DNA strands at the AT-rich region of *oriC.* This allows for the interaction of DnaA-ATP with ssDNA and in consequence - for the assembly of the replisome (DnaB helicase, DnaG primase, and DNA polymerase) on both single strands of the DNA [3–5]. ATP-DnaA is then hydrolyzed into its inactive DnaA-ADP form, and DnaA-ATP amount remains low until the next round of DNA replication [4,5]. Depending on the growth conditions, subsequent rounds of replication can commence while the previous ones are still ongoing. Several protein factors and specific DNA regions regulate access of DnaA to DnaA boxes at *oriC* (for example, SeqA and Fis) or formation of the oligomers competent in DNA unwinding. The latter type of control is exerted either directly, by blocking or enhancing DnaA binding to certain DnaA-boxes (IHF, DiaA and Fis) or indirectly, by promoting either ATP- or ADP-bound form of DnaA (Hda, *datA*, DARS) [4,5].

One such regulator, DiaA (DnaA initiator-associating factor) was shown to directly interact with the N-terminal domain (domain I) of DnaA and to stimulate initiation at *oriC* [6,7]. To initiate DNA replication, DnaA bound to the high-affinity DnaA boxes at *oriC* recruits DnaA-ATP to the low-affinity binding sites by forming a protein multimer. Through direct interaction with multiple DnaA molecules, DiaA tetramers aid DnaA-ATP multimer formation and stimulate cooperative binding of DnaA to low-affinity DnaA boxes [8]. DiaA (through Pro71,

Leu190, Phe191) interacts with specific DnaA residues (Phe46, Trp25, Trp50, Glu21) and the DnaA interaction surface is shared by DiaA and the DnaB helicase [7,8]. As a result, both proteins were shown to compete for binding to DnaA *in vitro* [8]. The competition is proposed to play a role in a tight temporal control of DnaB loading. Namely, after DiaA is released from the association with DnaA, the DnaB-DnaC complex can interact with DnaA. Subsequently the helicase can be loaded onto the ssDNA, which is a prerequisite for the DNA replication to start [8]. The cellular factor that leads to the release of DiaA from the complex remains unknown. This negative regulation of DnaB loading by DiaA could constitute a mechanism ensuring timely, synchronous initiation of chromosomal DNA replication at multiple *oriC*s in fast growing cell [7,8]. DiaA plays therefore both stimulating and inhibiting regulatory roles in DNA replication initiation. The importance of DiaA in DNA replication is highlighted by its wide conservation amongst bacteria, with homologues found in different classes of proteobacteria [9–11].

The crystal structure of *E. coli* DiaA together with mutational analysis revealed three regions with distinct functions within each DiaA monomer: (I) a region involved in multimerization of DiaA into a functional tetramer, (II) a DnaA interaction site, and (III) a well-conserved sugar isomerase (SIS) domain [7]. Mutations leading to the loss of DiaA function were found for each of these domains, suggesting that tetramer formation, direct interaction with DnaA, and the functional SIS domain are all necessary for the regulatory activity of DiaA.

The role of the SIS domain in DiaA function is unknown. Notably, the SIS domain closely resembles that of another *E. coli* protein, sedoheptulose 7-phosphate isomerase GmhA (alternative name - LpcA) and its homologues in other bacterial species [7,10,11]. GmhA catalyzes isomerization of D-sedoheptulose-7-phosphate (S7P) into D-glycero-D-manno-heptose-7-phosphate (M7P), which constitutes a step in the pathway of lipopolysaccharide (LPS) synthesis [12,13]. LPS is a part of the outer membrane of Gram-negative bacteria, and cells with defective LPS show higher cell wall permeability and increased susceptibility to certain antibiotics.

Structural studies of *E. coli* GmhA suggested that the isomerization of S7P to M7P occurs via enediol switch within a conserved catalytic site, with crucial residues being Glu-65, Gln-172, and His-180 [14,15].

Based on similarities between GmhA and DiaA, we performed a functional analysis of the SIS domain, with the aim to gain insights into its role in DiaA-mediated replication control. We show that *E. coli* DiaA binds the metabolite S7P. However, in contrast to GmhA, DiaA does not convert S7P to M7P. Comparison of the crystal structures available for the two proteins allowed us to design various mutations within the predicted S7P binding pocket of DiaA. We discovered that mutations of the SIS domain that abolished S7P binding or prevented oligomerization of DiaA resulted in perturbed and asynchronous chromosome DNA replication. Moreover, we present evidence that S7P influences DiaA-dependent DnaA activity *in vitro*. Consequently, our results show that mutations leading to decreased S7P levels *in vivo* result in a higher cellular DNA content despite slower growth rate of the mutants compared to wild-type strain. Altogether, our findings suggest that S7P might be the cellular regulator of DiaA linking DNA replication, cellular metabolism, and the cell cycle into a tightly regulated network.

Results

DiaA structure contains a well-conserved S7P-biding pocket

In order to characterize the role of the DiaA SIS domain we first asked whether DiaA could bind the same ligand as GmhA, the S7P. Therefore, we performed a comparison of available crystal structures of DiaA and GmhA in complex with S7P or M7P [7,13] (Figure 1a

and b). In these structures, GmhA interacts with the phosphate group of S7P or M7P via a well-conserved binding pocket that includes residues Ser119, Thr120, Ser121, and Ser124 (numbering according to *E. coli* GmhA sequence). Moreover, a wide network of GmhA residues interacts with the functional groups of S7P's or M7P's sugar moiety. Specifically, *E. coli* GmhA residues contacting S7P are: Ser55, His61, Glu65, Gln172, and His180. On the other hand, product-bound *Pseudomonas aeruginosa* GmhA interacts with M7P via its Glu64, Asn67, Arg68, and Gln172 (Figure 1a) (13). The importance of many of those residues for GmhA catalysis was confirmed by the lack of activity of the respective mutants *in vitro* [13]. Our structural comparison revealed conservation of most of the residues key for the GmhA-phosphosugar interaction in *E. coli* DiaA. Namely, in DiaA the predicted phosphate binding pocket consists of residues 117-122 (Ser 117, Thr118, Ser122 and non-conserved Arg119). Furthermore, some of the residues contacting the sugar moiety of S7P in GmhA are conserved in DiaA (Ser52, His58, Gln172), while others differ (Ser62 and Asn180). Similarly, the same amino acids are found in DiaA in three positions specific for GmhA-M7P product interaction (Asn65, Arg66, and Gln172), while Glu64 is replaced by a serine (Ser62) (Figure 1a and b). Interestingly, previously reported DiaA variant S52F, showed both lack of replication stimulation *in vitro* and aberrant initiation of DNA replication *in vivo* [7], strongly suggesting that DiaA S7P-binding motif may be important for the protein's activity as replication factor.

DiaA interacts with S7P in vitro

Given the structural similarities of *E. coli* DiaA and GmhA, we experimentally tested whether DiaA binds S7P. To assess DiaA-S7P interaction, we recombinantly expressed and purified both proteins and performed an electrophoretic mobility shift assay (EMSA) with radioactively labelled S7P as a substrate. We obtained labelled [^{32}P]-S7P by phosphorylation

of sedoheptulose with a [γ-^{32}P]-ATP in the presence of a specific kinase, CARKL [16]. As expected, GmhA addition led to a mobility shift confirming its ability to bind S7P (Figure 2a). Analogous shift was also observed for DiaA, in accordance with the presence of conserved S7P-binding pocket revealed by analysis of the crystal structure. The binding affinities of both proteins appear to be similar; however, the complexes formed with S7P by GmhA and DiaA migrated differently despite having very similar monomer molecular weights (20.8 and 21.1 kDa, respectively). This disparity in electrophoretic mobility of DiaA and GmhA is not a result of their association with S7P, since a similar difference was observed for the unbound proteins and the presence of S7P does not change the proteins' migration pattern (Figure S1a). In the absence of S7P, DiaA forms tetramers according to our gel filtration experiments (Figure S1b), in agreement with previous work [7]. GmhA has been reported to either form a dimer or a tetramer in solution [13,17]. Consistent with this, our assay indicated a dimeric form or an equilibrium between dimers and tetramers (Figure S1b). This result suggests distinct architectures of GmhA and DiaA complexes with S7P under gel electrophoresis conditions. Importantly, we did not observe S7P binding by DnaA (data not shown).

Changes in the predicted phosphosugar-binding pocket affect the DiaA-S7P interaction or tetramer formation

Our analysis confirmed that DiaA binds S7P. Next, we sought to determine whether the ability to bind S7P is important for DiaA function. Firstly, we tackled this problem by changing the key residues in the S7P-binding pocket of DiaA and testing effects of those changes on DiaA-S7P interaction and the protein's activity in the replication control. Therefore, we constructed vectors expressing the following protein variants: T118A, S122A, R119A, R119Q (phosphate group-binding pocket); S52A, H58Q, H58A, S62A, Q172E, N180E, N180A

(interaction with S7P's sugar moiety) and N65E, R66K and a double mutant N65E+R66K (residues specific for contact with M7P) (Figure 1b, Table 1).

To test whether S7P binding is affected by the mutations to the predicted binding site, we performed EMSAs with radiolabelled S7P and the purified DiaA variants (Figure 2b). Of the 17 variants tested, one – N180E – did not bind S7P (Figure 2b, lane 14; Figure 2c). We expected Asn180 to be important for S7P binding since the equivalent GmhA His180 was shown to be essential for GmhA activity [13]. Furthermore, amongst 62 sequences of DiaA homologues from bacterial species across the kingdom, the equivalent residue was invariably a histidine (like in *E. coli* GmhA) or an aspargine (like in *E. coli* DiaA; Figure 2d). It is worth noting that DiaA N180E still formed tetramers in solution like WT DiaA (Figure S1a and S1c). We used the N180E variant as a proxy for S7P binding-deficient DiaA in further *in vitro* and *in vivo* experiments linking the ability to bind S7P to DiaA function. No other single DiaA mutation abolished S7P binding.

Two DiaA variants (N65E, and N65E+R66K) appeared to form complexes with S7P that migrated faster on a gel, suggesting different oligomeric state than the wild-type DiaA (Figure 2b, lanes 6, 8; Figure S2). We observed similar differences in size-exclusion chromatography, where protein variant N65E eluted from the column later than the wild-type DiaA (Figure S1d). Given that DiaA was reported to form homotetramers (dimers of dimers) [7], we propose that the observed variants are dimers unable to associate to form higher oligomeric structures. Accordingly, the position Asn65 aligns with the dimer-dimer interface of DiaA tetramer (Figure 2e). Asn65 lies within helix α3 that makes interactions with helix α4 of a monomer belonging to the reciprocal dimer, and substitution of either of these residues for negatively charged glutamic acid likely destabilizes the dimer-dimer interaction. However, inability to tetramerize did not impair S7P binding by those protein variants. In fact, the results suggest that more DiaA-S7P complex formed in the presence of these variants than with wild-

type DiaA (Figure 2a, lanes 6 and 8), possibly due to increased access of the phosphosugar to the binding pocket when the second dimer is absent. Alternatively, it is possible that the mutated S7P binding pocket produces a slightly different conformation of each DiaA monomer/dimer, resulting in higher S7P affinity and an inability to form tetrameric complexes.

S7P binding is required for DiaA-dependent regulation of DNA replication

One of the functions of DiaA in bacterial cells is to ensure synchronous firing of multiple origins during multifork replication. To assess the roles of S7P binding of DiaA for its regulatory function in DNA replication, we replaced the *E. coli* chromosomal wild-type *diaA* gene with the 17 mutated variants analysed *in vitro* above. We then employed flow cytometry to measure the influence of DiaA mutations on the cellular DNA content. In this assay, replication initiation and cell division are blocked with antibiotics in an exponentially growing *E. coli* culture, and the number of chromosomes present in the cells after completion of ongoing replication rounds is estimated. In the wild-type cells, only even (2, 4, 8, or 16) numbers of chromosomes are expected. Accordingly, in fast growth conditions we observed cells with either 8 or 16 fully replicated chromosomes (Fig. 3a). In the absence of DiaA (*ΔdiaA*), this pattern was disturbed, indicating mis-regulation of DNA replication, as seen in previous studies (Figure 3b) [6]. Cells producing variant N180E (which did not bind S7P) showed an aberrant chromosome replication pattern comparable to that of a *ΔdiaA* strain (Figure 3c) suggesting that the ability to bind S7P is directly related to DiaA function in regulation of DNA replication. Similar results were obtained for the strains producing the DiaA variants impaired in tetramer formation (N65E, N65E+R66K, Figure 3d and e), confirming that tetramerization of DiaA is necessary for the replication control. The remaining DiaA variants showed replication patterns comparable with that of the wild-type DiaA (see for example R66K, R119S

in Figure 3f and g), which is in line with our previous conclusion that these mutations do not have a negative impact on S7P-DiaA interaction *in vitro*.

DiaA N180E interacts with DnaA

DiaA exerts its replication factor function by a direct interaction with the N-terminal domain of DnaA [6,7]. Since DiaA variant N180E which does not bind S7P, showed impaired replication control *in vivo*, we asked whether the observed effects are caused by disturbed physical interaction between DiaA and DnaA. To assess that, we performed pull-down experiments with purified His-tagged DnaA as "bait" and untagged DiaA and its variants as "prey" (Figure 4a, Figure S3). In the case of DiaA variant N180E, we observed DnaA interaction at a level similar to that of the wild-type DiaA (Figure 4a and b), suggesting that inability to bind S7P does not have an effect on DnaA-DiaA binding. On the contrary, impaired tetramerization of the DiaA N65E mutant, in line with previously published results [7], decreased its interaction with DnaA, as indicated by the reduced amount of DiaA N65E remaining on the resin with bound his-DnaA (Figure 4a).

Alteration of the S7P metabolic pathway affects DNA replication control

Based on the above finding that *diaA* mutants producing the protein variant unable to bind S7P show altered replication control, we next asked whether similar effects can be evoked by reduction of the cellular S7P pool. We hypothesized that the cellular levels of S7P could modulate DNA replication timing. S7P is a precursor for both LPS and nucleotide synthesis, making it a possible linker between chromosome duplication process, nucleotide synthesis and cell's growth. It is produced in the non-oxidative branch of the pentose phosphate pathway from

D-ribose 5-phosphate and D-xylulose 5-phosphate by two transketolases TktA and TktB, the former being the major source of the cellular S7P pool. To test whether a decrease in the S7P levels affects the initiation of DNA replication, we wanted to compare chromosomal DNA content of exponentially growing wild-type cells and *ΔtktA* mutants using flow cytometry (Figure 5a). However, this comparison is not straightforward since *ΔtktA* strain displays slower growth rate than its wild-type counterpart (41.5 vs 21.7 min) and smaller cell size [18] (1.38 vs 3,6 μm^3) (Figure 5b) whereas both parameters can affect the number of chromosomes present in cells. Therefore, we decided to measure chromosomal content in relation to cell volume and growth rate in both strains. In order to test our method, we assessed average cell size, chromosome number and growth rate of MG1655 strain cultivated in media supporting different growth rates. As expected, the slower the cells were growing, the smaller was their size and chromosome number per cell (Figure 5c and d, Figure S4). When grown in LB medium *ΔtktA* mutants contained in majority either 4 or 8 fully replicated chromosomes, in comparison to 8 and 16 chromosomes present in the wild-type cells (Figure 5a). However, the ratio of chromosomes to cell volume was much higher in *ΔtktA* mutants, suggesting that mechanisms coupling initiation of DNA replication to cell volume are perturbed in cells devoid of major transketolase activity (Figure 5c). This result supports the involvement of S7P in the DNA replication control, however it suggests that S7P binding by DiaA exerts a negative role during its initiation stage.

S7P binding negatively affects the activity of DiaA in stimulation of DnaA oligomerization in the presence of oriC

The primary role of DiaA in the control of *E. coli* DNA replication is the stimulation of DnaA binding to DnaA-boxes present at *oriC* (8). Our results suggest that S7P binding by

DiaA affects its activity as a replication factor. However, there was an apparent discrepancy with respect to the effect of DiaA-S7P complex formation on replication timing between the results of the cell cyle analysis of *tktA* and *diaA* N180E mutants. To gain insights into the influence of S7P binding for DiaA function, we investigated the DiaA-dependent effect on DnaA-*oriC* interaction in the presence and absence of S7P, using EMSA assay (Figure 6). As expected, DnaA on its own forms distinct complexes with *oriC* appearing as shifted bands in an EMSA. These complexes likely include a small number of DnaA monomers bound to the high-affinity DnaA-boxes (Figure 6, lane 2), and are not affected by addition of S7P alone (Figure 6, lane 8, 9). Upon addition of DiaA, a higher-molecular weight complex likely representing multimers of DnaA bound to both high- and low-affinity DnaA boxes can be observed (lanes 3 and 6). These slow-migrating complexes do not form when DiaA had been pre-incubated with S7P before addition to the reaction (Figure 6, lanes 4 and 7). Interestingly, the complexes of higher molecular weight were still formed when DiaA and S7P have been added simultaneously to the reaction without pre-incubation (data not shown). Taken together, these data suggest that S7P-bound DiaA might represent an inactive form of the protein in terms of promoting DnaA oligomerization on *oriC*. This result is also consistent with DNA replication starting too early during the cell cycle of *tktA* mutants.

DiaA does not isomerize S7P into M7P but its isomerase activity can be stimulated by restoration of the key catalytic residues of GmhA

Detection of S7P binding by DiaA suggests that the protein contains an active S7P-binding pocket similar to that of GmhA. Since the function of GmhA is to isomerize S7P into M7P, we asked whether DiaA can also perform this catalytic function. To answer that, we utilized an assay previously used to assess the function of GmhA and its variants, relying

on synthesis of D-glycero-D-manno-heptose 1-phosphate and release of the free phosphate which can be quantified [19]. Briefly, we purified the components of the heptose synthesis pathway, GmhB and HldE (Figure 7a). Subsequently, GmhB, and HldE were incubated with either GmhA or DiaA in the presence of S7P. Only an active S7P isomerase would lead to the formation of a green complex between Malachite Green, molybdate and the free phosphate. As expected, the reaction in the presence of GmhA led to conversion of S7P to M7P and subsequent release of the free phosphate as detected by the change of colour (Figure 7b). No free phosphate, comparable to the no-protein control, and therefore no conversion of S7P to M7P could be detected in the presence of DiaA. This suggests that while DiaA can bind S7P, it does not isomerize it into M7P.

We wondered whether the absence of isomerase activity of DiaA could be due to the lack of conservation of the key catalytic residues within the binding pocket. Namely, in GmhA, Glu65 and His180 [13], or alternatively Glu65 and Gln172 were proposed to act as the acid and base for the enediol switch leading to S7P isomerization [20]. These residues are only partially conserved in DiaA: Gln172 is present but Glu65 and His180 of GmhA are replaced by DiaA Ser62 and Asn180, respectively (Figure 1a). Another difference lies within the phosphate binding pocket, where the GmhA Ser121 is substituted by Arg119 in DiaA. We mutagenized these residues of DiaA (individually and together) to resemble those of GmhA, creating the following DiaA variants: S62E, R119S, N180H and the triple mutant S62E+R119S+N180H (Figure 1b). All of them bound S7P *in vitro* (Figure S2).

We tested these DiaA variants for the ability to isomerize S7P to M7P with the molybdate/malachite green phosphate assay as described in the preceding paragraph. Since wild-type DiaA did not isomerize S7P we used the signal obtained in the presence of GmhA as the 100% S7P to M7P conversion control (Figure 7c). The single-mutation variants of DiaA showed limited ability to isomerize S7P compared to wild-type DiaA (Figure 7c and data not

shown), but the differences were not statistically significant. However, introduction of three changes (S62E, R119S, and N180H) was sufficient to turn DiaA from an inactive into an active isomerase as indicated by significant (p=0.013) increase in free phosphate detection compared to the wild-type DiaA, at 9.5% of the GmhA isomerization level. Interestingly, similar phosphate detection levels (10%) were seen for a single mutant S62E, although this result was not statistically significant (p=0.113). It is worth noting that both the S62E and the S62E+R119S+N180H mutants showed increased electrophoretic mobility (Figure 2b), suggesting formation of smaller oligomers than wild-type DiaA. This result was confirmed in the case of the triple mutant by its earlier elution from a gel filtration column (Figure S1 e and f). The restoration of DiaA S7P isomerization ability in the S62E+R119S+N180H variant provides a proof-of-concept for the idea that DiaA possesses an S7P-binding pocket, which can be turned into a functional isomerase catalytic centre. It also indicates that additional residues of GmhA might provide a structural framework required for high levels of S7P isomerization or that the ability to form tetramers might be important for catalysis.

Discussion

How DNA replication is coordinated with cell growth and division in bacterial cells is an outstanding question. Mean size of growing *E. coli* cells in different media depends on their growth rate, and this relation is known as the growth law. It has been proposed recently that bacterial cell size might be determined by the relative rates of surface and volume synthesis [21]. Namely, in slower growing cells the rate of cell surface synthesis exceeds the rate of volume synthesis, whereas the opposite relation is observed in fast growing cells. Thus, accumulation of cell surface precursors, more rapid in slow growing than in fast growing cells, was proposed to constitute an indicator of cell volume growth for the cell division machinery. Cell volume

seems also to be the key determinant of the initiation of DNA replication as DNA synthesis was shown to start at a constant volume per chromosome [22,23] . What constitutes the signal or signals that convey the information about cell dimensions to the replication machinery remains elusive. Control of the replication regulatory protein DiaA by a metabolite that links nucleotide and cell surface synthesis, as described in this work, constitutes a feasible mechanism coupling cell growth with DNA replication initiation.

Structural studies of DiaA revealed the presence of sugar isomerase (SIS) domain that had previously denoted proteins engaged in metabolic processes but not with DNA replication. So far, the importance of the SIS domain for DiaA function remained unclear. In this work, we attempted to elucidate the role of the SIS domain by creating structurally guided DiaA-ligand binding assays as well as SIS domain mutations, and studying their effect on DiaA function *in vitro* and *in vivo*.

E. coli DiaA SIS domain closely resembles the SIS domain of GmhA (Figure 1 and b). GmhA active centre binds the substrate S7P and isomerizes it into product M7P. Both S7P and M7P are necessary for the formation of LPS and therefore constitute important intermediates in *E. coli* cell envelope metabolism, but neither compound has been linked directly to DNA replication. Here, we showed that the wild-type DiaA binds S7P, but does not isomerize it *in vitro* (Figure 2a, 7b).

To elucidate the role of the SIS domain in the function of DiaA as a regulator of DNA replication, we identified and mutagenized SIS domain residues that could be required for its function. To date, no structure of DiaA with S7P substrate has been solved, therefore we used the available structures of the protein's closest homologue, *E. coli* GmhA, to identify the relevant residues (Figure 1).

Surprisingly, amongst seventeen DiaA variants with mutated SIS domain, only a single variant, N180E, did not bind S7P (Figure 2b and c). In GmhA, a corresponding residue His180

is absolutely conserved between proteins from different bacterial species, and was proposed to act as a catalytic residue in S7P to M7P conversion (Figure 2d) [13]. Interestingly, substitution of DiaA Asn180 to alanine did not abolish S7P binding suggesting that the presence of Asn180 is not essential for S7P binding by DiaA. Instead, in the N180E variant, the interaction with S7P is likely disrupted by the introduction of a negative charge to the binding pocket by substituting asparagine for glutamic acid (Figure 2c). Since no other DiaA mutation abolished S7P binding, we conclude that multiple interactions between DiaA residues and S7P act to assure redundancy such that no single amino acid mutation tested abolishes S7P binding. Further mutagenesis studies based on amino acid conservation in DiaA homologues will shed light onto residues essential for S7P binding.

We used the DiaA N180E variant as a model to understand the functional implications of impaired S7P binding by DiaA in context of its function in bacterial DNA replication. *E. coli* cells producing DiaA N180E showed asynchronous and delayed initiation of DNA replication suggesting that S7P binding is a prerequisite for DiaA function in regulation of timing of *oriC* firing. The observed effect could not be attributed to the lack of DiaA-DnaA interactions since these could be observed with wild-type and mutant DiaA variant alike (Figure 4a and b). The importance of S7P for DNA replication timing during the cell cycle is also supported by the finding that *E. coli* metabolic mutant *tktA,* with lower cellular S7P concentration, exhibits higher chromosomal content per cell volume than the wild-type cells. Despite slower growth rate and smaller cell dimensions (Figure 5b), *tktA* cells contained chromosomes in a number characteristic for larger and faster growing wild-type cells (figure 5c). This suggests earlier initiation of replication during the cell cycle, at lower cellular mass per origin in *tktA* mutants. This result implies inhibitory role of S7P in initiation of DNA replication and is also in line with the negative effect of S7P on DiaA-dependent formation of high molecular weight DnaA-DNA complexes observed *in vitro* (Figure 6). However, the latter conclusions seem to be

in contradiction with the negative impact of mutation abolishing DiaA-S7P interaction on DNA replication *in vivo*. Nevertheless, it is possible that DiaAN180E variant is more similar in its conformation and properties to S7P-bound DiaA and remains in a constant "off" state with respect to stimulation of DNA replication. Replacement of Asp180 to glutamate seems to have no major impact on protein's conformation since DiaA N180E retains the ability to tetramerize and interact with DnaA (Figure 4 and S1).

To summarize, our results link the formation of DiaA-S7P complexes to DnaA oligomerization and formation of specific DnaA complexes at *oriC* (Figure 5b), but the detailed molecular mechanism is yet to be elucidated. We envision that S7P is the regulatory factor modulating the timing of the replication start. A mechanism involving S7P could couple the DNA replication to cell growth since S7P is a substrate for production of cell envelope components. The concentration of S7P could reflect the ratio of surface to volume synthesis and constitute information about the size increase for the replication machinery. S7P as an intermediary metabolite in the pentose phosphate pathway, providing substrates for NTPs synthesis, may also connect nucleotide metabolism to DNA replication. Further work is required to elucidate the impact of flux modulation through the pentose phosphate pathway on the timing of DNA replication.

Considering structural and sequence similarities between the SIS domains of DiaA and GmhA, we propose that they originated from a single GmhA-like protein replicated in an ancestral bacterial genome. In fact, both proteins have been previously described as isotypes [11]. It is imaginable that the redundant copy of this protein lost its ability to isomerize S7P and the two copies diverged to perform two distinct functions. Evolution of protein function preceded by a gene duplication event is a well-described mechanism [24]. Such mechanism of evolution of DiaA is supported by the fact that many bacteria encode two related proteins with GmhA-like SIS domain; partial restoration of isomerization function in DiaA by SIS

domain mutagenesis (Figure 7c) further supports this idea. It also implies that the mechanism of regulation of DiaA homologues' activity by S7P may be conserved in other bacterial species. Since some bacteria encode only a single GmhA homologue, it would be interesting to see whether this protein combines the functions of GmhA and DiaA, or whether different mechanisms are at play. *P. aeruginosa* isomerase GmhA, for instance, contains amino acid residues that were proven crucial for DiaA-DnaA interaction in *E. coli* [7].

In summary, the presented work elucidates for the first time the role of the SIS domain in DiaA function as a regulator of DNA replication initiation. Our results suggest that pentose phosphate metabolite S7P acts as a cellular regulator of DiaA-promoted DnaA-*oriC* complex formation required for initiating DNA replication. Altogether, we believe that these results will increase our understanding of the mechanisms controlling bacterial cell cycle.

Methods

Plasmids, strains and primers

E. coli strains used in this study are presented in Table S1. K12-derivative MG1655 was used as a wild type strain. *ΔtktA* and *ΔdiaA* strains were constructed by P1 transduction from Keio collection strains. DiaA chromosomal variants were generated with standard λ-red dependent recombination system[25]. To amplify linear DNA carrying mutated *diaA* and chloramphenicol resistance gene, we modified pKD3 by cloning *diaA* upstream of the chloramphenicol resistance cassette and performing site-directed mutagenesis as described below. Plasmids and primers used in this study are listed in Table S2 and S3, respectively.

Cloning and mutagenesis

All cloning procedures were performed using standard restriction techniques [26] or restriction-free cloning as described by van den Ent and Lowe [27]. Site-directed mutagenesis of pET28-DiaA and pKD3-DiaA was performed with single 5'-phosphorylated primer method. Briefly, plasmid DNA containing the *diaA* gene was PCR-amplified using a single mutagenic primer previously 5'-phosphorylated with polynucleotide kinase and circularized with Taq ligase. Purified PCR product was digested with DpnI and transformed into DH5a cells. Constructs were verified by sequencing.

Protein expression and purification

DiaA wild-type protein and its variants were overexpressed in *E. coli* BL21 (DE3) as N-terminal fusions with hexahistidine and Small Ubiquitin-like Modifier (SUMO) tags for 18 hours at 20 °C after addition of 1 mM isopropyl β-D-1-thiogalactopyranoside (IPTG). Cells were lysed by sonication in buffer A (25 mM HEPES-KOH pH 7.5, 250 mM KCl, 5% glycerol, 0.2 mM tris(2-carboxyethyl)phosphine (TCEP), 15 mM imidazole) supplemented with 1.5 mM phenylmethanesulfonylfluoride (PMSF) and an EDTA-free protease inhibitor tablet (ThermoScientific). The lysate was cleared by centrifugation. The proteins were purified from the soluble fraction of the lysate by Ni-affinity chromatography on a 5 ml HisTrap column (GE Healthcare). The proteins were eluted with buffer B (25 mM HEPES-KOH pH 7.5, 250 mM KCl, 5% glycerol, 0.2 mM TCEP, 0.5 M imidazole) and dialyzed into buffer C (25 mM HEPES-KOH pH 7.5, 250 mM KCl, 5% glycerol, 0.2 mM TCEP) in the presence of His-Ulp1 (SENP2) protease. The tags and the protease were removed on a Ni-affinity column. Finally, the proteins were purified by size-exclusion chromatography on a Superose 12 10/300 GL gel filtration

column (GE Healthcare). Protein concentration was estimated using NanoDrop Spectrophotometer (Thermo Scientific) at 280 nm and aliquots of purified protein were frozen in liquid nitrogen and stored at -70°C.

Proteins GmhA, GmhB, and HldE were overexpressed and purified as above.

DnaA was purified as above with DnaA-specific buffers: cells were sonicated in buffer D (45 mM HEPES-KOH pH 7.6, 200 mM potassium glutamate, 10 mM magnesium acetate, 15% glycerol, 0.2 mM TCEP, 15 mM imidazole) containing 1.5 mM PMSF and an EDTA-free protease inhibitor tablet. Protein bound to the HisTrap column was eluted with buffer E (45 mM HEPES-KOH pH 7.6, 200 mM potassium glutamate, 10 mM magnesium acetate, 15% glycerol, 0.2 mM TCEP, 0.5 M imidazole). Gel filtration was performed in buffer F (45 mM HEPES-KOHpH 7.6, 200 mM potassium glutamate, 10 mM magnesium acetate, 15% glycerol, 0.2 mM TCEP).

Protein sizes and oligomeric states were assessed by analytical size exclusion chromatography on a Superdex 200 10/300 GL column (GE Healthcare) in buffer F (40 mM HEPES-KOH pH 7.5, 150 mM KCl, 1 mM EDTA, 2 mM DTT, 5% glycerol).

Binding assays

DiaA binding to S7P was tested by electrophoretic mobility shift assay (EMSA). Radioactively-labelled S7P was obtained by phosphorylation of sedoheptulose with a specific CARKL kinase [16] (both were a kind gift from Arvand Haschemi, Medical University of Vienna, Austria). Reaction was performed as follows: sedoheptulose (100 µM) was incubated for 3 hours at 30°C with [γ-^{32}P]- ATP and 50 µg/ml CARKL in the labelling buffer (25 mM HEPES-KOH pH 7.5, 20 mM KCl, 10 mM $MgCl_2$). Subsequently, the enzyme was inactivated for 30 min at 80°C. [^{32}P]-S7P was diluted to the final concentration of 20 µM, assuming 100 percent

of the reaction efficiency. Diluted substrate was incubated with DiaA (30μM or as indicated) in the reaction buffer (25 mM HEPES-KOH pH 7.5, 100 mM KCl, 10 mM $MgCl_2$, 5% glycerol, 1mM EDTA, 1 mM DTT) for 2 h at 37°C. The complexes were resolved on a native 10% Tris-glycine polyacrylamide gel for 3 hours at 12 V/cm of the gel, at room temperature. Gels were scanned using Typhoon FLA 7000 Phosphoimager, and images were quantified and analyzed with ImageQuant (GE Healthcare).

An EMSA with *oriC*, DnaA, and DiaA-S7P was performed using a fluorescently labelled 419 bp linear *oriC* DNA fragment. The fragment was amplified using a Cy5-labeled primer 5'-Cy5-oriC-F (5'-Cy5CCCGGGCCGTGGATTCTAC-3') and an unmodified primer oriC-R (5'-GAAGATCAACATTCTTGATCACG-3'). Indicated amounts of DiaA were pre-incubated with 5 mM S7P for 15 minutes at 20 °C, then incubated together with labelled *oriC* (3.3 nM) and DnaA (90 or 100 nM) in the binding buffer (40 mM HEPES-KOH pH 7.6, 50 mM potassium glutamate, 5 mM magnesium acetate, 0.5 mM DTT, 5% glycerol, 2 mM ATP, 0.1 μg/ml poly(dI-dC), 0.2 mg/ml BSA,) for 20 minutes at 20 °C. Reaction products were analyzed using 5% TBE PAGE at 4°C and visualyzed by Typhoon FLA 7000 Phosphoimager(GE Healthcare).

In vitro S7P to M7P isomerization assay

GmhA, DiaA, and DiaA variants (120 μg/ml or as indicated) were incubated with S7P (0.16 mM), GmhB (34μg/ml), HldE (9μg/ml) and ATP (8 μM) in the reaction buffer for 10 min at 37 °C and then for 5 min at 70 °C. The amount of released free phosphate was quantified with the Malachite Green Phosphate Assay Kit (Sigma-Aldrich) according to the manufacturer's instructions, using the EnSpire Multimode Plate Reader (Perkin-Elmer) at 640

nm. The reactions were repeated in triplicates; the p values were calculated using Student's Test.

Flow cytometry analysis

Cells were exponentially grown with aeration at 37°C, in LB medium containing 0.2% glucose or AB medium (15.1mM $(NH_4)_2SO_4$, 42.3 mM Na_2HPO_4, 22 mM KH2PO4, 51.3 mM NaCl, 0.1 mM $CaCl_2$, 1 mM $MgCl_2$, 0.003 mM $FeCl_3$, 10 µg/ml thiamine, and 25 µg/ml uridine) with one of the following carbon sources: 0.2% glucose (ABg), 0.2% glucose + 0.5% casamino acids (ABgc) or 0.4% sodium acetate (ABac). At OD_{600}=0.15, cells were treated with 150 µg/ml rifampicin, and 10 µg/ml cephalexin and incubated for 4 h, resulting in an integral number of chromosomes corresponding to the number of replication origins at the time of the antibiotic treatment. Cells were subsequently harvested, washed with TBS (20 mM Tris-HCl pH 7.5, 130 mM NaCl) and fixed in cold 70% ethanol overnight or longer. Prior to analysis, cells were resuspended in 50 mM sodium citrate followed by RNA digestion with RNaseA for 4 h. Chromosomal DNA was stained with 2 mM Sytox Green (Invitrogen) and total DNA content per cell was measured with BD FacsCalibur using 488 nm Argon Ion laser. MG1655 (WT) strain growing in AB medium (15.1 mM $(NH_4)_2SO_4$, 42.3 mM Na_2HPO_4, 22 mM KH2PO4, 51.3 mM NaCl, 0.1 mM $CaCl_2$, 1 mM $MgCl_2$, 0.003 mM $FeCl_3$,10 µg/ml thiamine, and 25 µg/ml uridine) with 0.4% sodium acetate or 0.2% glucose, subjected to the same antibiotic treatment, were used before each measurement series as a standard for cells containing 1/2 or 2/4 chromosomes, respectively.

Pull-down assays

His-DnaA (2 μM) was pre-incubated in HB buffer (45 mM HEPES-KOH pH 7.6, 100 mM KCl, 5% glycerol, 0.025% Triton X-100, 2mM ATP, 15 mM imidazole) for 5 min on ice and added to Ni-NTA magnetic beads (Qiagen) equilibrated in the same buffer. After 1 h of gentle shaking at 4 °C, the unbound His-DnaA was washed out with buffer HB. The beads were then incubated with 8 μM (calculated for the monomer) of DiaA for 2 hours at 4°C, with gentle shaking. Magnetic beads with bound proteins were collected using magnetic stand and washed twice with buffer HB and once with buffer HW (45 mM HEPES-KOH pH 7.6, 100 mM KCl, 5% glycerol, 0.025% Triton X-100, 2mM ATP, 40 mM imidazole). Proteins were eluted with 40 μl of 1x SDS sample buffer (50 mM Tris pH 6.8, 1% SDS, 10% glycerol, 25 mM DTT) and subjected to SDS-PAGE followed by Coomassie Brilliant Blue staining.

References

1. Parker, M. W., Botchan, M. R. & Berger, J. M. Mechanisms and regulation of DNA replication initiation in eukaryotes. *Crit. Rev. Biochem. Mol. Biol.* **52,** 107–144 (2017).
2. Jameson, K. H. & Wilkinson, A. J. Control of Initiation of DNA Replication in Bacillus subtilis and Escherichia coli. *Genes (Basel).* **8,** (2017).
3. Leonard, A. C. & Grimwade, J. E. The orisome: structure and function . *Frontiers in Microbiology* **6,** 545 (2015).
4. Hansen, F. G. & Atlung, T. The DnaA Tale. in *Front. Microbiol.* (2018).
5. Katayama, T. Initiation of DNA Replication at the Chromosomal Origin of E. coli, oriC. *Adv. Exp. Med. Biol.* **1042,** 79–98 (2017).
6. Ishida, T. *et al.* DiaA, a novel DnaA-binding protein, ensures the timely initiation of Escherichia coli chromosome replication. *J. Biol. Chem.* **279,** 45546–45555 (2004).
7. Keyamura, K., Fujikawa, N., Ishida, T., Ozaki, S. & Su, M. The interaction of DiaA

and DnaA regulates the replication cycle in E . − DnaA-specific initiation complexes The interaction of DiaA and DnaA regulates the replication cycle in E . coli by directly promoting ATP – DnaA-specific initiation complexes. *Genes Dev. 2097* 2083–2099 (2007). doi:10.1101/gad.1561207

8. Keyamura, K., Abe, Y., Higashi, M., Ueda, T. & Katayama, T. DiaA dynamics are coupled with changes in initial origin complexes leading to helicase loading. *J. Biol. Chem.* **284,** 25038–25050 (2009).
9. Natrajan, G., Noirot-Gros, M. F., Zawilak-Pawlik, A., Kapp, U. & Terradot, L. The structure of a DnaA/HobA complex from Helicobacter pylori provides insight into regulation of DNA replication in bacteria. *Proc. Natl. Acad. Sci.* **106,** (2009).
10. Natrajan, G., Hall, D. R., Thompson, A. C., Gutsche, I. & Terradot, L. Structural similarity between the DnaA-binding proteins HobA (HP1230) from Helicobacter pylori and DiaA from Escherichia coli. *Mol. Microbiol.* **65,** 995–1005 (2007).
11. Do, H. *et al.* Crystal Structure and Comparative Sequence Analysis of GmhA from Colwellia psychrerythraea Strain 34H Provides Insight into Functional Similarity with DiaA. *Mol. Cells* **38,** 1086–1095 (2015).
12. Kneidinger, B. *et al.* Biosynthesis pathway of ADP-L-glycero-beta-D-manno-heptose in Escherichia coli. *J. Bacteriol.* **184,** 363–369 (2002).
13. Taylor, P. L. *et al.* Structure and function of sedoheptulose-7-phosphate isomerase, a critical enzyme for lipopolysaccharide biosynthesis and a target for antibiotic adjuvants. *J. Biol. Chem.* **283,** 2835–2845 (2008).
14. Taylor, P. L. & Wright, G. D. Novel approaches to discovery of antibacterial agents. *Anim. Heal. Res. Rev.* **9,** 237–246 (2008).
15. Brooke, J. S. & Valvano, M. A. Molecular cloning of the Haemophilus influenzae gmhA (lpcA) gene encoding a phosphoheptose isomerase required for

lipooligosaccharide biosynthesis. *J. Bacteriol.* **178,** 3339–3341 (1996).

16. Haschemi, A. *et al.* The sedoheptulose kinase CARKL directs macrophage polarization through control of glucose metabolism. *Cell Metab.* **15,** 813–826 (2012).
17. Valvano, M. A., Messner, P. & Kosma, P. Novel pathways for biosynthesis of nucleotide-activated glycero-manno-heptose precursors of bacterial glycoproteins and cell surface polysaccharides. *Microbiology* **148,** 1979–1989 (2002).
18. Westfall, C. S. & Levin, P. A. Comprehensive analysis of central carbon metabolism illuminates connections between nutrient availability, growth rate, and cell morphology in Escherichia coli. *PLOS Genet.* **14,** e1007205 (2018).
19. De Leon, G. P., Elowe, N. H., Koteva, K. P., Valvano, M. A. & Wright, G. D. An in vitro screen of bacterial lipopolysaccharide biosynthetic enzymes identifies an inhibitor of ADP-heptose biosynthesis. *Chem. Biol.* **13,** 437–441 (2006).
20. Harmer, N. J. The Structure of Sedoheptulose-7-Phosphate Isomerase from Burkholderia pseudomallei Reveals a Zinc Binding Site at the Heart of the Active Site. *J. Mol. Biol.* **400,** 379–392 (2010).
21. Harris, L. K. & Theriot, J. A. Relative Rates of Surface and Volume Synthesis Set Bacterial Cell Size. *Cell* **165,** 1479–1492 (2016).
22. Wallden, M., Fange, D., Lundius, E., Baltekin, O. & Elf, J. The synchronization of replication and division cycles in individual E. coli cells. *Cell* **166,** 729–739
23. Zheng, H. *et al.* Interrogating the Escherichia coli cell cycle by cell dimension perturbations. *Proc. Natl. Acad. Sci. U. S. A.* **113,** 15000–15005 (2016).
24. Conant, G. C. & Wolfe, K. H. Turning a hobby into a job: how duplicated genes find new functions. *Nat. Rev. Genet.* **9,** 938–950 (2008).
25. Datsenko, K. A. & Wanner, B. L. One-step inactivation of chromosomal genes in Escherichia coli K-12 using PCR products. *Proc. Natl. Acad. Sci. U. S. A.* **97,** 6640–5

(2000).

26. Russell., S. and. *Molecular Cloning: a laboratory manual 3rd Edition.* (CSHL Press.).

27. van den Ent, F. & Lowe, J. RF cloning: a restriction-free method for inserting target genes into plasmids. *J. Biochem. Biophys. Methods* **67,** 67–74 (2006).

Acknowledgements

We thank Prof. Arvand Haschemi (Medical University of Vienna, Vienna, Austria) for his generous gift of sedoheptulose and CARKL kinase. We also thank dr Beata Walter, dr Lidia Boss, and Robert Droczek for assistance with experiments. This work was supported by the National Science Center (Poland) No. [UMO-2014/13/B/NZ2/01139 to M.G., UMO-2016/23/N/NZ2/02378 to J.M.O.].

Author contribution

A.B. – designed and performed experiments, wrote the manuscript; J.M-O. – designed and performed experiments, analyzed the data, wrote the manuscript; M.B. – wrote the manuscript; J.G. – performed experiments; T.W. – consulted and performed experiments, revised the manuscript; A.Z-P. – consulted experiments, revised the manuscript; M.G. – conceptualized the work, interpreted the data, revised the manuscript.

Competing interests

The authors declare no competing interests.

Figures

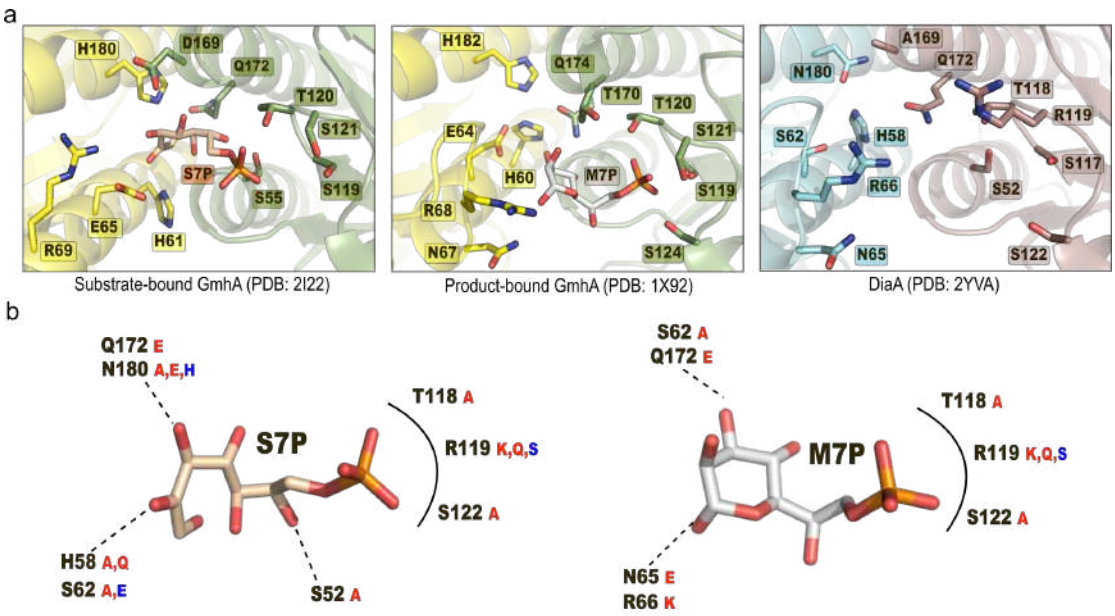

Fig. 1. Structural similarity of the DiaA SIS domain to the S7P/M7P biding pocket of GmhA a) Residues important for S7P substrate (left panel) and M7P product (middle panel) binding in the active center of GmhA, and the equivalent residues in the potential DiaA S7P binding pocket (right panel). The cartoon representations of the two adjacent monomers are shown in green and yellow for GmhA or in cyan and pink for DiaA. Conserved residue side chains are shown as sticks with atomic colouring b) Structural models of S7P and M7P together with potential ligand-binding residues of DiaA. Proposed hydrogen bonds are marked by dashed lines; proposed phosphate binding pocket – by solid line. Alterations introduced to disrupt S7P/M7P binding are depicted in red and those designed to restore isomerase catalytic centre- in blue.

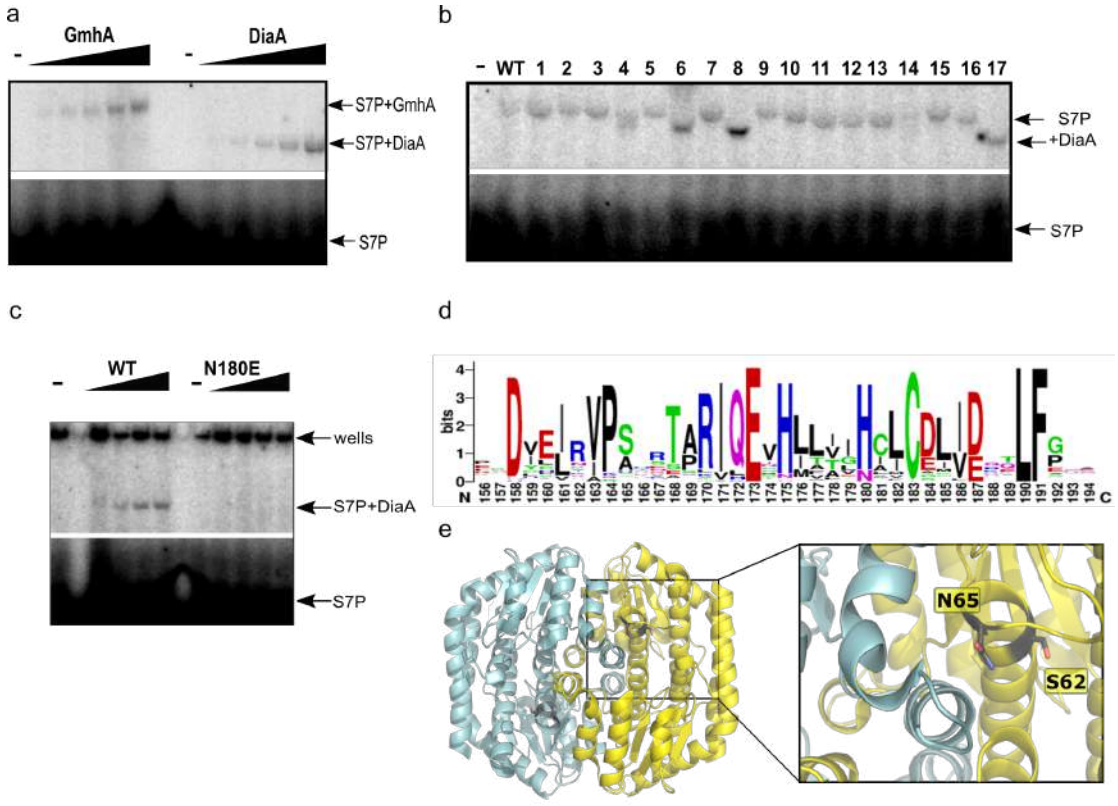

Fig. 2. DiaA binds S7P *in vitro* and this interaction can be abolished by changing conserved Arg180. a) S7P binding assay with purified DiaA and GmhA. Radioactively labelled S7P was incubated with increasing concentrations (4-30 μM) of the proteins as indicated above the gel. Positions of the resulting complexes are indicated by arrows. b) Properties of the DiaA variants with alterations in the SIS domain. EMSA of the complexes formed with S7P by the following DiaA variants: wild-type (WT), S52A(1), H58Q (2), H58A (3), S62E (4), S62A (5), N65E (6), R66K (7), N65E+R66K (8), T118A+S122A (9), R119K (10), R119Q (11), R119S (12), Q172E (13), N180E (14), N180H (15), N180A (16), S62E+R119S+N180H (17). Positions of the complexes are indicated by arrows. c) DiaA N180E variant does not bind S7P. Radioactively labelled S7P was incubated with increasing concentrations (4-30 μM) of the wild-type (WT) or mutant protein as indicated above the gel. Positions of the formed complexes are indicated by arrows. d) Sequence conservation of DiaA residue 180, with invariable histidine or asparagine at that position in 62 bacterial species. e) Position of DiaA residues Asn65 and Ser62

within the tetramerization region of DiaA. Both residues (shown as sticks with atomic colouring) lie on the interface between two adjacent DiaA dimers (in yellow and cyan).

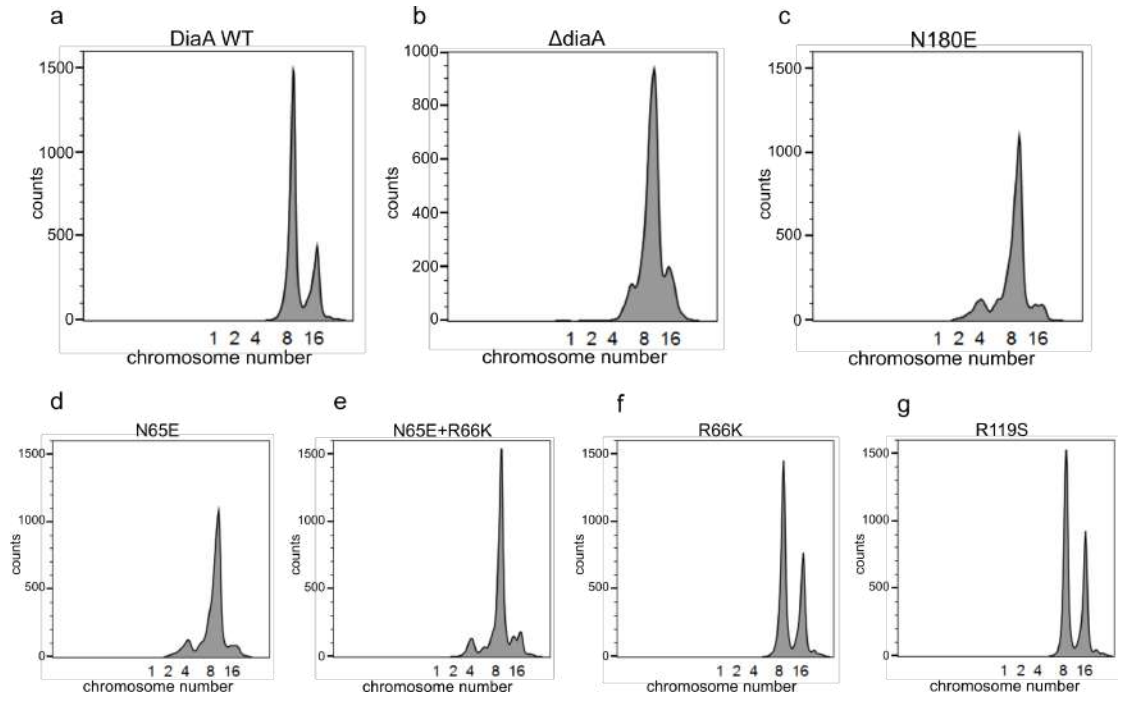

Fig. 3. Mutation impeding S7P binding results in aberrant replication control. Flow cytometry analysis of chromosomal DNA content in (a) wild-type strain, (b) knock-out DiaA strain, (c-g) strains carrying selected DiaA variants replacing the wild-type gene at its native position. The cell counting was performed following replication run-out and DNA staining with Cytox Green. Positions of the cell fractions containing 2, 4, 8, or 16 chromosomes are indicated based on the wild-type slow- (2 and 4) and fast-growth (8 and 16) control samples.

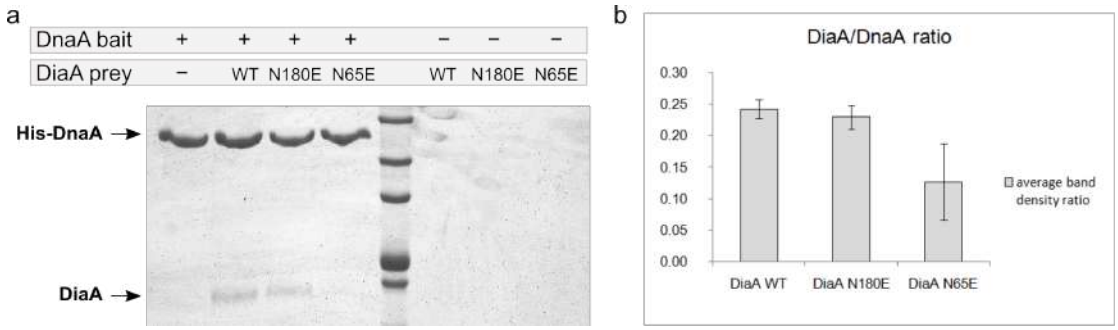

Fig. 4. ***In vitro*** **characterization of the DiaA-DnaA interactions**. a) Pull-down assay employing tagged DnaA and wild-type DiaA or its variants. DiaA-DnaA direct interaction is not disturbed in DiaA variant unable to bind S7P (N180E), but is reduced in the variant unable to tetramerize (N65E). b) Relative binding of wt and mutated DiaA variants to DnaA assessed by densitometry. Bars indicate standard deviation determined from 3 independent experiments.

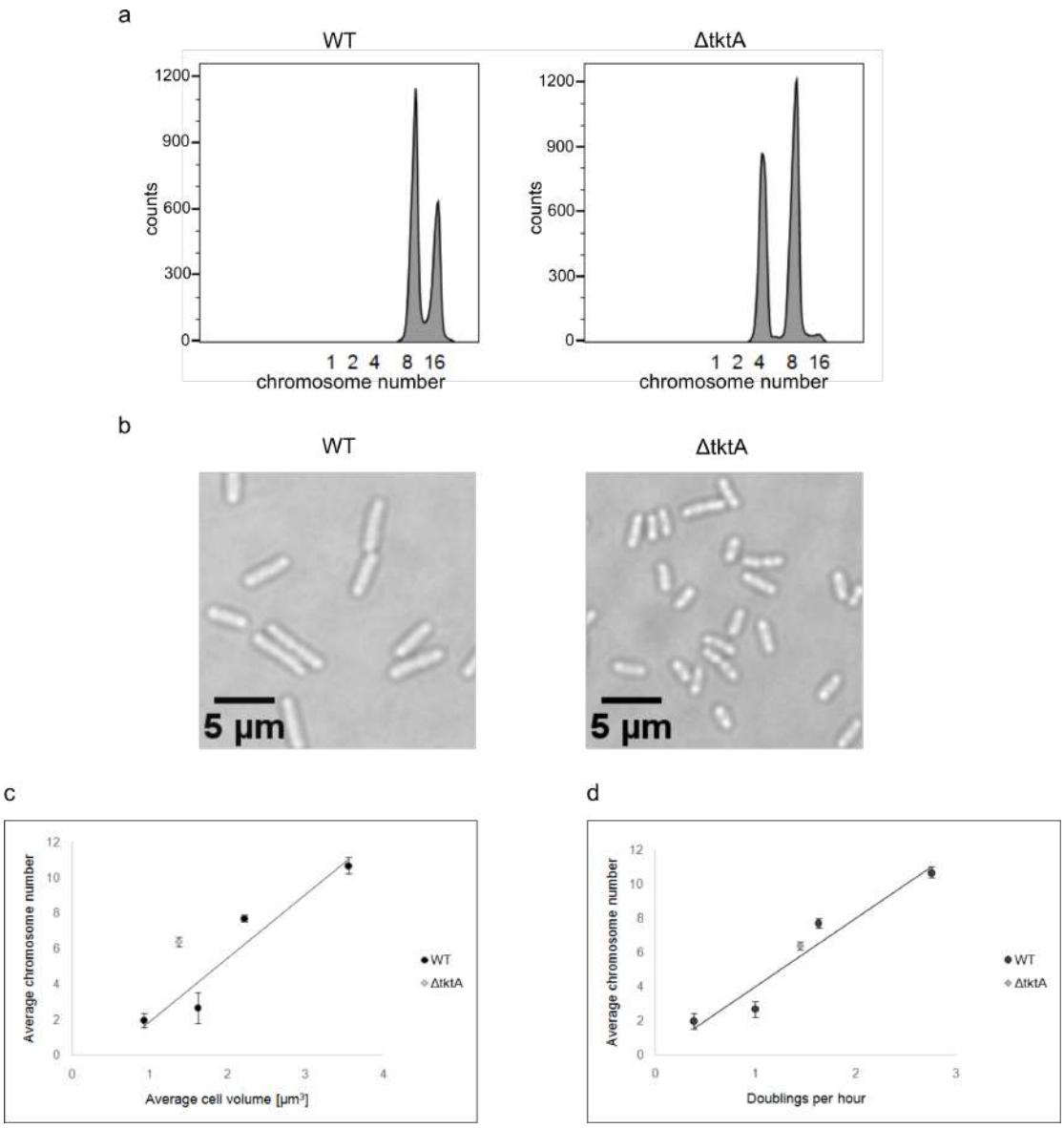

Fig. 5. Depletion of the cellular S7P pool by the *tktA* deletion influences DNA replication control. a) Flow cytometry analysis of chromosomal DNA content in the cell populations of the wild-type strain and the *ΔtktA* mutant, performed following replication run-out and DNA staining with Sytox Green. Positions of the cell fractions containing 2, 4, 8 or 16 chromosomes are indicated based on the wild-type slow- (2 and 4) and fast-growth (8 and 16) control samples. b) Morphology comparison of the wild-type and *ΔtktA* mutant cells. Phase-contrast images have the same 5 microns scale bar. c) Relation of chromosomal content to cell volume in wild-type cells (black circles) growing in media supporting different growth rates: LB, ABgc, ABg, ABac

(as described in Methods). This relation for *ΔtktA* mutants growing in LB medium is shown by grey circle. The number of chromosomes in cell populations was determined by flow cytometry. Cell volume was calculated on the basis of microscope images; 800 cells were analysed for each sample. Bars indicate standard deviation determined from 3 independent experiments (n=3). d) Relation of chromosomal content to growth rate in wild-type cells (black circles) cultivated under nutrient conditions supporting different growth rates: LB, ABgc, ABg, ABac (as described in Methods). This relation for *ΔtktA* mutants growing in LB medium is shown by grey circle. The number of chromosomes in cell populations was determined by flow cytometry. Bars indicate standard deviation determined from 3 independent experiments.

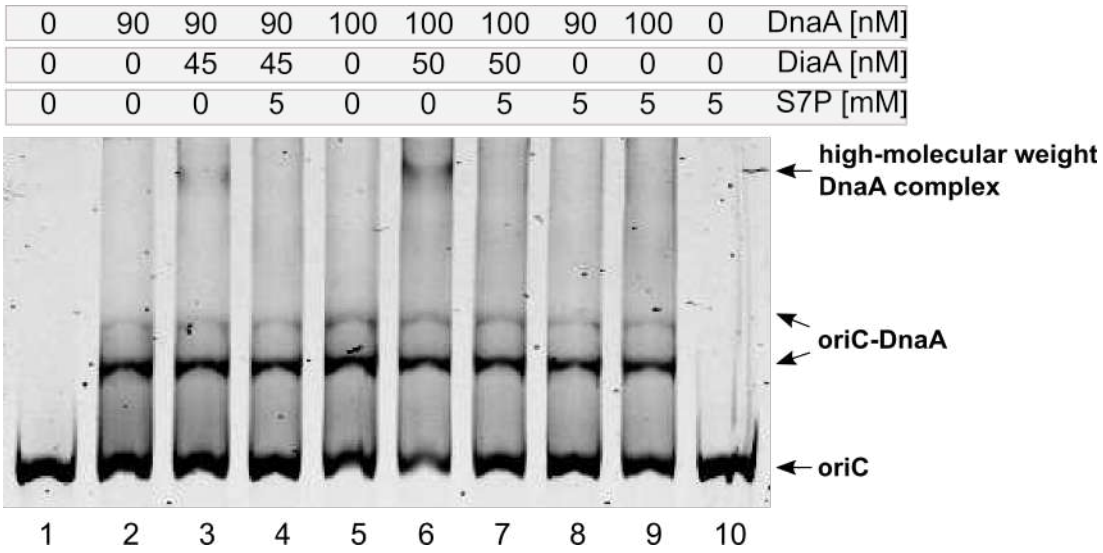

Fig. 6. S7P binding influences DiaA activity EMSA with fluorescently-labelled oriC DNA fragment investigating the effects of DiaA-S7P complex on DnaA oligomerization on oriC. High molecular weight DnaA-oriC complexes do not form in the presence of the pre-formed DiaA-S7P complex

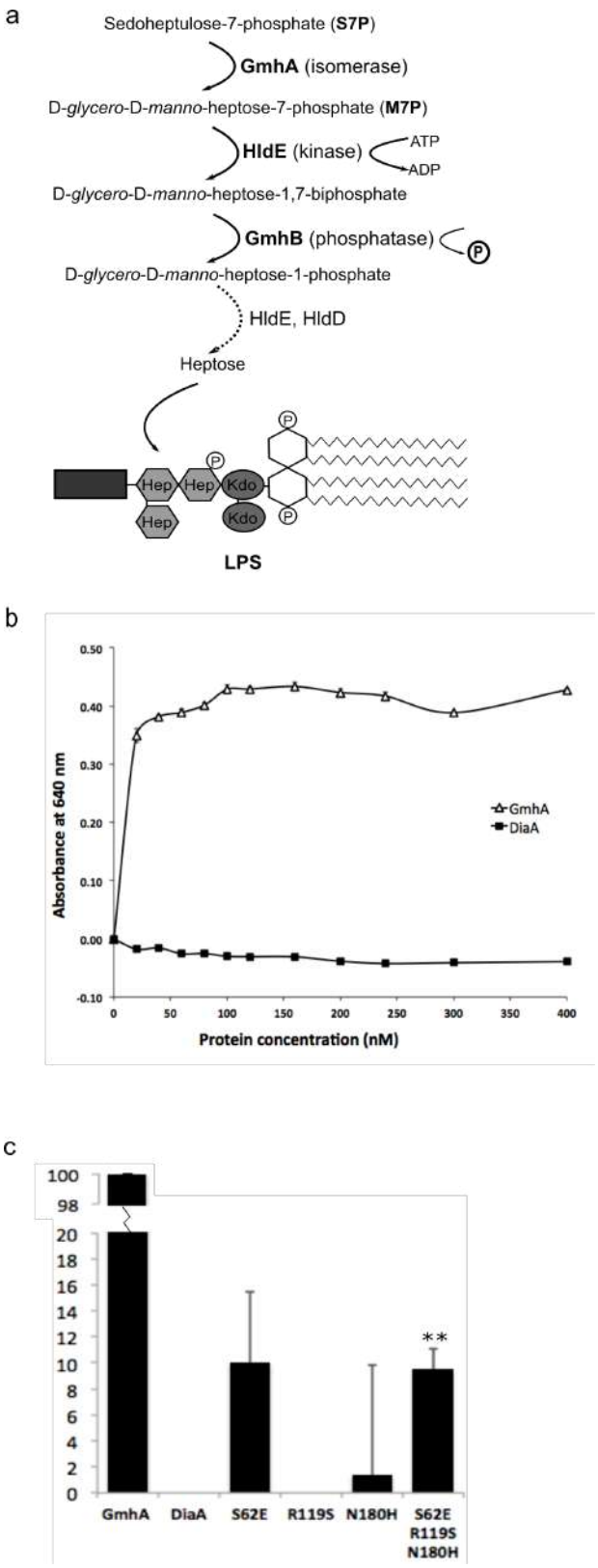

Fig. 7. DiaA does not isomerize S7P to M7P but its catalytic activity can be stimulated as the key catalytic centre residues converge with those of GmhA a) Initial stages of LPS inner core synthesis pathway, utilized in this work to measure GmhA and DiaA isomerase activity.

Enzyme names are shown in bold. The released free phosphate is shown as circled P. b) GmhA and DiaA isomerase activity as measured by phosphate release in the Malachite Green/molybdate/phosphate green complex formation assay. c) Isomerization activity of the DiaA variants as measured by phosphate release in the Malachite Green/molybdate/phosphate green complex formation assay, shown as a percentage of GmhA isomerization activity. Bars indicate standard deviation determined from 3 independent experiments (n=3). **p< 0.05 (Student's test).

Table 1. Summary of the performed mutational analysis of the predicted S7P-binding pocket of DiaA. Catalytic residues of GmhA are highlighted in red. GmhA residues are numbered according to *E. coli* GmhA sequence for phosphate binding pocket and S7P-interacting residues or to *P. aeruginosa* sequence for M7P-interacting residues. Asterisk denotes residues involved in both S7P and M7P interactions.

Predicted function of the protein region	**DiaA residue**	**GmhA residue**	**Characteristics of the protein variants**			
			Altered residue(s)	**S7P binding**	**Tetramerization**	**interaction with DnaA**
S7P/M7P phosphate binding pocket	Thr118	Thr120	T118A+S122A	+	+	ND
	Ser122	Ser124				
	Arg119	Ser121	R119K	+	+	ND
			R119Q	+	+	ND
			R119S	+	+	ND
Interaction with the functional groups of S7P	Ser52	Ser55	S52A	+	+	ND
	His58	His61	H58Q	+	+	ND
			H58A	+	+	ND
	Ser62	Glu65*	S62A	+	+	ND
			S62E	+	-	<wt
	Gln172	Gln172*	Q172E	+	+	ND
	Asn180	His180	N180E	-	+	+
			N180A	+	+	ND
			N180H	+	+	ND
			S62E+R119S+N180H	+	-	ND
Interaction with the functional groups of M7P	Asn65	Asn67	N65E	+	-	<wt
	Arg66	Arg68	R66K	+	+	ND
			N65E+R66K	+	-	ND

Suplement

Supplementary figures

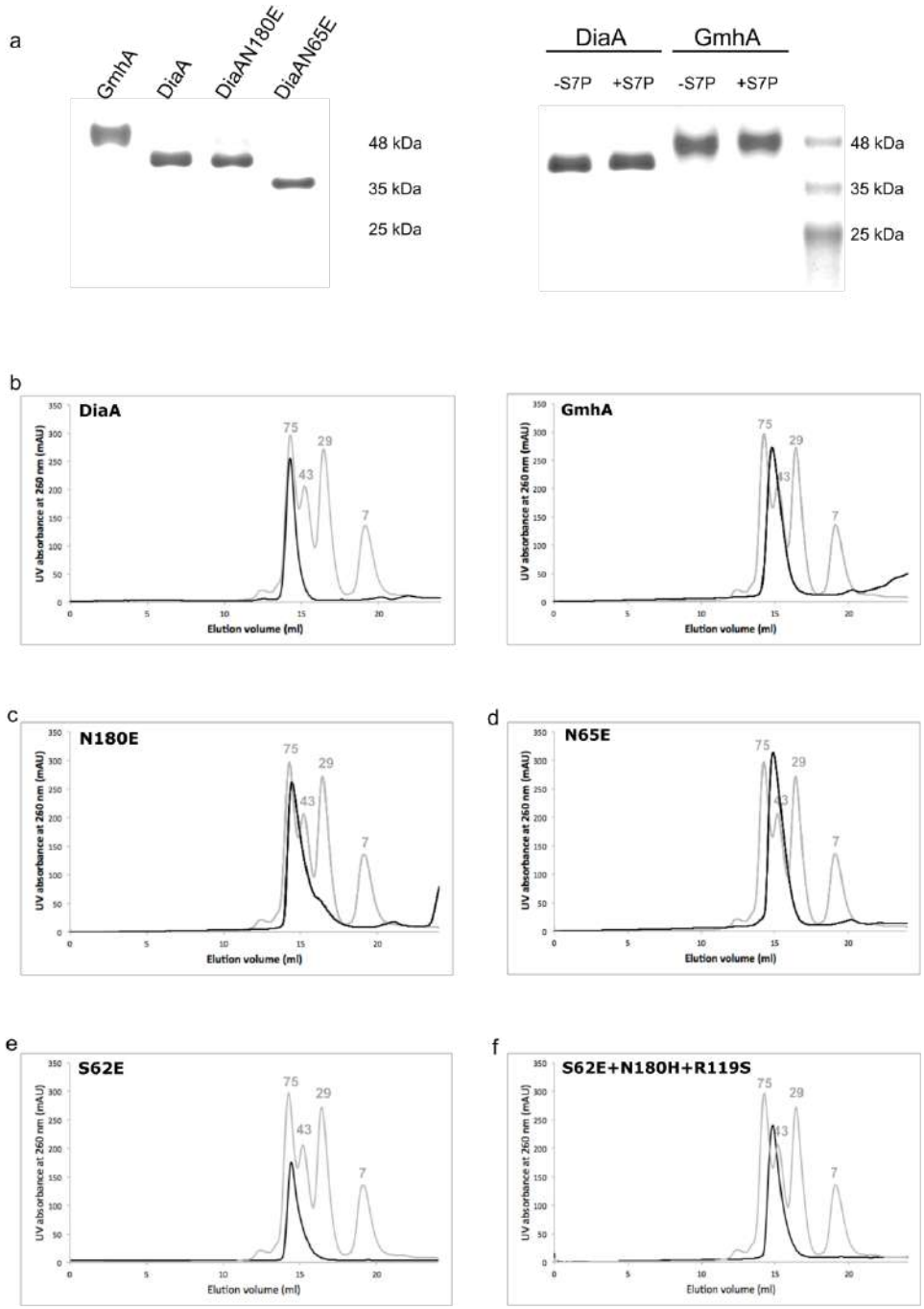

Fig. S1. (a) Native acrylamide gel electrophoresis of GmhA and DiaA and its variants, in the presence and absence of S7P (as indicated); (b) Analysis of protein size by analytical size-exclusion chromatography. Elution profiles of DiaA and GmhA from a Superdex 200 gel filtration column, detected at 260 nm, overlaid with protein standard with sizes as indicated. The elution profiles suggest that DiaA forms tetramers in solution, while GmhA forms smaller species likely corresponding to the dimer-tetramer equilibrium.

(**c-f**) **Oligomerization states of DiaA variants as analysed by size-exclusion chromatography on a Superdex 200 gel filtration column.** The complexes were detected at 260 nm, and the elution profiles overlaid with protein standard (sizes as indicated). DiaA N180E (c) and S62E (d) form tetramers in solution, while N65E (e) and the triple mutant S62E+N180H+R119S (f) remain dimeric in these conditions.

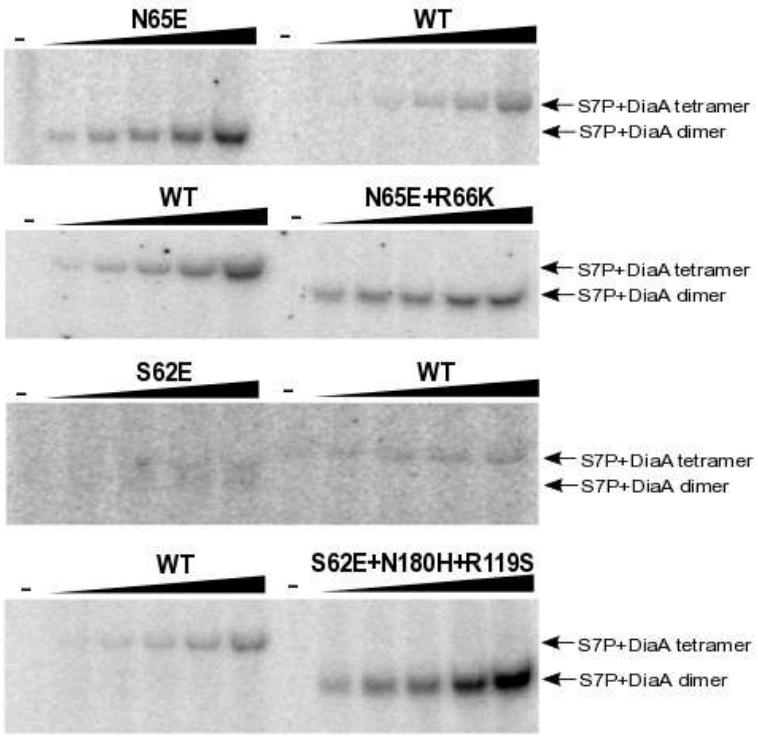

Fig. S2. EMSA showing S7P biding by the indicated DiaA variants. Radioactively labelled S7P was incubated with increasing concentrations (4-30 µM) of. DiaA N65E, N65E+R66K, S62E, or S62E+N180H+R119S. Resulting complexes were separated on a native polyacrylamide gel and visualized by autoradiography. Positions of the formed complexes are indicated by arrows.

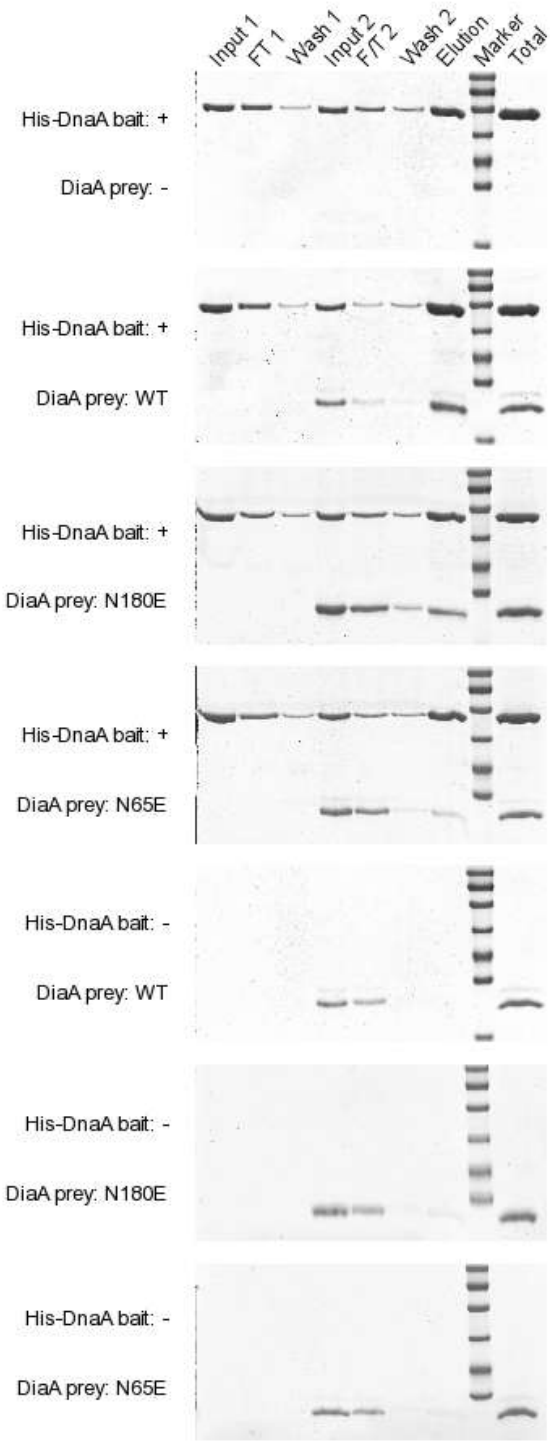

Fig. S3. Pull-down assay with His-DnaA 'bait' and DiaA (wild-type and variants) 'prey' on Nickel beads. Lanes: Input – loaded DnaA (1) or DiaA (2) sample; F/T –unbound proteins in the flow-through; Wash – wash with buffer containing 40 mM imidazole; Elution – elution with SDS sample buffer. The presence of DiaA or its variants in the elution fraction containing His-DnaA (top three panels) indicates direct interaction with His-DnaA since DiaA does not interact

with the beads on its own (lower three panels). The total amounts of loaded proteins are shown for reference.

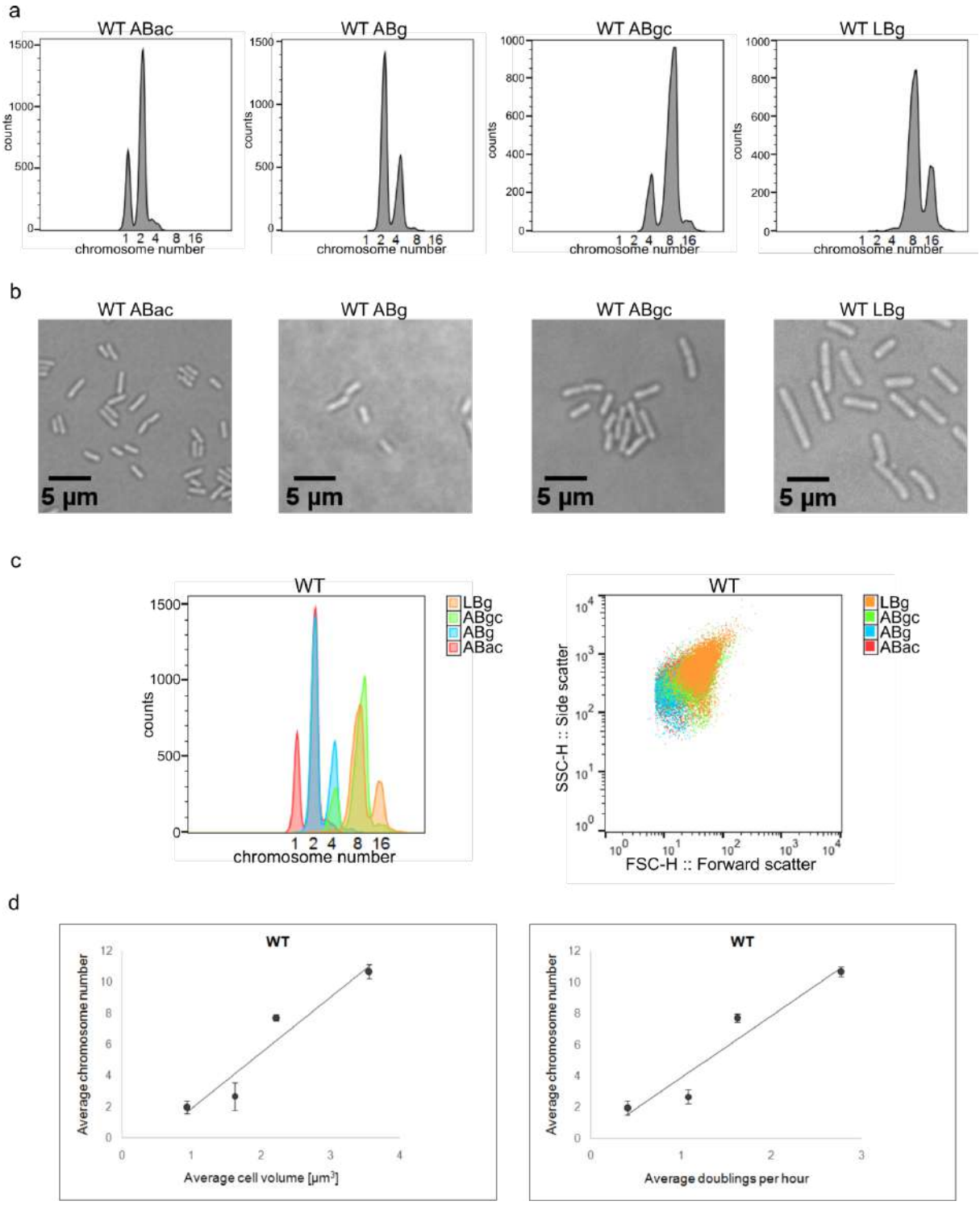

Fig. S4. Chromosomal content in wild-type cells cultivated in media supporting different growth rates: LB, ABgc, ABg, ABac (as described in Materials and Methods) a) Flow cytometry analysis of chromosomal DNA content in wild-type cell population performed following replication run-out and DNA staining with Sytox Green. Positions of the cell fractions

containing 1, 2, 4, 8 or 16 chromosomes are indicated. b) Morphology comparison of the wild-type cells under different growth rates. Phase-contrast images have the same 5 microns scale bar. c) Histogram showing positions of peaks produced in flow cytometry experiment by cells containing different chromosome number, from all tested media (left panel). (right panel) Scatter plot of flow cytometry forward scatter (FSC) and side scatter (SSC) for cells grown under all tested conditions d) Relation of chromosomal content to cell volume (left panel) or doubling time (right panel) in wild-type cells growing in media supporting different growth rates. The number of chromosomes in cell populations was determined by flow cytometry. Cell volume was calculated on the basis of microscope images; 800 cells were analysed for each sample. Bars indicate standard deviation determined from 3 independent experiments (n=3).

Supplementary tables

Table 1. *Escherichia coli* strains used in this study

strain	genotype	description
MG1655 (WT)	K-12 F⁻ λ⁻ *ilvG⁻ rfb-50 rph-1*	Wild type strain
MG1655 diaA_S52A	K-12 F⁻ λ⁻ *ilvG⁻ rfb-50 rph-1 diaA::diaAS52A:catR*	*diaA* chromosomal mutants
MG1655 diaA_H58Q	K-12 F⁻ λ⁻ *ilvG⁻ rfb-50 rph-1 diaA::diaAH58Q:catR*	
MG1655 diaA_H58A	K-12 F⁻ λ⁻ *ilvG⁻ rfb-50 rph-1 diaA::diaAH58A:catR*	
MG1655 diaA_S62E	K-12 F⁻ λ⁻ *ilvG⁻ rfb-50 rph-1 diaA::diaAS2E:catR*	
MG1655 diaA_S62A	K-12 F⁻ λ⁻ *ilvG⁻ rfb-50 rph-1 diaA::diaAS62A:catR*	
MG1655 diaA_N65E	K-12 F⁻ λ⁻ *ilvG⁻ rfb-50 rph-1 diaA::diaAN65E:catR*	
MG1655 diaA_R66K	K-12 F⁻ λ⁻ *ilvG⁻ rfb-50 rph-1 diaA::diaAR66K:catR*	
MG1655 diaA_N65E_R66K	K-12 F⁻ λ⁻ *ilvG⁻ rfb-50 rph-1 diaA::diaAN65ER66K:catR*	
MG1655 diaA_T118A_S122A	K-12 F⁻ λ⁻ *ilvG⁻ rfb-50 rph-1 diaA::diaAT118AS122A:catR*	
MG1655 diaA_R119K	K-12 F⁻ λ⁻ *ilvG⁻ rfb-50 rph-1 diaA::diaAR119K:catR*	
MG1655 diaA_R119Q	K-12 F⁻ λ⁻ *ilvG⁻ rfb-50 rph-1 diaA::diaAR119Q:catR*	
MG1655 diaA_R119S	K-12 F⁻ λ⁻ *ilvG⁻ rfb-50 rph-1 diaA::diaAR119S:catR*	
MG1655 diaA_Q172E	K-12 F⁻ λ⁻ *ilvG⁻ rfb-50 rph-1 diaA::diaAQ172E:catR*	
MG1655 diaA_N180E	K-12 F⁻ λ⁻ *ilvG⁻ rfb-50 rph-1 diaA::diaAN180E:catR*	

MG1655 diaA_N180H	K-12 F^- λ^- *ilvG*$^-$ *rfb-50 rph-1 diaA::diaAN180H:catR*	
MG1655 diaA_N180A	K-12 F^- λ^- *ilvG*$^-$ *rfb-50 rph-1 diaA::diaAN180A:catR*	
MG1655 diaA_S62E_R119S	K-12 F^- λ^- *ilvG*$^-$ *rfb-50 rph-1 diaA::diaAS62ER119S:catR*	
MG1655 diaA_S62E_N180H_R119S	K-12 F^- λ^- *ilvG*$^-$ *rfb-50 rph-1 diaA::diaAS62EN180HR119S:catR*	
MG1655 ΔdiaA (kan)	K-12 F^- λ^- *ilvG*$^-$ *rfb-50 rph-1 diaA::kanR*	*diaA* knockout strain (kanamycine restistant)
MG1655 ΔdiaA (cm)	K-12 F^- λ^- *ilvG*$^-$ *rfb-50 rph-1 diaA::catR*	*diaA* knockout strain (chloramphenicol restistant)
MG1655 ΔtktA	K-12 F^- λ^- *ilvG*$^-$ *rfb-50 rph-1 tktA::kanR*	*tktA* knockout strain (kanamycine restistant)
BL21 (DE3)	*E. coli* str. B F^- *ompT gal dcm lon hsdS*$_B$(r_B^- m_B^-) λ(DE3 [*lacI lacUV5-T7p07 ind1 sam7 nin5*]) [*malB*$^+$]$_{K\text{-}12}$(λ^S)	T7 expression strain for protein purification
BW25142	lacIq, rrnB3, del(lacZ)4787, hsdR514, DE(araBAD)567,DE(rhaBAD)568, del(phoBR)580, rhp-1, galU95, del(endA)9,uidA(delMluI)::pir116, recA1	Host strain (pir+) for pKD3 plasmid (and derivatives)
DH5α	F^- *endA1 glnV44 thi-1 recA1 relA1 gyrA96 deoR nup G purB20* ϕ80d*lacZ*ΔM15 Δ(*lacZYA-argF*)U169, hsdR17(r_K^- m_K^+), λ^-	

Table 2. Plasmids used in this study.

plasmid	description
pET28	T7 expression vector
pET28-DiaA	T7 expression vector with N-terminal His-SUMO gene fusions
pET28-DnaA	
pET28-GmhA	
pET28-GmhB	
pET28-HldE	
pET28-DiaA S52A	T7 expression vector with N-terminal His-SUMO gene fusions for DiaA mutants expression and purification.
pET28-DiaA H58Q	
pET28-DiaA H58A	
pET28-DiaA S62E	
pET28-DiaA S62A	
pET28-DiaA N65E	
pET28-DiaA R66K	
pET28-DiaA N65E R66K	
pET28-DiaA T118A S122A	

pET28-DiaA R119K	
pET28-DiaA R119Q	
pET28-DiaA R119S	
pET28-DiaA Q172E	
pET28-DiaA N180E	
pET28-DiaA N180H	
pET28-DiaA N180A	
pET28-DiaA T118A	
pET28-DiaA S62A R119S	
pKD3	Plasmid bearing FRT-flanked chloramphenicol resistance casette
pKD3-DiaA S52A	Plasmid bearing FRT-flanked chloramphenicol resistance casette and a mutated diaA gene to amplify linear PCR product used for λ-red recombination
pKD3-DiaA H58Q	
pKD3-DiaA H58A	
pKD3-DiaA S62E	
pKD3-DiaA S62A	
pKD3-DiaA N65E	
pKD3-DiaA R66K	
pKD3-DiaA N65E R66K	
pKD3-DiaA T118A S122A	
pKD3-DiaA R119K	
pKD3-DiaA R119Q	
pKD3-DiaA R119S	
pKD3-DiaA Q172E	
pKD3-DiaA N180E	
pKD3-DiaA N180H	
pKD3-DiaA N180A	
pKD3-DiaA T118A	
pKD46	Plasmid containing λ-red recombination system under the control of arabinose inducible promoter

Table 3. Primers used in this study.

primer	5’-3’ sequence	description
p28_gmhA_for_BamHI	GATCGGATCCATGTACCAGGATCTTATTCGTAACGAACTG	Primers for *diaA* and *gmhA* cloning into pET28 using BamHI and XhoI
p28_gmhA_rev XhoI	GATCCTCGAGTTACTTAACCATCTCTTTTTCAATCAACTGGATC	
p28_diaA_for BamHI	GATCGGATCCGTGCAAGAAAGAATTAAAGCTTGCTTCAC	
p28_diaA_rev XhoI	GATCCTCGAGTTAATCATCCTGGTGAGGGAAAAGC	
p28_gmhB RF for	GATCGGATCCGTGGCGAAGAGCGTACCC	Primers for restriction free cloning into pET28
p28_gmhB RF rev	ATCCTCGAGTCATTGTGCCGGTTTTGCTGC	
p28_hldE RF for	GATCGGATCCATGAAAGTAACGCGCCAGAG	
p28_hldE RF rev	GATCCTCGAGTTAGCCTTTTTTATCCTGTTGGATCTTC	
p28_dnaA RF for	CCAGGAACAAACCGGTGGATCCGTGTCACTTTCGCTTTGGC	

p28_dnaA RF rev	GGTGGTGGTGCTCGAGAGGCCTTTACGATGACAATGTTCTGATTAAA	
T7for	TAATACGACTCACTATAGGG	pET28 screening/sequencing primers
T7 rev	CAAGACCCGTTTAGAGGCC	
pKD3_diaA RF for	GCAGCATTACACGTCTTGAGCGATTGTGCAAGAAAGAATTAAAGCTTGC	Primers for restriction free cloning into pKD3
pKD3_diaA RF rev	TTCGAAGCAGCTCCAGCCTACATTAATCATCCTGGTGAGGGAAAA	
pKD3 for	AGATTGCAGCATTACACGTCTTG	pKD3 screening/sequencing primers
pKD3 rev	TATGGCAATGAAAGACGGTGAG	
S52A	CAAAATCCTCTGTTGTGGTAATGGAACTGCCGCTGCCAATGCACAG	Primers for *diaA* mutagenesis
H58Q	GCTGCCAATGCACAGCAGTTTGCTGCCAGCATGATCAAC	
H58A	CCGCTGCCAATGCACAGGCTTTTGCTGCCAGCATGATCAAC	
S62E	CAATGCACAGCATTTTGCTGCCGAAATGATCAACCGTTTCGAAACGGAG	
S62A	CAATGCACAGCATTTTGCTGCCGCCATGATCAACCGTTTCGAAACGGAG	
N65E	GCATTTTGCTGCCAGCATGATCGAACGTTTCGAAACGGAGCGG	
R66K	CATTTTGCTGCCAGCATGATCAACAAATTCGAAACGGAGCGGCC	
N65E R66K	GCATTTTGCTGCCAGCATGATCGAGAAATTCGAAACGGAGCGGC	
T118A S122A	CGCCCGTGGCAACGCCCGCGATATTGTTAAAGCAGTTGAAG	
R119K	GGAGATGTATTGTTAGCCATTTCCACCAAAGGCAACAGCCGCGATATTG	
R119Q	GAGATGTATTGTTAGCCATTTCCACCCAGGGCAACAGCCGCGATATTG	
R119S	GGAGATGTATTGTTAGCCATTTCCACCTCTGGCAACAGCCGCGATATGG	
Q172E	CGCATCGTAGTGCTCGCATTGAAGAAATGCATATGCTGACGGTAAATTGC	
N180E	CAGGAAATGCATATGCTGACGGTAGAATGCCTGTGCGATCTGATCG	
N180H	CAGGAAATGCATATGCTGACGGTACATTGCCTGTGCGATCTGATCG	
N180A	CAGGAAATGCATATGCTGACGGTAGCTTGCCTGTGCGATCTGATCG	
T118A	CGGGAGATGTATTGTTAGCCATTTCCGCCCGTGGCAACAGCC	
DiaA_RED_HR for	GATTAAGGATGCCTTTAATGACCACTCATAATTAAGGTTTAAGGATTAGCGTGCAAGAAAGAATTAAAGCTTGC	Primers for λ-red based integration of *diaA* variants into E. coli chromosome. Contain 50 bp homology to the genome integration site.
DiaA_RED_HR rev	AGCGCGGAAATAAGGACTGCGATTGGCGATAATGCCTTCATGTATTCTCCATGGGAATTAGCCATGGTCC	
DiaA upstream for	TTTGATACTGTGGATTGCCGGTTC	

DiaA downstream rev	GACACTGCGTGGGTCAGTTG	Screening/sequencing primers to confirm proper integration of *diaA* chromosomal mutants.

Wkład autorów – oświadczenia

Uniwersytet Gdański

mgr Joanna Morcinek-Orłowska
Katedra Genetyki Molekularnej Bakterii
Wydział Biologii
Uniwersytet Gdański

Gdańsk, 01.06.2025 r.

Oświadczenie o wkładzie w publikację

Oświadczam, że mój wkład w manuskrypt artykułu oryginalnego:

Bebel A*, Morcinek-Orłowska J*, Banzhaf M, Galińska J, Waldminghaus T, Zawilak-Pawlik A, Glinkowska M, Interaction of the replication factor DiaA and primary metabolite sedoheptulose 7-phosphate regulates DNA replication in Escherichia coli

*wkład równorzędny

obejmował:

- zaprojektowanie i wykonanie eksperymentów (udział w konstrukcji wektorów ekspresyjnych i oczyszczaniu białek, określenie stanu oligomerycznego białek, udział w identyfikacji wiązania DiaA-S7P *in vitro* i określeniu aktywności enzymatycznej, analiza wiązania DiaA-DnaA in vitro, analiza wiązania DnaA do *oriC* w obecności DiaA, analiza ilości chromosomów i czasu inicjacji replikacji metodą cytometrii przepływowej po zatrzymaniu replikacji dla szczepów *E. coli* z mutacjami w genie diaA i delecjami genów metabolicznych)
- analizę uzyskanych wyników i wizualizację danych
- napisanie wstępnej wersji manuskryptu, wspólnie z Aleksandrą Bebel

Joanna Morcinek-Orłowska

Wydział Biologii
Uniwersytetu Gdańskiego
Katedra Genetyki
Molekularnej Bakterii

tel. +48 58 523 60 65
e-mail: mol.KGB@ug.edu.pl

ul. Wita Stwosza 59
80-309 Gdańsk

www.ug.edu.pl

Dr. Aleksandra Bebel
BIMOVIS GmbH
Nikola-Tesla-Str. 1
69124 Heidelberg
Niemcy

Heidelberg, 10.06.2025

Oświadczenie o wkładzie w manuskrypt publikacji

Oświadczam, że mój wkład w manuskrypt artykułu oryginalnego:

Bebel A*, Morcinek-Orłowska J*, Banzhaf M, Galińska J, Waldminghaus T, Zawilak-Pawlik A, Glinkowska M, Interaction of the replication factor DiaA and primary metabolite sedoheptulose 7-phosphate regulates DNA replication in *Escherichia coli*

*wkład równorzędny

obejmował:

- analizę struktury DiaA oraz GmhA, zaprojektowanie mutagenezy miejscowo-specyficznej
- zaprojektowanie i wykonanie eksperymentów (konstrukcja wektorów ekspresyjnych, oczyszczanie białek, identyfikacja wiązania DiaA-S7P in vitro, określenie aktywności enzymatycznej GmhA i DiaA in vitro, uczestnictwo w analizie ilości chromosomów i czasu inicjacji replikacji metodą cytometrii przepływowej po zatrzymaniu replikacji)
- analizę uzyskanych wyników i wizualizację danych
- napisanie wstępnej wersji manuskryptu, wspólnie z Joanną Morcinek-Orłowską

Aleksandra Bebel

mgr Justyna Galińska
Cebertowicza 4/32
80-809 Gdańsk
e-mail: justyna.galinska95@gmail.com

Gdańsk, 26.05.2025

Oświadczenie o wkładzie w manuskrypt publikacji

Oświadczam, że mój wkład w manuskrypt artykułu oryginalnego:

Bebel A*, Morcinek-Orłowska J*, Banzhaf M, Galińska J, Waldminghaus T, Zawilak-Pawlik A, Glinkowska M, Interaction of the replication factor DiaA and primary metabolite sedoheptulose 7-phosphate regulates DNA replication in *Escherichia coli*

*wkład równorzędny

obejmował:

- udział w wykonaniu części eksperymentów (oczyszczanie białek, analiza ilości chromosomów i czasu inicjacji replikacji metodą cytometrii przepływowej po zatrzymaniu replikacji dla szczepów delecyjnych *E. coli*)

26.05.25
Justyna Galińska

TECHNISCHE UNIVERSITÄT DARMSTADT

Technical University Darmstadt | Schnittspahnstraße 12 | 64287 Darmstadt, Germany

Faculty of Biology

Molecular Microbiology

Prof. Dr.
Torsten Waldminghaus

Schnittspahnstraße 12
64287 Darmstadt
Germany

Tel. +49 (0) 6151 / 16 - 20332
Fax +49 (0) 6151 / 16 - 23672
torsten.waldminghaus@tu-darmstadt.de

Darmstadt, 25-11-17

To whom it may concern

Author contribution statement

I hereby declare that my contribution to the research article:

Bebel A*, Morcinek-Orłowska J*, Banzhaf M, Galińska J, Waldminghaus T, Zawilak-Pawlik A, Glinkowska M, Interaction of the replication factor DiaA and primary metabolite sedoheptulose 7-phosphate regulates DNA replication in *Escherichia coli*

*equal contribution

included:

- providing the expertise on flow cytometry and replication run-out method
- performing initial flow cytometry assays after replication run-out on genomic *diaA* mutants
- advisory support on data analysis
- revision of the final manuscript

Prof. Dr. Torsten Waldminghaus

Uniwersytet Gdański

dr hab. Monika Glinkowska, prof. UG
Katedra Genetyki Molekularnej Bakterii
Wydział Biologii
Uniwersytet Gdański

Gdańsk, 09.06.2025 r.

Oświadczenie o wkładzie w manuskrypt publikacji

Oświadczam, że mój wkład w manuskrypt artykułu oryginalnego:

Bebel A*, Morcinek-Orłowska J*, Banzhaf M, Galińska J, Waldminghaus T, Zawilak-Pawlik A, Glinkowska M, Interaction of the replication factor DiaA and primary metabolite sedoheptulose 7-phosphate regulates DNA replication in Escherichia coli

*wkład równorzędny

obejmował:

- zaplanowanie badań i koncepcji artykułu
- nadzorowanie przeprowadzonych eksperymentów oraz analizy danych, interpretację uzyskanych wyników
- rewizję wstępnej wersji manuskryptu, przygotowanie ostatecznej wersji manuskryptu
- kierowanie projektem Opus 14, w ramach którego sfinansowano większość badań

Monika Glinkowska

Wdział Biologii
Uniwersytetu Gdańskiego
Katedra Genetyki
Molekularnej Bakterii

tel. +48 58 523 60 65
e-mail: mol.KGB@ug.edu.pl

ul. Wita Stwosza 59
80-309 Gdańsk

www.ug.edu.pl

Finansowanie

Badania wchodzące w skład niniejszej rozprawy doktorskiej zostały sfinansowane z następujących źródeł:

1. **Projekt NCN OPUS** UMO-2014/13/B/NZ2/01139, Charakteryzacja sieci oddziaływań białkowych jakie tworzą komponenty kompleksu replikacyjnego *Escherichia coli* w różnych warunkach wzrostu komórek - na drodze do pełnego modelu koordynacji replikacji DNA z metabolizmem u bakterii, kierownik projektu: dr hab. Monika Glinkowska, prof. UG.
2. **Projekt NCN PRELUDIUM** UMO-2016/23/N/NZ2/02378, Analiza interakcji białko-metabolit oraz modyfikacji potranslacyjnych głównych białkowych regulatorów replikacji *Escherichia coli* w różnych warunkach wzrostu komórek, kierownik projektu: mgr Joanna Morcinek-Orłowska.
3. **Projekt NCN OPUS** UMO-2017/27/B/NZ2/00747, Mechanizmy koordynacji cyklu komórkowego bakterii – trop DiaA, kierownik projektu: dr hab. Monika Glinkowska, prof. UG.

Dorobek naukowy

Publikacje:

1. **Morcinek-Orłowska J**, Walter B, Forquet R, Cysewski D, Carlier M, Mozolewski M, Meyer S, Glinkowska M. Interaction networks of *Escherichia coli* replication proteins under different bacterial growth conditions. Sci Data. 2023 Nov 10;10(1):788. doi: 10.1038/s41597-023-02710-1. PMID: 37949936.
2. **Morcinek-Orłowska J**, Zdrojewska K, Węgrzyn A. Bacteriophage-Encoded DNA Polymerases - Beyond the Traditional View of Polymerase Activities. Int J Mol Sci. 2022 Jan 7;23(2):635. doi: 10.3390/ijms23020635. PMID: 35054821.
3. **Morcinek-Orłowska J**, Galińska J, Glinkowska MK. When size matters - coordination of growth and cell cycle in bacteria. Acta Biochim Pol. 2019 Apr 10;66(2):139-146. doi: 10.18388/abp.2018_2798. PMID: 30970043.
4. Skowron PM, Sobolewski I, Adamowicz K, **Morcinek-Orłowska J**, Gaffke L, Jaroszewicz W, Łubkowska B, Pierzynowska K, Zylicz-Stachula A, Węgrzyn G. The first thermophilic phage display system. Mater Today Bio. 2025 Jun 10;33:101960. doi: 10.1016/j.mtbio.2025.101960. PMID: 40585032; PMCID: PMC12205831.
5. Maciąg-Dorszyńska M, **Morcinek-Orłowska J**, Barańska S. Concise Overview of Methodologies Employed in the Study of Bacterial DNA Replication. Int J Mol Sci. 2025 Jan 7;26(2):446. doi: 10.3390/ijms26020446. PMID: 39859162; PMCID: PMC11764726.
6. Pierzynowska K, **Morcinek-Orłowska J**, Gaffke L, Jaroszewicz W, Skowron PM, Węgrzyn G. Applications of the phage display technology in molecular biology, biotechnology and medicine. Crit Rev Microbiol. 2023 Jun 4:1-41. doi: 10.1080/1040841X.2023.2219741. PMID: 37270791.
7. Jaroszewicz W, **Morcinek-Orłowska J**, Pierzynowska K, Gaffke L, Węgrzyn G. Phage display and other peptide display technologies. FEMS Microbiol Rev. 2022 Mar 3;46(2):fuab052. doi: 10.1093/femsre/fuab052. PMID: 34673942.
8. Boss L, Górniak M, Lewańczyk A, **Morcinek-Orłowska J**, Barańska S, Szalewska-Pałasz A. Identification of Three Type II Toxin-Antitoxin Systems in Model Bacterial

Plant Pathogen *Dickeya dadantii* 3937. Int J Mol Sci. 2021 May 31;22(11):5932. doi: 10.3390/ijms22115932. PMID: 34073004.

9. Krause K, Maciąg-Dorszyńska M, Wosinski A, Gaffke L, **Morcinek-Orłowska J**, Rintz E, Bielańska P, Szalewska-Pałasz A, Muskhelishvili G, Węgrzyn G. The Role of Metabolites in the Link between DNA Replication and Central Carbon Metabolism in *Escherichia coli*. Genes (Basel). 2020 Apr 19;11(4):447. doi: 10.3390/genes11040447. PMID: 32325866.

Doniesienia zjazdowe:

1. 6th BIO Life Science Congress, 17-20.09.2025, Poznań.

   Poster: **Joanna Morcinek-Orłowska***, Karolina Zdrojewska*, Roksana Dosz, Alicja Węgrzyn, Michał R. Szymański. Hold on tight: N-terminal region enables low-temperature activity of phage-derived Efa DNA polymerase.

2. IV Sympozjum Bakteriofagowe, 4-6.09.2025, Gdańsk.

   Poster: **Joanna Morcinek-Orłowska***, Karolina Zdrojewska*, Roksana Dosz, Alicja Węgrzyn, Michał R. Szymański. Domena N-terminalna fagowej polimerazy DNA Efa umożliwia aktywność w ujemnych temperaturach.

3. III Sympozjum Bakteriofagowe, 5-7.09.2024, Gdańsk.

   Wystąpienie: **Joanna Morcinek-Orłowska**, Karolina Zdrojewska, Roksana Dosz, Grzegorz Węgrzyn, Alicja Węgrzyn, Michał R. Szymański. Badania funkcjonalne polimerazy DNA z bakteriofaga vB_EfaS-271 – rola domeny N-terminalnej w dysocjacji struktur drugorzędowych na matrycy DNA.

4. 7th DNA polymerases meeting, 28-31.08.2024, Warszawa.

   Poster: **Joanna Morcinek-Orłowska**, Karolina Zdrojewska, Grzegorz Węgrzyn, Alicja Węgrzyn, Michał R. Szymański. Functional studies on the DNA polymerase from vB_EfaS-271 bacteriophage – the role of N-terminal domain in handling secondary structures on DNA template.

5. Sympozjum Bakteriofagowe, 8-10.09.2022, Gdańsk.

   Poster: **Joanna Morcinek-Orłowska**, Weronika Jaroszewicz, Ireneusz Sobolewski, Beata Łubkowska, Katarzyna Adamowicz, Piotr M. Skowron and Grzegorz Węgrzyn.

Construction of novel phage display system based on thermophilic *Geobacillus stearothermophilus* phage TP84.

6. FEMS Viruses of Microbes 2022, 18-22.06.2022, Guimarães (Portugalia).

   Poster: **Joanna Morcinek-Orłowska**, Weronika Jaroszewicz, Ireneusz Sobolewski, Beata Łubkowska, Katarzyna Adamowicz, Piotr M. Skowron and Grzegorz Węgrzyn. Construction of novel phage display system based on thermophilic *Geobacillus stearothermophilus* phage TP84.

7. EMBO/EMBL Symposium: New Approaches and Concepts in Microbiology, 10-13.07.2019, Heidelberg (Niemcy).

   Poster: **Joanna Morcinek-Orłowska**, Aleksandra Bebel, Justyna Galińska, Torsten Waldminghaus, Anna Zawilak-Pawlik and Monika Glinkowska. The interaction between replication factor DiaA and primary metabolite sedoheptulose-7-phosphate directly regulates DNA replication in *Escherichia coli*.

8. II Konferencja Doktorantów Pomorza BioMed Session, 7.12.2018, Gdańsk.

   Poster: **Joanna Morcinek-Orłowska**, Aleksandra Bebel, Justyna Galińska, Torsten Waldminghaus, Anna Zawilak-Pawlik and Monika Glinkowska. The interaction between replication factor DiaA and primary metabolite sedoheptulose-7-phosphate directly regulates DNA replication in *Escherichia coli*.

9. 9th Central European Genome Stability and Dynamics Meeting, 13-14.09.2018, Warszawa.

   Poster: **Joanna Morcinek-Orłowska**, Aleksandra Bebel, Justyna Galińska, Torsten Waldminghaus, Anna Zawilak-Pawlik and Monika Glinkowska. The interaction between replication factor DiaA and primary metabolite sedoheptulose-7-phosphate directly regulates DNA replication in *Escherichia coli*.

10. 8th Central European Genome Stability Meeting, 29-30.09.2017, Budapeszt (Węgry).

    Poster (współautorstwo): Gabriela Baranowska, Anna Barg-Wojas, **Joanna Morcinek-Orłowska**, Jakub Muraszko and Dorota Dziadkowiec. Influence of Rrp1, Rrp2 and Srs2 overexpression on chromosome segregation and genome stability.

11. 6th Central European Genome stability and Dynamics Meeting, 9-10.10.2015, Szeged (Węgry).

Poster (współautorstwo): Anna Barg. Jakub Muraszko, **Joanna Morcinek**, Ireneusz Litwin, Antony M. Carr, Dorota Dziadkowiec, Interactions of *Schizosaccharomyces pombe rrp1+* and *rrp2+* with other genes involed in DNA damage response.

12. 8th International Fission Yeast Meeting, 21-26.06.2015, Kobe (Japonia).
    Poster: **Joanna Morcinek**, Jakub Muraszko, Anna Barg, Antony M. Carr, Dorota Dziadkowiec, Interactions of *Schizosaccharomyces pombe rrp1+* and *rrp2+* with other genes involved in the DNA damage response.

Nagrody i wyróżnienia:

1. **Wyróżnienie** podczas III Sympozjum Bakteriofagowego, Gdańsk, 5-7.09.2024, za **wystąpienie**: **Joanna Morcinek-Orłowska**, Karolina Zdrojewska, Roksana Dosz, Grzegorz Węgrzyn, Alicja Węgrzyn, Michał R. Szymański. Badania funkcjonalne polimerazy DNA z bakteriofaga vB_EfaS-271 – rola domeny N-terminalnej w dysocjacji struktur drugorzędowych na matrycy DNA.
2. **Current Opinion Biology Prize** na Międzynarodowej Konferencji EMBO/EMBL Symposium: New Approaches and Concepts in Microbiology, Heidelberg, 10-13.07.2019, za **poster**: **Joanna Morcinek-Orłowska**, Aleksandra Bebel, Justyna Galińka, Torsten Waldminghaus, Anna Zawilak-Pawlik, Monika Glinkowska. The interaction between replication factor DiaA and primary metabolite sedoheptulose-7-phosphate directly regulates DNA replication in *Escherichia coli*.
3. **III nagroda** w konkursie prezentacji popularnonaukowych podczas warsztatów „Kuźnia Młodych Talentów" Akademii Młodych Uczonych PAN, Jabłonna, 18-21.09.2018, za **prezentację popularnonaukową**: **Joanna Morcinek-Orłowska**, Aleksandra Bebel, Monika Glinkowska. Na tropie pośredników, czyli powiązania między replikacją DNA a metabolizmem komórki bakteryjnej.
4. **Best Poster Award** na konferencji 9th Central European Genome Stability and Dynamics Meeting, Warszawa, 13-14.09.2018, za **poster**: **Joanna Morcinek-Orłowska**, Aleksandra Bebel, Justyna Galińka, Torsten Waldminghaus, Anna Zawilak-Pawlik, Monika Glinkowska. The interaction between replication factor DiaA and primary

metabolite sedoheptulose-7-phosphate directly regulates DNA replication in *Escherichia coli*.

5. **Wyróżnienie** za prezentację posteru podczas II Konferencji Doktorantów Pomorza BioMed Session, Gdańk, 7.12.2018 za **poster**: **Joanna Morcinek-Orłowska**, Aleksandra Bebel, Justyna Galińka, Torsten Waldminghaus, Anna Zawilak-Pawlik, Monika Glinkowska. The interaction between replication factor DiaA and primary metabolite sedoheptulose-7-phosphate directly regulates DNA replication in *Escherichia coli*.

Kierownictwo projektów badawczych:

1. **Projekt NCN PRELUDIUM** UMO-2016/23/N/NZ2/02378, Analiza interakcji białko-metabolit oraz modyfikacji potranslacyjnych głównych białkowych regulatorów replikacji *Escherichia coli* w różnych warunkach wzrostu komórek.
2. **Projekt Młodzi Naukowcy** 538-L250-B150-18, Wpływ acetylacji syntetazy fosforybozylopirofosforanu na mechanizm regulacji inicjacji replikacji *Escherichia coli*.
3. **Projekt Młodzi Naukowcy** 538-L250-B519-17, Rola syntetazy fosforybozylopirofosforanu jako potencjalnego regulatora inicjacji replikacji *Escherichia coli*.